Aptacapteur impédimétrique à base d'hydrogel pour la détection du Diclofenac

Getnet Sewnet Kassahun

PSL UNIVERSITÉ PARIS

THÈSE DE DOCTORAT
DE L'UNIVERSITÉ PSL

Préparée à École Nationale Supérieure de Chimie de Paris

Hydrogel Matrix Grafted Impedimetric Aptasensor for the Detection of Diclofenac

Aptacapteur Impédimétrique à base d'hydrogel pour la détection du Diclofenac

Soutenue par

Getnet Sewnet KASSAHUN

Le 20-12-2019

Ecole doctorale n° 406

Chimie moléculaire de Paris centre

Spécialité

Chimie moléculaire

Composition du jury :

Michel Cassir Professeur, ENSCP	*Président*
Jean Gamby Chargé de recherche, Université Paris-Saclay	*Rapporteur*
Claude Jolivalt Professeur, Sorbonne Université	*Rapporteuse*
Pierre-Henry Aubert Professeur, Université de Cergy-Pontoise	*Examinateur*
Yvette Tran Maitre de conférences, ESPCI	*Examinatrice*
Fethi Bedioui Directeur de recherche, ENSCP	*Directeur de thèse*

Chimie Paris ParisTech | PSL

To the one who gave me a chance to live and gave me strength and faith to overcome all difficulties, our **HEAVENLY FATHER**.

Acknowledgments

Undertaking this PhD has been a truly life-changing experience for me and it would not have been possible to do it without the support and guidance that I received from many people along the way. As I sit down to write this acknowledgement, it is difficult to find the words to adequately express appreciation for the contributions of the many people who have made the completion of the task possible.

Anyway, I would like to first thank my PhD advisors, Dr. Fethi Bedioui, Dr.Cyrine Slim and Dr.Sophie Grieveau for their endless support during these past three years. I thank them wholeheartedly, not only for their tremendous academic support and their insightful discussions about the research, but also for the extra miles they have taken to make my Ph.D. experience productive. It is very much appreciated! Many thanks also to Dr. Yvette Tran who collaborated in this thesis under the framework of the SATELIT project, for her contributions of time, ideas, discussions and supervisory role throughout the entire PhD. I am also very grateful to another project collaborator, Brunno Brenson for the many insightful discussions and guidance especially about the AFM.

I would like to thank my lab mates, and whom I would like to call friends: Menel Ben Ferej, Samantha Bourg, Jérémie Gouyon,Yuan Yuan,Sarah Boumati, Marion Gaudeau and Cindy lele, for their continued support and encouragement. This dissertation would not have been definitely possible without their contributions. A very special thank you to Sophie Julliard and Joffrey Champvert for the collaborative work undertaken on this project and most importantly for their friendship. I would like to thank also Francisco Cedano, Guillome, Ekkachai Martwong, and all the trainees and PhD students whom I met and have worked with at the ESPCI for making my experience in the SIMM lab exciting and fun. Thank you Romain Botella, for the friendship and those wonderful discussions about the ATR-FTIR.

I gratefully acknowledge the funding received towards my PhD from CAMPUS FRANCE and the Ministry of education of Ethiopia and I would also like to acknowledge the PSL (“Investissements d’avenir”, program ANR-10-IDEX-0001-02 PSL) and support of Institute Pierre-Gilles de Gennes (équipement d’excellence, “Investissements d’avenir”, program ANR-10-EQPX-0034).Thanks also to all the authors of the articles and books listed in the bibliography of this thesis.

I also have to thank the members of my PhD thesis committee, Dr Grégory Lefèvre and Dr. Virginie Lair for their helpful career advice, supervision and suggestions in general. For this dissertation, I would like to thank the jury committee members: Professeur Claude Jolivalt, Dr. Jean Gamby, Professeur Pierre-Henry Aubert, Professeur Michel Cassir and Dr. Yvette Tran for their time and interest to participate in the committee.

Last but not least, I would like to express my deepest gratitude to my family and friends at home, Ethiopia. This dissertation would not have been possible without their warm love, continued patience, and endless support. I would like especially to say a heartfelt thank you to my Mum, Alemnesh, and Dad, Sewnet, for always believing in me and encouraging me to follow my dreams. And most of all for my loving, supportive, encouraging, and patient wife, Samrawit Melke, whose faithful support and sacrificial care for me and our new born son, Isaac, made it possible for me to complete this work. I would very much like to acknowledge the encouragement and support provided by friends of mine residing in Ethiopia, who have also shared in all the pain, frustration, and fun of producing the thesis. Finally, Thank you to all those who have sacrificed things in their own lives to accommodate things in mine.

Thank You!
Getnet S. Kassahun
Paris, France
November 2019.

If you can’t fly, then **run**. If you can’t run, then **walk**. If you can’t walk, then **crawl**, but by all means, **keep moving**.

-Martin Luther King Jr.

Thesis Outline

This thesis has been organized into three chapters. Chapter one is a review of literature detailing about emerging pollutants and the electrochemical methods used for the detection of diclofenac mainly over the last two decades. Aptamer immobilization methods and polymer hydrogel thin films are also discussed in this section. In chapter two are detailed the experimental steps for the construction of the aptasensor *i.e.* the material and methods used for: the fabrication of surface attached hydrogel thin films with tunable and well controlled chemistry, the covalent immobilization of aptamers on the surface attached hydrogel thin film, and also the techniques used for characterization of the aptasensor.

The results of the research undertaken and discussion of the performance of the biosensor is presented in chapter three. In this chapter, each step of the aptasensor construction were analyzed using several techniques including ellipsometry, ATR-IR, Profilometry, AFM, cyclic voltammetry and electrochemical impedance spectroscopy, for a full characterization in terms of topographic, electric and analytical properties.

The final section of the thesis recapitulates the major achievements and conclusions drawn from the research work and recommends future directions for the continuation of this work. Thus, this thesis spans the whole range from design and construction, via characterization to the application of functional PAA hydrogel as matrix for development of an aptasensor.

TABLE OF CONTENTS

LIST OF FIGURES

LIST OF TABLES

LIST OF ACRONYMS AND ABBREVIATIONS

B

BIA-MPA	Batch injection analysis with amperometric detection

C

CNTs	Carbon nanotubes
CPEs	Carbon paste electrodes
CO	Codeine
CE-C^4D	Capacitively coupled contactless conductivity detection
CZE	Capillary zone electrophoresis
CB	Conduction band

D

DCL	Diclofenac
DOP	Dioctylphthalate
DBP	Dibutylphthalate
DNP	Dinonylphthalate
DNS	Dinonylsebacenate
DPV	Differential pulse voltammetry

E

EPs	Emerging pollutants
EDCs	Endocrine disrupting chemicals
EU	European Union
E2	17-beta-estradiol
EE2	17-alpha-ethinylestradiol
EAS	Electrode-active substance
EZM	Esomeprazole
EIS	Electrochemical impedance spectroscopy
ELISA	Enzyme-linked immunosorbent assay
ECL	Electrochemiluminescence
ECLIA	Electrochemiluminescence immunoassay
EDC	1-(3-dimethylaminopropyl)-3-ethyl carbodiimide

F

FFT SWV	Fast Fourier Transform Square-Wave Voltammetry
FIA-MPA	Flow injection analysis with multiple-pulse amperometric

G

GC	Gas chromatography
GCE	Glassy carbon electrode

H

HPLC-MS-MS	High performance liquid chromatography combined with tandem mass spectroscopy

I

ISEs	Ion selective electrodes
IA	Ionic associate
IND	Indomethacin

L

LPME	Liquid-phase micro extraction
LC	Liquid chromatography
LOD	Limit of detection
LOQ	Limit of quantitation
LSV	Linear Sweep Voltammetry
LFD	Lateral flow device
LC−MS	liquid chromatography−mass spectrometry

M

MS	Mass Spectroscopy
MWCNT–IL|CCE	Multiwalled carbon nanotube and ionic liquid modified carbon ceramic electrode
MWCNTs	Multi walled Carbon Nanotubes
MIP	Molecular Imprinted Polymer

N

NORMAN Group	Network of reference laboratories, research centers and related organizations for monitoring emerging environmental substances
NSAID	Nonsteroidal anti-inflammatory drug
NHS	N-hydroxysulfosuccinimide

P

PPCPs	Pharmaceuticals and personal care products
PVC	Poly(vinyl chloride)
PEC	Photoelectrochemical
PtNPs	Platinum nanoparticles
PEI	Polyethyleneimine
PEC	Photoelectrochemical

Q

QTRAP	Triple-quadrupole linear ion trap mass spectrometer
QCM	Quartz crystal microbalance

R

rGO	Reduced graphene oxide

S

SPE	Solid-phase extraction
SPME	Solid-phase microextraction
SWV	Square wave voltammetry
SELEX	Systematic evolution of ligands by exponential enrichment
SAM	Self-assembled monolayers
SPR	Surface plasmon resonance

T

TOF-MS	Time-of-flight mass spectrometry
TCP	Tricresylphosphtate

U

UV	Ultraviolet
UPLC–QqLIT–MS/MS	Ultra-high performance liquid chromatography coupled to mass spectrometry with hybrid triple quadrupole–linear ion trap
ULISA	Upconversion-linked immunosorbent assay

V

VB	Valence band

W

WWTPs	Wastewater treatment plants
WFD	Water Framework Directive

GENERAL INTRODUCTION

Pharmaceutical drugs have attracted much attention as suitable small organic molecule targets because of their potential applications. For example, detection of drug residues as contaminants in food and water is of great importance in the fields of environment and human health. One of the common drugs that have been used over the years is Diclofenac (noted as DCL), or 2-(2-((2,6-dichlorophenyl)amino) phenyl)acetic acid. This nonsteroidal anti-inflammatory drug (NSAID) possesses analgesic, anti-inflammatory, and antipyretic properties [1]. However, its environmental effects are harmful [2]. Sold under the brand name Voltaren® among others, DCL is frequently pre-scribed for rheumatic complaints, acute joint inflammation and mild to moderate pain[3,4]. Due to its wide use, DCL residues have often been detected in freshwater environments [5,6]. Thus, DCL is considered an emerging pollutants (EP) as a consequence of its occurrence in surface waters and its potential toxicity towards aquatic organisms[7,8]. EPs comprise a wide assortment of substances (e.g. endocrine disruptors, pharmaceuticals and personal care products) characterized by an extensive distribution in the environment due to their massive everyday use and persistence[9,10].

EPs, commonly present at trace concentrations, have been associated with negative effects on human and animal health (e.g. nervous system damage, toxicity or disruption of the immune system)[11]. Several studies have described harmful effects to different organisms when exposed to environmental levels of DCL[12,13]. These may vary from a few ng L^{-1} to tens of mg L^{-1} [14] in waste and environmental waters. Taking the above-mentioned aspects into account, the quantification of DCL in environmental waters is of great importance, not only to improve the current state of knowledge regarding its pathways, fate and effects in the environment, but also to determine the efficiency of waste water treatment plants [15]. Until now, its detection mostly relied on conventional techniques, such as HPLC [16,17] and GC/MS [18]. Though highly sensitive, these analytical techniques are time-consuming, expensive, require a lot of expertise to be operated and are not easy to be deployed in the field. Overcoming these limitations, electrochemical methods have attracted attention in recent years for environmental, pharmaceutical and biological compounds analysis and they offer numerous advantages over optical, piezoelectric or thermal detection. In comparison with optical methods, electrochemical transduction offers several benefits including simple-to-operate, rapid, cost effective, highly sensitive and selective,

compatible with novel micro-fabrication techniques, disposable, easy to miniaturize and robust [19–24]. Electrochemical reactions usually provide an electronic signal directly, avoiding the requirement of expensive signal transduction equipment [25–27].

Among the electrochemical methods, various amperometric [28–31]and potentiometric techniques [32–35]have been reported for the determination of DCL. Modified electrodes including Cu-doped zeolite-expanded graphite-epoxy electrode [36] and catalytic DCL electrooxidation on graphene or carbon nanotubes[37,38] have been also used. In order to improve the limit of detection (LOD), biomolecules that are specific for the DCL have been utilized by using antibodies also [39,40].

When it comes to electrochemical sensing, aptasensors are promising biosensors, as they take advantage of using aptamers as a recognition element [41]. Aptamers are short single-stranded nucleic acid oligomers (DNA or RNA) capable of folding into highly organized, complex structures enabling ligation to molecular targets with high affinity [42]. Their multiple advantages include their high specificity and affinity [43–46], their easy and highly reliable production by enzymatic or chemical synthesis [43,44], their regenerability by simple means [45,47] and their storability [45,48]. They are also stable, with no loss of activity under a wide range of buffer conditions, and resistant to harsh treatments such as physical or chemical denaturation. Aptamers can be functionalized, offering diverse immobilization ways [49].

Thus, combination of the excellent characteristics of aptamers and the leading detection platform techniques, such as optical, electrochemical, or mass sensitive techniques with high sensitivity and specificity draws a promising view for the application of the aptasensors for the detection of harmful small toxic chemicals and their real-time monitoring in the environments [51]. Among the different electrochemical detection techniques, electrochemical impedance spectroscopy (EIS) has appeared as a promising strategy [50,51]. Studies on detection of DCL using aptasensors are rarely reported to the best of our knowledge, and recently a very few EIS aptasensors have been designed and constructed based on monitoring the interfacial property changes [52,53].

In this work, we have developed a novel aptasensor for DCL. To this end, a new class of surface-attached hydrogel thin films was grafted on conductive transducer and used as biocompatible matrix for aptamer immobilization, tuned for the conception of biosensor. The polymeric network environment: favors the stable immobilization of the aptamer by providing the aptamer excellent environments to preserve its active and functional structure, provides the ability to immobilize a

large amount of the aptamer and favors the selective affinity of the aptamer to the target [54]. Surface-attached hydrogel thin films present then many advantages as immobilization matrix: they are stable, robust, multiscale and multifunctional materials, with thickness widely ranging from low nanometers to high micrometers. The deformability, permeability and porosity of the hydrogel films can also be easily and finely adjusted with the film thickness and the network crosslinks density.

A simple and versatile approach for the synthesis of reliable and reproducible hydrogel films, so-called CLAG process (Cross-Linking And Grafting), was followed in this study. The process consists in preforming functionalized polymers using thiol-ene click chemistry. The advantages of the approach, as described by Chollet *et al.* [55], is that the synthesis of preformed reactive chains avoids the difficulty of working under controlled atmosphere as oxygen inhibits radical polymerization. This versatile approach provides then the facile adjustment of chemical properties (platform for covalent immobilization) and physical properties (size and architecture) of hydrogel films.

Each step of the biosensor construction was analyzed, using various techniques for a full characterization in terms of topographic, electric and analytical properties. Morphological characterization of the biosensing surface was done by atomic force microscopy (AFM) to measure the thickness and determine the topography of the hydrogel film, while Attenuated Total Reflectance-Fourier Transform Infra-Red (*ATR-FTIR*) spectroscopy was used to evidence the presence of functional groups. Cyclic Voltammetry (CV) and EIS were implemented for monitoring the interfacial properties on the electrode surface during the stepwise assembly of the biosensor. The electrochemical performance of the biosensor was studied using EIS for target detection with a change in the electron transfer resistance when the target captured onto the electrode. The following schematic representation summarizes the experimental steps for the construction of the aptasensor.

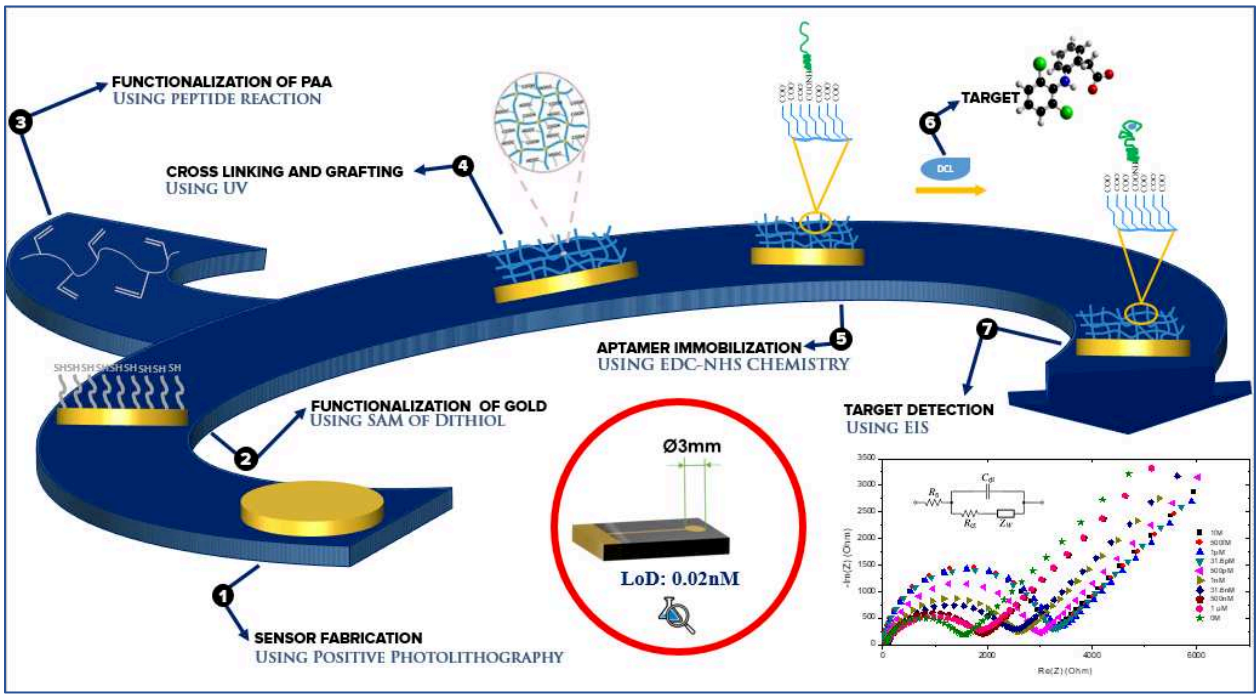
FUNCTIONALIZATION OF PAA
USING PEPTIDE REACTION
CROSS LINKING AND GRAFTING
USING UV
TARGET
DCL
APTAMER IMMOBILIZATION
USING EDC-NHS CHEMISTRY
TARGET DETECTION
USING EIS
FUNCTIONALIZATION OF GOLD
USING SAM OF DITHIOL
SENSOR FABRICATION
USING POSITIVE PHOTOLITHOGRAPHY
Ø3mm
LoD: 0.02nM

REFERENCES

[1] D.H. Solomon, J. Avorn, T. Stürmer, R.J. Glynn, H. Mogun, S. Schneeweiss, Cardiovascular outcomes in new users of coxibs and nonsteroidal antiinflammatory drugs: High-risk subgroups and time course of risk, Arthritis Rheum. 54 (2006) 1378–1389. https://doi.org/10.1002/art.21887.

[2] E.J. Tiedeken, A. Tahar, B. McHugh, N.J. Rowan, Monitoring, sources, receptors, and control measures for three European Union watch list substances of emerging concern in receiving waters – A 20 year systematic review, Sci. Total Environ. 574 (2017) 1140–1163. https://doi.org/10.1016/j.scitotenv.2016.09.084.

[3] R. Altman, B. Bosch, K. Brune, P. Patrignani, C. Young, Advances in NSAID Development: Evolution of Diclofenac Products Using Pharmaceutical Technology, Drugs. 75 (2015) 859–877. https://doi.org/10.1007/s40265-015-0392-z.

[4] T.J. Gan, Diclofenac: an update on its mechanism of action and safety profile, Curr. Med. Res. Opin. 26 (2010) 1715–1731. https://doi.org/10.1185/03007995.2010.486301.

[5] P. Paíga, L.H.M.L.M. Santos, S. Ramos, S. Jorge, J.G. Silva, C. Delerue-Matos, Presence of pharmaceuticals in the Lis river (Portugal): Sources, fate and seasonal variation, Sci. Total Environ. 573 (2016) 164–177. https://doi.org/10.1016/j.scitotenv.2016.08.089.

[6] Y. Zhang, S.-U. Geißen, C. Gal, Carbamazepine and diclofenac: Removal in wastewater treatment plants and occurrence in water bodies, Chemosphere. 73 (2008) 1151–1161. https://doi.org/10.1016/j.chemosphere.2008.07.086.

[7] B. Petrie, R. Barden, B. Kasprzyk-Hordern, A review on emerging contaminants in wastewaters and the environment: Current knowledge, understudied areas and recommendations for future monitoring, Water Res. 72 (2015) 3–27. https://doi.org/10.1016/j.watres.2014.08.053.

[8] S.D. Richardson, T.A. Ternes, Water Analysis: Emerging Contaminants and Current Issues, Anal. Chem. 86 (2014) 2813–2848. https://doi.org/10.1021/ac500508t.

[9] B. Albero, C. Sánchez-Brunete, A.I. García-Valcárcel, R.A. Pérez, J.L. Tadeo, Ultrasound-assisted extraction of emerging contaminants from environmental samples, TrAC Trends Anal. Chem. 71 (2015) 110–118. https://doi.org/10.1016/j.trac.2015.03.015.

[10] Q. Sui, X. Cao, S. Lu, W. Zhao, Z. Qiu, G. Yu, Occurrence, sources and fate of pharmaceuticals and personal care products in the groundwater: A review, Emerg. Contam. 1 (2015) 14–24. https://doi.org/10.1016/j.emcon.2015.07.001.

[11] Y. Luo, W. Guo, H.H. Ngo, L.D. Nghiem, F.I. Hai, J. Zhang, S. Liang, X.C. Wang, A review on the occurrence of micropollutants in the aquatic environment and their fate and removal during wastewater treatment, Sci. Total Environ. 473–474 (2014) 619–641. https://doi.org/10.1016/j.scitotenv.2013.12.065.

[12] B. Hoeger, B. Köllner, D.R. Dietrich, B. Hitzfeld, Water-borne diclofenac affects kidney and gill integrity and selected immune parameters in brown trout (Salmo trutta f. fario), Aquat. Toxicol. 75 (2005) 53–64. https://doi.org/10.1016/j.aquatox.2005.07.006.

[13] R. Triebskorn, H. Casper, V. Scheil, J. Schwaiger, Ultrastructural effects of pharmaceuticals (carbamazepine, clofibric acid, metoprolol, diclofenac) in rainbow trout (Oncorhynchus mykiss) and common carp (Cyprinus carpio), Anal. Bioanal. Chem. 387 (2007) 1405–1416. https://doi.org/10.1007/s00216-006-1033-x.

[14] A.J. Ebele, M. Abou-Elwafa Abdallah, S. Harrad, Pharmaceuticals and personal care products (PPCPs) in the freshwater aquatic environment, Emerg. Contam. 3 (2017) 1–16. https://doi.org/10.1016/j.emcon.2016.12.004.

[15] M. Cleuvers, Mixture toxicity of the anti-inflammatory drugs diclofenac, ibuprofen, naproxen, and acetylsalicylic acid, Ecotoxicol. Environ. Saf. 59 (2004) 309–315. https://doi.org/10.1016/S0147-6513(03)00141-6.

[16] C. Arcelloni, R. Lanzi, S. Pedercini, G. Molteni, I. Fermo, A. Pontiroli, R. Paroni, High-performance liquid chromatographic determination of diclofenac in human plasma after solid-phase extraction, J. Chromatogr. B. Biomed. Sci. App. 763 (2001) 195–200. https://doi.org/10.1016/S0378-4347(01)00383-8.

[17] B. Yilmaz, A. Asci, S.S. Palabiyik, HPLC Method for Determination of Diclofenac in Human Plasma and Its Application to a Pharmacokinetic Study in Turkey, J. Chromatogr. Sci. 49 (2011) 422–427. https://doi.org/10.1093/chrsci/49.6.422.

[18] P.-A. Auroux, D. Iossifidis, D.R. Reyes, A. Manz, Micro Total Analysis Systems. 2. Analytical Standard Operations and Applications, Anal. Chem. 74 (2002) 2637–2652. https://doi.org/10.1021/ac020239t.

[19] A. Sassolas, L.J. Blum, B.D. Leca-Bouvier, Electrochemical Aptasensors, Electroanalysis. 21 (2009) 1237–1250. https://doi.org/10.1002/elan.200804554.

[20] A. Hayat, J.L. Marty, Aptamer based electrochemical sensors for emerging environmental pollutants, Front. Chem. 2 (2014). https://doi.org/10.3389/fchem.2014.00041.

[21] M. Mir, M. Vreeke, I. Katakis, Different strategies to develop an electrochemical thrombin aptasensor, Electrochem. Commun. 8 (2006) 505–511. https://doi.org/10.1016/j.elecom.2005.12.022.

[22] L. Zhao, Y. Huang, Y. Dong, X. Han, S. Wang, X. Liang, Aptamers and Aptasensors for Highly Specific Recognition and Sensitive Detection of Marine Biotoxins: Recent Advances and Perspectives, Toxins. 10 (2018) 427. https://doi.org/10.3390/toxins10110427.

[23] H.B. Bostan, S.M. Taghdisi, J.L. Bowen, N. Demertzis, R. Rezaee, Y. Panahi, A.M. Tsatsakis, G. Karimi, Determination of microcystin-LR, employing aptasensors, Biosens. Bioelectron. 119 (2018) 110–118. https://doi.org/10.1016/j.bios.2018.08.003.

[24] S.G. Meirinho, L.G. Dias, A.M. Peres, L.R. Rodrigues, Voltammetric aptasensors for protein disease biomarkers detection: A review, Biotechnol. Adv. 34 (2016) 941–953. https://doi.org/10.1016/j.biotechadv.2016.05.006.

[25] G. Castillo, I. Lamberti, L. Mosiello, T. Hianik, Impedimetric DNA Aptasensor for Sensitive Detection of Ochratoxin A in Food, Electroanalysis. 24 (2012) 512–520. https://doi.org/10.1002/elan.201100485.

[26] A. Rhouati, A. Hayat, D.B. Hernandez, Z. Meraihi, R. Munoz, J.-L. Marty, Development of an automated flow-based electrochemical aptasensor for on-line detection of Ochratoxin A, Sens. Actuators B Chem. 176 (2013) 1160–1166. https://doi.org/10.1016/j.snb.2012.09.111.

[27] A. Rhouati, C. Yang, A. Hayat, J.-L. Marty, Aptamers: A Promising Tool for Ochratoxin A Detection in Food Analysis, Toxins. 5 (2013) 1988–2008. https://doi.org/10.3390/toxins5111988.

[28] J.A. Rodríguez, E. Barrado, Y. Castrillejo, J.R. Santos, J.L.F.C. Lima, Validation of a tubular bismuth film amperometric detector, J. Pharm. Biomed. Anal. 45 (2007) 47–53. https://doi.org/10.1016/j.jpba.2007.05.025.

[29] X. Yang, F. Wang, S. Hu, Enhanced oxidation of diclofenac sodium at a nano-structured electrochemical sensing film constructed by multi-wall carbon nanotubes–surfactant composite, Mater. Sci. Eng. C. 28 (2008) 188–194. https://doi.org/10.1016/j.msec.2006.11.006.

[30] M. Hajjizadeh, A. Jabbari, H. Heli, A.A. Moosavi-Movahedi, S. Haghgoo, Electrocatalytic oxidation of some anti-inflammatory drugs on a nickel hydroxide-modified nickel electrode, Electrochimica Acta. 53 (2007) 1766–1774. https://doi.org/10.1016/j.electacta.2007.08.026.

[31] P. Daneshgar, P. Norouzi, M. Ganjali, R. Dinarvand, A. Moosavi-Movahedi, Determination of Diclofenac on a Dysprosium Nanowire- Modified Carbon Paste Electrode Accomplished in a Flow Injection System by Advanced Filtering, Sensors. 9 (2009) 7903–7918. https://doi.org/10.3390/s91007903.

[32] M.C. Oliveira, E.H. Bindewald, L.H. Marcolino, M.F. Bergamini, Potentiometric determination of Diclofenac using an ion-selective electrode prepared from polypyrrole films, J. Electroanal. Chem. 732 (2014) 11–16. https://doi.org/10.1016/j.jelechem.2014.08.006.

[33] Zh.A. Kormosh, I.P. Hunka, Ya.R. Bazel, A potentiometric sensor for the determination of diclofenac, J. Anal. Chem. 64 (2009) 853–858. https://doi.org/10.1134/S1061934809080140.

[34] H.T. Elbalkiny, A.M. Yehia, S.M. Riad, Y.S. Elsaharty, Potentiometric diclofenac detection in wastewater using functionalized nanoparticles, Microchem. J. 145 (2019) 90–95. https://doi.org/10.1016/j.microc.2018.10.017.

[35] J. Lenik, A new potentiometric electrode incorporating functionalized β-cyclodextrins for diclofenac determination, Mater. Sci. Eng. C. 45 (2014) 109–116. https://doi.org/10.1016/j.msec.2014.08.072.

[36] F. Manea, M. Ihos, A. Remes, G. Burtica, J. Schoonman, Electrochemical Determination of Diclofenac Sodium in Aqueous Solution on Cu-Doped Zeolite-Expanded Graphite-Epoxy Electrode, Electroanalysis. 22 (2010) 2058–2063. https://doi.org/10.1002/elan.201000074.

[37] K. Sarhangzadeh, A.A. Khatami, M. Jabbari, S. Bahari, Simultaneous determination of diclofenac and indomethacin using a sensitive electrochemical sensor based on multiwalled

carbon nanotube and ionic liquid nanocomposite, J. Appl. Electrochem. 43 (2013) 1217–1224. https://doi.org/10.1007/s10800-013-0609-3.

[38] C. Karuppiah, S. Cheemalapati, S.-M. Chen, S. Palanisamy, Carboxyl-functionalized graphene oxide-modified electrode for the electrochemical determination of nonsteroidal anti-inflammatory drug diclofenac, Ionics. 21 (2015) 231–238. https://doi.org/10.1007/s11581-014-1161-9.

[39] M. Huebner, E. Weber, R. Niessner, S. Boujday, D. Knopp, Rapid analysis of diclofenac in freshwater and wastewater by a monoclonal antibody-based highly sensitive ELISA, Anal. Bioanal. Chem. 407 (2015) 8873–8882. https://doi.org/10.1007/s00216-015-9048-9.

[40] A. Hlaváček, Z. Farka, M. Hübner, V. Horňáková, D. Němeček, R. Niessner, P. Skládal, D. Knopp, H.H. Gorris, Competitive Upconversion-Linked Immunosorbent Assay for the Sensitive Detection of Diclofenac, Anal. Chem. 88 (2016) 6011–6017. https://doi.org/10.1021/acs.analchem.6b01083.

[41] A. Hayat, J.L. Marty, Aptamer based electrochemical sensors for emerging environmental pollutants, Front. Chem. 2 (2014). https://doi.org/10.3389/fchem.2014.00041.

[42] C.B. Joeng, J.H. Niazi, S.J. Lee, M.B. Gu, ssDNA aptamers that recognize diclofenac and 2-anilinophenylacetic acid, Bioorg. Med. Chem. 17 (2009) 5380–5387. https://doi.org/10.1016/j.bmc.2009.06.044.

[43] B. Strehlitz, C. Reinemann, S. Linkorn, R. Stoltenburg, Aptamers for pharmaceuticals and their application in environmental analytics, Bioanal. Rev. 4 (2012) 1–30. https://doi.org/10.1007/s12566-011-0026-1.

[44] F. Radom, P.M. Jurek, M.P. Mazurek, J. Otlewski, F. Jele?, Aptamers: Molecules of great potential, Biotechnol. Adv. 31 (2013) 1260–1274. https://doi.org/10.1016/j.biotechadv.2013.04.007.

[45] S. Balamurugan, A. Obubuafo, S.A. Soper, R.L. McCarley, D.A. Spivak, Designing Highly Specific Biosensing Surfaces Using Aptamer Monolayers on Gold, Langmuir. 22 (2006) 6446–6453. https://doi.org/10.1021/la060222w.

[46] S. Tombelli, M. Minunni, M. Mascini, Analytical applications of aptamers, Biosens. Bioelectron. 20 (2005) 2424–2434. https://doi.org/10.1016/j.bios.2004.11.006.

[47] C. Hamula, J. Guthrie, H. Zhang, X. Li, X. Le, Selection and analytical applications of aptamers, TrAC Trends Anal. Chem. 25 (2006) 681–691.

https://doi.org/10.1016/j.trac.2006.05.007.

[48] S. Tom, H.-E. Jin, S.-W. Lee, Aptamers as functional bionanomaterials for sensor applications, in: Eng. Nanobiomaterials, Elsevier, 2016: pp. 181–226. https://doi.org/10.1016/B978-0-323-41532-3.00006-3.

[49] M. Menger, J. Glökler, M. Rimmele, Application of Aptamers in Therapeutics and for Small-Molecule Detection, in: V. Erdmann, J. Barciszewski, J. Brosius (Eds.), RNA Med., Springer-Verlag, Berlin/Heidelberg, 2006: pp. 359–373. https://doi.org/10.1007/3-540-27262-3_18.

[50] A. Hayat, W. Haider, M. Rolland, J.-L. Marty, Electrochemical grafting of long spacer arms of hexamethyldiamine on a screen printed carbon electrode surface: application in target induced ochratoxin A electrochemical aptasensor, The Analyst. 138 (2013) 2951. https://doi.org/10.1039/c3an00158j.

[51] A. Hayat, S. Andreescu, J.-L. Marty, Design of PEG-aptamer two piece macromolecules as convenient and integrated sensing platform: Application to the label free detection of small size molecules, Biosens. Bioelectron. 45 (2013) 168–173. https://doi.org/10.1016/j.bios.2013.01.059.

[52] H. Derikvand, M. Roushani, A.R. Abbasi, Z. Derikvand, A. Azadbakht, Design of folding-based impedimetric aptasensor for determination of the nonsteroidal anti-inflammatory drug, Anal. Biochem. 513 (2016) 77–86. https://doi.org/10.1016/j.ab.2016.06.013.

[53] L. Kashefi-Kheyrabadi, M.A. Mehrgardi, Design and construction of a label free aptasensor for electrochemical detection of sodium diclofenac, Biosens. Bioelectron. 33 (2012) 184–189. https://doi.org/10.1016/j.bios.2011.12.050.

[54] L. Feng, L. Wang, Z. Hu, Y. Tian, Y. Xian, L. Jin, Encapsulation of horseradish peroxidase into hydrogel, and its bioelectrochemistry, Microchim. Acta. 164 (2009) 49–54. https://doi.org/10.1007/s00604-008-0030-5.

[55] B. Chollet, M. Li, E. Martwong, B. Bresson, C. Fretigny, P. Tabeling, Y. Tran, Multiscale Surface-Attached Hydrogel Thin Films with Tailored Architecture, ACS Appl. Mater. Interfaces. 8 (2016) 11729–11738. https://doi.org/10.1021/acsami.6b00446.

CHAPTER 1:
STATE OF THE ART

CHAPTER 1 : STATE OF THE ART

1.1 Emerging Pollutants: Generality

In the last decades, due to the industrial globalization and the rise in population, the increasing amount of hazardous compounds that have high impact on human wellbeing and environmental health have been of increasing concern [1]. These chemicals have been widely disseminated into the environment and some of them have never undergone safety testing, and a minimal assessment has been provided on their potential toxicity or the possible synergistic effects of simultaneous exposures to multiple chemicals [2,3].

Among these chemicals, emerging pollutants (EPs) have recently received a huge attention because of their increasing presence in the environment, their potential threats to environmental ecosystems, and the absence of routine monitoring programmes [4]. Emerging pollutants are defined by the NORMAN Group (Network of reference laboratories, research centers and related organizations for monitoring emerging environmental substances) as "synthetic or naturally occurring chemicals that are not commonly monitored in the environment but which have the potential to enter the environment and cause known or suspected adverse ecological and (or) human health effects" [5].

Emerging pollutants encompass a miscellaneous group of compounds, including pharmaceuticals and personal-care products, drugs of abuse and their metabolites, steroids and hormones, endocrine-disrupting compounds, surfactants, perfluorinated compounds, phosphate ester flame retardants, industrial additives and agents (e.g. benzotriazoles and benzothiazoles), siloxanes, artificial sweeteners, biocides, polar pesticides and their degradation products, and gasoline additives [6].

EPs exhibit wide variation in function, chemical structure and physiochemical properties, making it difficult to generalize about their behavior, persistence or impact in the environment. Most of these EPs are also designed to be biologically active, have a specific mode of action and to be persistent in the body, meaning they can impact humans and wildlife at trace concentrations which are often hard to detect and quantify using traditional analytical methods [7].

Occurrence of EPs can result from point (mainly urban and industry) or diffuse (agriculture) pollution. The transport of EPs from diffuse sources to the sink (water bodies) strongly depends

on the EPs properties [8] such as volatility, polarity, persistence and adsorption properties. EPs from urban or industrial waste water treatment plants are directly discharged into rivers where their environmental fate is of concern (degradation, sorption at the sediment, and transport in the aqueous phase). EPs can undergo significant biodegradation and transformation in effluent-impacted surface waters and groundwater.

The impacts of chronic exposure to trace concentrations of many EPs on wildlife and human health may be severe, thus it is critical to limit as much as possible the concentrations of this class of contaminants in our waterways [9]. Certain EPs can specifically impact the endocrine system of humans or wildlife; such chemicals are part of emerging pollutants known as endocrine disrupting chemicals (EDCs). Much of the growing interest in this field of research stems from fears that chronic exposure to EDCs (in bathing or drinking water, for example) may be linked to adverse human health conditions such as declining male fertility, birth defects, and breast and testicular cancers [10]. Furthermore, negative impacts of EDCs exposure on wildlife may include severe consequences such as feminization in fish [11]. Similar to EPs as a whole, EDCs are mainly thought to be transported into the aquatic environment *via* incomplete removal at wastewater treatment plants (WWTPs) [10].

Until recently, environmental regulations worldwide had not required explicit testing for any EPs in water bodies. However, given the growing concern about contamination of the aquatic environment with these compounds, legislation has recently begun to acknowledge this potential problem. Part of this effort is the Water Framework Directive (WFD, 2000/ 60/EC), which is an overarching piece of European environmental legislation aimed at protecting and improving water quality throughout the European Union (EU) [12].

Hence, in response to the growing EU concern about the release of untreated EPs into the aquatic environment, three compounds were included in the first watch list in 2013: diclofenac (DCL), 17-beta-estradiol (E2) and 17-alpha-ethinylestradiol (EE2). Besides the two pharmaceuticals (DCL and EE2) and the natural hormone (E2) that were previously recommended to be included by the Directive 39/2013/EU, the first watch list of 10 substances/groups of substances also refers to the three macrolide antibiotics (clarithromycin, azithromycin and erythromycin), other natural hormone (E1), some pesticides (oxadiazon, methiocarb, imidacloprid, thiacloprid, thiamethoxam, clothianidin, acetamiprid and triallate), a UVB filter (2-ethinylhexyl 4-methoxcinnamate) and an

antioxidant (2,6-di-tert-butyl-4-methylphenol) commonly used as a food additive [13]. This list, generally, presents emerging substances requiring further attention due to their high frequency of occurrence, the expected risk for human health and/or aquatic life, and/or for a lack of analytical techniques.

Among the 10 watch lists, Diclofenac is a nonsteroidal anti-inflammatory drug (NSAID) that possesses analgesic, anti-inflammatory, and antipyretic properties [14] with pKa value of 4.2 and log P of 3.9. The structure of DCL is shown on Figure 1.1. Sold under the brand name Voltaren®, among others, DCL is prescribed as oral tablets or a topical gel, frequently for rheumatic complaints, acute joint inflammation and mild to moderate pain [15,16]. Vieno et al. [17] reported that only 6–7% of the topical gel is absorbed, while the rest is washed off the skin or attaches to clothing. This is significant in regards to environmental contamination because a large percentage of topically applied DCL will end up washed down household drains, ultimately ending up in WWTP influent, and also they have found that between 65 and 75% of the orally administered dose is excreted through urine and 20–30% is excreted in faeces as the parent drug or metabolites.

Treated municipal wastewater effluent is considered to be the major vector of contamination of the aquatic environment with DCL [17] . DCL is considered as a recalcitrant compound, meaning its removal efficiency during conventional wastewater treatment is poor [9,18] and according to biodegradability studies, DCL biodegradation is slow or non-existent [19,20]. Thus, concentrations of this compound in effluent are generally high, and DCL is commonly released *via* this pathway into surface waters. Compared with E2 (~ 22 ng/L) and EE2(~ 7 ng/L), DCL(~ 131 ng/L) tends to be present in high concentrations in WWTP influents [21], and also among the most frequently detected compound in WWTPs effluents [9,18].

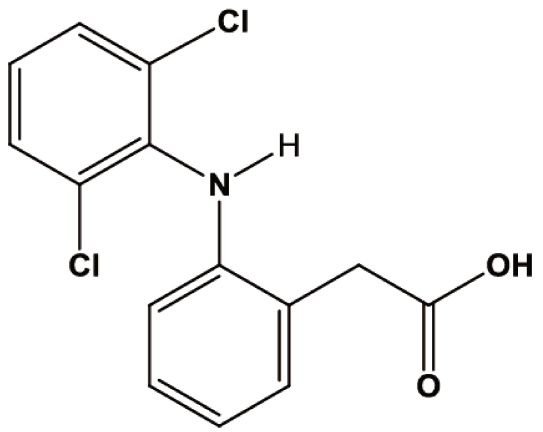

Figure 1.1: Chemical structure of Diclofenac

In general, DCL has been extensively found in various water bodies and the consumption of DCL is predicted to further grow, and its content will increase accordingly in the aquatic ecosystems [22–25]. Several studies have described harmful effects to different organisms when exposed to environmental levels of DCL [26,27]. These may vary from a few ng L^{-1} to tens of mg L^{-1} in waste and environmental waters [28]. Taking the above-mentioned aspects into account, the quantification of DCL is of great importance, not only to improve the current state of knowledge regarding its pathways, fate and effects in the environment, but also to determine the efficiency of waste water treatment plants [29].

1.2 Analytical Separative Methods for the Detection of DCL

As indicated above, as a result of long-term exposure, DCL is resulting in adverse effects on humans and wildlife. Therefore, it is important to develop analytical methodologies to detect and control the presence of DCL in very different kinds of samples, from urine, serum or plasma, to river and waste water, sediments or sewage sludge.

Generally, no analytical standard method is available for diclofenac, but the EPA method 1694 can be applied [41]. EPA method 1694 determines pharmaceuticals and personal care products (PPCPs) in environmental samples by high performance liquid chromatography combined with tandem mass spectroscopy (HPLC-MS-MS) using isotope dilution and internal standard quantitation techniques.

The analytical methods that are currently used for the detection and identification of NSAIDs such as DCL were reviewed by Olives et.al [42], including gas chromatography (GC) and liquid chromatography (LC) coupled with a variety of detection methods, including ultraviolet (UV) detection, diode array detection, fluorescence detection and tandem MS. In addition, more advanced extraction techniques such as SPE, SPME, and LPME are used for sample preparation and among them, SPE is the most popular and well-established technique because it is highly selective and robust [43].

The vast majority of analytical methods applied for accurate, selective and sensitive DCL detection and quantification in various samples have been based on separative techniques such as liquid chromatography (LC) coupled to different detection systems. For example, tandem mass spectrometry (LC-MS/MS) was used mainly due to its versatility and specificity , enabling the detection of target in the low ng/L range [42,44–46]. The hyphenation of MS detection with liquid chromatography, the suitability of analysis of DCL by LC as opposed to GC, is related to the fact that DCL is a polar compound [44].

A survey of the research articles dealing with analytical methods employed for quantitation of DCL is presented in Table 1.1. These analytical methods are given in part in the report “Analytical methods relevant to the European Commission's 2012 proposal on Priority Substances under the Water Framework Directive” [47]. As it can be seen in table 1.1, the analysis of DCL is dominated by LC-tandem mass spectrometric techniques because of its afore-mentioned merits compared to GC based techniques.

Table 1.1: Main analytical methods for the detection and quantification of DCL

No.	Extraction Method (volume)	Analysis method	Linearity (r^2)	LOD(ng/L)	LOQ (ng/L)	Reference
1	SPE (0.4 L)	LC/MS-MS	0.9998	36	10	[48]
2	SPE (surface water)	LC/MS-MS	0.9997	2	5	[49]
3	SPE (0.2 L); waste water	LC- QTRAP -MS-MS	0.9914	0.4	1	[50]
4	SPE (0.5 L) ; surface water	LC/MS-MS	0.9999	1	7	[51]
5	SPE (0.1 L)	LC-ion-trap-MS-MS	NA	0.15	0.49	[52]
6	SPE (0.1 L); surface water	LC/MS-MS	NA	0.7	2.4	[53]
7	SPE (0.5 L); surface water	UPLC–QqLIT–MS-MS	NA	4.1	13.5	[54]

Bueno et al. [50] developed a strategy for the analysis of a selected group of 56 organic pollutants in wastewater (38 pharmaceuticals and 10 of their most frequent metabolites, 6 pesticides, and 2 disinfectants). The LC-MS methodology applied is based on the use of a hybrid triple-quadrupole linear ion trap mass spectrometer (QTRAP) in combination with time-of-flight mass spectrometry (TOF-MS). Quantification was performed by LC-QTRAP-MS operating under selected reaction monitoring (SRM) mode in both positive and negative electrospray ionization. Unequivocal identification was provided by the acquisition of three SRM transitions per compound in most of the cases and by LCTOF-MS analysis, which allows obtaining accurate mass measurements of the identified compounds with errors lower than 2 ppm. Additionally, the use of TOF-MS permits retrospective analysis, since the full spectrum is recorded at all times with a high sensitivity. The methodology was successfully applied to a monitoring study intended to characterize wastewater effluents of six sewage treatment plants in Spain and the joint application of both techniques provided very good results in terms of accurate quantification and unequivocal confirmation as can be seen table 1.1.

A most recent article by Petrović et al. [54] covers the analysis of the occurrence of pharmaceuticals in waste, surface, underground, and drinking water collected from 25 locations in

the northern part of Serbia. Ultra-high performance liquid chromatography coupled to mass spectrometry with hybrid triple quadrupole–linear ion trap (UPLC–QqLIT–MS/MS) multi-residue method was applied to determine 81 pharmaceuticals from different therapeutic classes in extracts of surface, underground, drinking and waste waters (industrial and municipal) using solid phase extraction pretreatment. The lowest LOQ of 0.49 ng/l reported by Grujic et al.[52], for DCL water samples, were obtained using solid-phase extraction and extracts were analyzed by liquid chromatography–ion trap–tandem mass spectrometry with electrospray ionization in both positive and negative ionization mode. In general, in most of the publications reviewed here, DCL is often analyzed together with other pharmaceuticals within multi-compound analytical methods. LOQ in the low ng/l range is achievable.

In summary, the detection of DCL mostly relies on conventional techniques and these analytical techniques, though highly sensitive, have limitations of being time-consuming, expensive, requiring a lot of expertise to be operated and uneasiness to be deployed in the field [30,31,35,55].

1.3 Electroanalytical Methods for Detection of Diclofenac

Overcoming the limitations of the separative analytical techniques such as expensiveness, time consuming and the difficulty to deploy in the field, electrochemical methods have attracted attention in recent years for environmental, pharmaceutical and biological compounds analysis due to their fast response, sensitivity, accuracy, lower cost, high dynamic range and simplicity [30,32–40]. Among the electrochemical methods, amperometric [56–59] and potentiometric methods [35,55,60,61] have been reported for the determination of DCL. Generally, several parameters such as the electrode material, modifier nature, and modification method are effective on the performance of an electrochemical sensor.

1.3.1 Potentiometric Methods

Potentiometric sensors are being used for pharmaceutical tracing in the environment as an alternative technologies [62–65], as they have the advantages of being ecofriendly, simple design, provide the portability for *in situ* monitoring and use small amounts of sample as well as providing sensitive and consistent measurements at reasonable costs [66]. Specifically, ion selective membrane electrodes have been successfully used for both *in vitro* and *in vivo* assays of pharmaceutical products [67], as well as environmental pollutants [68–76].

An ion-selective electrode (ISE) is a transducer that converts the activity of a specific ion dissolved in a solution into an electrical potential [77]. Ion-selective membranes are permselective, that is, they behave as ion-exchangers where the ion of interest (also called analyte or primary ion) may freely partition into and out of the membrane material. The counter ion of the analyte does not extract into the membrane phase while any ion-exchanger site of the membrane is confined to its phase and does not partition into the sample either [78].

Potentiometric methods using ion selective electrodes (ISEs) for DCL detection in pharmaceutical preparation and biological fluids are mainly based on using cationic exchangers (as iron(II)-phthalocyanine, safranine T, crystal violet, rhodamin B, nickel(II) bathophenanthroline, Fe(III) tetraphenylporphyrin-chlorid, Fe(III) tetrakis(pentafluorophenyl)porphyrin-chloride, Manganese (III) porphyrin, neutral dye, 2,4,6-tri(2-pyridyl)-s-triazine iron(II), astrafloxin, Basic dye BIK) [79–88] , β-cyclodextrin[35] or graphite matrix [89]. To our knowledge, only one ISEs were constructed for determination of DCL in water sample by using imidazolium–diclofenac ion associate in a plasticized poly(vinyl chloride) (PVC) membrane on planar carbon electrodes, with an intermediate poly(3,4-ethylenedioxythiophene) layer [90].

A few potentiometric diclofenac-selective sensors based on a plasticized poly (vinyl chloride) membrane were developed over the past two decades. These membrane electrodes were used as a sensor for assaying diclofenac in pharmaceutical formulations. In this regard, Kormosh et al., developed electrodes containing ions of opposite electrical charge of DCL, an ionic associate (IA) of diclofenac, with neutral red [86] and basic dye Astrafloxin FF [88], as electrode-active substances in plasticized ISE .The response found was linear over the diclofenac concentration range 5×10^{-5} to 5×10^{-2} M with the slope of the electrode function being 30.0 ± 1.1 – 44.0 ± 1.2 mV/ dec^{-1} and 59.0 ± 1.2 mV/ dec^{-1} respectively. Studies of the electrochemical properties of the ISE with different contents of the ionic associate provided evidence that the best results were obtained with membranes containing 5–20% IA and 5–9% IA of diclofenac with neutral red and Astrafloxin FF respectively, as an electrode-active substance, even if all ISE responded to over the wide range diclofenac concentrations. The authors reported that the increase in the IA concentration led to membrane heterogeneity and degradation of their mechanical and electrochemical properties.

Some potentiometric ISEs based on plastic membrane containing an ionophore immobilized on transducer surface have also been reported [81,91–94]. Specifically, Kormosh et al. [81,91,92] developed different diclofenac sensitive electrodes by incorporation of ion pair complex formed between DCL and butyl rhodamine B and DCL with Safranine T dye into graphite matrix (Figure 1.2). The plan to use the ion pair complex as an electrode-active substance in the preparation of the ion-selective electrode was successful and exhibited a linear response over the concentration range of $5.0 \times 10^{-5} – 5.0 \times 10^{-2}$ mol L^{-1} at pH 6–12, and a detection limit of approximately 10^{-5} mol L^{-1} with a slope between 47– 61 mV dec^{-1}. Using a similar approach, Maleki et al.[94] prepared an ion pair complex between DCLand silver which showed a Nernstian response (58.9 ± 0.2 mV dec^{-1}) and a linear range from 5.2×10^{-5} to 1.1×10^{-2} mol L^{-1} at 25 ± 1 °C.

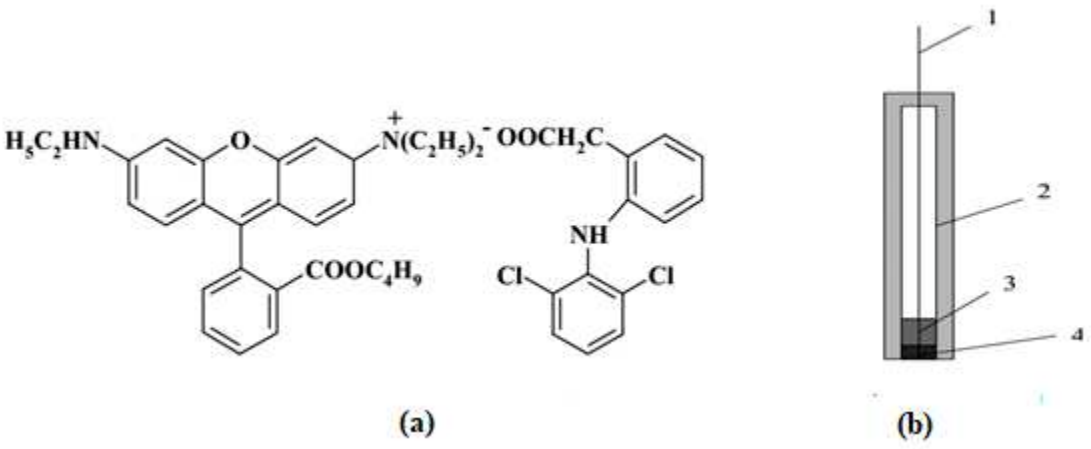

Figure 1.2:(a) Ion associate of diclofenac with butyl rhodamine B and (b) Diclofenac electrode: 1- Cu wire (conductor cable), 2- PVC tube, 3- Alloy of Vud, 4-Sensor pellet (graphite |IA| TCP)

Conductive polymers were also used for membrane preparation applied for ISE construction. Among them, Oliveira et al., [60] developed a potentiometric sensor by incorporating DCL anion into polypyrrole (PPy) film during polymer electrochemical synthesis on graphite electrode in order to form a membrane with selective potentiometric response for the dopant ion . The potentiometric ion-selective sensor based on a doped PPy film exhibited a linear dynamic response in the concentration range from 3.1×10^{-4} to 1.1×10^{-2} mol L^{-1} of DCL with a limit of detection of 190 µmol L^{-1}. The sequence of steps involved during the PPy formation and doping of the polymer chain by DCL is represented in Figure 1.3.

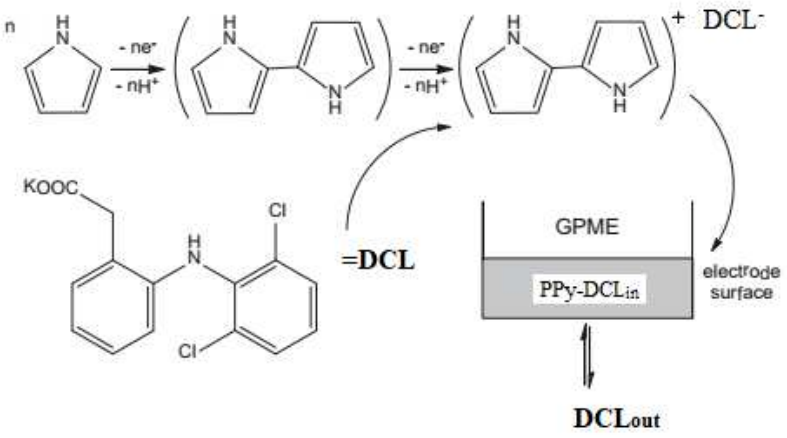

Figure 1.3: Schematic representation of involved steps during the preparation of polypyrrole membrane doped with Diclofenac anion. [60]

There are a few potentiometric studies concerning the use of cyclodextrins as ionophores in membrane electrodes selective for detection of DCL in wastewater samples and pharmaceutical dosage form [35,55]. Lenik [35] reports on the preparation of such diclofenac-selective membrane electrode incorporating heptakis (2,3,6-tri-O-benzoyl)-β-cyclodextrin, plasticized with 2-nitrophenyloctyl ether, with a limit of detection of 14 μmol L^{-1}. Recently, Elbalkiny et al. [55] developed a (CV-Fe (β-CD) sensor by conjugating functionalized nano-sized magnetized iron oxide (MNP-Fe_3O_4) particles with crystal violet (CV) cationic exchanger and β-Cyclodextrins (β-CD), with a Nernstian slope of -58.7 ± 1 mV dec^{-1} over the concentration range 1.0×10^{-7} to 1.0×10^{-2} mol L^{-1} of Diclofenac with a limit of detection of 1.1×10^{-7} mol L^{-1}. The incorporation of β-cyclodextrin together with magnetite ferric oxide in the inner solution composition enabled the construction of potentiometric sensors that demonstrated a good potentiometric selectivity for diclofenac with respect to a number of interfering ions and organic species. The membrane sensor was successfully applied for the determination of diclofenac in wastewater samples and dosage form without sample pretreatment steps prior to its analysis.

In general, the modification of electrodes is one of the most important developments to increase the DCL detection and the electron transfer rate at the electrode surface. The sensitivity and selectivity of the Ion selective electrodes reviewed here, for diclofenac monitoring in pharmaceutical wastewater and dosage form, have shown to depend not only on the nature of an electrode active substance used but also on the content of the electrode active substance in the composition and the properties of the solvent mediators employed. The analytical characteristics

of published potentiometric methods for Diclofenac analysis based on ISE are listed below in (Table 1.2). The sensitivity, working range, detection limit and selectivity of membrane sensors demonstrated significant dependence on the type of plasticizers. For most of the articles referenced in the table, the results of the DCL assay were validated and found in good agreement with reference methods like HPLC and the proposed electrodes exhibited long lifetime, good stability, sensitivity, precision, and selectivity.

Table 1.2: Comparative potentiometric characteristics of diclofenac–selective sensors.

Composition of membrane	pH range	Slope (mV/dec)	Response time(s)	ISE lifetime (weeks)	Linear concentration range (M)	Detection limit (M)	Ref.
Nickel(II) bathophenanthroline	8–12	55.1 ± 0.2	<35	8	5×10^{-5}–1×10^{-2}		[80]
α-Cyclodextrin–tetradecylammonium bromide–2-nitrophenyloctyl ether	8.2–12.7	56.6 ± 1.0	<20	5	5×10^{-6}–1×10^{-2}	-	[95]
2,4,6-tri(2-pyridyl)-s-triazine iron(II)	5.5-9.9	-56± 1	15	12	1×10^{-2}–1×10^{-6}	3.4×10^{-6}	[87]
Fe(II) phthalocyanine–tridodecylmethylammonium chloride–dibutyl sebacate	5.5-9	61.0 ± 1.0	<10	16	9×10^{-6}–1×10^{-2}	5.4×10^{-6}	[83]
Hexadecylpyridinium bromide–dibutyl phthalate	6.0–9.0	-59.0 ± 1.0	<10	>3	1×10^{-5}–6×10^{-2}	4.0×10^{-6}	[93]
Fe (III) tetraphenyl porphyrin chloride	9.9	−59.3 ± 0.4	10		1×10^{-5}–1×10^{-2}	1.5×10^{-5}	[82]
Pt|Hg2(DFC)2|Graphite	6.5-9.0	58.1 ± 0.8	10–30	20	5×10^{-5} – 1×10^{-2}	3.2×10^{-5}	[89]
Ag(I)–diclofenac–dioctyl phthalate	6.0–9.5	-58.9 ± 0.2	10	12	5×10^{-5}–1×10^{-2}	3.2×10^{-5}	[94]
Bovine serum albumin	6.9	60.0 ± 1.0	-	-	1×10^{-6} – 1×10^{-2}	-	[96]
Basic dye Safranine T	6-12	47±1.0	2-4	13	5×10^{-5} - 5×10^{-2}	3.2×10^{-5}	[97]
Basic dye crystal violet	6-11	59 ± 1	-	-	5.0×10^{-5}-5.0×10^{-2}	2.5×10^{-5}	[79]
Rhodamin B	8	60	3		1×10^{-5} - 5×10^{-2}	1×10^{-5}	[84]
Basic dye BIK	7–11	60.0 ± 1.1	2–3	16–20	1×10^{-4} – 5×10^{-2}	5.0×10^{-5}	[98]
Butyl rhodamine| Graphite	6-11	61.0 ± 2.0	3-11	24	1×10^{-4}-5×10^{-2}	3.9×10^{-5}	[99]
Neutral Red	5-12	44.0± 1.2	3-10	16	5×10^{-5} -5×10^{-2}	5.0×10^{-5}	[86]

Astrafloxacin FF	9–12	59.0 ± 1.2	2–3	>17	5×10^{-5}–5×10^{-2}	3.2×10^{-5}	[61]
Manganese(III)-tetrakis(3-hydroxyphenyl)porphyrin chloride	5.5-11.5	-59.7 ± 0.6	-	-	$3 \times 10^{-6} – 1 \times 10^{-2}$	1.5×10^{-6}	[85]
Modified graphite pencil electrode (MGPE) with doped polypyrrole films	3	48.2	-	-	3.1×10^{-4} - 1.1×10^{-2}	1.9×10^{-4}	[60]

1.3.2 Amperometric Methods

The electrochemical methods here are based on the electrooxidation of DCL (Figure 1.4), where the anodic current responses are correlated with the amount of the drug in the sample of interest. Voltammetry is a potentiodynamic technique, based on measuring the current arising from oxidation or reduction reactions at the working electrode surface, when a controlled potential variation is imposed. Amperometry is based on the application of a constant potential to a working electrode, and the subsequent measurement of the current generated by the oxidation/reduction of an electroactive analyte [100]. From the broad spectrum of available electroanalytical methods for detection of DCL, cyclic voltammetry [101], differential pulse voltammetry [102] and square wave voltammetry [103] are the principal techniques most frequently used. Among the voltammetric methods for determining the diclofenac, differential pulse voltammetry mode is favored because the peaks are sharper and better defined at lower concentration with a lower background current and improved resolution[101].

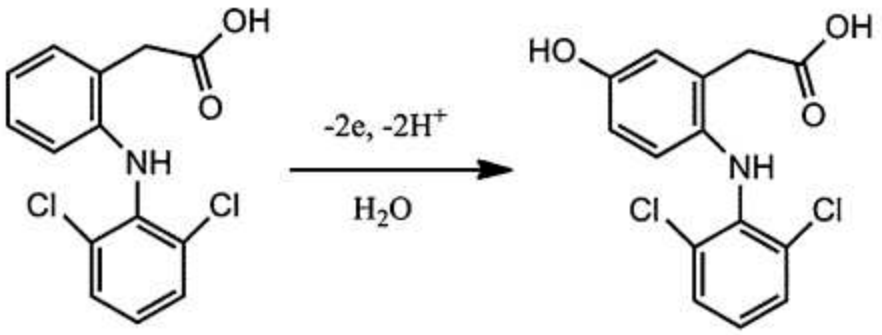

Figure 1.4: Proposed oxidation mechanism of DCL. [104]

There are different methods for development of electrochemical DCL sensors starting from unmodified electrodes to different composites incorporating nanomaterials, DNA, ionic liquids or various inorganic mediators. Voltammetry and amperometry at bare/unmodified electrodes have its own challenges because the electrooxidation of diclofenac sodium proceeds very slowly but also it represents an interesting alternative, in particular when high sensitivity is not required. This approach has been realized by use of a simpler system, resulting in reduced costs for both production and use, and long-term stability.

For instance, Yilmaz and Ciltas, [104] developed an Linear Sweep Voltammetry (LSV) for determination of diclofenac at Pt disc electrode in pharmaceutical formulations. The LSV method was aimed at developing an easy and rapid assay method for diclofenac without any time--consuming sample preparation steps for routine analysis. Can you add a figure to illustrate the LSV obtained with DCL. They reported a linear range to be over the concentration range of 16-118 μmol/L with limits of quantification (LOQ) of 16.2 μmol/L.

But the quest for over-potential diminution and fouling minimization has required electrode modification with a view to increase sensitivity and obtain more prominent peak separation. These properties are required mainly in complex media such as biological samples particularly prone to interferences, where DCL coexists with other electroactive species. Voltammetry/amperometry at modified electrodes will be detailed below.

1.3.2.1 Modified Electrodes with Carbon Nanotubes

Carbon nanotubes (CNTs) exhibits superconducting, metallic and semiconducting transport of electrons and it contains a hollow core which is suitable for the storage of guest molecules [105]. The subtle electronic properties of CNTs suggest that they are able to promote electron transfer when used as the electrode material in electrochemical reactions. These properties provided a new manner of electrode surface modification for designing new electrochemical sensors and novel electrocatalytic materials [106].

Compared with other studies that have been reported on the voltammetric determination of DCL using modified ionic liquid carbon nanotube paste electrodes [107–109], the work of Goodarzian et al., [110] on square wave voltammetric determination of diclofenac in liquid phase, using a novel ionic liquid multiwall carbon nanotubes paste electrode, is shown to have the better dynamic range, limit of detection and sensitivity for DCL analysis. The oxidation peak potential for the direct electrochemistry of DCL at a surface of the ionic liquid carbon nanotubes paste electrode (IL/CNTPE) appeared at 750 mV that was about 70 mV lower than the oxidation peak potential at the surface of the traditional carbon paste electrode under similar condition.The proposed method is reported to have a linearity to DCL concentrations over the concentration range of 0.3 – 750 μmol L^{-1}, and detection limit of 0.09 μmol L^{-1}.

Voltammetric determination of DCL using multi-walled carbon nanotubes (MWNTs)–dihexadecyl hydrogen phosphate (DHP) film-coated glassy carbon electrode (GCE) was developed by Yang et al., [57]. The oxidation peak current of DCL at the nano-structured film-modified electrode increased significantly compared with that at a bare glassy carbon electrode. This was mainly attributed to the large surface area and strong adsorptive properties of the MWNTs providing more reaction sites. The sensor showed a limit of detection of 8.0×10^{-8} mol/L using LSV.

Multiwalled carbon nanotube and ionic liquid modified carbon ceramic electrode (MWCNT–IL|CCE) was employed by Sarhangzadeh et al., [102] for the simultaneous determination of diclofenac and indomethacin (IND). The procedure of CCE modification with MWCNT–IL composite exhibited high electrocatalytic activity to oxidation of DCL and IND and led to a linear calibration plot over a range of concentrations of 0.05–50 μmol L^{-1} for DCL (and 1–50 μmol L^{-1} for IND))with a detection limits of 18 and 260 nM for DCL and IND, respectively.

An electrochemical sensor developed by modification of carbon paste electrodes using NiO-SWCNTs as conductive mediator and 2, 4-dimethyl-N/-[1-(2, 3-dihydroxy phenyl) methylidene] aniline (DDPM) as electro-catalyst (NiO-SWCNTs/DDPM/CPE) was reported by Akbarian et al., [111] for determination of DCL in the existence of mefenamic acid and morphine. This article proposed an analytical procedure for simultaneous determination of diclofenac, morphine and mefenamic acid. The NiOSWCNTs/DDPM/CPE showed good capability for determination of diclofenac, morphine and mefenamic acid with oxidation potentials at + 0.25 V, 0.45 V and 0.70 V respectively (see Figure 1.5). The calibration curves obtained at SWV were linear calibration curves obtained at SWV were linearin the ranges of 0.04-1200, 0.9-400, and 1.0-600 µM, with detection limits of 0.008, 0.4 and 0.5 µM for diclofenac, morphine and mefenamic acid, respectively.

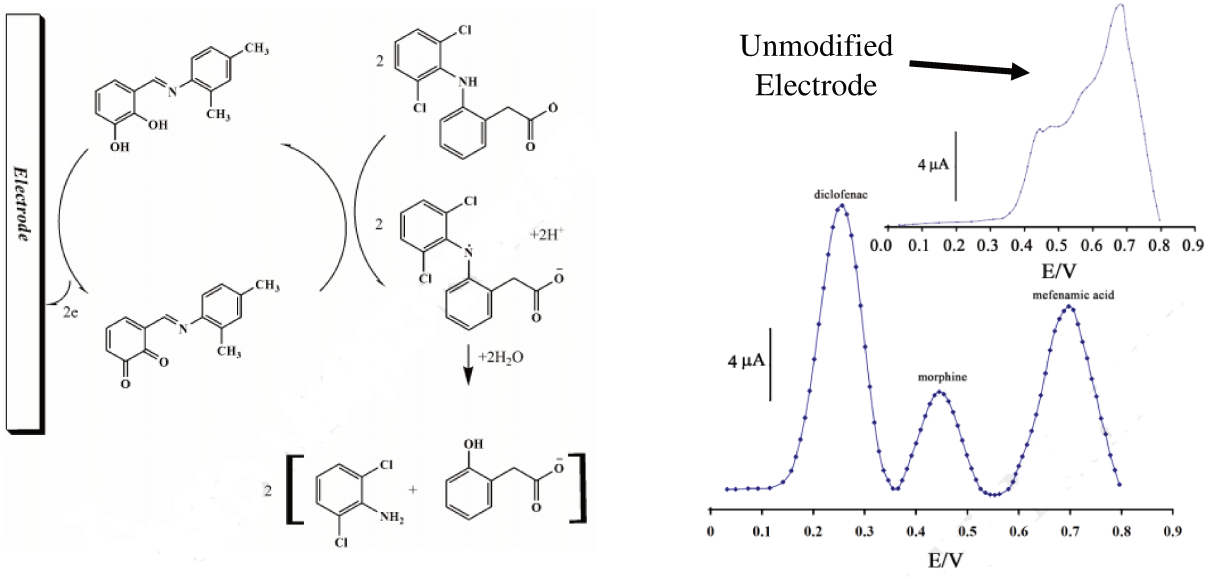

Figure 1.5: Diclofenac oxidation at NiO-SWCNTs/DDPM/CPE surface for simultaneous analysis of diclofenac, morphine and mefenamic acid. [112]

Combining edge plane pyrolytic graphite electrodes and square wave voltammetry, Goyal et al., [112] developed a sensor for detection of DCL that has a linear range of 10–1000 nM with a low detection limit of 6.2 nM .The edge plane sites in EPPGE contributed in making it an efficient sensor by enhancing the kinetics of the electrochemical process. Based on this work, the effect of modifying an edge-plane pyrolytic graphite electrode with single-wall carbon nanotubes was

studied [113] for the detection of DCL and the oxidation of diclofenac occurred in two well-defined peaks having peak potentials of 439 and 854 mV at pH 7.2. Under the optimum conditions, the calibration curve studied using square wave voltammetry (SWV) was linear in the range from 1 to 500 nM for peak I and from 25 to 1500 nM for peak II. The detection limit is 0.82 and 22.5 nM for peaks I and II, respectively, and the detection limit at peak I is almost 10 times lower than observed at bare pyrolytic graphite electrode.

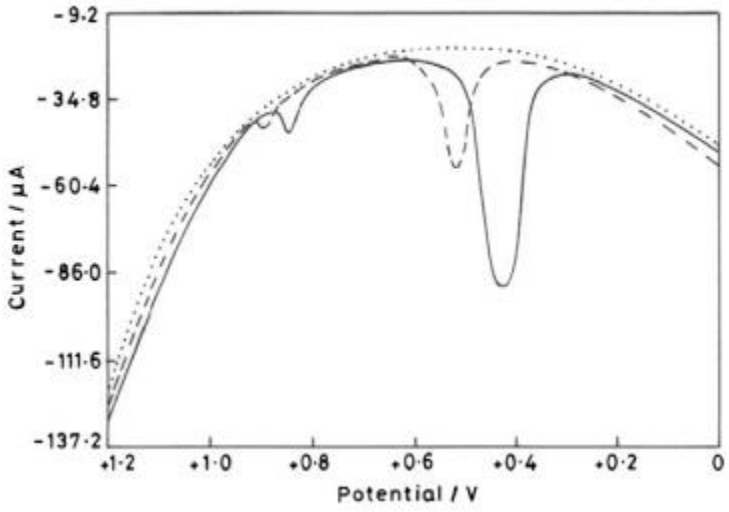

Figure 1.6: Comparison of square-wave voltammograms of 250 nM diclofenac (pH 7.2) at (a) SWCNT modified EPPGE (—), (b) bare EPPGE (- - - - -) and (c) background PBS at pH 7.2 at SWCNT modified EPPGE (. . ....). [113]

1.3.2.2 Modified Electrodes with Nanoparticles and Nanocomposites

It has been demonstrated that the electrochemical performance of an electrode is influenced by its electron conductivity and accessible surface areas. Hence, in order to enhance the electrochemical performance of the sensors; the effective strategy is the design of composites by combining highly electro-catalytic active materials with excellent conductivity substances to modify the electrode surface. In this regard, several techniques have been developed to improve sensitivity using nanoparticles and nanocomposites for detection of DCL, and some selected articles are reviewed below.

In an attempt to enhance the electrochemical performance of DCL sensor, Eteya *et al*., [114] combine highly electro-catalytic active materials with excellent conductive materials to modify the electrode surface. Among the various bimetallic materials, they chose gold–platinum (Au–Pt)

bimetallic nanoparticle as it is a promising system that shows excellent electro-catalytic activity towards many electrochemical reactions [115–117], and in order to improve the catalytic activity of the nanoparticles as a result of their high surface energy and large surface to–volume ratio inflicted aggregation, they used multi walled carbon nanotubes (MWCNTs) due to their superior properties such as good biocompatibility, high surface area, strong mechanical strength and high electrical conductivity [118–120]. Due to the synergetic effects of gold–platinum (Au–Pt) bimetallic nanoparticles and the multi walled carbon nanotubes, the sensor exhibited a good electro-catalytic activity towards the DCL and the linear range was found to be between 0.5-1000 µmol/L with a detection limit of 0.3 µmol/L.

Shalauddin et al., [103] developed a sensor for determination of DCL by combining the significant catalytic property of multi-walled carbon nanotubes (MWCNTs) and the excellent adsorption capacity and film forming ability of Chitosan. Under the optimum conditions, the electrochemical response of DCL for the hybrid composite MWCNTs/CTs-Cu/GCE was reported to be linear in the range of 0.3 and 200 µmol L^{-1} with the detection limit of 0.021 µmol L^{-1} at pH 4.0 using square wave voltammetry (SWV) techniques.

Arvand et al., [107] modified glassy carbon electrode with with nanocomposite consisting of $Cu(OH)_2$ nanoparticles, hydrophobic ionic liquid 1-ethyl-3-methylimidazolium hexafluorophosphate ($EMIMPF_6$) and multiwalled carbon nanotubes. Using differential pulse voltammetry (DPV), the prepared electrodeis reported to have a linear range from 0.18 to 119 µM, with a detection limit of 0.04 µmolµmol L^{-1}.

Manea *et al*., [121] developed a Cu-Doped Zeolite-modified expanded graphite-epoxy composite (CuZEGE) electrode for a new alternative quantitative determination of DCL in aqueous solutions. The linear dependence of the current obtained by DPV versus diclofenac concentration indicated good sensitivity and selectivity with a limit of detection for DCL to be 5×10^{-8} molmol L^{-1}.

A simple carboxyl-functionalized graphene oxide-modified electrode was reported by Karuppiah et al., [122] with a limit withaof 0.09 µmol L^{-1} using LSV. On the other hand, El-Wekil et al.,[123] developed carbon paste electrode (CPE) modified with reduced graphene oxide (rGO) and $Co(OH)_2$ nano-flakes (CHNF) for the simultaneous electrochemical analysis of esomeprazole (EZM) and DCL in binary mixture. The modified electrode exhibited significantly improved electro-analytical response compared to the unmodified bare CPE, a linear simultaneous

electrochemical analysis of esomeprazole (EZM) and DCL in binary mixture. The modified electrode exhibited significantly improved electro-analytical response compared to the unmodified bare CPE, a linearresponse in the range of 2.5- 155×10^{-8} M and 1.5-105×10^{-8} M with detection limits of 8×10^{-9} M and 5×10^{-9} M for DCL and EZM, respectively.

A detection technique called Fast Fourier Transform Square-Wave Voltammetry (FFT SWV), based on measurements of electrode admittance as a function of potential, was reported by Daneshgar et al., [59] using carbon paste electrode modified by dysprosium nanowires (DyNW), for detection of DCL. The approach is designed to separate the voltammetric signal and background signal in the frequency domain by using a discrete Fast Fourier Transformation (FFT) method. The calibration curves were reported to be linear over the concentration range of 0.01-1.0 μmolμmol L^{-1}, with a limit of detection being 2.0 × 10 nmol L^{-1}.

1.3.2.3 Voltammetric and Amperometric Methods Coupled to Separative Methods

There are just a few techniques reported that utilizes the coupling of a separative methods to amperometric methods.Among these,following their prior work [124] that demonstrated flow injection analysis with multiple-pulse amperometric (FIA-MPA) detection can be successfully used for the determination of DCL in pharmaceutical formulations using an unmodified working electrode , Gimenes et al., [125] came up with two electrochemical methods for fast and simultaneous determination of codeine (CO) and DCL. The first one is based on batch injection analysis with amperometric detection (BIA-MPA) and the second one is based on capillary electrophoresis with capacitively coupled contactless conductivity detection (CE-C^4D). The inspiration for the utilization of capillary electrophoresis with capacitively coupled contactless conductivity detection (CE-C^4D) is related to the fact that it was widely used for the separation and simultaneous determination of ionic compounds [126,127] and has a short analysis time, low cost, high separation efficiency, and low consumption of reagents and samples [128].

The BIA-MPA method is highly-precise (RSD of 1.1% and 0.9% for DCL and CO, respectively; n=10), fast (300 injections h^{-1}) and relatively has a low detection limits (1.1 and 1.0 μmol L^{-1} for DCL and CO, respectively). The proposed CE-C^4D method allows the determination of CO and DCL in less than 1 min with high precision (RSD of 0.3% and 0.7% for DCL and CO, respectively; n=10) and low detection limits (11 and 21 μmol L^{-1} for DCL and CO, respectively).

Because amperometric detection provides excellent sensitivity for the small dimensions associated with capillary zone electrophoresis (CZE) while offering a high degree of selectivity toward electroactive species and low cost [129], Jin and Zhang, [130] employed capillary zone electrophoresis for the determination of DCL using an end-column amperometric detection with a carbon fiber microelectrode. The limit of detection is reported to be 2.5 X 10^{-6} mol L^{-1} (*S/N*=2) with the relative standard deviation being 0.8% for the migration time and 4.7% for the electrophoretic peak current.

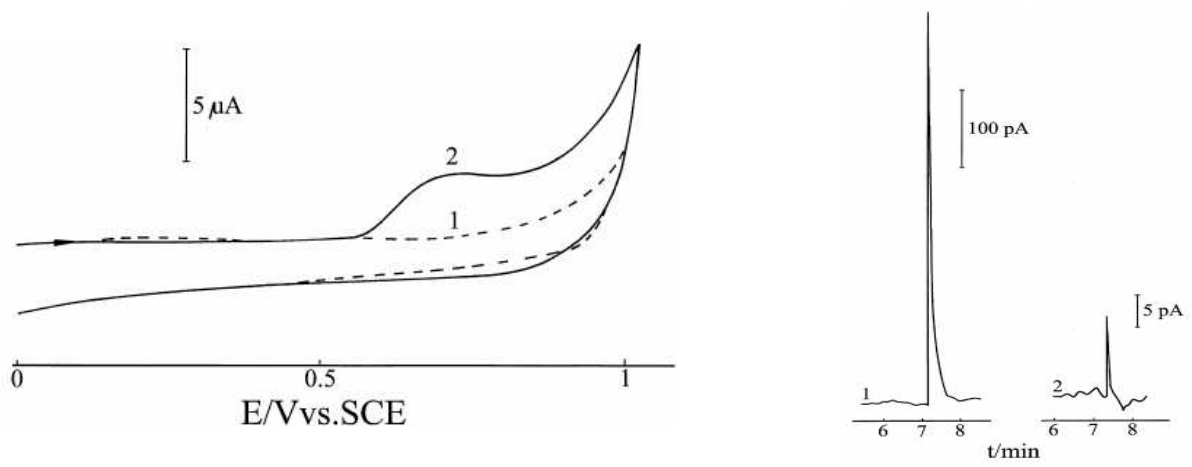

(A) (B)

Figure 1.7:(A) Typical cyclic voltammogram of diclofenac sodium at the carbon fiber array electrode: 1, 0.120 mol/L Na2 HPO4 –0.080 mol/L NaH2PO4 ; 2, (1) + 1.0 10-4mol/l diclofenac sodium. V=20 mV/s.(B) Typical electropherograms of diclofenac sodium. Concentration of diclofenac sodium: 1, 5.0010^{-4} mol/l; 2, 9.90 10^{-6} mol/l. E_d=0.83 V

1.3.3 Electrochemiluminescence Method

Electrochemiluminescence is a means of converting electrical energy into light (radiative energy). It involves the production of reactive intermediates from stable precursors at the surface of an electrode. These intermediates then react under a variety of conditions to form excited states that emit light [131].

There are a few immunological assays reported for the determination of diclofenac in different samples over the last decades. These immunochemical techniques, performed in different formats such as ELISA on microtiter plates, biosensors (immunosensors), and lateral flow device (LFD), take advantage of the highly selective binding by antibodies [132]. In the past, for diclofenac, a

highly sensitive and specific ELISA based on a polyclonal diclofenac antiserum prepared in rabbit was developed by Deng et al., [133] which allows the determination of DCL in the low ppt range. It was successfully applied to different samples [133–139]. Because of the limited availability of these polyclonal antibodies, Huebner et al., [145] developed an ELISA for the analytical determination of the pharmaceutical diclofenac in water samples based on monoclonal antibodies. Compared with the earlier polyclonal antibody-based assay, similar LOD value in the low ng/L range was obtained by the new ELISA. As a new assay format, Hlaváček et al.,[140] developed a sensitive competitive immunoassay for the detection of DCL in water using an upconversion-linked immunosorbent assay (ULISA), by exploiting the unique photophysical characteristics of Photon-upconverting nanoparticles (UCNPs) that emit light of shorter wavelength under near-infrared excitation and thus avoids optical background interferences. The optimized ULISA reached a detection limit of 0.05 ng DCL per mL. This performance came close to a conventional enzyme linked immunosorbent assay (ELISA) without the need for an enzyme-mediated signal amplification step.

Recently, electrochemiluminescence (ECL), combining electrochemistry and chemiluminescence analysis, has attracted extensive attentions due to its high sensitivity detection, simplified optical setup and low background noise [141–146]. By integrating the specific recognition of immunoassay between antigen and antibody and the brilliant properties of ECL, the ECL immunoassay (ECLIA) has become a powerful analytical tool for highly sensitive and specific detection of clinical samples. The ECL intensity mainly depends on the rate of electrochemical reaction, the efficiency of the excited state product and the luminescent efficiency of the excited state material. Hence, the chosen of luminophores and the conductivity of other nanomaterials are crucial for the entire work.

In line with this, an ultrasensitive competitive electrochemiluminescent (ECL) immunosensor for detecting DCL was fabricated using multiwalled carbon nanotubes and gold nanoparticles (MWCNTs-AuNPs) as a matrix for immobilizing antigen by Hu et al., [147] , with graphene oxide coupled graphite-like carbon nitride (GO-g-C_3N_4) as signal probe. The matrix used is reported to have not only contributed for immobilizing a large amount of coating antigen but also facilitated the electronic transmission rate to enhance the ECL intensity. The wide linearity for the detection of DCL in the range of 0.005-1000 ng mL^{-1} with a detection limit of 1.7 pg mL^{-1} is attributed to

the dual signal amplification strategy by using synergetic effect of GO-g-C_3N_4 and MWCNTs-AuNPs composite for the sensitive detection of DCL (figure 1.8).

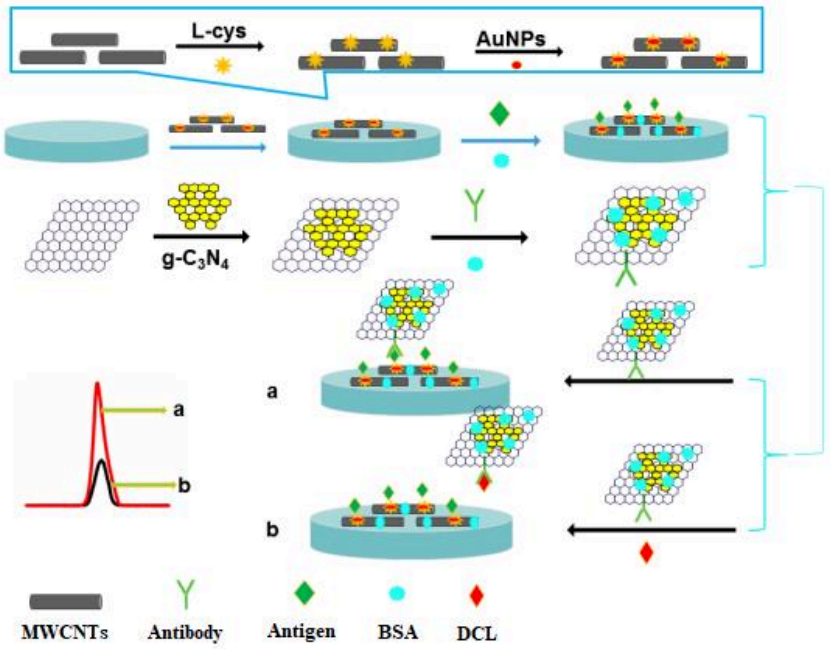

Figure 1.8: Illustrative ECL detection mechanism for DCL based on GCE/ MWCNTs-AuNPs. [147]

Very recently Wang et al.,[36] developed a novel electrochemiluminescent (ECL) immunosensor for detecting DCL using poly(etherimide)-poly(3,4-ethylene dioxythiophene): poly(styrene sulfonate) functionalized graphene oxide and CdSe@CdS quantum dots (QDs-PEI-GO/PEDOT) as bioreceptor for conjugating DCL antibody to magnify signal. The novelty comes from the fact that it is the first time that GO/PEDOT has been applied to ECL sensor field and they proved that compared with GO, the GO/PEDOT exhibited a higher conductivity and more stable chemical property. The reason for the improved sensitivity, selectivity of the sensor and very low detection limit of 0.33 pg mL^{-1} was attributed to the fact that the electrode was modified with gold nanorods (AuNRs), which increased the load capacity of DCL coating antigen through Au-N bond, and the competitive immunoassay method chosen for structuring the immunosensor. The immunosensor revealed a wider detection range of 0.001-800 ng mL^{-1}.

1.3.4 Photoelectrochemical Methods

Photoelectrochemical (PEC) sensors are based on photo-induced electron transfer processes at electrode/interfaces, have recently attracted considerable research interests due to their advantages of high sensitivity, simple instrument, easy miniaturization and low cost [148,149]. In the construction of PEC sensors, the photoactive materials play a crucial role in the performance of PEC sensors. In relation to this, Do Prado et al., [150] developed a photoelectrochemical sensor for the detection of DCL in urine. This sensor was fabricated using a film of bismuth vanadate modified with reduced graphene oxide, forming the nanocomposite ($BiVO_4$/rGO). The modification of the semiconductor with rGO aims to increase the efficiency of the generated photocurrent during DCL electro-oxidation. The broad work potential range, high surface area, faster charge transfer and high electrocatalytic activity of the rGO, combined with $BiVO_4$, have made the nanocomposite a suitable material for fluorine-doped thin oxide (FTO) glass electrode modification. The PEC sensor is highly linear over a concentration range from 9.6×10^{-9} to 9.2×10^{-6} mol L^{-1} with a detection limit of 4.2×10^{-9} mol L^{-1}.

Figure 1.9 presents a photocurrent generation in the BiVO4/rGO for DCL and under visible light irradiation. In step A, there occurs the electrochemical process for the oxidation of the ionic form of the DCL, releasing $1H^+$ and $1e^-$ to the production of a radical anion. This radical reacts with the water in the chemical process of step B, when cleavage of the molecule occurs to produce 2,6-dichloroaniline and the radical anion 2-(2-hydroxy prop-2-enyl) phenol. In step C, the electron released in the electrochemical process is collected by the holes generated in the valence band (VB) of the $BiVO_4$ under irradiation. The occurrence of this phenomenon avoids recombination between the holes of the VB and the electrons promoted to the conduction band (CB) when the $BiVO_4$ is illuminated. Consequently, the electrons of the CB are transferred to the transducer and the increase of the photocurrent is proportional to the amount of the DCL electro-oxidized in the sample.

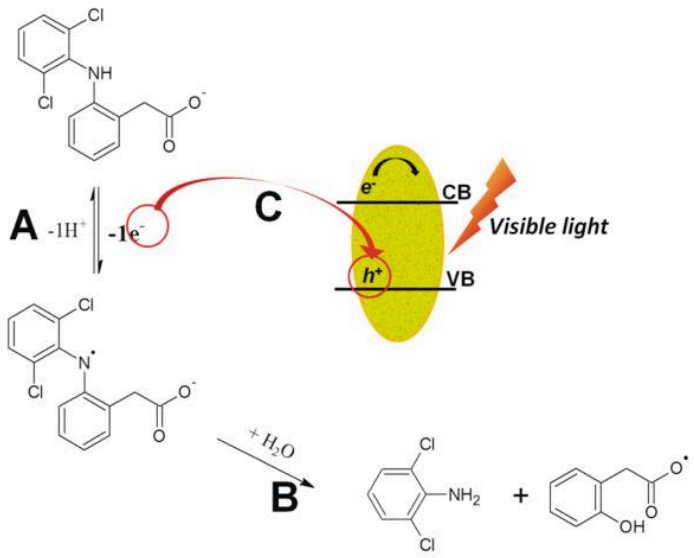

Figure 1.9: Scheme of the photocurrent generation in the BiVO4/rGO for DCL and under visible light irradiation.[150]

As it has been mentioned above, the sensitivity of PEC sensors could be generally improved by promoting the performance of photo catalysts. However, PEC sensing is based on photocatalytic reactions which are usually not specific to analytes. To overcome this problem, much effort has been paid to improve the selectivity of PEC sensors by introduction of various recognition elements such as molecular imprinted polymers, enzymes, antibodies and aptamers [151–154]. Among the various recognition elements, aptamers, well-known antibody mimetics possessing high recognition ability to specific targets, have been intensively utilized to construct highly selective PEC aptasensors for a wide range of analytes including inorganic ions, proteins, cells, antibiotics and organic compounds [155–160]. In connection with this, PEC aptasensors reported by Okoth et al., [161] and Shi et al. [162] are discussed in section 1.4 of this manuscript.

In summary, the photoelectrochemical sensors based on on/off photocurrent responses present advantages that can be inferred from the lower LOD values obtained in a broad range of DCL concentrations. The stability of the baseline and the high intensity of the photocurrents based on the efficiency of the electro-oxidation of small amounts of the DCL have caused the photoelectrochemical sensors to become more sensitive than the others techniques.

Table 1.3: Comparative analytical parameters for detection of DCL using several methods

No.	Detection method	Modifier	Linear range (M)	LOD	Refs.
1	**Potentiometry**	Membrane electrodes incorporating β-cyclodextrins	5.0×10^{-5} - 1.0×10^{-2}	14 μM	[35]
2	**Potentiometry**	PVC Matrix Membrane	1.0×10^{-4} - 5.0×10^{-2}	50 μM	[92]
3	**Potentiometry**	Membrane containing β- cyclodextrin coupled with magnetite ferric oxide (CV-Fe(beta-CD))	1.0×10^{-2} - 1.0×10^{-5}	11μM	[55]
4	**Amperometry**		10×10^{-6}–50×10^{-6}	1.1 μM	[125]
5	**DPV**	Multiwalled carbon nanotube and ionic liquid modified carbon ceramic electrode (MWCNT–IL|CCE)	0.05×10^{-6} - 50×10^{-6}	18nM	[102]
6	**SWV**	composite (MWCNTs/CTS-Cu/GCE)	0.3×10^{-6} - 200×10^{-6}	0.021 μM	[103]
7	**LSV**	A multi-walled carbon nanotubes (MWNTs)–dihexadecyl hydrogen phosphate (DHP) film-coated glassy carbon electrode (MWNTs–DHP/GCE)	0.17×10^{-6}- 2.5×10^{-6}	80nM	[57]
8	**SWV**	NiOSWCNTs/DDPM/CPE	0.04×10^{-6}-1200×10^{-6}	0.008μM	[111]
9	**SWV**	Edge plane pyroltic graphite	0.01×10^{-6}-1×10^{-6}	0.006μM	[112]
10	**DPV**	A diclofenac (DCL) imprinted polymer	5-80 mg L^{-1}	1.1 mg L^{-1}	[30]
11	**SWV**	Carbon paste electrode (CPE) modified with reduced graphene oxide (rGO) and Co(OH)2 nano-flakes (CHNF).	2.5×10^{-8} -155×10^{-8}	8 nM	[123]

12	**DPV**	Functionalized multi-walled carbon nanotubes (f-MWCNTs) and gold–platinum bimetallic nanoparticles (Au–PtNPs) (Au–PtNPs/fMWCNTs/Au)	0.5×10^{-6} - $1000\ 10^{-6}$	0.3 μM	[114]
13	**DPV**	Cu-doped zeolite-modified expanded graphite-epoxy composite (CuZEGE) electrode	2×10^{-5} -3×10^{-7}	50 nM	[121]
14	**DPV**	MWCNTs/Cu(OH)2 nanoparticles/IL nanocomposite modified electrode	0.18×10^{-6} - 119×10^{-6}	0.04 μM	[107]
15	**DPV**	IL/CNTPE	0.5×10^{-6} -300×10^{-6}	0.02μM	[108]
16	**SWV**	Multiwall carbon nanotubes (MWCNTs) (ionic liquid carbon nanotubes paste electrode (IL/CNTPE))	0.3×10^{-6} –750×10^{-6}	0.09 μM	[110]
17	**LSV**	GO-COOH/GCE	1.2×10^{-6} –400×10^{-6}	0.09 μM	[122]
18	**SWV**	Edge-plane pyrolytic graphite electrode (EPPGE) coated with single-wall carbon nanotubes	0.02×10^{-6} -1.5×10^{-6}	0.02μM	[113]
19	**DPV**	Tyrosine-modified carbon paste electrodes (TCPEs)	10×10^{-6} -140×10^{-6}	3.28 μM	[107]
20	**EIS**	DCL Aptamer immobilized on the surface of the glassy carbon electrode (GCE)(GCE/AHA/Aptamer)	0 - 5×10^{-6} ;10×10^{-6} - 1×10^{-9}	0.27μM	[40]
21	**EIS**	Platinum nanoparticles(PtNPs) on carbon nanotubes (CNTs) functionalized with polyethyleneimine (PEI) (PtNPs/PEI/CNTs/Aptamer)	10×10^{-9} - 200×10^{-9}	2.7 nM	[163]
22	**ECL**	GO-g-C3N4 and MWCNTs-AuNPs composite	0.005-1000 ng mL^{-1}	1.7 pg mL^{-1}	[147]
23	**ECL**	QDs-PEI-GO/PEDOT	0.001-800 ng mL^{-1}	3.3×10^{-4}ng mL^{-1}	[36]
24	**ECL**	Pd nanoparticles (PdNPs) and Core@Shell quantum dots decorated poly(etherimide) (PEI)-graphene oxide (GO) ((PdNPs/PEI-GO-QDs))	0.001 - 1000 ngmL^{-1}	0.3 pg mL^{-1}	[164]

25	**ECL**	Electrografting of two functional diazonium salts	0.1×10^{-12} to 0.1×10^{-9}	25pg L^{-1}	[165]
32	**PEC**	DCL Aptamer/Gold nanoparticles (Au NPs) and graphene-doped CdS (GR-CdS)(Aptamer/Au/GR-CdS)	1×10^{-9} - 150×10^{-9}	0.78 nM	[161]
34	**Amperometry**	$Ni(OH)_2$-nickel electrode	196×10^{-6}-2650×10^{-6}	31.7µM	[58]
38	**NPV**	Carbon nanotube paste	2×10^{-6}–100×10^{-6}	0.8µM	[166]

Photoelectrochemical **(PEC);** Differential Pulse Voltammetric (**DPV**) ;electrochemiluminescent (**ECL**) immunosensor ;Linear Sweep Voltammetry **(LSV)** ;Electrochemical Impedance Spectroscopy **(EIS)**

1.4 Electrochemical Aptasensors for the detection of Diclofenac

According to the International Union of Pure and Applied Chemistry (IUPAC), a biosensor is a self-contained integrated device capable of providing quantitative or semi-quantitative analytical information using a biological recognition element, which is retained in direct spatial contact with a suitable transducer responsible for detecting the biological reaction and converting it into a measurable signal [167].

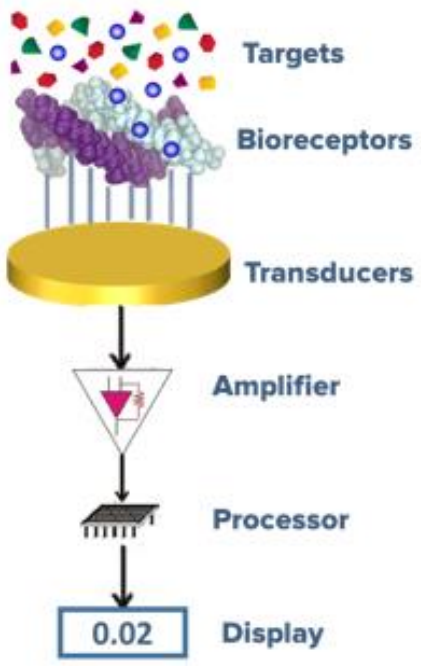

Figure 1.10: Schematic representation of a biosensor

The biological sensing material or bio-receptor may be a protein such as an enzyme or antibody, aptamer, a whole microbial cell, or even a plant or animal tissue. The signal transducer determines the extent of the biorecognition event and converts it into a measurable electronic signal, which can be recorded by the end user[168]. An aptasensor is hence, a particular class of biosensor where the biological recognition element is a DNA or RNA aptamer. Electrochemical biosensors have high sensitivity, selectivity, ability to operate in turbid solutions and rapid analysis, and are amenable to miniaturization[169].

1.4.1 Aptamers

Aptamers are short single-stranded oligomers (ssDNA or RNA), which are able to bind their target molecules with high specificity and selectivity. Binding occurs because of their specific and complex three-dimensional shape characterized by stems, loops, bulges, hairpins, pseudoknots, triplexes, or quadruplexes. The aptamer-target binding results from structure compatibility, stacking of aromatic rings, electrostatic and van der Waals interactions, and hydrogen bondings, or from a combination of these effects [170].

Aptamers have drawn considerable attention as significant recognition elements for the construction of various kinds of biosensors [171–174]. They have unique properties such as high specificity, low expense, small size, easy chemical modification, and more importantly remarkable flexibility, along with the fact that their design is not time consuming at all [175–181]. In recent years, a variety of techniques such as surface plasmon resonance [179,182,183], optical techniques [184–186]), quartz crystal microbalance[187] and electrochemical techniques [171,188–191] have been applied for aptamer-based biosensors.

Aptamers are generated by an *in vitro* selection process called SELEX (systematic evolution of ligands by exponential enrichment) which was first reported in 1990 [192,193]. The SELEX method has permitted the identification of unique RNA/DNA molecules, from very large populations of random sequence oligomers (DNA or RNA libraries), which bind to the target molecule with very high affinity and specificity.

Aptamers show a very high affinity for their targets, with dissociation constants typically from the micromolar to low picomolar range, comparable to those of some monoclonal antibodies, sometimes even better. The high affinity of aptamers for their targets is given by their capability of folding upon binding their target molecule: they can incorporate small molecules into their nucleic acid structure or integrate into the structure of larger molecules such as proteins [170]. In comparison to antibodies, aptamer receptors have a number of advantages that make them very promising in analytical and diagnostic applications. The main advantage is the overcoming of the use of animals for their production. Aptamers are isolated by *in vitro* methodologies that are independent of animals, and an *in vitro* combinatorial library can be generated for any target including toxins or small molecules. Moreover, the aptamer selection process can be manipulated to obtain aptamers which bind a specific region of the target under different conditions [179]. In

addition, aptamer can be easily functionalized by their ends to facilitate immobilization on supports.

Others advantages of aptamers in comparison to other biological recognition elements is the possibility to develop them for toxic substances as the frequently used biological recognition elements enzymes and antibodies cannot be developed for toxic targets. Pharmaceuticals are shown to have poisonous effects at least when used in high doses. Therefore, the development of antibodies for pharmaceuticals is a difficult thing to deal with.

It is well known that antibodies and aptamers can bind the relative target with high specificity and affinity. However, aptamers offer numerous advantages over antibodies that make them very promising in several applications, as summarized in Table 1.4.

Table 1.4: Comparison between aptamers and antibodies.

Aptamer	**Antibody**
In vitro production	*In vivo* production
Automated synthesis and screening	Production process complicated and expensive
Identification of small molecules, toxins and drugs	Limited to molecules that produce an immuno-response. Small molecules require conjugation to a hapten
Can function at different T and pH	Only works under physiological conditions
Production highly reproducible	Variations in lot to lot
Easily labeled in precise locations	Labeling can cause loss of afinity
Simple transportation and storage	Sensitive to temperature and humidity changes

Another advantage of aptamers is their higher temperature and pH stability. Aptamers are very stable and can recover their native, active conformation after thermal denaturation. They are stable to long-term storage and can be transported at room temperature. Whilst antibodies are temperature and pH sensitive proteins that can suffer irreversible denaturation, and they also have a limited shelf life [194].

1.4.2 Aptamer Immobilization Methods

The preparation of aptasensor necessitates the immobilization of aptamers onto the electrode surface. The control of this step is essential in order to ensure high orientation, reactivity, accessibility and stability of the surface-aptamer. Different surfaces could be used for aptamer immobilization depending on the kind of aptasensors; these include bulk metals, such as gold, or other solid phases, such as resins, polymers, silicates, or nanomaterials. The most common immobilization techniques used in aptasensors are described in detail below, and the choice of a suitable immobilization strategy is determined by the physicochemical properties of both the surface and the aptamer. An ideal material for aptasensor development, for achievement of high sensitivity and selectivity, should allow the effective immobilization of the aptamer on its surface, guarantee a robust interaction between the target and the aptamer, as well as exhibit a negligible nonspecific adsorption of the label and a sensitive detection of the biological event [195]. The achievement of high sensitivity and selectivity requires minimization of nonspecific adsorption and the stability of the immobilized aptamers [196]. Table 1.5 summarizes the main aptamer immobilization methods in relation to the sensing surface and the relative advantages and challenges. It is well known that the correct immobilization of aptamers and the density of the aptamers influence the accuracy and the sensitivity of aptasensors.

Table 1.5: Main immobilization strategies of aptamers. [195]

No.	Immobilizing methods	Principle	Advantages	Disadvantages
1	Physical adsorption	Direct immobilization of aptamer on surfaces by electrostatic forces or van der Waals forces	Simple and rapid	Weak attachment
				Random orientation of aptamers
			Direct method (no linkers are required)	Poor reproducibility
				Desorption by detergent
2	Covalent binding of activated aptamer on functionalized surfaces	Activation of aptamer followed by chemical binding to the surface's functional group	Increased specificity of aptasensors	Chemical modifications are required
			Good stability	Use of linker molecules
			High binding strength	Slow and irreversible
			Decreased interference signal due to nonspecific adsorption	Possible interference factors such as surfactants, cross-linking agents, could be present
			Wide range of flexibility	The optimum reaction conditions of chemical reagents, aptamers, and targets must be considered
3	Covalent binding of modified aptamer on activated surfaces	Chemical binding between the surface's functional groups and the aptamer's modified group		
4	Covalent binding by entrapment	Chemical binding between the surface's functional groups and the aptamer's modified group	Increased amount of aptamer on the surface	Complexity of the procedure for entrapped matrix synthesis
			Higher coupling density	
			Flexibility for chemical modification	
			Can be used as coating on other substrates	

5	Covalent binding by electrografting	Chemical binding between the surface's functional groups and the aptamer's modified group	Uniform, controlled, and efficient immobilization of aptamer	Long incubation times for the reaction
			Improved sensitivity	Requirement for complex equipment for immobilization
			Reduced nonspecific signals	
6	Self-assembly	Specific adsorption of the aptamer's modified group to the surface	Stability	Possible leaching of biomolecules from the support and Possible denaturation
			Oriented recognition	
			Prevention of nonspecific adsorption	
			Easy to be produced	
7	Avidin–biotin binding (affinity coupling)	Interaction between the biotin group of the aptamer and amine group of the avidine	High specificity and functionality	Great influence of pH values on avidin
			Potential to be reversible	Poor reproducibility
			Increased amount of aptamers on the sensor surface	Problem of crowding effect
			Reduced incidence of nonspecific adsorption	
			Improved sensor signal-to-noise ratio	
8	Electrochemical adsorption	Adsorption controlled by a potential	Rapid and efficient	Great influence of the pH Unpredictable arrangement of the aptamer on the surface
				Large electrostatic repulsion and steric hindrance

1.4.2.1 Physical Adsorption

The direct physical adsorption of aptamer is the easiest way to immobilize an aptamer to surfaces without using reagents or modified aptamer sequences through weak, labile bonds with active substrate sites [195,197,198]. The physical adsorption could be either wet or dry. In the first case, a solution of aptamer is incubated onto the electrode surface and then it is let dry. While in the second case, the electrode is left in contact with a solution of aptamer for a specific time [199]. This binding strategy is based on electrostatic, van der Waals interactions, hydrogen bonds, and hydrophobic interactions of the reactants. The adsorption is a complex interplay between the chemical properties, structure, and porosity of the surface with the aptamer to be adsorbed. Thanks to the negative charges of aptamers resulting from the anionic phosphate group contained in each base and to its hydrophobic effect, the aptamer can bind several positively charged surfaces, including gels, carbon, metal oxide, polymers, and membranes or functionalized surfaces, in a simple and fast way [200,201].

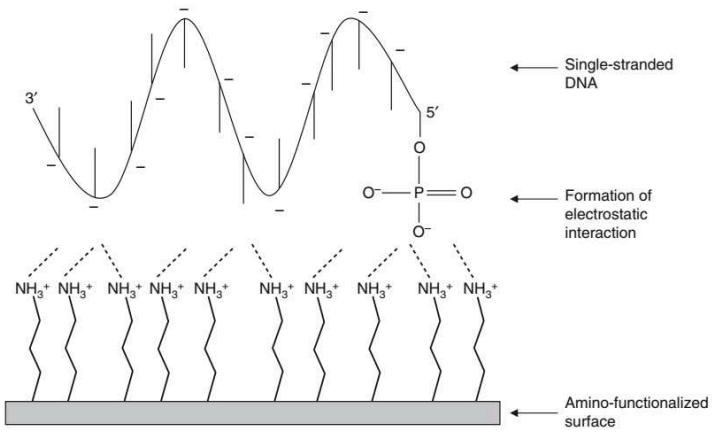

Figure 1.11:Electrostatic interactions on charged surfaces [201]

The resulting immobilized aptamers are likely to be heterogeneous and randomly oriented on the surface because each molecule can form many contacts in different orientations to minimize repulsive interactions with the substrate and previously adsorbed DNA probes. The limitation of physical adsorption is the poor stability, the weak attachment of aptamer to the surface and random orientation of aptamers, poor reproducibility, and easy desorption (i.e. by detergent) [202,203].

1.4.2.2 Covalent Binding

Immobilization of aptamers onto the electrode surface can be could also carried out by means of covalent binding between a molecule attached to the electrode surface and a reactive group of the aptamer. Different types of covalent binding technique have been reported in the literature [204–206], considering that aptamers can be easily functionalized by their ends to facilitate their immobilization (eg. -amino, -tiol, biotin, etc.). The immobilization of aptamers onto surfaces through covalent binding can be performed mainly by the immobilization of activated aptamers (typically at its 5′- or 3′-end) on functionalized surfaces or in the immobilization of modified aptamer on activated surfaces. In the last case, both the aptamer and the surface present a reactive pair of functional groups. The covalent immobilization of activated aptamer on a surface is characterized by the activation of the phosphate group of the aptamer to allow it to react with the modified surface. The carbodiimide method, the reactive anhydrides method and the activated ester method are the three activation methods used for this technique [201].

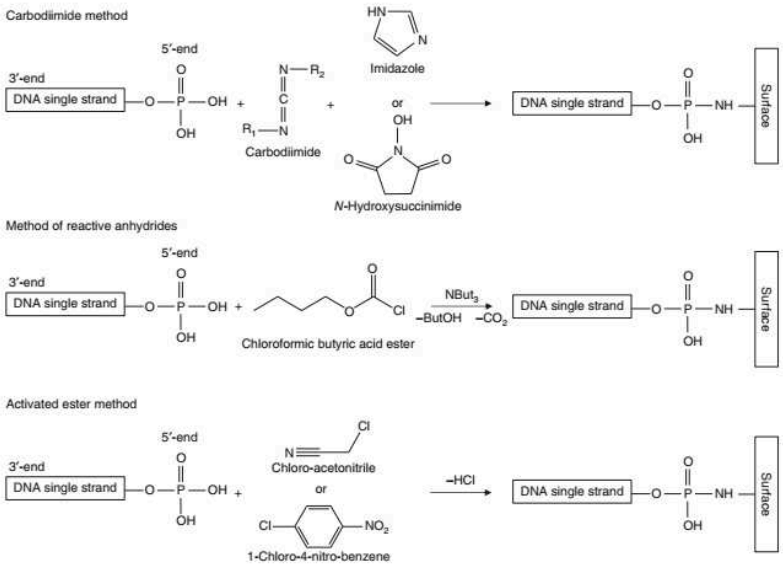

Figure 1.12: DNA activation and covalent coupling on amino-functionalized surfaces. [201]

The use of activated surfaces for immobilization of the modified aptamer increases the specificity of the aptasensors and decreases nonspecific adsorption. The kind of surface activation strategy depends on the type of terminal functional groups linked to the aptamer. Surfaces can be activated using zero-length cross-linkers or bifunctional cross-linkers. Zero-length cross-linkers are reactive molecules that activate functional groups on surfaces without any chain elongation or

incorporation in molecules that have to be attached and are used for the "direct coupling" of the aptamers to the surface.

The most common functional groups of zero-length cross-linkers include hydroxyl (-OH), amine ($-NH_2$), carboxyl (-COOH), and aldehyde (-CHO) that react with modified aptamers containing an amine group [201,202].The most used protocol is based on the formation of a covalent bond between the aptamer and the electrode surface through the activation of a carboxylic acid with carbodiimide 1-(3-dimethylaminopropyl)-3-ethyl carbodiimide (EDC) and N-hydroxysulfosuccinimide (NHS) for reaction with an amine group [131].

This method provides the benefits by structural flexibility and chemical stability, thus improving biorecognition efficiency. However, it presents some drawbacks, it requires chemical modifications of the surface, which make the assay time consuming, and aptamers have to be modified, which make the assay more expensive than others immobilization techniques.

1.4.2.3 Streptavidin (or Avidin)-Biotin Binding (Affinity Coupling)

The high specificity and affinity between avidin (or a related derivative such as streptavidin or neutravidin) and biotin are widely used in the immobilization of aptamers onto the sensor surfaces [207,208] [209] [210]. Avidin (or streptavidin) is a biotin binding protein that contains four identical subunits. Each subunit contains one binding site for biotin. Streptavidin and avidin are large tetrameric molecules (70 kDa) with four identical binding sites, and biotin is a small molecule that binds with high affinity binding site with an affinity constant of 1×10^{-15} M [211]. It is considered one of the strongest interactions in nature, with a K_d value of 10^{-15} M for avidin and 10^{-13} M for streptavidin. Avidin and streptavidin are tetrameric proteins that have four identical binding sites for biotin and high affinity for this molecule due to conserved amino acid sequences and structure.

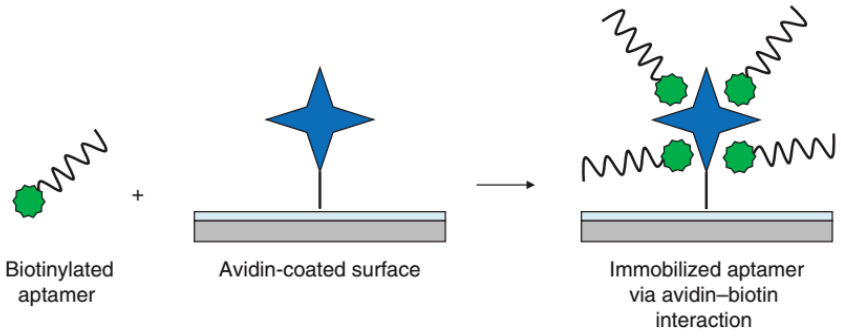

Figure 1.13: Immobilization of biotinylated aptamers to avidin-coated surfaces. [195]

The strength of the noncovalent avidin-biotin interaction could be comparable to antigen/ antibody and ligand/receptor [212].The stability of this interaction is nearly equal to that of a covalent bond. Actually, this interaction can only be broken under very extreme conditions. This is a two steps method, where the solid surface is first modified with streptavidin or avidin (deposition by physical adsorption or covalent interaction or immobilization into a composite material), followed by step of biotinylated aptamers are added to form the complex. This immobilization technique provides a good orientation of the aptamers onto the electrode surface, which causes a high specificity. However, streptavidin and avidin are expensive and it requires biotinylated aptamers which increases the production cost.

In summary, biotin-labeled aptamers interacted with avidin can be fixed on a variety of sensor surfaces, and the aptasensors can be used to detect various targets, such as proteins, antibiotics, biotoxins, and so on. Specifically, compared with other fixation methods, each streptavidin molecule can bind four biotinylated aptamers. This would increase the amount of aptamers on the sensor surfaces, reduce the incidence of nonspecific adsorption, and improve sensor signal-to-noise ratio of the sensor. Drawbacks include influence of pH values on avidin, poor reproducibility, and crowding effect [197,203,213].

1.4.2.4 Self-Assembled Monolayers (SAM)

Self-assembled monolayers (SAM) technique is a spontaneous formation of monolayers by chemisorption and self-organization of long-chain molecules onto a substrate. This technique provides a reproducible, ultrathin, and well-ordered layer suitable for further modification with aptamers, which improve sensitivity, speed, and reproducibility. Factors like good control at the molecular level, easy preparation in the laboratory, and the very small amount of chemicals needed

for their preparation make SAMs an excellent platform for aptamers iommobolisation [213]. The most extensively studied class of SAMs is derived from the adsorption of sulfur-based compounds such as thiols, disulphides on metals, including gold, silver, copper, and palladium [214], with SAMs based on the strong adsorption of sulfur compounds on gold as one of the most important class [215,216]. Gold is the standard surface used for SAM production for many reasons: it is easy to obtain, it is an inert metal that does not react with most chemicals, and thin gold films can be easily integrated into several technologies[214]. The thiol groups demonstrate affinity towards the noble metal surface allowing the formation of covalent bonds between the sulfur and gold atoms [217,218] .

Advantages of using SAM surfaces with aptamers include uniformity of the monolayer, resistance to nonspecific adsorption of interfering molecules, the ability to include multiple aptamers or other moieties (mixed SAMs), and ease of preparation and integration into techniques such as quartz crystal microbalance (QCM) and surface plasmon resonance (SPR). However, long aptamers with larger numbers of amine groups (in their base unit) have a greater probability of nonspecific binding to the gold surface; furthermore, the cost of the thiol-modified aptamers is higher than the non-modified or amine-modified aptamers.

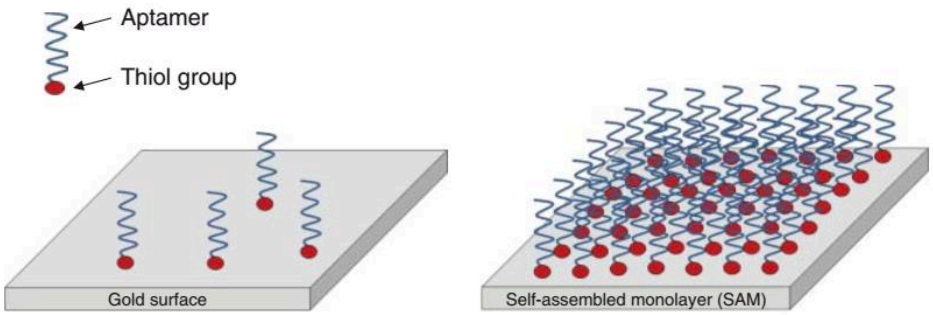

Figure 1.14: Representative immobilization of thiolated aptamers on gold surface. Large-scale immobilization of the thiolated aptamers forms a self-assembled monolayer (SAM).[195]

1.4.2.5 Electrochemical Adsorption

The electrochemical adsorption is an adsorption controlled by a potential to an electrode. This immobilization method is widely used for immobilizing rapidly and efficiently nucleic acids on screen-printed carbon transducers since the electrostatic binding of aptamer to positively charged carbon electrodes is sufficiently strong [219]. In particular, the positive charge applied to the electrodes generates a potential that enhances the stability of the aptamer through the electrostatic attraction between the positively charged surface and the negatively charged sugar-phosphate backbone of DNA.

.

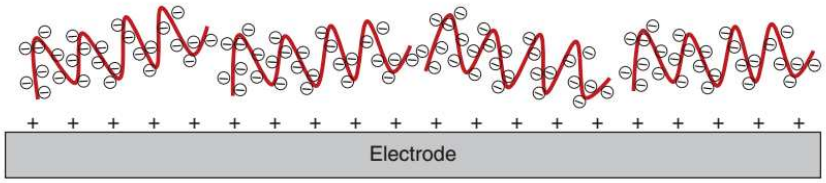

Figure 1.15: Example of electrochemical adsorption between the negatively charged sugar-phosphate backbone of aptamer and a positively charged electrode.

1.4.3 Aptamer-based Diclofenac Detection Systems

A literature review shows that there are just a very few reports on the aptamer based DCL detection systems that depend on optical, piezoelectric or electrochemical transduction techniques. Among these techniques, electrochemical techniques have been recognized as a powerful tool for fast access to biochemical information in aptamer-target complex due to their high sensitivity, fast response, easy operation, possibility of minituarization, relatively compact, as well as low production cost [171,188–191].

1.4.3.1 Impedimetric aptasensors

Taking into consideration the capability of the EIS technique to study the interfacial characteristics at the electrode surface in order to detect the changes occurring as a result of a small perturbation applied to the system, many studies have been attempted to assess the significance of EIS in characterizing biomolecule-functionalized electrodes, and also for monitoring biorecognition events that occur on the electrode surfaces [220–222]. In addition to its simple operation and high sensitivity [36-38], EIS is also a nondestructive technique and that makes it extremely attractive for electrochemical biosensing assays[188,223–225]. Among the different electrochemical techniques available, impedance has widely been used in aptasensors. This can be due to the fact

that it allows to perform label-free detection which makes the assay rapid, simple and low cost. However, sometimes labelling are required in order to increase selectivity and enhance sensitivity.

Among the very few reports on the impedimetric sensor for detection of DCL using aptasensors, a label free electrochemical aptasensor for detection of DCL was developed by Kashefi-Kheyrabadi and Mehrgardi, [40] by covalently immobilizing amino-functionalized diclofenac aptamer on glassy carbon electrode surface. To the best of our knowledge, this is the first attempt made to use aptasensors for detection of DCL. In this manuscript, the DCL was sandwiched between two aptamers on the surface of a glassy carbon electrode. The blocking of $[Fe(CN)6]^{3-/4-}$ as a negative probe to the surface by the negatively charged aptamer is reported to slow down the electron-transfer kinetics of the redox probe and the changes in the charge transfer resistance was monitored using electrochemical impedance spectroscopic (EIS) techniques. The calibration plot for the aptasensor developed showed to have two different linear dynamic ranges over 0 – 5 µM and 10 µM to 1 mM with a detection limit of 2.7×10^{-7} M.

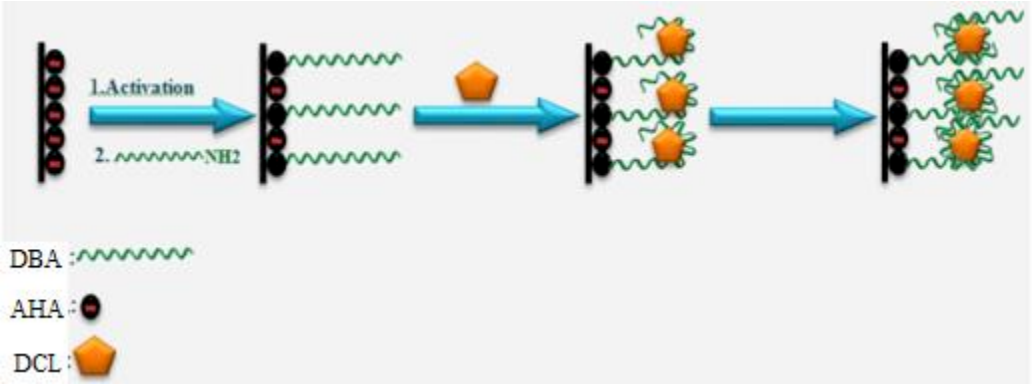

Figure 1.16:Schematic presentation of different steps of biosensor construction where DBA is the amino-functionalized diclofenac binding aptamer and AHA is the 6-aminohexanoic acid[40]

Recently, Derikvand et al., [163] developed an electrochemical DCL aptasensor based on a novel sensing nanocomposite with highly dispersed platinum nanoparticles (PtNPs) on carbon nanotubes (CNTs) functionalized with polyethyleneimine (PEI) as a platform for immobilization of DCL aptamer. The PtNPs/PEI/CNTs nanocomposite developed provided abundant $–NH_2$ groups for the immobilization of DCL specific aptamer. Derikvand et al. used Nickel-hexacyanoferrate (NiHCF) as signal probe for detection of DCL, which they manage to cast on the surface of PtNPs/PEI/CNTs nanocomposite by an electrodeposition method.

The formation of DCL–aptamer complexes at the sensing interface was monitored using electrochemical impedance spectroscopy (EIS) by monitoring the differences of the electron transfer resistance (Rct) before and after adding different concentration of DCL from 10 to 200 nM with a detection limit of 2.7 nM. The lower detection limit and wider linear range was attributed to the superior electron transfer of NiHCF and the densely populated aptamers at the surface of the electrode.

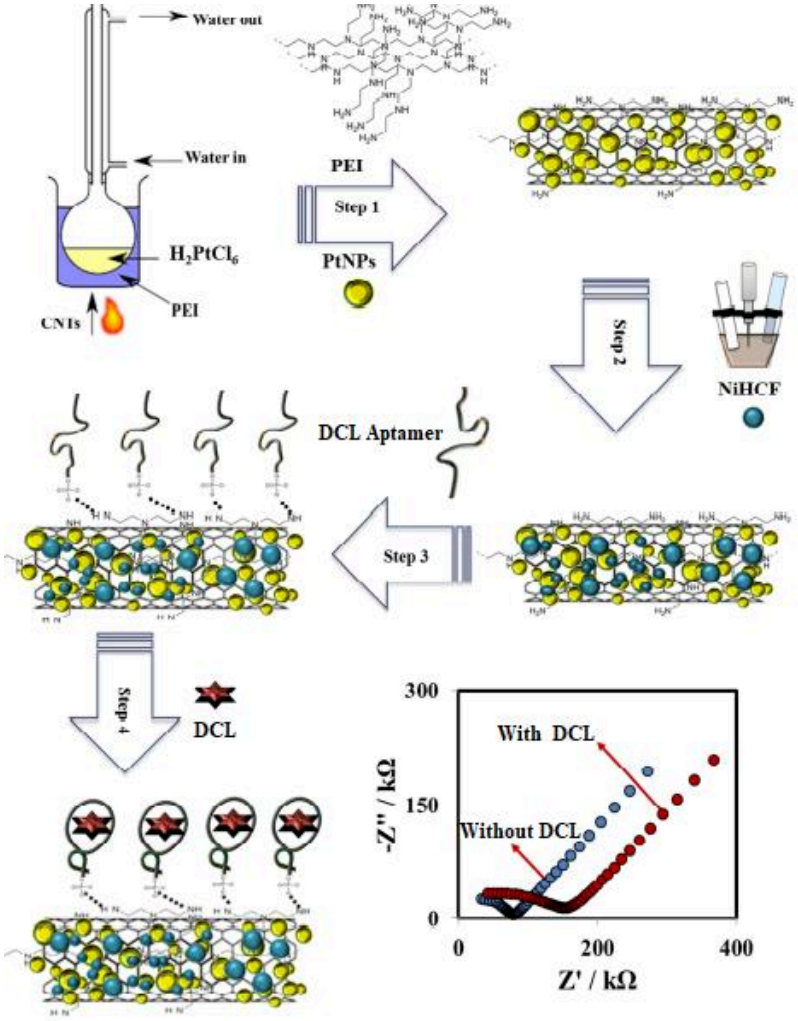

Figure 1.17: Schematic presentation of different steps of an aptamer construction based on the use of PtNPs/PEI/CNTs nanocomposite. [40]

1.4.3.2 Photoelectrochemical aptasenors

Photoelectrochemical (PEC) sensors, a sensing technique based on photo-induced electron transfer processes at electrode/interfaces, have recently attracted considerable research interests due to their advantages of high sensitivity, simple instrument, easy miniaturization and low cost [148,149]. In connection with this, Okoth et al., [161] developed a label-free photoelectrochemical aptasensor utilizing gold nanoparticles (Au NPs) and graphene-doped CdS (GR-CdS) for detection of DCL in pharmaceutical and environmental samples. Okoth et al. reported that the Au/GR-CdS modified electrode exhibited a high and stable photocurrent response upon visible light illumination, due to the excellent electrical and optical property of GR as well as the high absorption efficiency of CdS in the visible region. The Au NPs were incorporated with GR-CdS to further increase the photocurrent response and to immobilize the SH-terminated aptamer as a biorecognition element. The PEC aptasensor developed exhibited high sensitivity, excellent selectivity and good stability with a linear response being in the range of 1 to 150 nM and a detection limit of 0.78 nM, which can be attributed to the merits of great stability and high sensitivity of Au/GR-CdS and the excellent selectivity of the DCL binding aptamer.

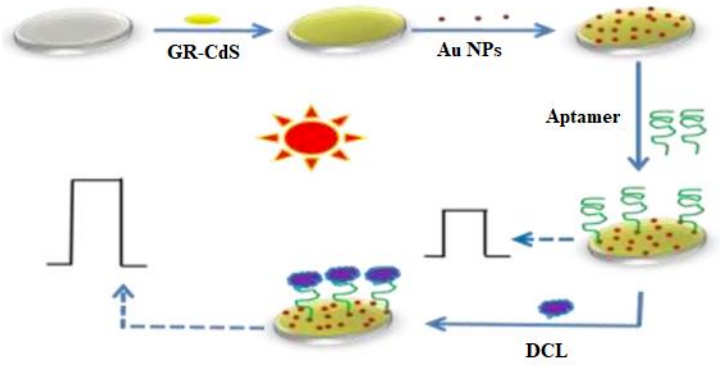

Figure 1.18: Schematic illustration on the fabrication process of DCL PEC aptasensor based on the use of gold nanoparticles and graphene doped. [161]

Recently, another photoelectrochemical aptasensor for diclofenac detection, based on visible/near-infrared (vis/NIR) light-responsive vanadyl-phthalocyanine/graphitic carbon nitrid nanosheet (VOPc/CN) nanocomposites, was developed by Shi et al. [162]. In this work, the first coupling of CN and VOPc with a facile solution–phase method was prepared and applied to PEC sensing. The prepared VOPc/CN composites gave excellent PEC signals relative to pure CN and VOPc and the authors proved that the VOPc, as a photosensitizer introduced into CN, can extend the light absorption boundary to the visible/NIR area and impede the recombination of photogenerated carriers on the surface of CN, causing an increase in the photo-to-current conversion efficiency. They reported the PEC signal of the VOPc/CN nanocomposites improved 2.7 and 12.42-fold compared with pure VOPc and CN, respectively. Due to the specific interaction between DCL and the aptamer, and the excellent photoelectric property of the VOPc/CN composites, the fabricated PEC biosensor (aptamer/CS/VOPc/CN/ITO) exhibited superior performances with high sensitivity, a low detection limit of 0.03 nM and a wide linear response, in the range of 0.1-500 nM.

1.5 Polymer Hydrogel Thin films as a Matrix for Aptamer Immobilization

Hydrogel is a three-dimensional cross-linked network of hydrophilic polymer chains, which can absorb up to 90% (by weight) water when submerged in water. One of the most remarkable properties of hydrogels is the very low polymer content. Due to the special structure, hydrogels are soft materials behaving as soft solids, with the properties ranging from soft and weak to hard and tough. In water, the hydrogel system can be treated as a dispersion of water molecules within a solid in which the solid is the continuous phase and the liquid is the discontinuous phase [226,227].

Owing to specific interactions between the polymer chains and water and many possible structures of the networks, kinds of complex polymer hydrogels are available. These two keys parameters can be initially designed to obtain particular materials with required properties. Based on the type of cross-linking, hydrogels are classified in two groups: chemically crosslinked hydrogels and physically cross-linked hydrogels. For chemically cross-linked hydrogels, the polymer chains are cross-linked through covalent bonds, which are irreversible if no chemical degradation occurs. These hydrogels behave as elastic solids, with the conservation of the permanent shape under self-weight (no flowing phenomenon) and no physical modification. On the contrary, in the case of physically cross-linked hydrogels, the interactions between the polymer chains at the cross-linking points are reversible, including Van der Waals interactions [228]: hydrogen bonding [229], ionic [230,231] or hydrophobic interactions [232,233], etc.

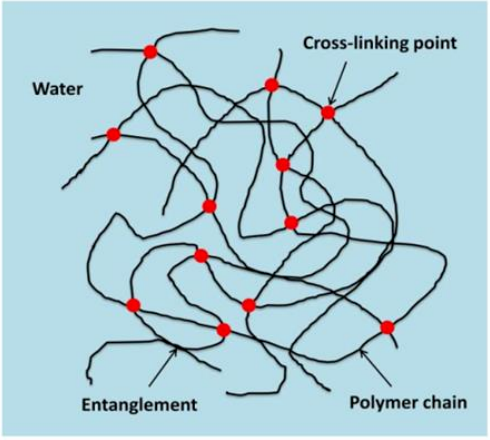

Figure 1.19: schematic representation of a (chemically or physically) cross-linked polymer network.

Many inherent properties of polymer hydrogels predetermine their irreplaceable position for numerous applications, among which the most important is their high water content that makes them biocompatible and allows the diffusion process of water soluble compound through the polymer networks[234]. Based on this property, various uses of hydrogels have been explored including their use in sensing applications. Stimulus-sensitive hydrogels may act as active sensing material. Such gels are sensitive to small changes in the environment and give the response to physical stimuli (temperature, light, pressure, electric field, ionic strength, and magnetic field) [235], chemical stimuli (pH, ions or biological stimuli (glucose, enzyme and antigen) through volume changes [236]. Another application of hydrogels in biosensors is a protection and coating function of sensor parts to prevent undesired interaction with biological molecules or cells. Their open porous structure and hydrophilic environment allows diffusion of analytes through the hydrogel matrix [234].

Beyond simple protection, hydrogels can be used as immobilization matrix for the biosensing elements. Essential criteria in designing biosensors with high selectivity and sensitivity are receptors that have to be immobilized in their native conformation to be able to specifically interact with the analyte, while support material should be resistant to unspecific adsorption. Furthermore, the quality of sensing and the sensitivity level mainly depend on accessibility and activity of the immobilized sensing molecules. Hydrogels provide excellent environments for biomolecules to preserve their active and functional structure [237]. As hydrogels may easily be tailored in their properties, they can form an ideal platform for this purpose.

1.5.1 Synthesis Methods of Hydrogel Thin Films

Recent advances in nanotechnology have led to increased interest in hydrogel thin films, as they can be rendered multifunctional and multiresponsive. The hydrogel thin films are very promising since they associate both advantages of hydrogel and films. On the one hand, hydrogel thin films are attractive as an approach to responsive surfaces and interfaces, where the hydrogel architecture offers much potential in competition with layer-by-layer (LbL) assemblies and grafted polymer layers. Thin films of chemically cross-linked hydrogels are usually prepared by the following two methods:

i. Cross-linking copolymerization by mixing monomers and multifunctional co-monomers;

ii. Cross-linking functionalized (co)polymers with reactive groups or with high-energy irradiation.

In the first approach, copolymerization and cross-linking take place simultaneously. Solvent based free radical polymerization techniques are widely employed. The reaction mixture containing monomers, the cross-linker and the initiator is confined between two planar substrates (one is functionalized to attach the hydrogel film and the other is non-sticky to detach the film) separated by spacers, and then is polymerized and cross-linked in situ [238]. Among all the free radical polymerization techniques, UV-initiated polymerization has drawn great attention because it realizes micro-patterning of hydrogel films by using a projection mask[238–241]. However, this technique may have its limits for thick hydrogel films due to the volume absorption of the UV beam. Plasma polymerization is another attractive deposition technique used to fabricate highly cross-linked hydrogel thin films (typical thickness ranging from tens to hundreds of nanometers), thanks to its advantageous features, like one-step, solvent-free and vapor-phase.

In the second approach, crosslinking of polymer chains in dry state is carried out after coating a thin film of functionalized (co)polymers to obtain hydrogel. So far, various techniques for coating have been developed, like spin-coating, dip-coating, spray-coating, etc. As for crosslinking, different techniques are available according to the chemical composition of the polymer. For example, after spin-coating, thin layers of mixed PVA/PAA chains are dried and then thermally crosslinked at 130°C via esterification reaction to produce pH-responsive hydrogel thin films [242,243].

While for copolymers that contain photo-reactive pendent groups or monomers, their crosslinking can be achieved either by the addition of photoinitiators[244] or by UV irradiation[245–248]. The crosslinking technique based on UV irradiation is broadly used, because it is compatible with photolithography and allows the preparation of hydrogel films with a wide range of dry thickness (from nanometres to tens of microns) [249,250]. As a matter of fact, high-energy irradiation (e.g., electron beam, γ-rays, UV-light) on polymer chains induces random chain scission resulting in free-radicals, which are then recombinated, leading to the formation of a crosslinked polymer network [251]. The crosslinking density is supposedly decided by the ratio of crosslinkers and/or the irradiation dose.

1.5.2 Swelling of Hydrogel Thin Films

Hydrogels are usually defined by their degree of swelling. A crosslinked polymer hydrogels swell but not dissolve when water or a solvent enters it. The swelling properties, which usually use degree of swelling to define hydrogels, depend on many factors such as network density, solvent nature, and polymer solvent interaction parameter [252]. The swelling of hydrogels depends on swelling and elastic forces. A hydrogel containing hydrophilic functional groups and ions can generate strong interactions with swelling medium, which cause hydrogels expansion. On the other hand, cross-links prevent infinite expansion of the network by generating elastic forces. Therefore, a cross-linked hydrogel in water may experience expansion and contraction depending on the magnitude of individual forces.

The swelling of isotropic bulk hydrogels is uniform in all directions. In contrast, the swelling of surface-attached hydrogel thin films is highly anisotropic. In fact, their in-plane (lateral) swelling is restricted by the chemical attachment of the polymer networks to the surface, and their volumetric expansion is available only in the direction normal to the substrate plane[253]. Thus, the swelling behavior of the hydrogel thin films is strongly influenced by the surface confinement.

It has been observed that the surface-attached polymer networks swell much less than the non-attached bulk networks of the same cross-link density[238]. The surface confinement has also an effect on the surface topography of the hydrogel thin films apart from their swelling properties. Actually, the strong osmotic force in the lateral dimension can induce a mechanical stress which may cause the delamination of the hydrogel films from the substrate [254,255] and the wrinkling

of the free surface of the gel films. In particular, the wrinkling was observed in 100 mm-thick gel films [256] and 150 nm-thick gel membranes [257,258].

For surface-attached gel films, the volumetric swelling ratio is the ratio of the volume fraction of polymer in air to the volume fraction of polymer in water. If attached networks swell only perpendicularly to the surface with no swelling parallel to the surface, then the linear swelling ratio and the volumetric swelling ratio is the same, in other words:

$$s_F = \frac{\Phi_a}{\Phi_\omega} = \frac{h_\omega}{h_a} \tag{1.1}$$

1.6 Thesis Objectives

Current efforts in the development of biosensors for the accurate and sensitive analysis of emerging pollutants such as diclofenac mainly focus on new platforms for biomolecule immobilization, and it is in this context that the objectives of the thesis were set. Hence, the general objective of this PhD thesis was to develop a novel class of surface attached hydrogel thin film on conductive transducer as biocompatible matrix for aptamer immobilization, for screening detection of diclofenac using electrochemical impedance spectroscopy as highly sensitive transduction technique. In order to carry out the main objectives, the following specific objectives were established.

(i) The fabrication of surface attached hydrogel thin films with tunable and well controlled chemistry
(ii) The covalent immobilization of aptamers on hydrogel films
(iii) Characterization of the biosensing electrodes at every stage of the aptamer construction

The main novelty of this work lies in the unique combination of the versatility of the hydrogel thin films with the aptamer, for the possibility of developing a miniaturized and portable electrochemical biosensor for DCL detection. Another element of novelty in this assay is in its ability to use covalent grafting of the thin film on to the electrode surface, and also the covalent immobilization of the aptamer on to the surface of the functionalized hydrogel thin film, in an effort to have a rather stable aptasensor platform.

REFERENCES

[1] D. Streimikiene, Environmental indicators for the assessment of quality of life, Intellectual Economics, 9 (2015) 67–79.

[2] P.J. Landrigan, L.R. Goldman, Children's Vulnerability To Toxic Chemicals: A Challenge And Opportunity To Strengthen Health And Environmental Policy, Health Affairs, 30 (2011) 842–850.

[3] R.G. Ahmed, S. Incerpi, F. Ahmed, A. Gaber, The Developmental and Physiological Interactions between Free Radicals and Antioxidant Defense System: Effect of Environmental Pollutants, (2013) 38.

[4] Tiedeken et al - 2017 - Monitoring, sources, receptors, and control measur.pdf, (n.d.).

[5] WELCOME TO THE NORMAN NETWORK | NORMAN, (n.d.).

[6] A.A. Bletsou, J. Jeon, J. Hollender, E. Archontaki, N.S. Thomaidis, Targeted and non-targeted liquid chromatography-mass spectrometric workflows for identification of transformation products of emerging pollutants in the aquatic environment, TrAC Trends in Analytical Chemistry, 66 (2015) 32–44.

[7] K. Fent, A. Weston, D. Caminada, Ecotoxicology of human pharmaceuticals, Aquatic Toxicology, 76 (2006) 122–159.

[8] M. Farré, S. Pérez, K. Gajda-Schrantz, V. Osorio, L. Kantiani, A. Ginebreda, D. Barceló, First determination of C60 and C70 fullerenes and N-methylfulleropyrrolidine C60 on the suspended material of wastewater effluents by liquid chromatography hybrid quadrupole linear ion trap tandem mass spectrometry, Journal of Hydrology, 383 (2010) 44–51.

[9] P. Verlicchi, M. Al Aukidy, E. Zambello, Occurrence of pharmaceutical compounds in urban wastewater: Removal, mass load and environmental risk after a secondary treatment—A review, Science of The Total Environment, 429 (2012) 123–155.

[10] A. Nikolaou, S. Meric, D. Fatta, Occurrence patterns of pharmaceuticals in water and wastewater environments, Analytical and Bioanalytical Chemistry, 387 (2007) 1225–1234.

[11] J.P. Sumpter, A.C. Johnson, 10th Anniversary Perspective: Reflections on endocrine disruption in the aquatic environment: from known knowns to unknown unknowns (and many things in between), Journal of Environmental Monitoring, 10 (2008) 1476.

[12] THE EUROPEAN PARLIAMENT AND THE COUNCIL OF THE, EUROPEAN UNION, The Water Framework Directive (WFD, 2000/ 60/EC), 2000.

[13] R.N. Carvalho, L. Ceriani, A. Ippolito, T. Lettieri, Development of the first Watch List under the Environmental Quality Standards Directive - Directive 2008/105/EC, as ammended by Directive 2013/39/EU in the field of water policy, 2015.

[14] D.H. Solomon, J. Avorn, T. Stürmer, R.J. Glynn, H. Mogun, S. Schneeweiss, Cardiovascular outcomes in new users of coxibs and nonsteroidal antiinflammatory drugs: High-risk subgroups and time course of risk, Arthritis & Rheumatism, 54 (2006) 1378–1389.

[15] R. Altman, B. Bosch, K. Brune, P. Patrignani, C. Young, Advances in NSAID Development: Evolution of Diclofenac Products Using Pharmaceutical Technology, Drugs, 75 (2015) 859–877.

[16] T.J. Gan, Diclofenac: an update on its mechanism of action and safety profile, Current Medical Research and Opinion, 26 (2010) 1715–1731.

[17] N. Vieno, M. Sillanpää, Fate of diclofenac in municipal wastewater treatment plant — A review, Environment International, 69 (2014) 28–39.

[18] C. Miège, J.M. Choubert, L. Ribeiro, M. Eusèbe, M. Coquery, Removal efficiency of pharmaceuticals and personal care products with varying wastewater treatment processes and operating conditions – conception of a database and first results, Water Science and Technology, 57 (2008) 49–56.

[19] J. Quintana, S. Weiss, T. Reemtsma, Pathways and metabolites of microbial degradation of selected acidic pharmaceutical and their occurrence in municipal wastewater treated by a membrane bioreactor, Water Research, 39 (2005) 2654–2664.

[20] A. Joss, E. Keller, A.C. Alder, A. Göbel, C.S. McArdell, T. Ternes, H. Siegrist, Removal of pharmaceuticals and fragrances in biological wastewater treatment, Water Research, 39 (2005) 3139–3152.

[21] E.J. Tiedeken, A. Tahar, B. McHugh, N.J. Rowan, Monitoring, sources, receptors, and control measures for three European Union watch list substances of emerging concern in receiving waters – A 20 year systematic review, Science of The Total Environment, 574 (2017) 1140–1163.

[22] H.-R. Buser, T. Poiger, M.D. Müller, Occurrence and Fate of the Pharmaceutical Drug Diclofenac in Surface Waters: Rapid Photodegradation in a Lake, Environ. Sci. Technol., 32 (1998) 3449–3456.

[23] E. Nie, M. Yang, D. Wang, X. Yang, X. Luo, Z. Zheng, Degradation of diclofenac by ultrasonic irradiation: Kinetic studies and degradation pathways, Chemosphere, 113 (2014) 165–170.

[24] S.-W. Nam, C. Jung, H. Li, M. Yu, J.R.V. Flora, L.K. Boateng, N. Her, K.-D. Zoh, Y. Yoon, Adsorption characteristics of diclofenac and sulfamethoxazole to graphene oxide in aqueous solution, Chemosphere, 136 (2015) 20–26.

[25] S. Álvarez, R.S. Ribeiro, H.T. Gomes, J.L. Sotelo, J. García, Synthesis of carbon xerogels and their application in adsorption studies of caffeine and diclofenac as emerging contaminants, Chemical Engineering Research and Design, 95 (2015) 229–238.

[26] B. Hoeger, B. Köllner, D.R. Dietrich, B. Hitzfeld, Water-borne diclofenac affects kidney and gill integrity and selected immune parameters in brown trout (Salmo trutta f fario), Aquatic Toxicology, 75 (2005) 53–64.

[27] R. Triebskorn, H. Casper, V. Scheil, J. Schwaiger, Ultrastructural effects of pharmaceuticals (carbamazepine, clofibric acid, metoprolol, diclofenac) in rainbow trout (Oncorhynchus mykiss) and common carp (Cyprinus carpio), Anal Bioanal Chem, 387 (2007) 1405–1416.

[28] A.J. Ebele, M. Abou-Elwafa Abdallah, S. Harrad, Pharmaceuticals and personal care products (PPCPs) in the freshwater aquatic environment, Emerging Contaminants, 3 (2017) 1–16.

[29] M. Cleuvers, Mixture toxicity of the anti-inflammatory drugs diclofenac, ibuprofen, naproxen, and acetylsalicylic acid, Ecotoxicology and Environmental Safety, 59 (2004) 309–315.

[30] M. Mostafavi, M.R. Yaftian, F. Piri, H. Shayani-Jam, A new diclofenac molecularly imprinted electrochemical sensor based upon a polyaniline/reduced graphene oxide nano-composite, Biosensors and Bioelectronics, 122 (2018) 160–167.

[31] K. Kwaśniewska, R. Gadzała-Kopciuch, K. Cendrowski, Analytical Procedure for the Determination of Zearalenone in Environmental and Biological Samples, Critical Reviews in Analytical Chemistry, 45 (2015) 119–130.

[32] H. Karimi-Maleh, P. Biparva, M. Hatami, A novel modified carbon paste electrode based on NiO/CNTs nanocomposite and (9, 10-dihydro-9, 10-ethanoanthracene-11, 12-dicarboximido)-4-ethylbenzene-1, 2-diol as a mediator for simultaneous determination of cysteamine, nicotinamide adenine dinucleotide and folic acid, Biosensors and Bioelectronics, 48 (2013) 270–275.

[33] A.A. Ensafi, H. Karimi-Maleh, S. Mallakpour, M. Hatami, Simultaneous determination of N-acetylcysteine and acetaminophen by voltammetric method using N-(3,4-dihydroxyphenethyl)-3,5-dinitrobenzamide modified multiwall carbon nanotubes paste electrode, Sensors and Actuators B: Chemical, 155 (2011) 464–472.

[34] B.J. Sanghavi, S.M. Mobin, P. Mathur, G.K. Lahiri, A.K. Srivastava, Biomimetic sensor for certain catecholamines employing copper(II) complex and silver nanoparticle modified glassy carbon paste electrode, Biosensors and Bioelectronics, 39 (2013) 124–132.

[35] J. Lenik, A new potentiometric electrode incorporating functionalized β-cyclodextrins for diclofenac determination, Materials Science and Engineering: C, 45 (2014) 109–116.

[36] C. Wang, T. Jiang, K. Zhao, A. Deng, J. Li, A novel electrochemiluminescent immunoassay for diclofenac using conductive polymer functionalized graphene oxide as labels and gold nanorods as signal enhancers, Talanta, 193 (2019) 184–191.

[37] S. Wang, Q. Liu, H. Li, Y. Li, N. Hao, J. Qian, W. Zhu, K. Wang, Fabrication of label-free electrochemical impedimetric DNA biosensor for detection of genetically modified soybean by recognizing CaMV 35S promoter, Journal of Electroanalytical Chemistry, 782 (2016) 19–25.

[38] M. Asif, A. Aziz, M. Azeem, Z. Wang, G. Ashraf, F. Xiao, X. Chen, H. Liu, A review on electrochemical biosensing platform based on layered double hydroxides for small molecule biomarkers determination, Advances in Colloid and Interface Science, 262 (2018) 21–38.

[39] A.L. Sanati, H. Karimi-Maleh, A. Badiei, P. Biparva, A.A. Ensafi, A voltammetric sensor based on NiO/CNTs ionic liquid carbon paste electrode for determination of morphine in the presence of diclofenac, Materials Science and Engineering: C, 35 (2014) 379–385.

[40] L. Kashefi-Kheyrabadi, M.A. Mehrgardi, Design and construction of a label free aptasensor for electrochemical detection of sodium diclofenac, Biosensors and Bioelectronics, 33 (2012) 184–189.

[41] Method 1694: Pharmaceuticals and Personal Care Products in Water, Soil, Sediment, and Biosolids by HPLC/MS/MS, (2007) 77.

[42] A. I. Olives, V. Gonzalez-Ruiz, M. Antonia Martin, Isolation and Quantitative Methods for Analysis of Non-Steroidal Anti-Inflammatory Drugs, Anti-Inflammatory & Anti-Allergy Agents in Medicinal Chemistry, 11 (2012) 65–95.

[43] J. Wu, L. Zhang, Z. Yang, A Review on the Analysis of Emerging Contaminants in Aquatic Environment, Critical Reviews in Analytical Chemistry, 40 (2010) 234–245.

[44] P. Vazquez-Roig, C. Blasco, Y. Picó, Advances in the analysis of legal and illegal drugs in the aquatic environment, TrAC Trends in Analytical Chemistry, 50 (2013) 65–77.

[45] K. Fischer, E. Fries, W. Körner, C. Schmalz, C. Zwiener, New developments in the trace analysis of organic water pollutants, Applied Microbiology and Biotechnology, 94 (2012) 11–28.

[46] F. Hernández, M. Ibáñez, R. Bade, L. Bijlsma, J.V. Sancho, Investigation of pharmaceuticals and illicit drugs in waters by liquid chromatography-high-resolution mass spectrometry, TrAC Trends in Analytical Chemistry, 63 (2014) 140–157.

[47] R. Loos, European Commission, Joint Research Centre, Institute for Environment and Sustainability, Analytical methods relevant to the European Commission's 2012 proposal on priority substances under the water framework directive, Publications Office, Luxembourg, 2012.

[48] C. Hao, L. Lissemore, B. Nguyen, S. Kleywegt, P. Yang, K. Solomon, Determination of pharmaceuticals in environmental waters by liquid chromatography/electrospray ionization/tandem mass spectrometry, Analytical and Bioanalytical Chemistry, 384 (2005) 505–513.

[49] M. Gros, M. Petrović, D. Barceló, Development of a multi-residue analytical methodology based on liquid chromatography–tandem mass spectrometry (LC–MS/MS) for screening and trace level determination of pharmaceuticals in surface and wastewaters, Talanta, 70 (2006) 678–690.

[50] M.J. Martínez Bueno, A. Agüera, M.J. Gómez, M.D. Hernando, J.F. García-Reyes, A.R. Fernández-Alba, Application of Liquid Chromatography/Quadrupole-Linear Ion Trap Mass Spectrometry and Time-of-Flight Mass Spectrometry to the Determination of

Pharmaceuticals and Related Contaminants in Wastewater, Analytical Chemistry, 79 (2007) 9372–9384.

[51] M. Gros, M. Petrović, D. Barceló, Tracing Pharmaceutical Residues of Different Therapeutic Classes in Environmental Waters by Using Liquid Chromatography/Quadrupole-Linear Ion Trap Mass Spectrometry and Automated Library Searching, Analytical Chemistry, 81 (2009) 898–912.

[52] S. Grujić, T. Vasiljević, M. Laušević, Determination of multiple pharmaceutical classes in surface and ground waters by liquid chromatography–ion trap–tandem mass spectrometry, Journal of Chromatography A, 1216 (2009) 4989–5000.

[53] M. Gros, S. Rodríguez-Mozaz, D. Barceló, Fast and comprehensive multi-residue analysis of a broad range of human and veterinary pharmaceuticals and some of their metabolites in surface and treated waters by ultra-high-performance liquid chromatography coupled to quadrupole-linear ion trap tandem mass spectrometry, Journal of Chromatography A, 1248 (2012) 104–121.

[54] M. Petrović, B. Škrbić, J. Živančev, L. Ferrando-Climent, D. Barcelo, Determination of 81 pharmaceutical drugs by high performance liquid chromatography coupled to mass spectrometry with hybrid triple quadrupole–linear ion trap in different types of water in Serbia, Science of The Total Environment, 468–469 (2014) 415–428.

[55] H.T. Elbalkiny, A.M. Yehia, S.M. Riad, Y.S. Elsaharty, Potentiometric diclofenac detection in wastewater using functionalized nanoparticles, Microchemical Journal, 145 (2019) 90–95.

[56] J.A. Rodríguez, E. Barrado, Y. Castrillejo, J.R. Santos, J.L.F.C. Lima, Validation of a tubular bismuth film amperometric detector, Journal of Pharmaceutical and Biomedical Analysis, 45 (2007) 47–53.

[57] X. Yang, F. Wang, S. Hu, Enhanced oxidation of diclofenac sodium at a nano-structured electrochemical sensing film constructed by multi-wall carbon nanotubes–surfactant composite, Materials Science and Engineering: C, 28 (2008) 188–194.

[58] M. Hajjizadeh, A. Jabbari, H. Heli, A.A. Moosavi-Movahedi, S. Haghgoo, Electrocatalytic oxidation of some anti-inflammatory drugs on a nickel hydroxide-modified nickel electrode, Electrochimica Acta, 53 (2007) 1766–1774.

[59] P. Daneshgar, P. Norouzi, M. Ganjali, R. Dinarvand, A. Moosavi-Movahedi, Determination of Diclofenac on a Dysprosium Nanowire- Modified Carbon Paste Electrode Accomplished in a Flow Injection System by Advanced Filtering, Sensors, 9 (2009) 7903–7918.

[60] M.C. Oliveira, E.H. Bindewald, L.H. Marcolino, M.F. Bergamini, Potentiometric determination of Diclofenac using an ion-selective electrode prepared from polypyrrole films, Journal of Electroanalytical Chemistry, 732 (2014) 11–16.

[61] Zh.A. Kormosh, I.P. Hunka, Ya.R. Bazel, A potentiometric sensor for the determination of diclofenac, Journal of Analytical Chemistry, 64 (2009) 853–858.

[62] S.A.A. Almeida, A.M. Heitor, M.C.B.S.M. Montenegro, M.G.F. Sales, Sulfadiazine-selective determination in aquaculture environment: Selective potentiometric transduction by neutral or charged ionophores, Talanta, 85 (2011) 1508–1516.

[63] T.F.A. Sousa, C.G. Amorim, M.C.B.S.M. Montenegro, A.N. Araújo, Cyclodextrin based potentiometric sensor for determination of ibuprofen in pharmaceuticals and waters, Sensors and Actuators B: Chemical, 176 (2013) 660–666.

[64] C.O. Cunha, R.C.R. Silva, C.G. Amorim, S.A. Júnior, A.N. Araújo, M.C.B.S.M. Montenegro, V.L. Silva, Tetracycline Potentiometric Sensor Based on Cyclodextrin for Pharmaceuticals and Waste Water Analysis, Electroanalysis, 22 (2010) 2967–2972.

[65] S.M. Riad, F.I. Khattab, H. Salem, H.T. Elbalkiny, Ion-Selective Membrane Sensors for the Determination of Ciprofloxacin Hydrochloride in Water and Pharmaceutical Formulation, 6 (2014) 14.

[66] V.V. Coşofre, R.P. Buck, Recent Advances in Pharmaceutical Analysis with Potentiometric Membrane Sensors, Critical Reviews in Analytical Chemistry, 24 (1993) 1–58.

[67] V. K. Gupta, A. Nayak, S. Agarwal, B. Singhal, Recent Advances on Potentiometric Membrane Sensors for Pharmaceutical Analysis, CCHTS, 14 (2011) 284–302.

[68] V.K. Gupta, H. Karimi-Maleh, R. Sadegh, Simultaneous Determination of Hydroxylamine, Phenol and Sulfite in Water and Waste Water Samples Using A Voltammetric Nanosensor, Int. J. Electrochem. Sci., 10 (2015) 14.

[69] S.K. Srivastava, V.K. Gupta, M.K. Dwivedi, S. Jain, Caesium PVC–crown (dibenzo-24-crown-8) based membrane sensor, Anal. Proc., 32 (1995) 21–23.

[70] V.K. Gupta, M.R. Ganjali, P. Norouzi, H. Khani, A. Nayak, S. Agarwal, Electrochemical Analysis of Some Toxic Metals by Ion–Selective Electrodes, Critical Reviews in Analytical Chemistry, 41 (2011) 282–313.

[71] V.K. Gupta, L.P. Singh, R. Singh, N. Upadhyay, S.P. Kaur, B. Sethi, A novel copper (II) selective sensor based on Dimethyl 4, 4′ (o-phenylene) bis(3-thioallophanate) in PVC matrix, Journal of Molecular Liquids, 174 (2012) 11–16.

[72] S.K. Srivastava, V.K. Gupta, S. Jain, PVC-Based 2,2,2-Cryptand Sensor for Zinc Ions, Anal. Chem., 68 (1996) 1272–1275.

[73] V.K. Gupta, S. Kumar, R. Singh, L.P. Singh, S.K. Shoora, B. Sethi, Cadmium (II) ion sensing through p-tert-butyl calix[6]arene based potentiometric sensor, Journal of Molecular Liquids, 195 (2014) 65–68.

[74] V.K. Gupta, A.K. Singh, L.K. Kumawat, Thiazole Schiff base turn-on fluorescent chemosensor for Al3+ ion, Sensors and Actuators B: Chemical, 195 (2014) 98–108.

[75] V.K. Gupta, N. Mergu, L.K. Kumawat, A.K. Singh, Selective naked-eye detection of Magnesium (II) ions using a coumarin-derived fluorescent probe, Sensors and Actuators B: Chemical, 207 (2015) 216–223.

[76] V.K. Gupta, N. Mergu, L.K. Kumawat, A.K. Singh, A reversible fluorescence "off–on–off" sensor for sequential detection of aluminum and acetate/fluoride ions, Talanta, 144 (2015) 80–89.

[77] E. Bakker, Ion-Selective Electrodes, in: Reference Module in Chemistry, Molecular Sciences and Chemical Engineering, Elsevier, 2018: p. B9780124095472144000.

[78] E. Pungor, The Theory of Ion-Selective Electrodes, Anal. Sci., 14 (1998) 249–256.

[79] Z. Kormosh, I. Hunka, Y. Bazel, N. Kormosh, A. Laganovsky, I. Mazurenko, A new diclofenac membrane sensor based on its ion associate with crystal violet Application to diclofenac determination in urine and pharmaceuticals, JICS, 4 (2007) 408–413.

[80] S.S.M. Hassan, R.M. Abdel-Aziz, M.S. Abdel-Samad, Plastic membrane electrode for selective determination of diclofenac (voltaren) in pharmaceutical preparations, Analyst, 119 (1994) 1993.

[81] Z. Kormosh, I. Hunka, Y. Bazel, Potentiometric determination of diclofenac in pharmaceutical formulation by membrane electrode based on ion associate with base dye, Chinese Chemical Letters, 18 (2007) 1103–1106.

[82] E.M.G. Santos, A.N. Araújo, C.M.C.M. Couto, M.C.B.S.M. Montenegro, Potentiometric behaviour of ion selective electrodes based on iron porphyrins: The influence of porphyrin substituents on the response properties and analytical determination of diclofenac in pharmaceutical formulations, Journal of Pharmaceutical and Biomedical Analysis, 42 (2006) 535–542.

[83] S.S.M. Hassan, W.H. Mahmoud, M.A.F. Elmosallamy, M.H. Almarzooqi, Iron(II)-phthalocyanine as a novel recognition sensor for selective potentiometric determination of diclofenac and warfarin drugs, Journal of Pharmaceutical and Biomedical Analysis, 39 (2005) 315–321.

[84] Z. Kormosh, I. Hunka, Y. Bazel, A. Laganovsky, I. Mazurenko, N. Kormosh, Determination of diclofenac in pharmaceuticals and urine samples using a membrane sensor based on the ion associate of diclofenac with Rhodamine B, Open Chemistry, 5 (2007).

[85] D. Vlascici, S. Pruneanu, L. Olenic, F. Pogacean, V. Ostafe, V. Chiriac, E.M. Pica, L.C. Bolundut, L. Nica, E. Fagadar-Cosma, Manganese(III) Porphyrin-based Potentiometric Sensors for Diclofenac Assay in Pharmaceutical Preparations, Sensors, 10 (2010) 8850–8864.

[86] Zh.A. Kormosh, I.P. Hunka, Y.R. Bazel, An ion-selective sensor for assay of diclofenac in medicines, Pharm Chem J, 43 (2009) 428–430.

[87] S.S.M. Hassan, W.H. Mahmoud, M.A.F. Elmosallamy, M.H. Almarzooqi, Determination of diclofenac in pharmaceutical preparations using a novel PVC membrane sensor, (2003) 4.

[88] Zh.A. Kormosh, I.P. Hunka, Ya.R. Bazel, A potentiometric sensor for the determination of diclofenac, J Anal Chem, 64 (2009) 853–858.

[89] A.O. Santini, H.R. Pezza, L. Pezza, Determination of diclofenac in pharmaceutical preparations using a potentiometric sensor immobilized in a graphite matrix, Talanta, 68 (2006) 636–642.

[90] E. Brennan, P. Futvoie, J. Cassidy, B. Schazmann, An ionic liquid-based sensor for diclofenac determination in water, International Journal of Environmental Analytical Chemistry, 97 (2017) 588–596.

[91] Z. Kormosh, I. Hunka, Y. Bazel, An electrode immobilized in a graphite matrix with ion pair complex for the determination of diclofenac in pharmaceuticals, (2008) 9.

[92] Z. Kormosh, I. Hunka, Y. Bazel, Preparation and Characterization of a Diclofenac Sensitive Electrode Based on a PVC Matrix Membrane, Acta Chim. Slov., (2008) 7.

[93] M. Shamsipur, F. Jalali, S. Ershad, Preparation of a diclofenac potentiometric sensor and its application to pharmaceutical analysis and to drug recovery from biological fluids, Journal of Pharmaceutical and Biomedical Analysis, 37 (2005) 943–947.

[94] R. Maleki, A.A. Matin, R. Hosseinzadeh, et al., PVC membrane sensor for diclofenac: applications in pharmaceutical analysis and drug binding studies, Pharmazie, (2007) 672–677.

[95] A.M. Pimenta, A.N. Araújo, M.C.B.S.M. Montenegro, Simultaneous potentiometric and fluorimetric determination of diclofenac in a sequential injection analysis system, Analytica Chimica Acta, 470 (2002) 185–194.

[96] R. Hosseinzadeh, R. Maleki, A.A. Matin, Interaction of Diclofenac with Bovine Serum Albumin Investigated by Diclofenac-Selective Electrode, Acta Chim. Slov., (2007) 6.

[97] Z. Kormosh, I. Hunka, Y. Bazel, Potentiometric determination of diclofenac in pharmaceutical formulation by membrane electrode based on ion associate with base dye, Chinese Chemical Letters, 18 (2007) 1103–1106.

[98] Z. Kormosh, I. Hunka, Y. Bazel, Preparation and Characterization of a Diclofenac Sensitive Electrode Based on a PVC Matrix Membrane, Acta Chim. Slov., (2008) 7.

[99] Z. Kormosh, I. Hunka, Y. Bazel, An electrode immobilized in a graphite matrix with ion pair complex for the determination of diclofenac in pharmaceuticals, (2008) 8.

[100] A.J. Bard, L.R. Faulkner, Electrochemical methods: fundamentals and applications, 2nd ed, Wiley, New York, 2001.

[101] B.K. Chethana, S. Basavanna, Y. Arthoba Naik, Voltammetric Determination of Diclofenac Sodium Using Tyrosine-Modified Carbon Paste Electrode, Industrial & Engineering Chemistry Research, 51 (2012) 10287–10295.

[102] K. Sarhangzadeh, A.A. Khatami, M. Jabbari, S. Bahari, Simultaneous determination of diclofenac and indomethacin using a sensitive electrochemical sensor based on multiwalled carbon nanotube and ionic liquid nanocomposite, Journal of Applied Electrochemistry, 43 (2013) 1217–1224.

[103] M. Shalauddin, S. Akhter, S. Bagheri, M.S. Abd Karim, N. Adib Kadri, W.J. Basirun, Immobilized copper ions on MWCNTS-Chitosan thin film: Enhanced amperometric sensor

for electrochemical determination of diclofenac sodium in aqueous solution, International Journal of Hydrogen Energy, 42 (2017) 19951–19960.

[104] B. Yilmaz, U. Ciltas, Determination of diclofenac in pharmaceutical preparations by voltammetry and gas chromatography methods, Journal of Pharmaceutical Analysis, 5 (2015) 153–160.

[105] J.J. Davis, K.S. Coleman, B.R. Azamian, C.B. Bagshaw, M.L.H. Green, Chemical and Biochemical Sensing with Modified Single Walled Carbon Nanotubes, Chem. Eur. J., 9 (2003) 3732–3739.

[106] R.R. Gaichore, A.K. Srivastava, Multiwalled carbon nanotube-4-tert-butyl calix[6]arene composite electrochemical sensor for clenbuterol hydrochloride determination by means of differential pulse adsorptive stripping voltammetry, J Appl Electrochem, 42 (2012) 979–987.

[107] M. Arvand, T.M. Gholizadeh, M.A. Zanjanchi, MWCNTs/Cu(OH)2 nanoparticles/IL nanocomposite modified glassy carbon electrode as a voltammetric sensor for determination of the non-steroidal anti-inflammatory drug diclofenac, Materials Science and Engineering: C, 32 (2012) 1682–1689.

[108] A.A. Ensafi, M. Izadi, H. Karimi-Maleh, Sensitive voltammetric determination of diclofenac using room-temperature ionic liquid-modified carbon nanotubes paste electrode, Ionics, 19 (2013) 137–144.

[109] H. Razmi, K. Sarhang-Zadeh, R. Mohammad-Rezaei, Electrochemical Behavior and Voltammetric Determination of Diclofenac at a Multi-Walled Carbon Nanotube-Ionic Liquid Composite Modified Carbon Ceramic Electrode, Analytical Letters, 46 (2013) 1885–1896.

[110] M. Goodarzian, M.A. Khalilzade, F. Karimi, V. Kumar Gupta, M. Keyvanfard, H. Bagheri, M. Fouladgar, Square wave voltammetric determination of diclofenac in liquid phase using a novel ionic liquid multiwall carbon nanotubes paste electrode, Journal of Molecular Liquids, 197 (2014) 114–119.

[111] Y. Akbarian, M. Shabani-Nooshabadi, H. Karimi-Maleh, Fabrication of a new electrocatalytic sensor for determination of diclofenac, morphine and mefenamic acid using synergic effect of NiO-SWCNT and 2, 4-dimethyl-N/-[1- (2, 3-dihydroxy phenyl) methylidene] aniline, Sensors and Actuators B: Chemical, 273 (2018) 228–233.

[112] R.N. Goyal, S. Chatterjee, B. Agrawal, Electrochemical investigations of diclofenac at edge plane pyrolytic graphite electrode and its determination in human urine, Sensors and Actuators B: Chemical, 145 (2010) 743–748.

[113] R.N. Goyal, S. Chatterjee, A.R.S. Rana, The effect of modifying an edge-plane pyrolytic graphite electrode with single-wall carbon nanotubes on its use for sensing diclofenac, Carbon, 48 (2010) 4136–4144.

[114] M.M. Eteya, G.H. Rounaghi, B. Deiminiat, Fabrication of a new electrochemical sensor based on Au Pt bimetallic nanoparticles decorated multi-walled carbon nanotubes for determination of diclofenac, Microchemical Journal, 144 (2019) 254–260.

[115] J. Zhou, Y. Zhao, J. Bao, D. Huo, H. Fa, X. Shen, C. Hou, One-step electrodeposition of Au-Pt bimetallic nanoparticles on MoS 2 nanoflowers for hydrogen peroxide enzyme-free electrochemical sensor, Electrochimica Acta, 250 (2017) 152–158.

[116] S. Nantaphol, T. Watanabe, N. Nomura, W. Siangproh, O. Chailapakul, Y. Einaga, Bimetallic Pt–Au nanocatalysts electrochemically deposited on boron-doped diamond electrodes for nonenzymatic glucose detection, Biosensors and Bioelectronics, 98 (2017) 76–82.

[117] M. Cui, J. Huang, Y. Wang, Y. Wu, X. Luo, Molecularly imprinted electrochemical sensor for propyl gallate based on PtAu bimetallic nanoparticles modified graphene–carbon nanotube composites, Biosensors and Bioelectronics, 68 (2015) 563–569.

[118] S. Zhang, B. Li, Q. Sheng, J. Zheng, Electrochemical sensor for sensitive determination of nitrite based on the CuS–MWCNT nanocomposites, Journal of Electroanalytical Chemistry, 769 (2016) 118–123.

[119] X. Du, Z. Zhang, C. Zhang, Y. Zhang, Q. Chen, One-step electrodeposition of poly (3,4-ethylenedioxythiophene) on carboxylated multi-wall carbon nanotubes and its application in ascorbic acid sensing, Journal of Electroanalytical Chemistry, 782 (2016) 84–90.

[120] M. Jin, X. Zhang, Q. Zhen, Y. He, X. Chen, W. Lyu, R. Han, M. Ding, An electrochemical sensor for indole in plasma based on MWCNTs-chitosan modified screen-printed carbon electrode, Biosensors and Bioelectronics, 98 (2017) 392–397.

[121] F. Manea, M. Ihos, A. Remes, G. Burtica, J. Schoonman, Electrochemical Determination of Diclofenac Sodium in Aqueous Solution on Cu-Doped Zeolite-Expanded Graphite-Epoxy Electrode, Electroanalysis, 22 (2010) 2058–2063.

[122] C. Karuppiah, S. Cheemalapati, S.-M. Chen, S. Palanisamy, Carboxyl-functionalized graphene oxide-modified electrode for the electrochemical determination of nonsteroidal anti-inflammatory drug diclofenac, Ionics, 21 (2015) 231–238.

[123] M.M. El-Wekil, S.A. Alkahtani, H.R.H. Ali, A.M. Mahmoud, Advanced sensing nanomaterials based carbon paste electrode for simultaneous electrochemical measurement of esomeprazole and diclofenac sodium in human serum and urine samples, Journal of Molecular Liquids, 262 (2018) 495–503.

[124] D.T. Gimenes, J.M. de Freitas, R.A.A. Munoz, E.M. Richter, Flow-Injection Amperometric Method for Determination of Diclofenac in Pharmaceutical Formulations Using a Boron-Doped Diamond Electrode, Electroanalysis, 23 (2011) 2521–2525.

[125] D.T. Gimenes, R.R. Cunha, M.M.A. de C. Ribeiro, P.F. Pereira, R.A.A. Muñoz, E.M. Richter, Two new electrochemical methods for fast and simultaneous determination of codeine and diclofenac, Talanta, 116 (2013) 1026–1032.

[126] J.A. Fracassi da Silva, C.L. do Lago, An Oscillometric Detector for Capillary Electrophoresis, Anal. Chem., 70 (1998) 4339–4343.

[127] A.J. Zemann, E. Schnell, D. Volgger, Contactless Conductivity Detection for Capillary Electrophoresis, (n.d.) 5.

[128] A.A. Elbashir, H.Y. Aboul-Enein, Recent applications and developments of capacitively coupled contactless conductivity detection (CE-C ^{4} D) in capillary electrophoresis: Recent applications of CE-C4D, Biomed. Chromatogr., 28 (2014) 1502–1506.

[129] P.D. Voegel, R.P. Baldwin, Electrochemical detection in capillary electrophoresis, Electrophoresis, 18 (1997) 2267–2278.

[130] W. Jin, J. Zhang, Determination of diclofenac sodium by capillary zone electrophoresis with electrochemical detection, Journal of Chromatography A, 868 (2000) 101–107.

[131] H. Chen, Q. Chen, Y. Zhao, F. Zhang, F. Yang, J. Tang, P. He, Electrochemiluminescence aptasensor for adenosine triphosphate detection using host–guest recognition between metallocyclodextrin complex and aptamer, Talanta, 121 (2014) 229–233.

[132] M. Huebner, E. Weber, R. Niessner, S. Boujday, D. Knopp, Rapid analysis of diclofenac in freshwater and wastewater by a monoclonal antibody-based highly sensitive ELISA, Anal Bioanal Chem, 407 (2015) 8873–8882.

[133] A. Deng, M. Himmelsbach, Q.-Z. Zhu, S. Frey, M. Sengl, W. Buchberger, R. Niessner, D. Knopp, Residue Analysis of the Pharmaceutical Diclofenac in Different Water Types Using ELISA and GC−MS, Environ. Sci. Technol., 37 (2003) 3422–3429.

[134] D. Knopp, A. Deng, M. Letzel, M. Taggart, M. Himmelsbach, Q.-Z. Zhu, I. Peröbner, B. Kudlak, S. Frey, M. Sengl, W. Buchberger, C. Hutchinson, A. Cunningham, D. Pain, R. Cuthbert, A. Raab, A. Meharg, G. Swan, Y. Jhala, V. Prakash, et al., Immunological Determination of the Pharmaceutical Diclofenac in Environmental and Biological Samples, in: I.R. Kennedy, K.R. Solomon, S.J. Gee, A.N. Crossan, S. Wang, F. Sánchez-Bayo (Eds.), Rational Environmental Management of Agrochemicals, American Chemical Society, Washington, DC, 2007: pp. 203–226.

[135] A.B. Riemer, S. Gruber, I. Pali-Schöll, T. Kinaciyan, E. Untersmayr, E. Jensen-Jarolim, Suppression of gastric acid increases the risk of developing Immunoglobulin E-mediated drug hypersensitivity: human diclofenac sensitization and a murine sensitization model, Clinical & Experimental Allergy, 40 (2010) 486–493.

[136] S. Rau, U. Hilbig, G. Gauglitz, Label-free optical biosensor for detection and quantification of the non-steroidal anti-inflammatory drug diclofenac in milk without any sample pretreatment, Anal Bioanal Chem, 406 (2014) 3377–3386.

[137] M. Pschenitza, E.S. Gavrilova, S.A. Tarasov, D. Knopp, R. Niessner, O.I. Epstein, Application of a heterogeneous immunoassay for the quality control testing of release-active forms of diclofenac, International Immunopharmacology, 21 (2014) 225–230.

[138] M. Saini, M.A. Taggart, D. Knopp, S. Upreti, D. Swarup, A. Das, P.K. Gupta, R. Niessner, V. Prakash, R. Mateo, R.J. Cuthbert, Detecting diclofenac in livestock carcasses in India with an ELISA: A tool to prevent widespread vulture poisoning, Environmental Pollution, 160 (2012) 11–16.

[139] A.K. Sharma, M. Saini, S.D. Singh, V. Prakash, A. Das, R. Bharathi Dasan, S. Pandey, D. Bohara, T.H. Galligan, R.E. Green, D. Knopp, R.J. Cuthbert, Diclofenac is toxic to the Steppe Eagle *Aquila nipalensis* : widening the diversity of raptors threatened by NSAID misuse in South Asia, Bird Conservation International, 24 (2014) 282–286.

[140] A. Hlaváček, Z. Farka, M. Hübner, V. Horňáková, D. Němeček, R. Niessner, P. Skládal, D. Knopp, H.H. Gorris, Competitive Upconversion-Linked Immunosorbent Assay for the Sensitive Detection of Diclofenac, Anal. Chem., 88 (2016) 6011–6017.

[141] W. Miao, Electrogenerated Chemiluminescence and Its Biorelated Applications, Chem. Rev., 108 (2008) 2506–2553.

[142] S. Motoc, F. Manea, A. Iacob, A. Martinez-Joaristi, J. Gascon, A. Pop, J. Schoonman, Electrochemical Selective and Simultaneous Detection of Diclofenac and Ibuprofen in Aqueous Solution Using HKUST-1 Metal-Organic Framework-Carbon Nanofiber Composite Electrode, Sensors, 16 (2016) 1719.

[143] H. Yang, H. Wang, C. Xiong, Y. Liu, R. Yuan, Y. Chai, An electrochemiluminescence immunosensor based on ABEI and FCA functionalized Platinum@Copper hierarchical trigonal bipyramid nanoframes, Electrochimica Acta, 213 (2016) 512–519.

[144] X. Fu, X. Tan, R. Yuan, S. Chen, A dual-potential electrochemiluminescence ratiometric sensor for sensitive detection of dopamine based on graphene-CdTe quantum dots and self-enhanced Ru(II) complex, Biosensors and Bioelectronics, 90 (2017) 61–68.

[145] F. Cai, Q. Zhu, K. Zhao, A. Deng, J. Li, Multiple Signal Amplified Electrochemiluminescent Immunoassay for Hg^{2+} Using Graphene-Coupled Quantum Dots and Gold Nanoparticles-Labeled Horseradish Peroxidase, Environ. Sci. Technol., 49 (2015) 5013–5020.

[146] Q. Zhu, F. Cai, J. Zhang, K. Zhao, A. Deng, J. Li, Highly sensitive electrochemiluminescent immunosensor based on gold nanoparticles-functionalized zinc oxide nanorod and poly(amidoamine)-graphene for detecting brombuterol, Biosensors and Bioelectronics, 86 (2016) 899–906.

[147] L. Hu, J. Zheng, K. Zhao, A. Deng, J. Li, An ultrasensitive electrochemiluminescent immunosensor based on graphene oxide coupled graphite-like carbon nitride and multiwalled carbon nanotubes-gold for the detection of diclofenac, Biosensors and Bioelectronics, 101 (2018) 260–267.

[148] X. Zhang, Y. Guo, M. Liu, S. Zhang, Photoelectrochemically active species and photoelectrochemical biosensors, RSC Adv., 3 (2013) 2846–2857.

[149] Z. Yue, F. Lisdat, W.J. Parak, S.G. Hickey, L. Tu, N. Sabir, D. Dorfs, N.C. Bigall, Quantum-Dot-Based Photoelectrochemical Sensors for Chemical and Biological Detection, ACS Appl. Mater. Interfaces, 5 (2013) 2800–2814.

[150] T.M. do Prado, F.H. Cincotto, O. Fatibello-Filho, F. Cruz de Moraes, Bismuth Vanadate/Reduced Graphene Oxide Nanocomposite Electrode for Photoelectrochemical Determination of Diclofenac in Urine, Electroanalysis, 30 (2018) 2704–2711.

[151] J. Gong, T. Fang, D. Peng, A. Li, L. Zhang, A highly sensitive photoelectrochemical detection of perfluorooctanic acid with molecularly imprined polymer-functionalized nanoarchitectured hybrid of AgI–BiOI composite, Biosensors and Bioelectronics, 73 (2015) 256–263.

[152] K. Yan, Y. Liu, Y. Yang, J. Zhang, A Cathodic "Signal-off" Photoelectrochemical Aptasensor for Ultrasensitive and Selective Detection of Oxytetracycline, Anal. Chem., 87 (2015) 12215–12220.

[153] W.-W. Zhao, Z.-Y. Ma, D.-Y. Yan, J.-J. Xu, H.-Y. Chen, *In Situ* Enzymatic Ascorbic Acid Production as Electron Donor for CdS Quantum Dots Equipped TiO_2 Nanotubes: A General and Efficient Approach for New Photoelectrochemical Immunoassay, Anal. Chem., 84 (2012) 10518–10521.

[154] Y.-J. Li, M.-J. Ma, J.-J. Zhu, Dual-Signal Amplification Strategy for Ultrasensitive Photoelectrochemical Immunosensing of α-Fetoprotein, Anal. Chem., 84 (2012) 10492–10499.

[155] M. Zhao, G.-C. Fan, J.-J. Chen, J.-J. Shi, J.-J. Zhu, Highly Sensitive and Selective Photoelectrochemical Biosensor for Hg^{2+} Detection Based on Dual Signal Amplification by Exciton Energy Transfer Coupled with Sensitization Effect, Anal. Chem., 87 (2015) 12340–12347.

[156] Y. Zang, J. Lei, Q. Hao, H. Ju, "Signal-On" Photoelectrochemical Sensing Strategy Based on Target-Dependent Aptamer Conformational Conversion for Selective Detection of Lead(II) Ion, ACS Appl. Mater. Interfaces, 6 (2014) 15991–15997.

[157] G.-L. Wang, J.-X. Shu, Y.-M. Dong, X.-M. Wu, W.-W. Zhao, J.-J. Xu, H.-Y. Chen, Using G-Quadruplex/Hemin To "Switch-On" the Cathodic Photocurrent of p-Type PbS Quantum Dots: Toward a Versatile Platform for Photoelectrochemical Aptasensing, Anal. Chem., 87 (2015) 2892–2900.

[158] F. Liu, Y. Zhang, J. Yu, S. Wang, S. Ge, X. Song, Application of ZnO/graphene and S6 aptamers for sensitive photoelectrochemical detection of SK-BR-3 breast cancer cells based on a disposable indium tin oxide device, Biosensors and Bioelectronics, 51 (2014) 413–420.

[159] O.K. Okoth, K. Yan, Y. Liu, J. Zhang, Graphene-doped Bi2S3 nanorods as visible-light photoelectrochemical aptasensing platform for sulfadimethoxine detection, Biosensors and Bioelectronics, 86 (2016) 636–642.

[160] Y. Liu, K. Yan, O.K. Okoth, J. Zhang, A label-free photoelectrochemical aptasensor based on nitrogen-doped graphene quantum dots for chloramphenicol determination, Biosensors and Bioelectronics, 74 (2015) 1016–1021.

[161] O.K. Okoth, K. Yan, J. Feng, J. Zhang, Label-free photoelectrochemical aptasensing of diclofenac based on gold nanoparticles and graphene-doped CdS, Sensors and Actuators B: Chemical, 256 (2018) 334–341.

[162] T. Shi, Z. Wen, L. Ding, Q. Liu, Y. Guo, C. Ding, K. Wang, Visible/near-infrared light response VOPc/carbon nitride nanocomposites: VOPc sensitizing carbon nitride to improve photo-to-current conversion efficiency for fabricating photoelectrochemical diclofenac aptasensor, Sensors and Actuators B: Chemical, 299 (2019) 126834.

[163] H. Derikvand, M. Roushani, A.R. Abbasi, Z. Derikvand, A. Azadbakht, Design of folding-based impedimetric aptasensor for determination of the nonsteroidal anti-inflammatory drug, Analytical Biochemistry, 513 (2016) 77–86.

[164] W. Chen, Q. Zhu, Q. Tang, K. Zhao, A. Deng, J. Li, Ultrasensitive detection of diclofenac based on electrochemiluminescent immunosensor with multiple signal amplification strategy of palladium attached graphene oxide as bioprobes and ceria doped zinc oxide as substrates, Sensors and Actuators B: Chemical, 268 (2018) 411–420.

[165] T.T.K. Nguyen, T.T. Vu, G. Anquetin, H.V. Tran, S. Reisberg, V. Noël, G. Mattana, Q.V. Nguyen, T. Dai Lam, M.C. Pham, B. Piro, Enzyme-less electrochemical displacement heterogeneous immunosensor for diclofenac detection, Biosensors and Bioelectronics, 97 (2017) 246–252.

[166] A. Ambrosi, R. Antiochia, L. Campanella, R. Dragone, I. Lavagnini, Electrochemical determination of pharmaceuticals in spiked water samples, Journal of Hazardous Materials, 122 (2005) 219–225.

[167] D. Thevenot, K. Toth, R. Durst, G. Wilson, Electrochemical biosensors: recommended definitions and classification, (2001) 12.

[168] D. Thevenot, K. Toth, R. Durst, G. Wilson, Electrochemical biosensors: recommended definitions and classification, Pure Appl. Chem., (1999) 17.

[169] J. Shah, E. Wilkins, Electrochemical Biosensors for Detection of Biological Warfare Agents, Electroanalysis, 15 (2003) 157–167.

[170] T. Hermann, D.J. Patel, Adaptive Recognition by Nucleic Acid Aptamers, Science, New Series, 287 (2000) 820–825.

[171] L. Hu, Z. Bian, H. Li, S. Han, Y. Yuan, L. Gao, G. Xu, [Ru(bpy) $_2$ dppz] $^{2+}$ Electrochemiluminescence Switch and Its Applications for DNA Interaction Study and Label-free ATP Aptasensor, Anal. Chem., 81 (2009) 9807–9811.

[172] S. Centi, S. Tombelli, M. Minunni, M. Mascini, Aptamer-Based Detection of Plasma Proteins by an Electrochemical Assay Coupled to Magnetic Beads, Anal. Chem., 79 (2007) 1466–1473.

[173] N. de-los-Santos-Álvarez, M.J. Lobo-Castañón, A.J. Miranda-Ordieres, P. Tuñón-Blanco, Modified-RNA Aptamer-Based Sensor for Competitive Impedimetric Assay of Neomycin B, J. Am. Chem. Soc., 129 (2007) 3808–3809.

[174] E. Golub, G. Pelossof, R. Freeman, H. Zhang, I. Willner, Electrochemical, Photoelectrochemical, and Surface Plasmon Resonance Detection of Cocaine Using Supramolecular Aptamer Complexes and Metallic or Semiconductor Nanoparticles, Analytical Chemistry, 81 (2009) 9291–9298.

[175] C.B. Joeng, J.H. Niazi, S.J. Lee, M.B. Gu, ssDNA aptamers that recognize diclofenac and 2-anilinophenylacetic acid, Bioorganic & Medicinal Chemistry, 17 (2009) 5380–5387.

[176] B. Strehlitz, C. Reinemann, S. Linkorn, R. Stoltenburg, Aptamers for pharmaceuticals and their application in environmental analytics, Bioanalytical Reviews, 4 (2012) 1–30.

[177] F. Radom, P.M. Jurek, M.P. Mazurek, J. Otlewski, F. Jele?, Aptamers: Molecules of great potential, Biotechnology Advances, 31 (2013) 1260–1274.

[178] S. Balamurugan, A. Obubuafo, S.A. Soper, R.L. McCarley, D.A. Spivak, Designing Highly Specific Biosensing Surfaces Using Aptamer Monolayers on Gold, Langmuir, 22 (2006) 6446–6453.

[179] S. Tombelli, M. Minunni, M. Mascini, Analytical applications of aptamers, Biosensors and Bioelectronics, 20 (2005) 2424–2434.

[180] C. Hamula, J. Guthrie, H. Zhang, X. Li, X. Le, Selection and analytical applications of aptamers, TrAC Trends in Analytical Chemistry, 25 (2006) 681–691.

[181] S. Tom, H.-E. Jin, S.-W. Lee, Aptamers as functional bionanomaterials for sensor applications, in: Engineering of Nanobiomaterials, Elsevier, 2016: pp. 181–226.

[182] K. Ohsawa, T. Kasamatsu, J. Nagashima, K. Hanawa, M. Kuwahara, H. Ozaki, H. Sawai, Arginine-modified DNA Aptamers That Show Enantioselective Recognition of the Dicarboxylic Acid Moiety of Glutamic Acid, Anal. Sci., 24 (2008) 167–172.

[183] J. Wang, A. Munir, H.S. Zhou, Au NPs-aptamer conjugates as a powerful competitive reagent for ultrasensitive detection of small molecules by surface plasmon resonance spectroscopy, Talanta, 79 (2009) 72–76.

[184] H. Huang, G. Jie, R. Cui, J.-J. Zhu, DNA aptamer-based detection of lysozyme by an electrochemiluminescence assay coupled to quantum dots, Electrochemistry Communications, 11 (2009) 816–818.

[185] N. Li, C.-M. Ho, Aptamer-Based Optical Probes with Separated Molecular Recognition and Signal Transduction Modules, J. Am. Chem. Soc., 130 (2008) 2380–2381.

[186] V. Pavlov, Y. Xiao, B. Shlyahovsky, I. Willner, Aptamer-Functionalized Au Nanoparticles for the Amplified Optical Detection of Thrombin, J. Am. Chem. Soc., 126 (2004) 11768–11769.

[187] C. Yao, Y. Qi, Y. Zhao, Y. Xiang, Q. Chen, W. Fu, Aptamer-based piezoelectric quartz crystal microbalance biosensor array for the quantification of IgE, Biosensors and Bioelectronics, 24 (2009) 2499–2503.

[188] J. Elbaz, B. Shlyahovsky, D. Li, I. Willner, Parallel Analysis of Two Analytes in Solutions or on Surfaces by Using a Bifunctional Aptamer: Applications for Biosensing and Logic Gate Operations, ChemBioChem, 9 (2008) 232–239.

[189] T. Hianik, J. Wang, Electrochemical Aptasensors - Recent Achievements and Perspectives, Electroanalysis, 21 (2009) 1223–1235.

[190] M. Mir, A.T.A. Jenkins, I. Katakis, Ultrasensitive detection based on an aptamer beacon electron transfer chain, Electrochemistry Communications, 10 (2008) 1533–1536.

[191] A. Sassolas, L.J. Blum, B.D. Leca-Bouvier, Electrochemical Aptasensors, Electroanalysis, 21 (2009) 1237–1250.

[192] A.D. Ellington, J.W. Szostak, In vitro selection of RNA molecules that bind specific ligands, Nature, 346 (1990) 818–822.

[193] C. Tuerk, L. Gold, Systematic evolution of ligands by exponential enrichment: RNA ligands to bacteriophage T4 DNA polymerase, Science, 249 (1990) 505–510.

[194] S.D. Jayasena, Aptamers: An Emerging Class of Molecules That Rival Antibodies in Diagnostics, Clinical Chemistry, (1999) 23.

[195] A. De Girolamo, M. McKeague, M. Pascale, M. Cortese, M.C. DeRosa, Immobilization of Aptamers on Substrates, in: Y. Dong (Ed.), Aptamers for Analytical Applications, Wiley-VCH Verlag GmbH & Co. KGaA, Weinheim, Germany, 2018: pp. 85–126.

[196] S. Nimse, K. Song, M. Sonawane, D. Sayyed, T. Kim, Immobilization Techniques for Microarray: Challenges and Applications, Sensors, 14 (2014) 22208–22229.

[197] S. Balamurugan, A. Obubuafo, S.A. Soper, D.A. Spivak, Surface immobilization methods for aptamer diagnostic applications, Analytical and Bioanalytical Chemistry, 390 (2008) 1009–1021.

[198] L. Zhou, M.-H. Wang, J.-P. Wang, Z.-Z. Ye, Application of Biosensor Surface Immobilization Methods for Aptamer, Chinese Journal of Analytical Chemistry, 39 (2011) 432–438.

[199] M. Du, T. Yang, C. Zhao, K. Jiao, Electrochemical logic aptasensor based on graphene, Sensors and Actuators B: Chemical, 169 (2012) 255–260.

[200] A. Sassolas, B.D. Leca-Bouvier, L.J. Blum, DNA Biosensors and Microarrays, Chem. Rev., 108 (2008) 109–139.

[201] C. Heise, F.F. Bier, Immobilization of DNA on Microarrays, in: Springer-Verlag, Berlin/Heidelberg, 2005.

[202] C. Wittmann, C. Marquette, DNA Immobilization, in: R.A. Meyers (Ed.), Encyclopedia of Analytical Chemistry, John Wiley & Sons, Ltd, Chichester, UK, 2012: p. a9210.

[203] S. Nimse, K. Song, M. Sonawane, D. Sayyed, T. Kim, Immobilization Techniques for Microarray: Challenges and Applications, Sensors, 14 (2014) 22208–22229.

[204] I. Bravo, T. García-Mendiola, M. Revenga-Parra, F. Pariente, E. Lorenzo, Diazonium salt click chemistry based multiwall carbon nanotube electrocatalytic platforms, Sensors and Actuators B: Chemical, 211 (2015) 559–568.

[205] F. Rohrbach, H. Karadeniz, A. Erdem, M. Famulok, G. Mayer, Label-free impedimetric aptasensor for lysozyme detection based on carbon nanotube-modified screen-printed electrodes, Analytical Biochemistry, 421 (2012) 454–459.

[206] D. Xie, C. Li, L. Shangguan, H. Qi, D. Xue, Q. Gao, C. Zhang, Click chemistry-assisted self-assembly of DNA aptamer on gold nanoparticles-modified screen-printed carbon electrodes for label-free electrochemical aptasensor, Sensors and Actuators B: Chemical, 192 (2014) 558–564.

[207] M.I. Pividori, A. Lermo, A. Bonanni, S. Alegret, M. del Valle, Electrochemical immunosensor for the diagnosis of celiac disease, Analytical Biochemistry, 388 (2009) 229–234.

[208] A. Bonanni, M.I. Pividori, M. del Valle, Application of the avidin–biotin interaction to immobilize DNA in the development of electrochemical impedance genosensors, Analytical and Bioanalytical Chemistry, 389 (2007) 851–861.

[209] K. Zhang, M. Xie, B. Zhou, Y. Hua, Z. Yan, H. Liu, L. Guo, B. Wu, B. Huang, A new strategy based on aptasensor to time-resolved fluorescence assay for adenosine deaminase activity, Biosensors and Bioelectronics, 41 (2013) 123–128.

[210] H. Bai, R. Wang, B. Hargis, H. Lu, Y. Li, A SPR Aptasensor for Detection of Avian Influenza Virus H5N1, Sensors, 12 (2012) 12506–12518.

[211] R.C. Ebersole, J.A. Miller, J.R. Moran, M.D. Ward, Spontaneously formed functionally active avidin monolayers on metal surfaces: a strategy for immobilizing biological reagents and design of piezoelectric biosensors, Journal of the American Chemical Society, 112 (1990) 3239–3241.

[212] J. Becker, M. Wilchek, Inactivation by avidin of biotin-modified bacteriophage, Biochimica et Biophysica Acta (BBA) - General Subjects, 264 (1972) 165–170.

[213] D. Samanta, A. Sarkar, Immobilization of bio-macromolecules on self-assembled monolayers: methods and sensor applications, Chem. Soc. Rev., 40 (2011) 2567.

[214] J.C. Love, L.A. Estroff, J.K. Kriebel, R.G. Nuzzo, G.M. Whitesides, Self-Assembled Monolayers of Thiolates on Metals as a Form of Nanotechnology, Chem. Rev., 105 (2005) 1103–1170.

[215] Y. Liu, T. Kwa, A. Revzin, Simultaneous detection of cell-secreted TNF-α and IFN-γ using micropatterned aptamer-modified electrodes, Biomaterials, 33 (2012) 7347–7355.

[216] X. Zhang, V.K. Yadavalli, Surface immobilization of DNA aptamers for biosensing and protein interaction analysis, Biosensors and Bioelectronics, 26 (2011) 3142–3147.

[217] Y. Wang, J. Feng, Z. Tan, H. Wang, Electrochemical impedance spectroscopy aptasensor for ultrasensitive detection of adenosine with dual backfillers, Biosensors and Bioelectronics, 60 (2014) 218–223.

[218] T. Bao, H. Shu, W. Wen, X. Zhang, S. Wang, A sensitive electrochemical aptasensor for ATP detection based on exonuclease III-assisted signal amplification strategy, Analytica Chimica Acta, 862 (2015) 64–69.

[219] I. Palchetti, M. Mascini, Electrochemical Adsorption Technique for Immobilization of Single-Stranded Oligonucleotides onto Carbon Screen-Printed Electrodes, in: C. Wittmann (Ed.), Immobilisation of DNA on Chips II, Springer-Verlag, Berlin/Heidelberg, 2006: pp. 27–43.

[220] C.C. Mayorga Martinez, E.F. Treo, R.E. Madrid, C.C. Felice, Evaluation of chrono-impedance technique as transduction method for a carbon paste/glucose oxidase (CP/GOx) based glucose biosensor, Biosensors and Bioelectronics, 26 (2010) 1239–1244.

[221] M. Shamsipur, S.H. Kazemi, M.F. Mousavi, Impedance studies of a nano-structured conducting polymer and its application to the design of reliable scaffolds for impedimetric biosensors, Biosensors and Bioelectronics, 24 (2008) 104–110.

[222] E. Katz, I. Willner, Probing Biomolecular Interactions at Conductive and Semiconductive Surfaces by Impedance Spectroscopy: Routes to Impedimetric Immunosensors, DNA-Sensors, and Enzyme Biosensors, Electroanalysis, 15 (2003) 913–947.

[223] A.-E. Radi, J.L. Acero Sánchez, E. Baldrich, C.K. O'Sullivan, Reusable Impedimetric Aptasensor, Analytical Chemistry, 77 (2005) 6320–6323.

[224] M.C. Rodriguez, A.-N. Kawde, J. Wang, Aptamer biosensor for label-free impedance spectroscopy detection of proteins based on recognition-induced switching of the surface charge, Chem. Commun., (2005) 4267.

[225] M. Zayats, Y. Huang, R. Gill, C. Ma, I. Willner, Label-Free and Reagentless Aptamer-Based Sensors for Small Molecules, J. Am. Chem. Soc., 128 (2006) 13666–13667.

[226] H. Omidian, K. Park, Hydrogels, in: J. Siepmann, R.A. Siegel, M.J. Rathbone (Eds.), Fundamentals and Applications of Controlled Release Drug Delivery, Springer US, Boston, MA, 2012: pp. 75–105.

[227] H. Omidian, K. Park, Engineered High Swelling Hydrogels, in: R.M. Ottenbrite, K. Park, T. Okano (Eds.), Biomedical Applications of Hydrogels Handbook, Springer New York, New York, NY, 2010: pp. 351–374.

[228] M. Rubinstein, A.V. Dobrynin, Associations leading to formation of reversible networks and gels, Current Opinion in Colloid & Interface Science, 4 (1999) 83–87.

[229] F. Ilmain, T. T., K. E., Volume transition in a gel driven by hydrogen bonding, Nature, 349 (1991) 400–401.

[230] R. Skouri, F. Schosseler, J.P. Munch, S.J. Candau, Swelling and Elastic Properties of Polyelectrolyte Gels, Macromolecules, 28 (1995) 197–210.

[231] C. Karakasyan, M. Legros, S. Lack, F. Brunel, P. Maingault, G. Ducouret, D. Hourdet, Cold Gelation of Alginates Induced by Monovalent Cations, Biomacromolecules, 11 (2010) 2966–2975.

[232] D.C. Tuncaboylu, M. Sari, W. Oppermann, O. Okay, Tough and Self-Healing Hydrogels Formed via Hydrophobic Interactions, Macromolecules, 44 (2011) 4997–5005.

[233] G. Miquelard-Garnier, C. Creton, D. Hourdet, Synthesis and Viscoelastic Properties of Hydrophobically Modified Hydrogels, Macromol. Symp., 256 (2007) 189–194.

[234] D. Buenger, F. Topuz, J. Groll, Hydrogels in sensing applications, Progress in Polymer Science, 37 (2012) 1678–1719.

[235] K.M. Gupta, S.R. Barnes, R.A. Tangaro, M.C. Roberts, D.H. Owen, D.F. Katz, P.F. Kiser, Temperature and pH Sensitive Hydrogels: An Approach Towards Smart Semen-Triggered Vaginal Microbicidal Vehicles, Journal of Pharmaceutical Sciences, 96 (2007) 670–681.

[236] B. Zhao, J.S. Moore, Fast pH- and Ionic Strength-Responsive Hydrogels in Microchannels, Langmuir, 17 (2001) 4758–4763.

[237] L. Feng, L. Wang, Z. Hu, Y. Tian, Y. Xian, L. Jin, Encapsulation of horseradish peroxidase into hydrogel, and its bioelectrochemistry, Microchimica Acta, 164 (2009) 49–54.

[238] M.E. Harmon, T.A.M. Jakob, W. Knoll, C.W. Frank, A Surface Plasmon Resonance Study of Volume Phase Transitions in *N* -Isopropylacrylamide Gel Films, Macromolecules, 35 (2002) 5999–6004.

[239] D. Bhatta, G. Christie, B. Madrigal-González, J. Blyth, C.R. Lowe, Holographic sensors for the detection of bacterial spores, Biosensors and Bioelectronics, 23 (2007) 520–527.

[240] R. Bashir, J.Z. Hilt, O. Elibol, A. Gupta, N.A. Peppas, Micromechanical cantilever as an ultrasensitive pH microsensor, Appl. Phys. Lett., 81 (2002) 3091–3093.

[241] L. Liang, Temperature-sensitive membranes prepared by UV photopolymerization of N-isopropylacrylamide on a surface of porous hydrophilic polypropylene membranes, Journal of Membrane Science, 162 (1999) 235–246.

[242] A. Richter, A. Bund, M. Keller, K.-F. Arndt, Characterization of a microgravimetric sensor based on pH sensitive hydrogels, Sensors and Actuators B: Chemical, 99 (2004) 579–585.

[243] J. Sorber, G. Steiner, V. Schulz, M. Guenther, G. Gerlach, R. Salzer, K.-F. Arndt, Hydrogel-Based Piezoresistive pH Sensors: Investigations Using FT-IR Attenuated Total Reflection Spectroscopic Imaging, Anal. Chem., 80 (2008) 2957–2962.

[244] F.R. Aussenegg, H. Brunner, A. Leitner, Ch. Lobmaier, Th. Schalkhammer, F. Pittner, The metal island coated swelling polymer over mirror system (MICSPOMS): a new principle for measuring ionic strength, Sensors and Actuators B: Chemical, 29 (1995) 204–209.

[245] M. Guenther, D. Kuckling, C. Corten, G. Gerlach, J. Sorber, G. Suchaneck, K. Arndt, Chemical sensors based on multiresponsive block copolymer hydrogels, Sensors and Actuators B: Chemical, 126 (2007) 97–106.

[246] S. Gupta, D. Kuckling, K. Kretschmer, V. Choudhary, H.-J. Adler, Synthesis and characterization of stimuli-sensitive micro- and nanohydrogels based on photocrosslinkable poly(dimethylaminoethyl methacrylate), J. Polym. Sci. A Polym. Chem., 45 (2007) 669–679.

[247] D. Matsukuma, K. Yamamoto, T. Aoyagi, Stimuli-Responsive Properties of *N* -Isopropylacrylamide-Based Ultrathin Hydrogel Films Prepared by Photo-Cross-Linking, Langmuir, 22 (2006) 5911–5915.

[248] J.M.D. Heijl, F.E. Du Prez, Fast, multi-responsive microgels based on photo-crosslinkable poly(2-(dimethylamino)ethyl methacrylate), Polymer, 45 (2004) 6771–6778.

[249] J. Hoffmann, M. Plötner, D. Kuckling, W.-J. Fischer, Photopatterning of thermally sensitive hydrogels useful for microactuators, Sensors and Actuators A: Physical, 77 (1999) 139–144.

[250] H. Liu, Y. Ito, Gradient micropattern immobilization of a thermo-responsive polymer to investigate its effect on cell behavior, J. Biomed. Mater. Res., 67A (2003) 1424–1429.

[251] I. Tokarev, S. Minko, Stimuli-responsive hydrogel thin films, Soft Matter, 5 (2009) 511–524.

[252] R. Jin, P.J. Dijkstra, J. Feijen, Rapid gelation of injectable hydrogels based on hyaluronic acid and poly(ethylene glycol) via Michael-type addition, Journal of Controlled Release, 148 (2010) e41–e43.

[253] R. Toomey, D. Freidank, J. Rühe, Swelling Behavior of Thin, Surface-Attached Polymer Networks, Macromolecules, 37 (2004) 882–887.

[254] J.S. Sharp, R.A.L. Jones, Micro-buckling as a Route Towards Surface Patterning, Adv. Mater., (2002) 4.

[255] J.S. Sharp, R.A.L. Jones, Swelling-induced morphology in ultrathin supported films of poly (d , l − lactide), Phys. Rev. E, 66 (2002) 011801.

[256] T. Tayoichi, S. Shao-Tang, H. Yoshitsugu, K. Seiji, K. John, H. Yoshiharu, A. Takayuki, Mechanical instability of gels at the phase transition, Nature, 325 (1987) 796–798.

[257] M. Orlov, I. Tokarev, A. Scholl, A. Doran, S. Minko, pH-Responsive Thin Film Membranes from Poly(2-vinylpyridine): Water Vapor-Induced Formation of a Microporous Structure, Macromolecules, 40 (2007) 2086–2091.

[258] I. Tokarev, M. Orlov, E. Katz, S. Minko, An Electrochemical Gate Based on a Stimuli-Responsive Membrane Associated with an Electrode Surface, J. Phys. Chem. B, 111 (2007) 12141–12145.

CHAPTER 2:
MATERIALS AND METHODS

CHAPTER 2 : MATERIALS AND METHODS

In this chapter are detailed the experimental steps for the construction of the aptasensor *i.e.,* the material and methods used for: the fabrication of surface attached hydrogel thin films with tunable and well controlled chemistry, the covalent immobilization of aptamers on the surface attached hydrogel thin film, and also the techniques used for characterization of the aptasensor.

2.1 Materials

2.1.1 Chemicals and Buffers

Poly(acrylic acid) (PAA) (M_W~250 kg/mol, 35 wt% solution in water), allylamine, N-hydroxysuccinimide (NHS), 1-ethyl-3-(3-dimethylaminopropyl) carbodiimide (EDC), 1,4-dithioerythritol (DTE), diclofenac (DCL), potassium ferricyanide [$K_3Fe(CN)_6$], potassium ferricyanide [$K_4Fe(CN)_6$], and potassium/sodium phosphate monobasic/dibasic were purchased from Sigma-Aldrich and were used as received. Sodium hydroxide, sodium chloride, chloroform, methanol, formic acid solvents were also purchased from Sigma-Aldrich.

PBS1 was used for activation of the carboxylic groups of the hydrogel, and PBS2 was used for the preparation of aptamer solution. 100 µM aptamer stock solution was prepared and stored at −20 °C and the working aptamer solutions were prepared by diluting to the desired final concentration. Other chemicals used in this study were of analytical grade and used as supplied unless otherwise stated. Deionized water (18.2 MΩ/cm) purified by a Pure Labflex system (Elga Water, Veolia, France) was used throughout the experiment for aqueous solution preparation. For the determination of DCL in water sample, a stock solution of 100 mM DCL was daily prepared, and was then diluted at different concentrations using 200 µL binding washing buffer (BWB).

Table 2.1: Names and compositions of the different buffer solutions employed in this thesis

Buffer Name	pH	Chemical Composition
PBS1	6.2	0.1 M KH_2PO_4 , 0.1 M NaOH
PBS2	7.4	0.1 M KH_2PO_4 ,0.1 M NaOH
BWB	7.4	2 mM Tris–HCl containing 10 mM NaCl, 0.5 mM KCl, 0.2 mM $MgCl_2$, 0.1 mM $CaCl_2$ and 5% ethanol
Phosphoric acid buffer	3	40 mM NaH_2PO_4,Phosphoric acid
Boric acid-borax buffer	9	0.2 M boric acid,0.05 M borax

The aptamer used for sensing (amine terminated fluorescently labeled DCL aptamer (75 bases)) had the 5'-/5AmMC6/ATA CCA GCT TAT TCA ATT GCA ACG TGG CGG TCA GTC AGC GGG TGG TGG GTT CGG TCC AGA TAG TAA GTG CAA TCT/36-FAM/-3' sequence [1] and was purchased from Integrated DNA technologies.

2.1.2 Equipment

Electrochemical Workstation

A conventional three-electrode cell was employed with a Saturated Calomel Electrode (SCE) as the reference electrode, a platinum wire as counter electrode and modified gold electrode as working electrode. All cyclic voltammograms and EIS measurements were carried out using a Bio-Logic instrument (Bio-Logic SP-300), see figure 2.1. EC-Lab software were used for the acquisition of the data and the control of the experiments.

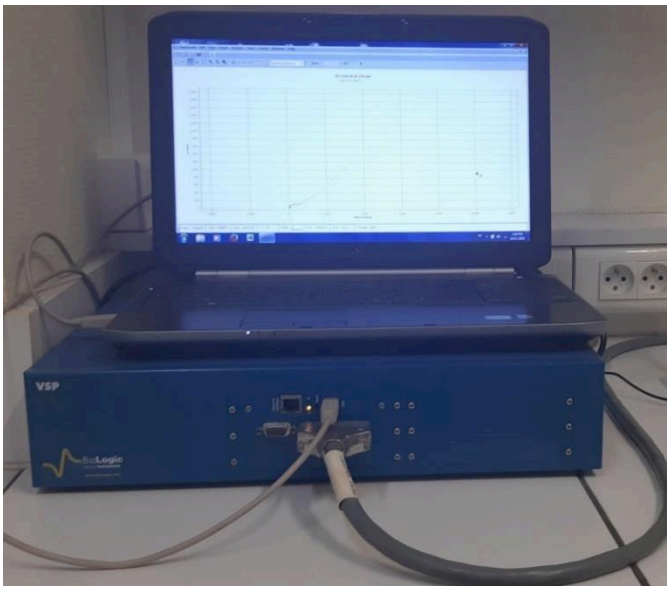

Figure 2.1: A photograph of Bio-Logic SP-300 equipment

Atomic Force Microscopy

AFM images were made at ESPCI and were acquired with a Bruker ICON microscope controlled by a Nanoscope V software, see figure 2.2. The thickness of the gold electrode and the PAA hydrogel is determined at the edge of the pattern. The height images of the surface of gold and the

hydrogel films in air were obtained in tapping mode at 300 kHz with a standard tip of stiffness 40 N/m. The roughness is defined as the half width of the height distribution histogram extracted from the images [2]. As very soft matter is probed, a tip with a lower stiffness is preferred if the adhesion is not preponderant. In our case, a compromise is chosen with a typical contact tip with a stiffness of 0.2 N/m.

To probe hydrogel films in water, the Peak Force mode is preferred when imaging soft matter in water. In this mode, the probe and the sample are intermittently brought into contact for a short period and can be viewed as a succession of approach-retract curves performed at high frequency (1 kHz) and limited by a maximum set force which can be finely tuned. This mode allows to reduce the lateral and shear forces during the scanning. The Peak Forces images in water were obtained using a cantilever of stiffness of 0.7 N/m, with a typical Force Set Point of 1nN. The amplitude of the tapping was about 200 nm. The size of the images is 1 μm.

Figure 2.2: A photograph of Bruker ICON AFM

Scanning Electron Microscope

A scanning electron microscope (SEM) was used to visualize the different stage of electrode construction. The secondary electron imaging of the different stages of construction was done using FEI Thermo Fischer Magellan SEM equipped with a FEG source, see figure 2.3.

Figure 2.3: A photograph of FEI Thermo Fischer Scanning Electron Microscope

ATR-FTIR Spectroscopy

For Attenuated Total Reflectance-Fourier Transform Infra-Red (ATR-FTIR) spectroscopy measurements, Agilent Cary 660 apparatus was used coupled with resolution Pro software, see figure 2.4. The spectra are recorded with a resolution of 4 cm^{-1} and a 256-scan accumulation. 1H NMR spectroscopy was recorded on a 400 MHz Bruker spectrometer. The solvents used was deuterium oxide (D_2O) for ene-functionalized poly (acrylic acid).

Figure 2.4: A photograph of Agilent Cary 660 apparatus

Ellipsometry

The laser *ellipsometer* SE 400adv was used to characterize the optical properties of the deposited gold layer (n, k), as well as the dry thicknesses of our hydrogel. A multilayer model of a flat film is applied for the fitting of the experimentally measured ellipsometric angles Ψ and Δ, including the native silica layer, the thiol layer and the gel layer.

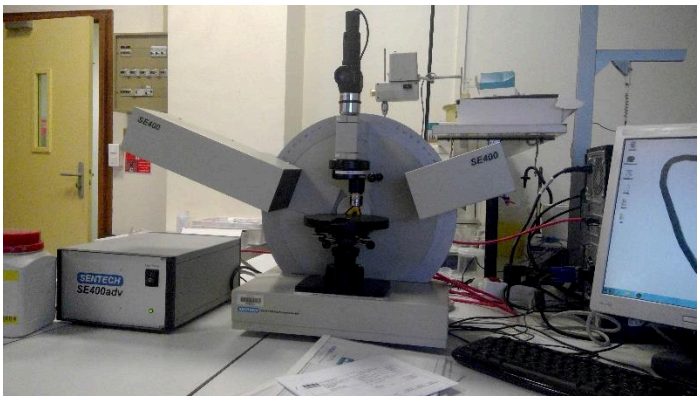

Figure 2.5: A photograph of Sentech SE-400 laser ellipsometer

Contact Angle Measurement

Contact angle measurements were performed for surface characterization of all layers in biosensors construction using the sessile drop method with KRUSS drop shape analyzer. During the experiments, a drop of distilled water was dripped into each surface. The drop profile was recorded with a CCD camera allowed monitoring the changes in contact angle for each surface. All reported data were given as the average of ten measurements ± SD.

Figure 2.6: A photograph of Drop shape analyzer

Thermal Evaporator System

Thermal Evaporation of gold was carried out through means of locally heating a small amount of gold to temperatures high enough to cause melting, where by energetic atoms of gold then escape and condense on cold surfaces undergoing solidification. A photograph of a BOC Edwards Auto 500 evaporator system is shown in Figure 2.7.

Figure 2.7: A photograph of a BOC Edwards Auto 500 evaporator system

Other equipment used:

- Pico plasma system (Diener electronic, Germany)
- WS-650HZ-23NPP Spin Coater (Laurell Technologies,USA)
- Vacuum drying oven VC-20 (Salvis Lab, Switzerland)
- Alpha 1-2 LDplus Freeze dryer (Martin Christ, Germany)
- UV lamp (Horiba Scientifc, Japan)
- UV-KUB 2 (Kloe, France)

2.1.3 Electrodes

A homemade working electrode was prepared, as a thin layer gold electrode deposited on silicon wafer using a positive photolithography process, see Figure 2.8. To this end, N-type phosphorous doped silicon wafer with 100 orientations (resistivity: 1-20 ohm.cm) were used as substrates in the preparation of evaporated gold films.

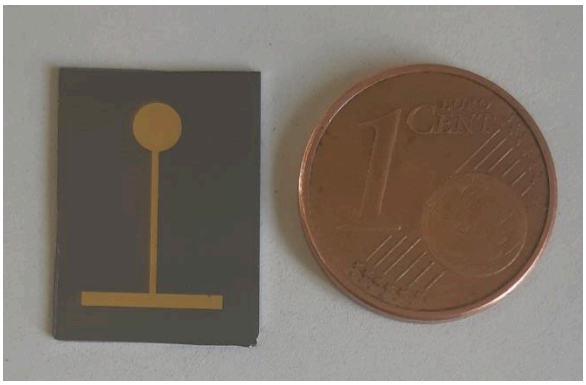

Figure 2.8: A photograph of the home-made gold electrode using positive photolithography process

2.2 METHODS

2.2.1 Fabrication of the gold electrode transducer

The detailed procedure and optimization for obtaining gold electrodes by the lift-off technique on a silicon wafer is detailed in the following chapter. Briefly, the silicon wafers were cleaned by oxygen plasma prior to coating to promote adhesion and cleanliness and a UV lithography and lift-off processes were used to pattern 100 nm gold onto 12 nm chromium adhesion layer deposited by electron-beam evaporation. Acetone removed the bulk of the resist and a 2 min ultra-sonication step removed residual resist. Finally, the wafers were diced to have the desired configuration.

2.2.2 Method for cleaning the gold film surface

As such, in electrochemical experiments, the quality of the active surface will affect the measurements. The peak currents in cyclic voltammetry and the frequency response during electrochemical impedance spectroscopy will be dependent on the surface composition of the gold. It has been demonstrated by our experiments that the gold electrodes fabricated using the photolithography process were subjected to ambient contaminants affecting the electrochemical behavior. Hence, before the evaporated gold is chemically modified for another use, it must be cleaned.

We slightly modified a protocol described by L. M Fischer *et al*. [3] in which they describe the application of nine treatments means to clean the surface of gold, including soaking an electrode in a solution of KOH (50 mM) and H_2O_2 at 25 % for 10 min and then do a potential sweep between -200 mV and -1200 mV (*vs* Ag/AgCl) at a scan rate of 50 mV/s in a solution of KOH at 50 mM.

Our modified protocol for cleaning the gold thin film electrode were cleaning in a solution of 50 mM NaOH and 25 % H_2O_2 for 30 minutes without doing a potential sweep. The electrodes were then characterized for the efficiency of the cleaning method by cyclic voltammetry at 50 mV/s in $K_3[Fe(CN)_6]$ aqueous solution to check the reversibility of redox couple and compare experimental to theoretical peak currents.

2.2.3 Functionalization of the gold electrode surface

In this study, the functionalization of the cleaned gold electrodes was performed by means of a self-assembled monolayer technique. Modification of electrodes by self-assembled monolayers are very attractive due to simplicity and quickness of this approach [4]. Well-defined self-assembled monolayer of thiols is formed as a result of strong chemisorption between gold and

sulfur atoms of thiols [5]. The self-assembled monolayer of thiols should expose the biggest number of functional groups for providing favorable thiol-ene click chemistry. To achieve the best analytical parameters for the sensor, we experimented (i) both dip coating the electrodes and spotting the solution on, (ii) different thiolation times but the optimized protocol used for the cleaned gold electrode was immersing into 1 mM fresh dithioerythritol (DTE) in chloroform for 2 hours at room temperature. The thiol-modified electrodes were then rinsed in chloroform in ultrasonic bath, to remove unreacted thiol, and dried with nitrogen flow.

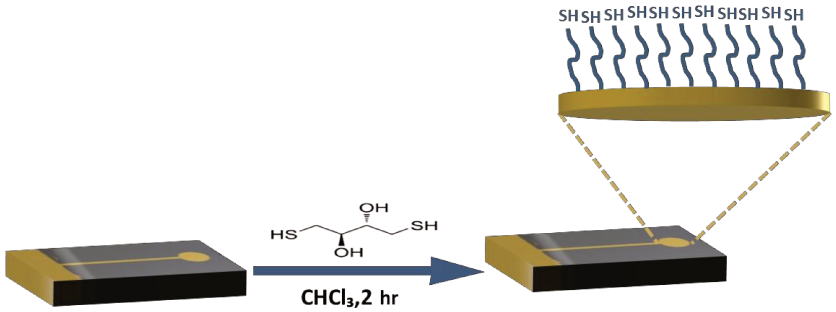

Figure 2.9: Dithiol functionalized gold surface

2.2.4 Synthesis of ene-reactive PAA polymer

Poly(acrylic acid) polymer chains were randomly functionalized with ene-groups at their carboxylic acid sites. A peptide reaction was used to graft allylamine onto polymer chains in the presence of EDC as the dehydration agent and NHS as the addition agent to increase yields and decrease side reactions [6]. Briefly, a 20 wt % solution of PAA in Milli-Q water was mixed with EDC and NHS at a pH of 4.5 for 2 hours at 60 °C. Allylamine was then added (the molar ratio AA/allylamine/EDC/NHS being set equal to 10/1/1.5/1.5) and the pH was adjusted to 10 before the reaction was allowed to proceed for 16 hours at 60°C Finally, the polymer was recovered through freeze-drying after 3 days of dialysis in 0.1 M NaCl solution and 3 days of dialysis in Milli-Q water. The functionalization hydrogel reaction is shown on Figure 2.10(A).

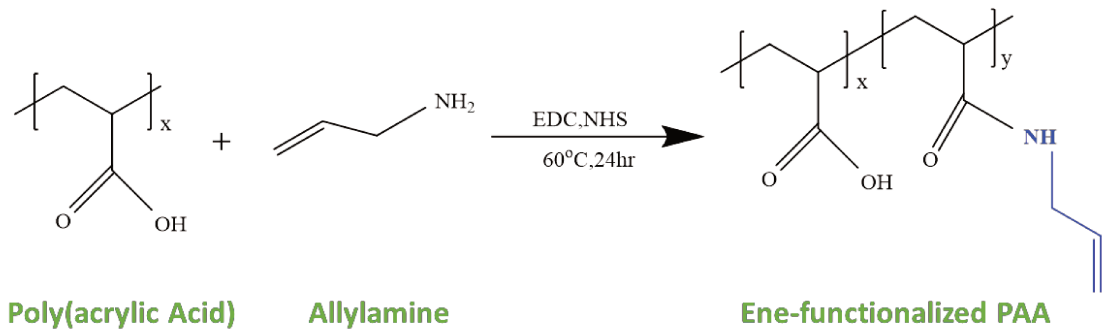

(A)

(B)

Figure 2.90:(A) A Schematic for functionalization of PAA, (B) A photograph of the synthesis of ene-functionalized PAA polymer

2.2.5 Synthesis of hydrogel films on gold electrodes

The different steps of hydrogel grafting are detailed in figure 2.11. Our synthesis strategy is inspired from the "grafting onto" technique, which consists in crosslinking and grafting the preformed and ene-reactive polymer chains through thiol-ene click chemistry. This strategy has the advantage of being well-controlled without any caution of no-oxygen atmosphere or addition of initiators. It enables a better control than the approach starting from monomers. A consequence of this approach is the facile patterning of hydrogel films as thiol-ene reaction can be selectively activated by UV irradiation (in addition to thermal heating).

Accordingly, the PAA hydrogel thin films were synthesized on the electrode surface by simultaneously cross-linking and grafting preformed polymer chains through thiol−ene click chemistry route as described by Chollet *et al*.[7] and Li *et al*. [2]. More precisely, preformed ene-reactive (functionalized) PAA is spin-coated on thiol-modified silicon gold electrode with dithiol (DTE) crosslinker. The mixture of methanol and formic acid 7:3 (V/V) containing ene-reactive PAA (at different concentrations and various molecular weight) and dithioerythritol crosslinker is dropped onto thiol-modified gold substrate. The ratio of dithioerythritol to ene-functionalized copolymer units is 15 times (corresponding to a molar excess of bifunctional dithioerythritol of 30). The conditions of spin-coating are fixed with the final angular velocity of 3000 rpm and the spinning time of 30 seconds. Patterns are obtained by performing the UV-light irradiation with common 8 Watt fluorescent lamp (= 254 nm) through a photomask. Aluminum foil were used as a mask for patterning. The photomask is placed over the spin-coated polymer film and the sample is irradiated for 2.5 hours. The hydrogel film were rinsed in methanol and sonicated before being dried under nitrogen to remove unreacted polymers so that remained polymers are chemically cross-linked and covalently grafted to the substrate.

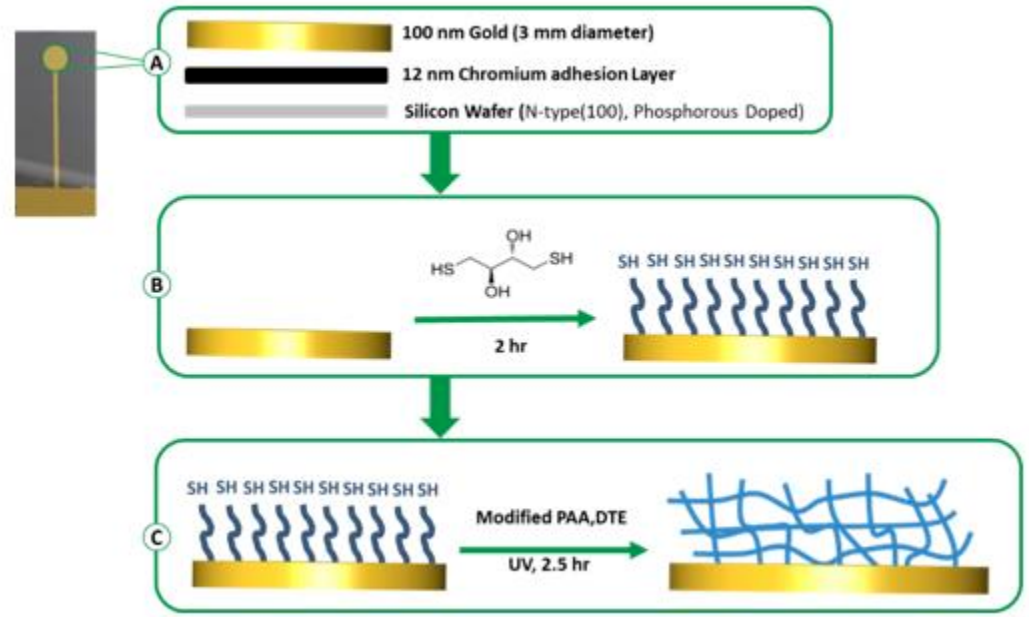

Figure 2.10:A general schematic representation of different steps to hydrogel grafting; (A) gold electrode made by positive photolithography; (B) thiol modification of the gold electrode; (C) hydrogel grafting using thiol-ene click chemistry.

2.2.6 Immobilization of aptamer on hydrogel-modified transducer

Covalent attachment of the amino-labelled aptamer solution on the PAA hydrogel modified electrode was performed by using *in situ* two-step attachment method. EDC/NHS activation of the electrode surface was performed inorder to create carboxylic groups required for the formation of amide mond *via* carbodiimide reaction.

Before aptamer immobilization technique, aptamer preconditioning was done in order to promote the loose conformation of the aptamer. For that, the aptamer solutions were heated at 75°C for 5 min and then, the solutions were cooled down for 15 minutes at room temperature. The modified electrode was incubated for 30 minutes at 20°C in phosphate buffer of pH 6.2 (PBS1) containing 50 mM EDC and 100 mM NHS. The electrode was subsequently rinsed with phosphate buffer of pH 7.4 (PBS2) and then incubated with 10 µM aptamer in phosphate buffer solution of pH 7.4 for 1 h at 20°C. After aptamer immobilization, the electrode was washed with phosphate buffer solution (PBS2) to remove unreacted aptamer (see Figure 2.12).

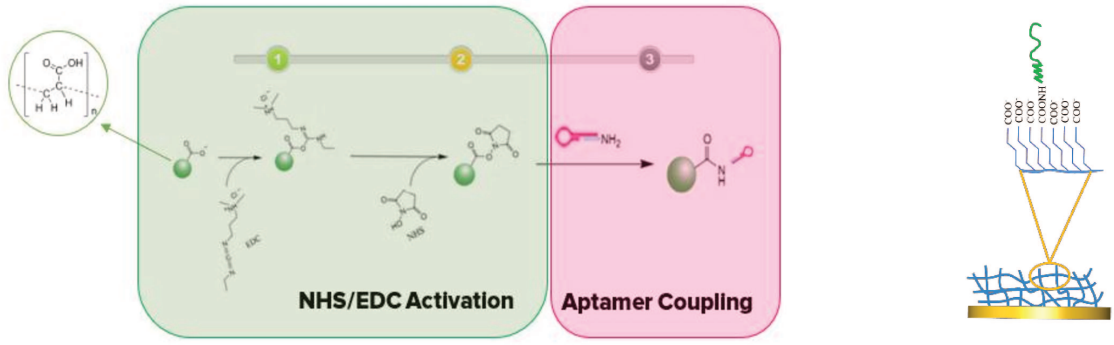

(A) (B)

Figure 2.112:(A) Schematic representation of the EDC/NHS surface modification and aptamer coupling. (B) A cross sectional schematic of aptamer coupling.

2.2.7 Target Detection

After aptamer immobilization, the biorecognition between aptamer and diclofenac was performed when the electrode was dipped in a solution containing diclofenac according to the scheme of the figure 2.13. The incubation of the aptamer-modified electrode in 200 µL BWB solution containing the desired concentration of the target took place for 50 min at room temperature. After detection, the biosensor was washed three times by using BWB buffer to remove any non-bound molecules of the diclofenac, at room temperature.

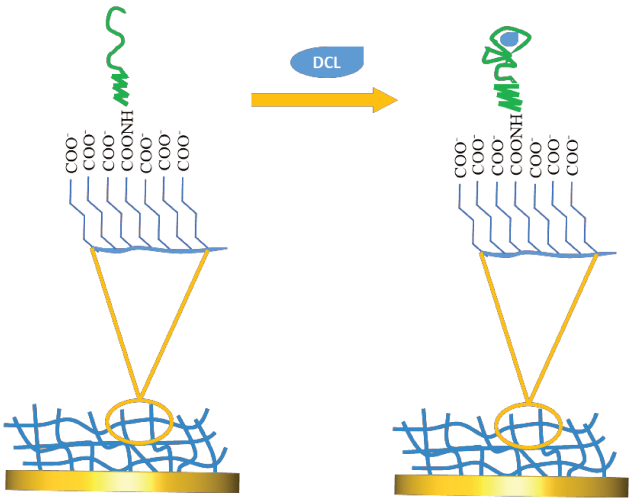

Figure 2.123:Cross-sectional schematic representation of the target detection after aptamer coupling

2.2.8 Determination of Analytic Characteristics, Operational and Storage Stabilities

For optimization study, the aptasensor were prepared and tested for different target concentrations at room temperature. The calibration curves were plotted for different diclofenac concentrations versus impedance response with standard deviation values and the linearity equations, linear range and limit of detection (LOD) value were determined.

The operational stability of the optimized aptasensor was determined by repetitive measurements of the target concentrations at room temperature in the same day. The storage stability of the aptasensor was examined by measuring the impedimteric responses every 7 day for the same target concentrations under the optimized conditions. Between each subsequent measurement the aptasensor were stored at 4 °C.

References

[1] C.B. Joeng, J.H. Niazi, S.J. Lee, M.B. Gu, ssDNA aptamers that recognize diclofenac and 2-anilinophenylacetic acid, Bioorg. Med. Chem. 17 (2009) 5380–5387. https://doi.org/10.1016/j.bmc.2009.06.044.

[2] M. Li, B. Bresson, F. Cousin, C. Fretigny, Y. Tran, Submicrometric Films of Surface-Attached Polymer Network with Temperature-Responsive Properties, Langmuir. 31 (2015) 11516–11524. https://doi.org/10.1021/acs.langmuir.5b02948.

[3] L.M. Fischer, M. Tenje, A.R. Heiskanen, N. Masuda, J. Castillo, A. Bentien, J. Émneus, M.H. Jakobsen, A. Boisen, Gold cleaning methods for electrochemical detection applications, Microelectron. Eng. 86 (2009) 1282–1285. https://doi.org/10.1016/j.mee.2008.11.045.

[4] S. Schneider, C. Partes, A. Wiesner, A. Terfort, Potential-induced phase transition of benzoxazole-2-thiol, naphthaleneoxazole-2-thiol and anthraceneoxazole-2-thiol monolayers on gold electrodes, Electrochimica Acta. 283 (2018) 167–173. https://doi.org/10.1016/j.electacta.2018.06.123.

[5] M. Shamsipur, S.H. Kazemi, A. Mehdinia, M.F. Mousavi, H. Sharghi, Electron Transfer Behavior through Densely Packed Self-Assembled Monolayers of a Novel Heteroaromatic Thiol Derivative onto the Gold Surface, Electroanalysis. 20 (2008) 513–519. https://doi.org/10.1002/elan.200704085.

[6] G. Miquelard-Garnier, S. Demeures, C. Creton, D. Hourdet, Synthesis and rheological behavior of new hydrophobically modified hydrogels with tunable properties, Macromolecules. 39 (2006) 8128–8139. https://doi.org/10.1021/ma061361n.

[7] B. Chollet, M. Li, E. Martwong, B. Bresson, C. Fretigny, P. Tabeling, Y. Tran, Multiscale Surface-Attached Hydrogel Thin Films with Tailored Architecture, ACS Appl. Mater. Interfaces. 8 (2016) 11729–11738. https://doi.org/10.1021/acsami.6b00446.

CHAPTER 3:

DESIGN, DEVELOPMENT AND CHARACTERIZATION OF AN IMPEDIMETRIC APTASENSOR FOR THE DETECTION OF DICLOFENAC BASED ON A NOVEL IMMOBILIZATION MATRIX

3.1 Fabrication and Characterization of the Gold Electrode Transducer

A very broad spectrum of electrode materials and forms has been used as transducer for developing electrochemical biosensors capable of providing a good analytical performance, simplicity of construction and low cost [1,2]. Gold surface is selected in this study owing to its inertness, high purity, great stability and its strong affinity towards thiol compounds, which render these electrodes very suitable for clinical diagnosis, food and environmental analysis, besides other applications [3,4].

The size and shape of the electrode surface also has an effect on the electrochemical response of the electrode, and in an effort to have a working electrode that is very clean metal surface with a well-defined geometry, we have expeimented different electrode configurations and process of fabrication of the electrode as seen in figure 3.1. The classic forms like gold disk electrodes are bulky and expensive. So as to take advantages of lower cost, disposability, and miniaturization benefits, we have fabricated and used patterned electrodes in this study.

As shown in figure 3.1, we started fabricating electrodes produced by evaporating a gold thin film on whole silicon wafer for a proof of concept of the chemistry we intended to utilize in this dissertation. Once the proof of concept was made with fig 3.1(A), we have experimented defining the area of the electrode using non-conductive adhesive tape(fig 3.1 (B)) and because of inability to have a well-defined structure and the need to achieve the above mentioned advantages of lower cost and miniaturization benefits, we used photolithography techniques to pattern the working electrodes. Because the silicon wafer used was not conductive enough to collect the electrochemical response as in configuration of fig 3.1 (C), we had to come up with a configuration containing an electrical contact/collecting part (fig 3.1 (D)).

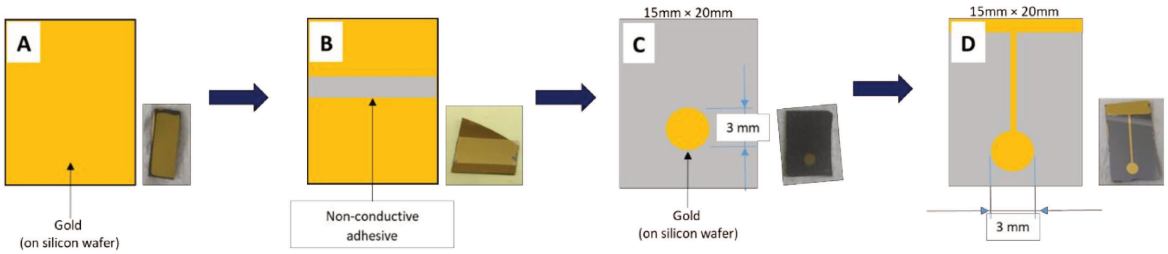

Figure 3.1: The different electrode configurations experimented in this study: (A) a gold thin film electrode, (B) a gold thin film electrode with non-conductive adhesive used to define the active area, (C) a patterned gold electrode using photolithography without electrical contact point for measuring the electrochemical response (D) a patterned gold electrode using photolithography with electrical contact point

Hence, in this study, this final configuration is used as an optimized size and shape of the electrode surface and in the subsequent sub section, its fabrication process is detailed. Briefly, following the standard positive photolithography and lift-off protocol didn't yield us a reproducible and stable gold electrode transducer and as a result, we slightly modified the standard photolithography procedure using the S1818 photo resist and the processes are detailed as following.

3.1.1 Sample Preparation

An important step in the fabrication of samples is the correct preparation of the substrate, and making sure that it is as clean as possible before anything else is done with it, as a dirty substrate will not give the necessary accuracy of feature sizes and dimensions due to the sensitive nature of process. Originally, simple conventional wet cleaning procedures of rinsing with acetone and ultra-pure water and then blow drying with nitrogen gas was done in addition to the standardized RCA cleaning and piranha cleaning methods [5,6]. Acetone and ultra-pure water cleaning and also the piranha cleaning method was ineffective in our case (See figure 3.11). The RCA cleaning method was very effective but in terms of environmental safety and economics, we chose cleaning using the oxygen plasma cleaning method.

The cleaning routine carried out was the cleaning of the silicon wafers using a nitrogen gun to remove visible dust and stray debris or particles on the surface and once this is done, the wafers were cleaned for 10 minutes using oxygen plasma cleaner shown in Figure 3.2 below. The wafer is then stored in a suitably sized wafer-carrier, and is then ready for further processing.

Figure 3.2: A photograph of the Plasma cleaner

3.1.2 Positive Photolithography Process

Once the substrate was cleaned, we performed the next step of fabrication which is photolithography. Photolithography is a very useful fabrication technique whereby a 'top-down' approach to achieving micrometer (and larger) feature sizes on a substrate can be carried out quickly and in parallel. This is done by coating a substrate with the photoresist, a light-sensitive polymeric solution then covering this with a patterned hard-mask and finally exposing all of this with a light source (typically UV light) which causes a chemical reaction in the photoresist to take place. Upon developing, the photoresist is then characterized for the mask-pattern with only the desired patterned areas remaining and the rest of the photoresist being dissolved in the solution.

Photoresist is a light-sensitive polymeric solution, which undergoes a chemical reaction upon illumination of UV light. Photoresists can either be Positive or Negative tone. Positive implies that the exposed areas become more soluble in a developer, whilst negative tone resists having their exposed areas become less soluble in a developer and remain after development. In this study, a positive S1818 photoresist was used. A schematic diagram of the photolithography and Lift-off process carried out is shown in Figure 3.3 below.

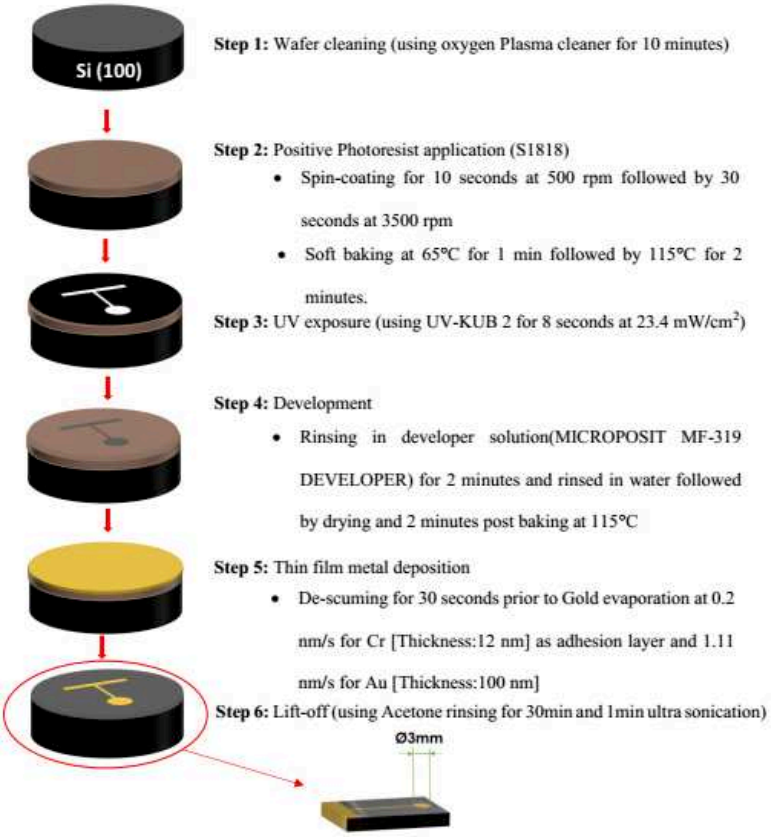

Figure 3.3: Fabrication of electrode using positive Photolithography and lift-off process

The photoresist is applied to the surface of the silicon wafer substrate through the use of spin-coating. This is where the sample is affixed to a spin-coating machine, (see Figure 3.4) which is programmed to rotate at 3500 revolutions per minute, and pouring on a small amount of photoresist which then spreads evenly across the sample to create a flat uniform area. This is necessary to allow good contact to be made with a hard-mask. The spin-coating took less than a minute to perform, with cycles in the speed and acceleration taking place to assure uniform spreading (see Table 3.1).

Figure 3.4: (A) A photograph of (from left-to-right) the positive photoresist (S1818) and the Spin Coater used in the preparation of samples for fabrication. (B) a photograph of a hot plate for soft baking

Once the resist has been spun onto the substrate, it is then transferred to a hotplate for soft baking at 65°C for 1 min followed by 115°C for 2 minutes to encourage evaporation of the solvent and a stronger adhesion to the substrate. This causes a solidification of the resist, which would otherwise be problematic for contact with the photomask if it were still viscous.

Following the spin-coating, the resist is then required to be exposed to UV light in order to make it selectively-soluble, and have a desired pattern. This is done with the use of a photomask as shown in Figure 3.5. The photomask was designed through the use of CleWin software, where the exact dimensions and features can be accurately controlled and fabricated using photo plotter. The exposure and masking system used was a UV-LED masking system (UV-KUB 2), and operated for 8 seconds at 23.4 mW/cm^2.

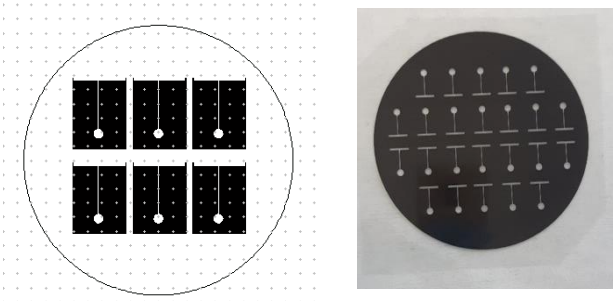

(A) (B)

Figure 3.5: (A) The photomask design (B) A photograph of the photomask

Figure 3.6: A photograph of the UV-KUB 2 system

Exposure of the samples takes place using contact mode (where the surface of the photoresist is brought very close and touching the mask), as this is the best means of achieving small feature sizes due to less optical scattering distance. The exposure times was optimized for the UV-KUB 2 system to be 8 seconds. Following exposure, it was crucial to leave the sample to 'rest' for 10-15 minutes or so before developing, to allow the photoactive chemistry to take place. Once the sample had been given adequate resting time after exposure, the development took place in a fume cupboard by submerging the sample in a glass beaker partly filled with MF-319 developer (Figure 3.7). A steady agitation was carried out to encourage solubility of the exposed resist. The optimized developing time, where the time the resist was seen to dissolve by a clouding effect and the absence of clouding signaling the end of development, was 2 minutes (See Figure 3.8). The sample was then removed from the solution and rinsed under deionized water for 1 minute, before being gently dried with a nitrogen gun and 2 minutes post baking at 115°C. Subsequently, to remove the residual photo resist a gentle oxygen plasma cleaning (de-scumming) was done for 30 seconds.

Figure 3.7: A photograph of developing stage

Table 3.1: Summary of the procedure used for processing S1818 photoresist

Process type	RPM	Spin Time (seconds)	Acceleration
Cycle 1	500	10	200
Cycle 2	3500	30	300
Prebake	Soft baking at 65°C for 1 min followed by 115°C for 2 minutes.		
Exposure	For 8 seconds at 23.4 mW/cm^2		
Development	Rinsing in MICROPOSIT MF-319 developer solution for 2 minutes and rinsing in water followed by drying and 2 minutes post baking at 115°C.		

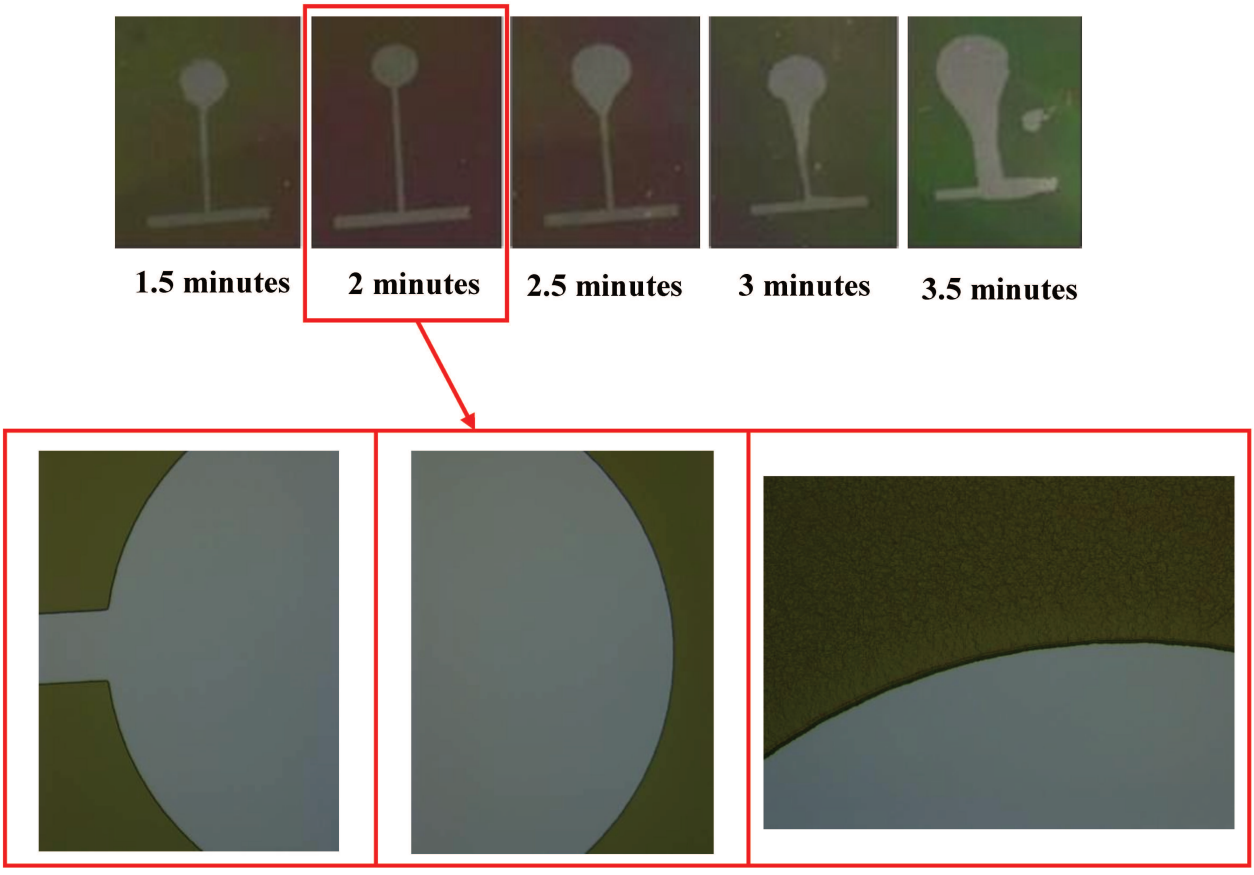

Figure 3.8: Study of the effect of development time on the lithography process

3.1.3 The Metal-Deposition and Lift-off Process

After the photolithography process is completed, gold metal deposition to fill the voids present in the developed photoresist was carried out. Because we used a positive photoresist, the metal patterning was the inverse pattern where the metallic structures that remain are the desired outcome, after lift-off. Thermal evaporation gold metal deposition procedures are carried out through means of locally heating a small amount of the gold metal to temperatures high enough to cause melting, whereby energetic atoms of this metal then escape and condense on cold surfaces undergoing solidification (Figure 3.9). To aid the adhesion of the gold structure to the surface and minimize damage or removal during lift-off, a thin layer of chromium was used.

Figure 3.9: A photo of BOC Edwards Auto 500 Evaporator system

When heating the gold metal, care was taken to maintain the current at low values to desorb any contaminants which may be present in the crucible and also adsorbed to the gold metal. Once the gold metal was ready to be evaporated, it was heated slowly up to the point at which melting occurs. To produce a nice uniform layer, the current was maintained low enough that the evaporation rate is between 0.04-0.11 nm s^{-1} for chromium, and between 0.4-0.65 nm s^{-1} for gold, as if the rate is too high then clustering may occur and the deposited metal layer will have an increased roughness.

Once the patterned voids in the photoresist were filled with 12 nm thin layer of chromium and 100 nm thick gold metal, we performed a lift-off process of the resist to leave behind only the metallic structures on the substrate. An image of gold electrodes on the whole 4 inch wafer produced by lift-off is shown in Figure 3.10. The optimized Lift-off process was carried out by submerging the

gold-coated sample in acetone solvent for 30 minutes and then ultra-sonicating for 45 seconds, to aid in the removal of the photoresist and metal which sits atop the resist.

(A)

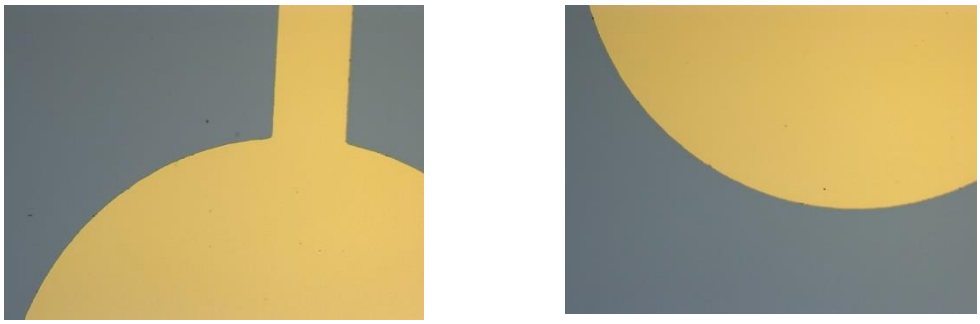

(B)

Figure 3.10: (A) A photograph of gold electrode transducer by deposition of 100 nm thick gold on 12 nm chromium adhesion layer onto a pre-patterned, developed photoresist, and subsequent lift-off processing in acetone solution. (B) Optical microscopy image of the gold electrode after lift-off.

An example of the spinning of a photoresist on a silicon wafer, in which debris or impurities on the surface caused unwanted 'streaks' and thickness variations of the resist leading to issues after developing and after lift-off process are indicated below in figure 3.11.

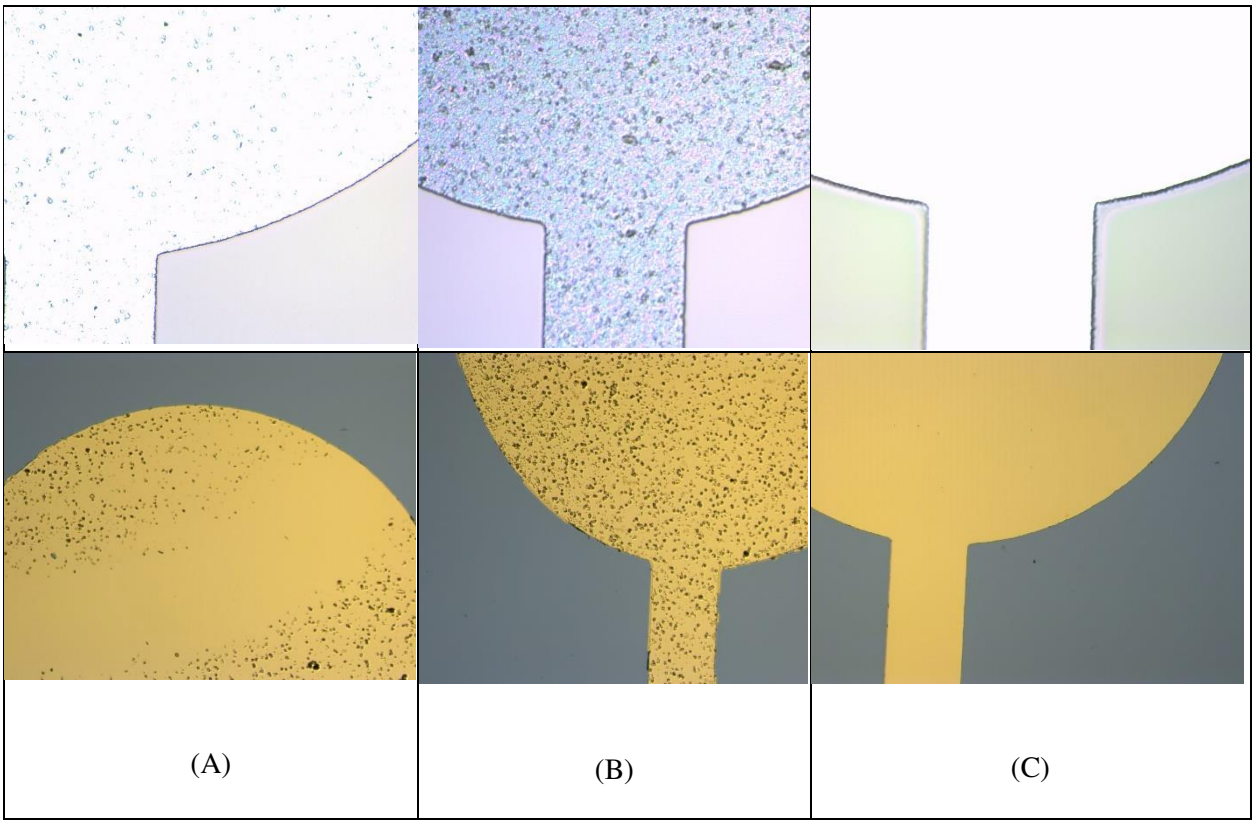

Figure 3.11: Photograph taken using optical microscopy after development and after lift-off stage (A) for Acetone and deionized water cleaned wafer (B) for Piranha cleaned wafer (C) Oxygen Plasma cleaned wafer. For all the three cases the development time and bathing time for the lift off stage were the same.

3.1.4 Cleaning the gold film surface

Before the evaporated gold is chemically modified for another use, we cleaned the electrode to ensure reliably clean gold surfaces and maximize stable coverage of thiol monolayer as it has been demonstrated by our electrochemical experiments that the gold electrodes fabricated using the photolithography process were subjected to contamination.

Hence, different gold cleaning methods were employed to clean our electrode including sulfuric acid potential cycling [7,8] and the potassium hydroxide potential sweep method [9]. After cleaning, the electrochemical behavior of $Fe(CN)_6^{3-/4-}$,used as a redox probe, was analyzed at

cleaned electrodes by cyclic voltammetry. The peak-current potential-differences obtained from cyclic voltammetry, ΔE, were used as main performance criteria to determine the cleanness of the gold electrode, a low peak-current potential-difference indicating a cleaner surface. Any increase in this value, ΔE, was interpreted to be caused by surface imperfections or contaminations.

The very common electrochemical cleaning technique of cycling the electrode potential in a sulfuric acid solution until a stable CV scan was achieved in 0.1M H_2SO_4 solution with a scan rate of 20 mV/s, for 30 cycles. However, the H_2SO_4 CV method appears to severely oxidize the gold and delivers a surface less clean than expected in our case.

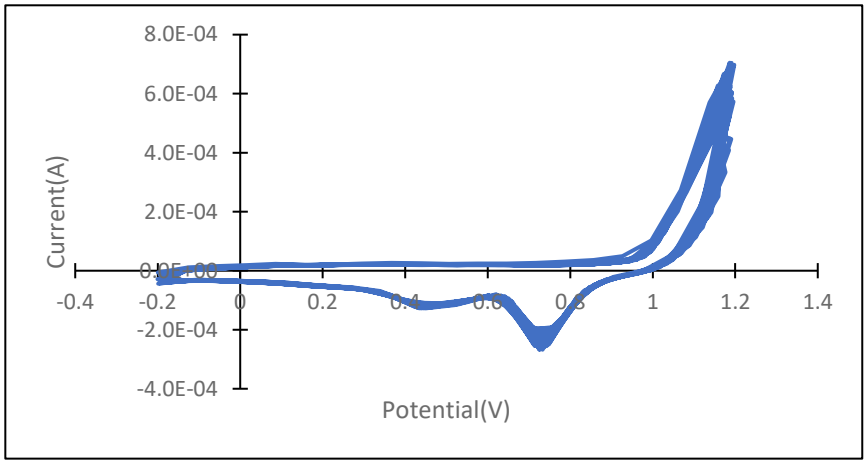

Figure 3.12: Cleaning of the electrode done by cycling the electrode in 0.1M H_2SO_4 solution for 30 cycles at 20 mV/s

As a result, a slightly modified protocol of the potassium hydroxide potential sweep method described by L. M Fischer et al. [10], in which they describe the soaking of an electrode in a solution of KOH (50 mM) and H_2O_2 at 25 % for 10 min and then do a potential sweep between -200 mV and -1200 mV (*vs* Ag/AgCl) at a scan rate of 50 mv/s in a solution containing KOH at 50 mM, was employed to produce a significantly cleaner and reproducible surface. As it is shown figure 3.13, the as-prepared gold electrode (after photo-lithography) is not perfectly cleaned. After pre-treatment with NaOH and H_2O_2, an increase in the oxidation current (x1.84) and a decrease in the ΔE are observed compared to the uncleaned electrode. The NaOH + H_2O_2 and NaOH sweep methods appear to deliver the cleanest gold electrodes compared with the common H_2SO_4 CV method.

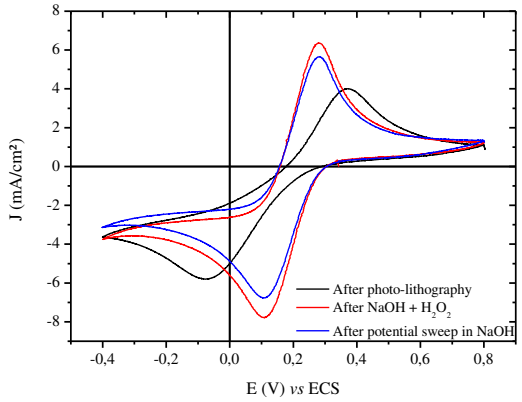

Figure 3.13 : Evolution of the current density in function of the potential applied in a solution of $[Fe(CN)_6]^{3-/4-}$ 50 mM + KCl 100 mM (50 mV/s) for the gold electrode after the photo-lithography (black), after the bath in NaOH (50 mM) + H_2O_2 (25 %) (red) and after the potential sweep in NaOH between -245 mV and -1245 mV vs SCE (blue).

Table 3.2: Comparison of the main electrochemical parameters for $[Fe(CN)_6]^{3-/4-}$ redox couple at gold electrode as a function of pre-treatment conditions for gold electrodes (deduced from cyclic voltammetry experiments at 50 mV/s)

Nature of the electrode	Ep_a (mV)	Ep_c (mV)	ΔEp (mV)	ΔJ_{ox} (mA/cm²)	ΔJ_{red} (mA/cm²)
After photo-lithography	369.3	-79	448.3	4.8	-6.16
After NaOH + H_2O_2	279.6	106.8	172.8	8.86	-7.88
After potential sweep	281.1	106.6	174.5	7.49	-6.79

Based on this method, our optimized modified protocol for cleaning the gold thin film electrode involves studying the influence of the bathing time from 10 minutes to 70 minutes in a solution of 50 mM NaOH and 25 % H_2O_2. As indicated above, the peak-to-peak separation, ΔEp, was used as a measure of electrochemical cleanliness of the electrode surface with a smaller ΔE indicating a cleaner surface. The results of the experiment show clearly that after the cleaning process, all electrodes showed a significant change in terms of the ΔE, and to see the influence of the timing bath, the ΔE and the ΔI_{ox} are reported below in the following two figures.

In figure 3.14, we can see that the ΔE decreases after the NaOH + H_2O_2 bath.

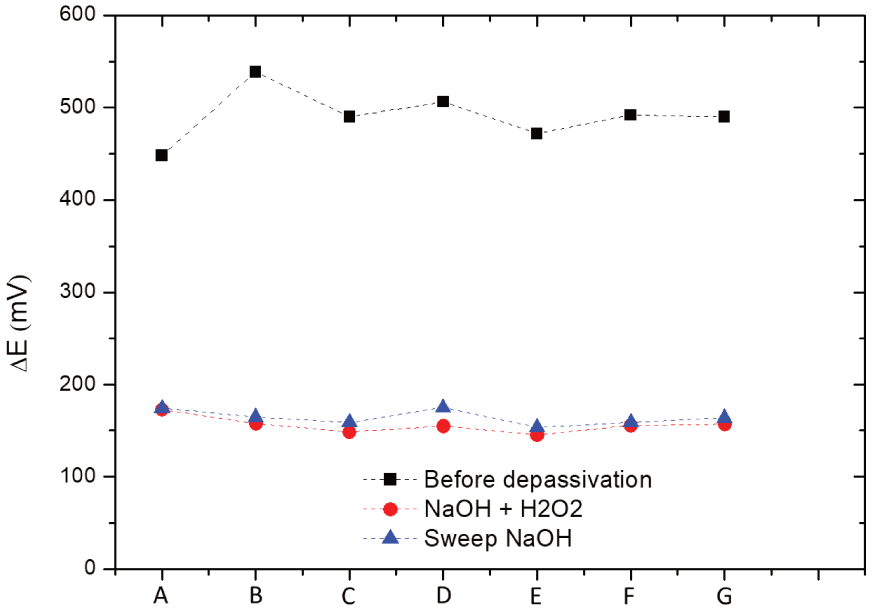

Figure 3.14: Evolution of the ΔE during the cleaning process for different bathing time :(A)10 minutes (B)20 minutes (C) 30 minutes (D)40 minutes (E)50 minutes (F) 60 minutes (G)70 minutes

In general, experiments were conducted on seven different electrodes to evaluate the effect of bathing time (10 to 70 minutes) and potential sweep on the electrode response towards ferri/ferrocyanide couple. The obtained results suggested that the bathing only NaOH+H_2O_2 (without potential sweeping) for 30 minutes is efficient to improve the electrode response. Exposure time higher than 30 minutes didn't improve the response and hence we chose to use the shortest time.

Furthermore, the electrode fabricated using the photolithography process was compared, for different parameters inlcuding its electrochemical activity, against/with commercial gold Drop Sens electrode in a solution of $[Fe(CN)6]^{3-/4-}$ (50 mM) and KCl (100 mM) (scan rate: 50 mV/s *vs* ECS) . As we can see in the figure 3.15, the cleaned gold electrode presents a better electrochemical response than the Drop Sens electrode with a smaller ΔE and a higher current density.

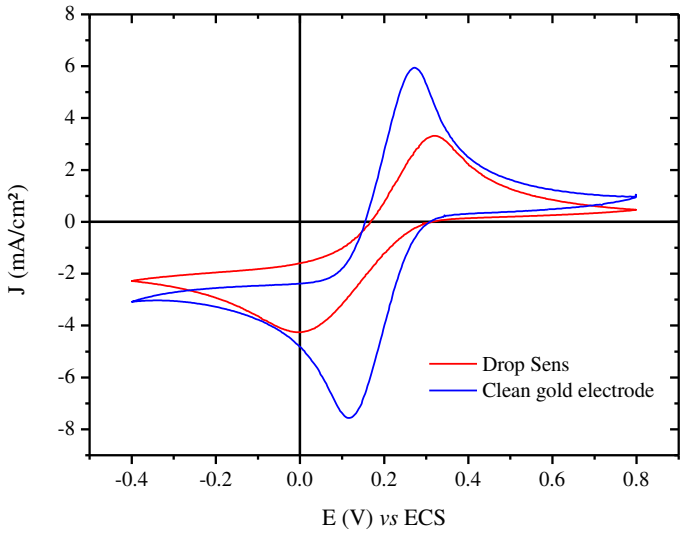

Figure 3.15 : Evolution of the current density in function of the potential applied in a solution of $[Fe(CN)6]^{3-/4-}$ 50 mM + KCl 100 mM (50 mV/s) for gold Drop Sens microelectrode (red) and the clean gold electrode (blue).

The AFM and SEM works done also evidenced the improved surface structure after cleaning in addition to the electrochemical properties (figure 3.16). The atomic force microscopy exploration of the surface of gold characterizes the gold as homogenous, with a root-mean-square (RMS) value of around 4 nm for mean roughness estimated from the half width of the height histogram of each image. The images acquired for the evaporated gold surface shows a fairly a smooth, homogeneous structure with small rounded grains.

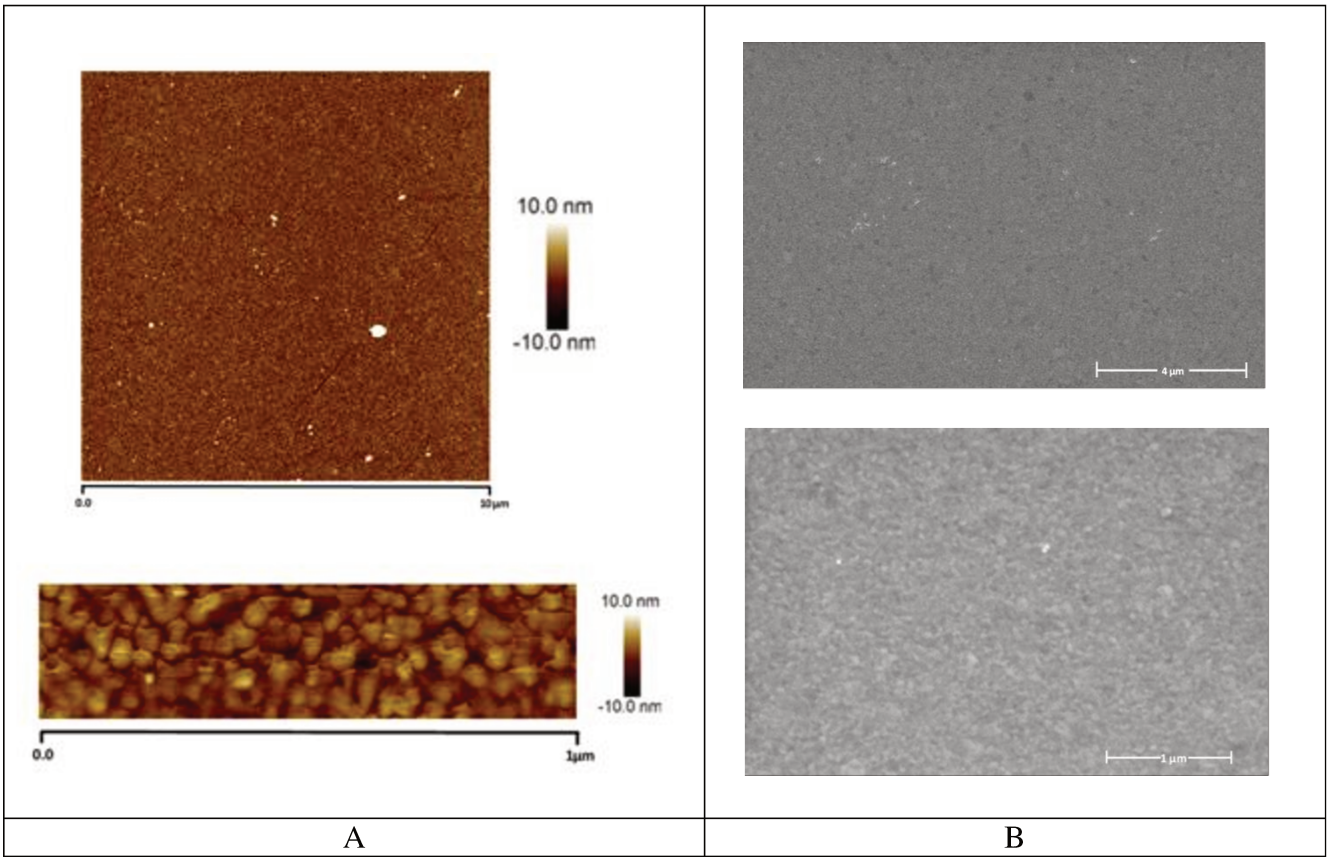

Figure 3.16: Topographic images of gold using AFM (A) and SEM (B).

3.2 Functionalization of the gold electrode surface

The gold surfaces obtained by evaporation of a gold film on the silicon wafer are functionalized with thiol self-assembled monolayer (SAM) using a solution of dithioerythritol (DTE) at 1 mM in chloroform. They are kept immersed in a sealed reactor to prevent evaporation of chloroform.

The modification of the gold surface by DTE was first characterized by using water contact angle measurements, by comparing WCA before and after gold immersion in DTE. It was shown that the contact angle was higher after SAM immobilization (75°) in comparison to bare gold electrode (62°) showing that the wettability of the gold surface decreases after thiol immobilization.

Then, electrochemical measurements and morphological characterization tools were used to confirm the presence of the DTE SAM. Different thiolation times (2 to 25 hours) have been tested for the formation of SAM to evaluate if the thiolation time will have an impact on the electrochemical response of the modified electrode. This was conducted by evaluating the

electrochemical behavior of ferri/ferrocyanide couple on the modified electrode by cyclic voltammetry.

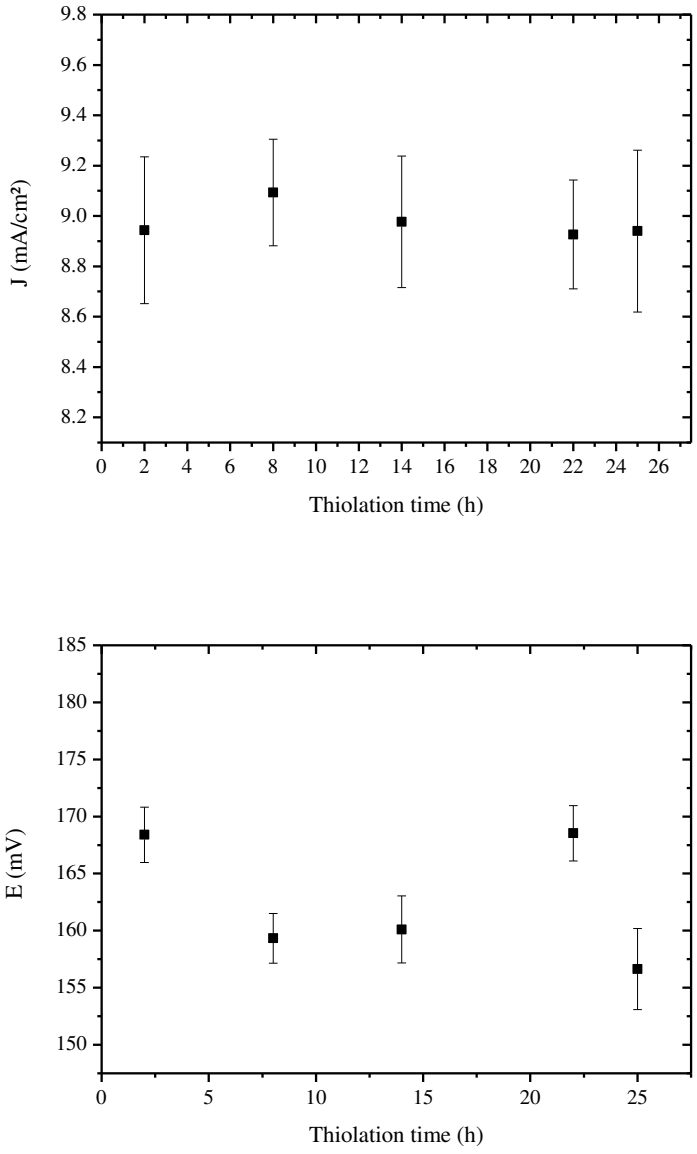

Figure 3.17: Evolution of the ΔE and ΔJ in function of the time of thiolation.

Comparing the trend of the ΔE with the trend of the ΔJ on figure 3.17, we can see that there is a concordance between them. Indeed, when the thiolation time is increased to 6h, there is a decrease in the current density and an increase in the ΔE. Then, when it comes to 22h, the current density observed as well as the ΔE are in the same range than for 2 hours. Given the standard deviation,

we can comfortably say that there is no significant thiolation time effect and hence we used 2 hours for SAM formation in this study.

Figure 3.18 shows the cyclic voltammetry at bare and DTE modified gold electrode obtained in a solution of ferri/ferrocyanide (50 mM each) in KCl 0.1 M. The voltammogram obtained shows not significant difference beween the thiol-modified electrode to that of the bare gold electrode. This is attributed to the fact that the thiol molecules form a non-dense monolayer [11]. The introduction of terminal groups (–SH, –COOH, –OH, $–NH_2$) instead of the $–CH_3$ group usually results in a decrease in self-assembled ordering [12]. Thus, the monolayer of DTE thiol small molecule on gold is too thin to effectively block electron transfer on a gold surface.

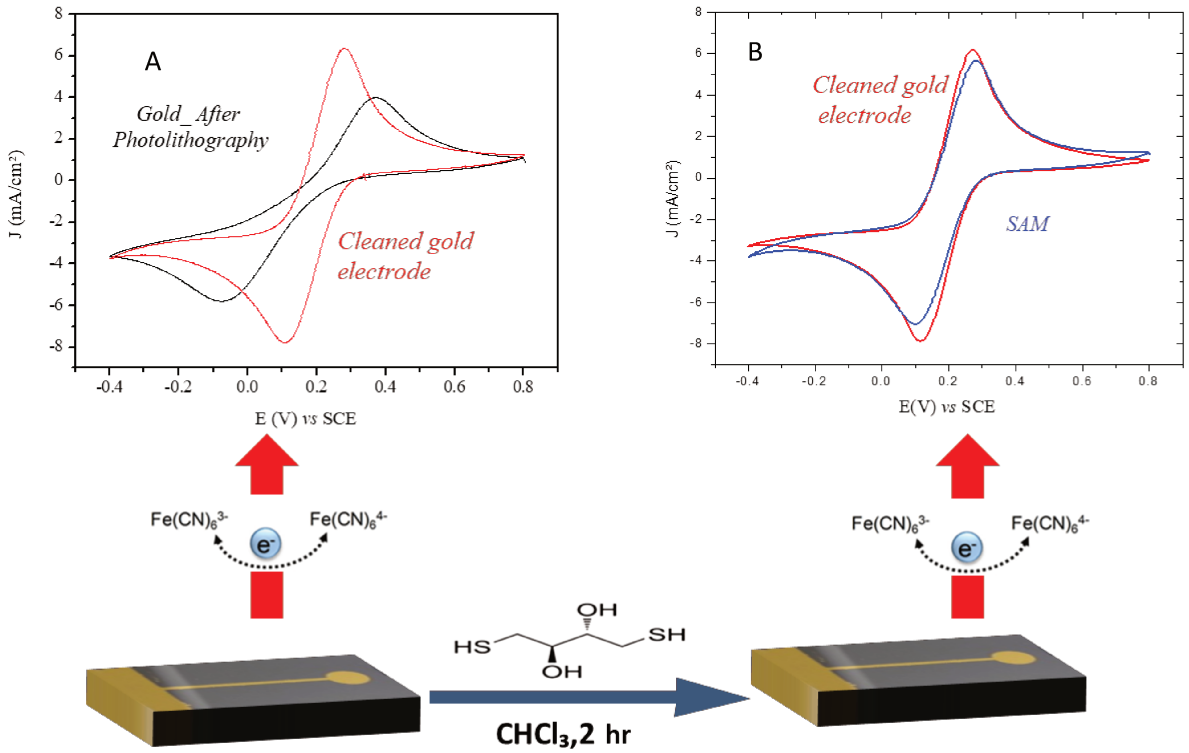

Figure 3.18: Evolution of the current density in function of the potential applied in a solution of $[Fe(CN)6]^{3-/4-}$ 50 mM + KCl 100 mM (50 mV/s) for (A) the gold electrode after the photo-lithography (black), after the bath in NaOH (50 mM) and H_2O_2 (25 %) (red). (B) DTE SAM on Au electrode after 2 hours of thiolation time (Blue)

We have performed reductive electro desorption curves to confirm the presence of covalently attached DTE to the gold substrate references. Indeed, it is possible to evaluate thiol immobilization by Au-S bond breaking by inducing reduction, as follows:

$$nRS{-}Au + ne^- \longrightarrow nRS^- + nAu$$

The electrolyte chosen in this case was 0.1 M NaOH because in the neutral medium the current peak related to the thiol electrodesorption overlaps partially with the hydrogen evolution reaction. The cathodic polarization curve shown in Figure 3.19-a corresponds to a clean (thiol SAM-free) gold substrate recorded from -0.4 to -1.4 V. Figure 3.19-b shows typical curves recorded for DTE-SAM on the gold prepared from the 1mM DTE solutions for 2 hours at room temperature. In comparison with the bare electrode, a reduction peak at around -0.9 V is observed at DTE modified gold electrode and may be attributed to the reductive desorption of the DTE from the gold electrode surface.

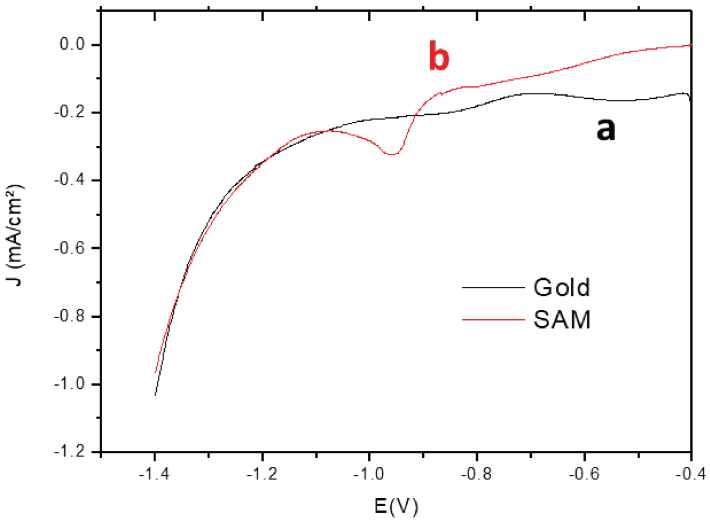

Figure 3.19 : current density vs. potential profiles for the reductive desorption of DTE.(a) Bare Gold, (b)Gold incubated in DTE 1mM for 2 hr. Measurements were made in NaOH 0.1M at a sweep rate of 0.05 V/s

Figure 3.20 shows cyclic voltammetry at bare gold and dithiol modified surfaces in electrolyte PBS at pH 7.4 containing no redox species indicating the peaks where gold oxidation and reduction of the oxide occur, as well as the region where there is only charging current. The CVs compare well with gold evaporated on silicon wafer references. Upon thiol monolayer formation on the gold surface, gold oxide formation and reduction are suppressed, as evidenced by the lack of peaks in the CV at the SAM-modified electrode seen in fig 3.20. The cyclic voltammetry of alkanethiol monolayer-coated electrodes in electrolyte solutions shows that the charging current drops dramatically in comparison to the bare metal electrode. This is consistent with the presence of a low dielectric constant between electrode and electrolyte.

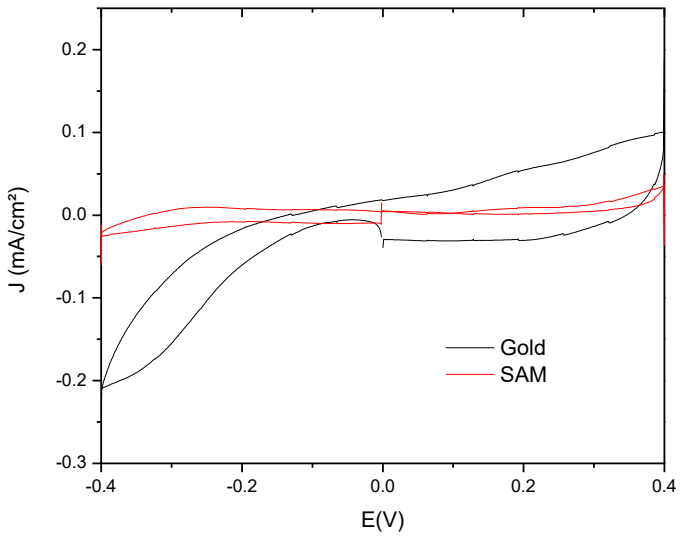

Figure 3.20: Cyclic voltammogram of a bare gold electrode and DTE SAM. The supporting electrolyte used was PBS at scan rate of 1 V/s

The interfacial surface properties of the SAM modified electrode were characterized using ATR-FTIR and the modification of the gold electrode using dithiol molecule has been confirmed by the presence of the necessary functional groups and is detailed in section 3.6.

3.3 Surface-attached hydrogel films with tunable and well controlled chemistry

3.3.1 Strategy of surface-attached hydrogel films

The fabrication of hydrogel films is delicate given that synthesis at surface is very sensitive due to a high surface to volume ratio. To overcome this difficulty, recently, a research group at ESPCI, SIMM, has developed a new, simple and versatile approach for the synthesis of reliable and reproducible hydrogel films that involves cross-linking and grafting preformed functionalized polymers using click chemistry [13]. Click chemistry is a term applied to chemical synthesis tailored to generate substances quickly and reliably by joining small units together. It is not a single specific reaction, but describes a way of generating products that follows examples in nature, which also generates substances by joining small modular units. Thiol-ene reaction involves the addition of a S-H bond across a double bond by either a free radical or ionic mechanism. It is essentially the sulfur version of the hydrosilylation reaction. Thiol-ene reaction is considered to be a "click" reaction as it carries all the desirable features of a click reaction, being highly efficient, simple to execute with no side products and proceeding rapidly to high yield [14].

The thiol-ene click chemistry is chosen since the thiol-ene reaction is advantageously performed without any initiator addition and can be activated by either thermal heating or UV-irradiation, resulting in facile patterning of hydrogel films. The principle of the thiol-ene click chemistry reaction is as follows (figure 3.21):

Figure 3.21: Principle of thiol-ene reaction

The fabrication of various architectures for polymer films was demonstrated in previous studies by SIMM team [13,15]: multilayer hydrogel films in which single-networks are stacked one onto the other, interpenetrating networks films with mixture of two networks in the same layer, nanocomposite hydrogel films where nanoparticles are stably trapped inside the mesh of the network.

Our research group collaborated with the SIMM laboratory in light of using the surface-attached hydrogel films as new immobilization matrix for development of aptasensors. So far, there are no studies, at least to the best of our knowledge, related to biosensors that utilizes these surface

attached hydrogel thin films as a matrix for aptamer immobilization despite their numerous advantages.

Based on this approach we have demonstrated an additional way of fabricating a surface attached film that avoids the thiol monolayer formation on surface of gold electrode. The later approach, which lets us to have a surface attached thin film by directly spin coating the polymer solution with excess dithiol cross linker directly on the gold surface accelerates the process of the sensor fabrication, and characterization tools including ATR-FTIR and voltammetric techniques have proofed and practicality of the method.

The responsive polymer used is Poly acrylic acid (PAA) and single network films were developed as immobilization matrix for biomolecule. Among various ionic hydrogels, poly(acrylic acid) (PAA) has attracted remarkable interests due to its superior biocompatibility[16–19] as well as its perfect water absorptivity and good thin-film formability [20–22]. Moreover, the high density of carboxylic acids makes it suitable for physical and chemical modification to form bio-functional surfaces [20], and thus, PAA has great potential to be deployed in rapidly emerging fields, such as tissue engineering, protein immobilization, biosensors, and biomedical devices [19,22–24].

The “grafting onto” strategy used in this work consists in cross-linking preformed functionalized polymers through thiol-ene click chemistry and consists of;

i. Ene-functionalize the homopolymer;
ii. The ene-functionalized polymer is solubilized in proper solvent and then the bifunctional thiol molecules are introduced into the solution as cross-linkers which are proportional to the ene groups in the polymer;
iii. The solution is deposited on the thiol-modified gold electrode and then spin-coated;
iv. Cross-linking and grafting-to-surface processes are achieved simultaneously by the thiol-ene reaction (see Figure 3.22).

The single reaction thiol-ene "click" chemistry is selected and used for its high efficiency, its stereoselectivity and its favorable thermodynamics. This reaction may be by free-radical additions and catalyzed Michael additions. We chose the radical addition activated UV exposure (Figure 3.22). Thiol-ene radical additions are advantageous because the step growth (propagation and chain-transfer steps) and chain growth (homopolymerization) processes can be effectively used to form homogeneous polymer networks. Basically, the thiol-ene radical addition combines

the benefits of photopolymerization reactions with the aforementioned advantages of click chemistry reactions.

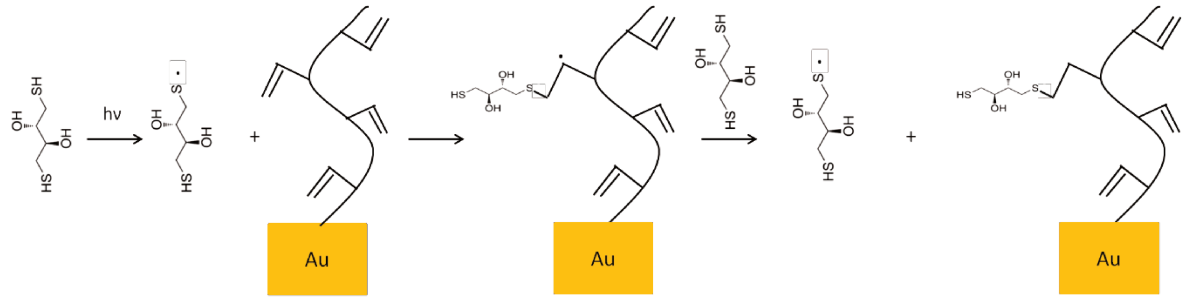

Figure 3.22: Mechanism of the simultaneous cross-linking and grafting of the PAA hydrogel on gold surface references

The grafting and crosslinking reactions are happening simultaneously. The activation causes the formation of thiyl radicals which propagate to the -en-function by anti-Markovnikov addition, forming a thioalkyl. The radical carbons formed will react with other thiols to form new thiyl radicals and the desired thioethers. In our case the second thiol of DTE can react, which allows the crosslinking with another polymer chain by the same reaction. This reaction has a total atom economy and it can be carried out in aqueous solvent and in the presence of oxygen.

3.3.2 Synthesis and Characterization of ene-functionalized PAA Homopolymer

The ratio of ene-groups is decisive for synthesis of hydrogel thin films by surface-grafting and cross-linking of ene-reactive chains through thiol-ene click reaction. It has been shown that the ratio of ene-groups has to be at least 1 mol % to allow the formation of hydrogel thin films. Below 1 mol % of ene-groups ratio, the formation of hydrogel films cannot occur due to low grafting density and cross-linking, the polymer chains being not sufficiently grafted and cross-linked to the chemical stability of the polymer networks on the surface. On the other hand, highly cross-linked hydrogels (with ene-groups ratio above 5 mol %) would not swell a lot, containing little water.

In this study, the PAA homopolymer chains were randomly functionalized with ene-groups at their carboxylic acid sites in Milli-Q water at room temperature in the presence of EDC/NHS couple. A peptide reaction was used to graft allylamine onto polymer chains in the presence of EDC as the

dehydration agent and NHS as the addition agent to increase yields and decrease side reactions [25]. The molar ratio AA/allylamine/EDC/NHS is set equal to 10/1/2/2. After 10 g AA (0.14 mol) is dissolved in 150 ml water, EDC/NHS couple is added into the solution under stirring. The solution with a pH adjusted to 4.5 is left under stirring for 2h. The acidic conditions promote the protonation of EDC, facilitating the coupling reaction. Then, the aqueous solution of allylamine is added to the medium, associated with the adjustment of the pH to 10 with NaOH, for the formation of the targeted amide bond through the nucleophilic attack of allylamine onto the carboxylic acid. The reaction is allowed to proceed for 24 hours. The final solution is dialyzed firstly in 0.1 M NaCl solution (to remove the unreacted EDC/NHS) for 3 days, and then in Milli-Q water for 3 days, solvent being changed twice a day. Finally, the polymer is recovered by freeze-drying. From ^{1}H NMR spectra, the ratio of ene-functionalization is calculated and a ratio of about 2% was found (figure 3.23).

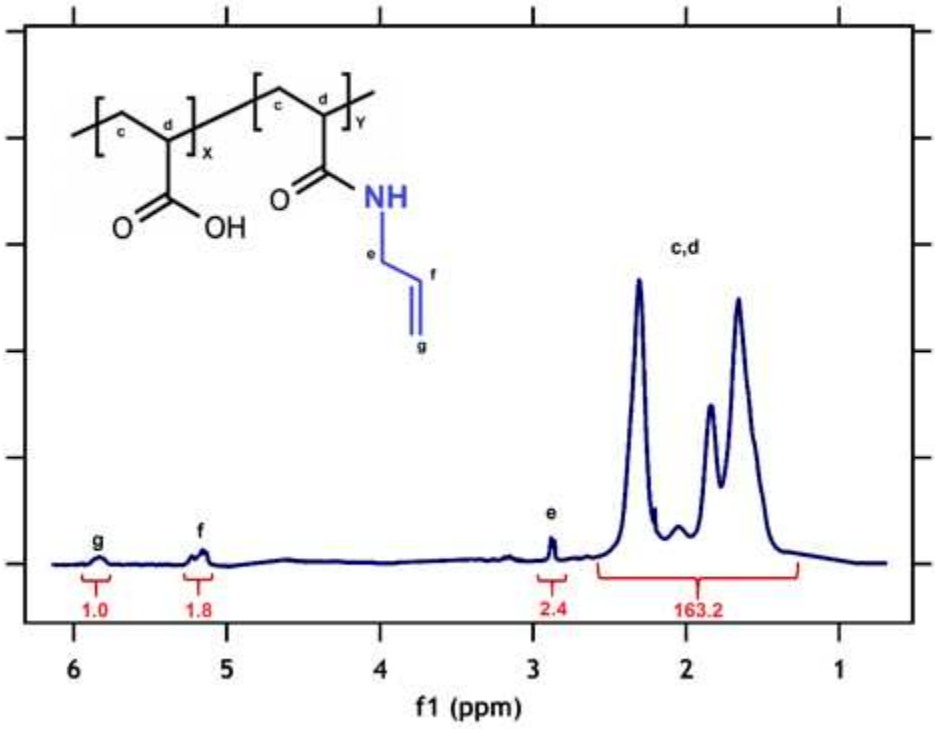

Figure 3.23 : ^{1}H NMR spectrum of ene-functionalized PAA(250K) in D_2O. Regions between 1.1 - 1.2 ppm (residual ethanol CH_2) - and 3.55-.3.65 ppm (residual ethanol CH_3) omitted in the interest of clarity.

3.3.3 Synthesis and Characterization of Hydrogel thin films on gold electrodes

3.3.3.1 Synthesis of PAA hydrogel films

The PAA surface-attached hydrogel films were synthesized by simultaneously crosslinking and grafting reactive PAA by thiol-ene reaction. A mixture of formic acid and methanol (30:70) is used as the solvent. A solution containing ene-reactive polymer and added dithioerythritol cross-linkers was dropped onto thiol-functionalized gold substrates for spin coating. The ratio of dithioerythritol to ene-reactive polymer units is 15 times (corresponding to a molar excess of bifunctional dithioerythritol of 30). This is necessary because disulfide bridges are formed between thiols during crosslinking. The formation of these "groups" dithiols make it possible to adjust the length of the crosslinking agent and facilitate the reaction. The conditions of spin-coating were fixed with the final angular velocity of 3000 rpm and the spinning time of 30 seconds. The samples were rinsed and sonicated in water during 1 min and finally dried with nitrogen flow to remove free chains. For deep UV irradiation, a common 8 Watt UV lamp (=254 nm) with photomasks was used.

3.3.3.2 2D Patterning of the Surface-attached Hydrogel

The formation of surface-attached hydrogel films can be achieved by either UV-irradiation or thermal activation. Deep selective UV-irradiation allows the activation of thiol-ene reaction without any initiator to simultaneously crosslink polymer chains and graft them on thiol modified substrate. In the past, there have been demonstrations of several techniques to pattern hydrogels including micro contact printing [26], ion beam lithography [21,27], micro molding [22,28], evaporation-induced self-assembly [29], wet etching [30], and photomask-based lithography [20].

Most of these techniques are time-consuming or require fastidious processing condition. The deep UV activation technique, in addition to time saving, it provides the ability to create patterns of surface-attached hydrogels. Hence, the patterning of hydrogels can be obtained using common fluorescent lamps with photomasks and in this study patterns were obtained by performing the UV-light irradiation with a commercial UV-lamp (electrical power = 8 W - 32W, UV-C, λ=254 nm) through a photomask. Specifically, the photomask is placed over the spin-coated polymer film and the sample was irradiated for an optimized 2.5 hours for the 8 W fluorescent lamp, in a home-made cardboard chamber at 5 cm distance from the UV lamp.

In an effort to develop a simple, low-cost and versatile method for patterning a thin layer of spin-coated poly(acrylic acid) (PAA), different potential masks were used. Adhesive tape, transparent film mask, Kapton film, Glass slide with 3 mm diameter holes, Adhesive tape coated glass slide with 3 mm diameter holes, 100 nm Chrome on glass slide with 3 mm diameter holes have been tested for the UV patterning before we finally optimized the utilization of Aluminium foil as a mask with 3 mm diameter holes to localize the hydrogel on the 3mm diameter electrode (figure 3.24). The masks were chosen based on their theoretical capacity to absorb and reflect deep UV.

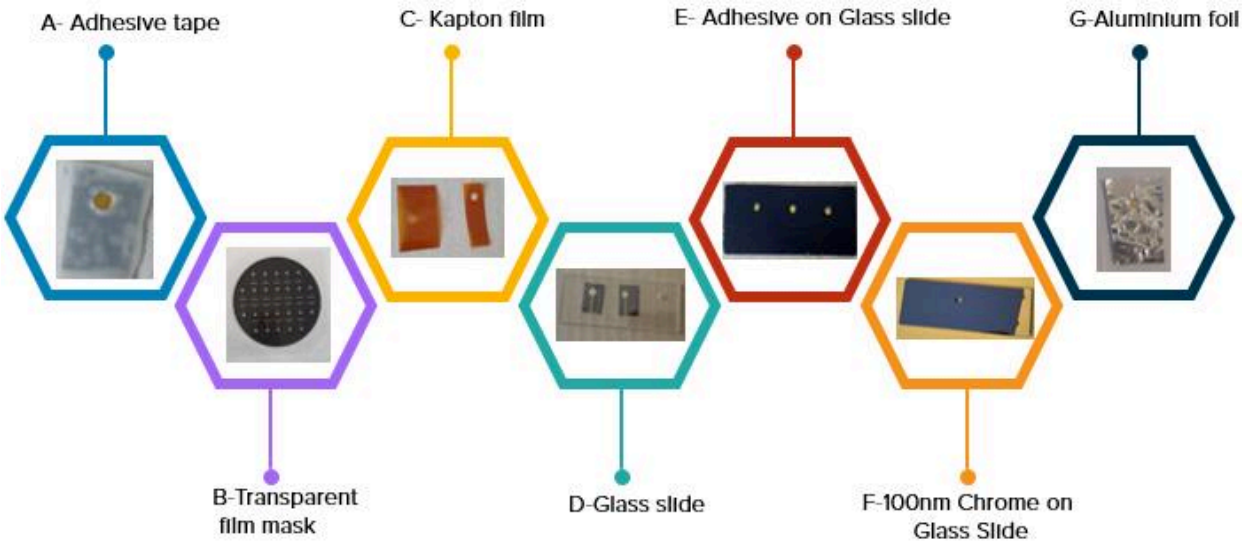

Figure 3.24 : Different masks prepared for patterning the PAA hydrogel on gold electrode (A) Adhesive tape with 3 mm diameter holes (B) Transparent film mask(C) Kapton film with 3 mm diameter holes (D) Glass slide with 3 mm diameter holes (E) Adhesive tape on glass slide with 3 mm diameter holes (F) 100nm Chrome evaporated on a glass Slide with 3 mm diameter holes.

Electrochemical activity and optical imaging techniques were used to identify an optimal mask that clearly demonstrates the facile micro-patterning of the surface-attached hydrogel with good resolution. Briefly, in a first step, the cross linking of the PAA has been performed without any mask in order to have a blank. Electrochemical results have been compared with the bare gold electrode and with SAM modification electrode. It can be observed that in presence of the polymer, there is a significant decrease in the current density and an increase in the ΔE. It has to be noted that the whole electrode is covered by the hydrogel, and so is the connection point. These results are taken as blank experiment. As it is shown in fig. 3.25 and 3.26, there is no significant improvement in the ΔE for the kapton film and the results obtained with the glass slide were better

in comparison. However, there is still an important decrease in the current density compared with electrodes with the SAM modification (2 times lower) and hence we deposited 100 nm chromium on the glass slide in order to be sure that the UV is blocked anywhere else than in the laser cut 3 mm diameter hole pattern. The use of chromium onto the surface of the glass slide slightly improved the results obtained and was more repeatable.

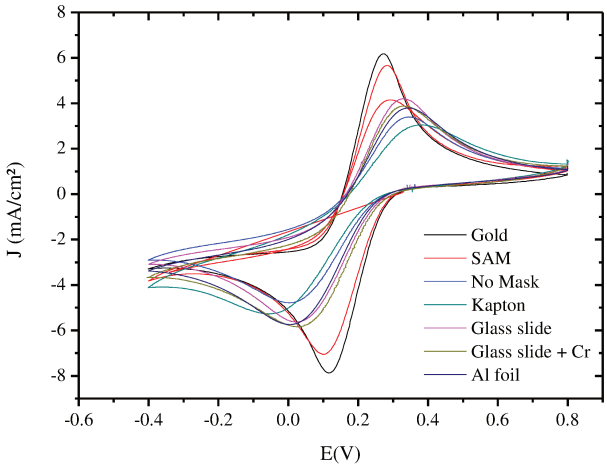

Figure 3.25 : Evolution of the current density in function of the potential applied in a solution of $[Fe(CN)6]^{3-/4-}$ 50 mM + KCl 100 mM (50 mV/s) for electrodes with PAA.

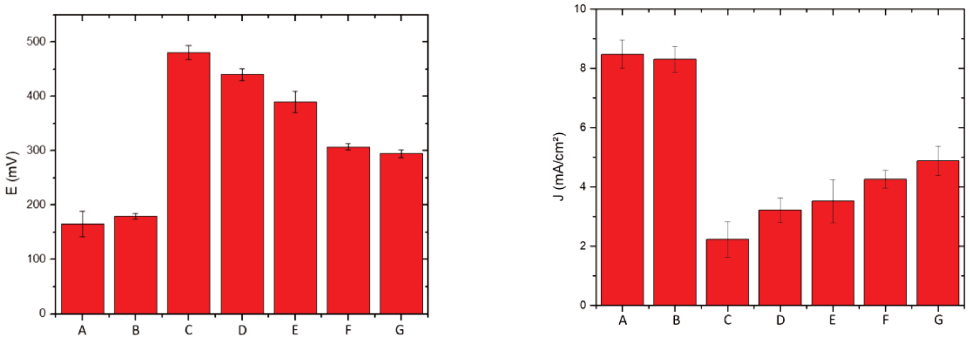

Figure 3.26 : Evolution of the ΔE and ΔJ for different masks used(A) Gold (B) SAM modified electrode (C) without mask (D) Kapton mask (E) Glass slide mask (F) 100nm Chrome evaporated on a glass Slide with 3 mm diameter holes(G) Aluminum foil

Finally, utilization of aluminum foil as a mask resulted in a decreased separation potential and an increased current density in comparison to the other masks. Moreover, imaging techniques proved that that the patterning was better with aluminum foil than the mask used as seen in figure 3.27 and as a result, aluminum foil was chosen and used in this study as a mask for facile 2D patterning of surface attached PAA hydrogel with good resolution.

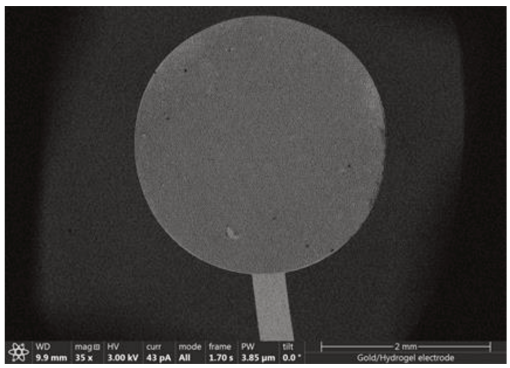

(A)

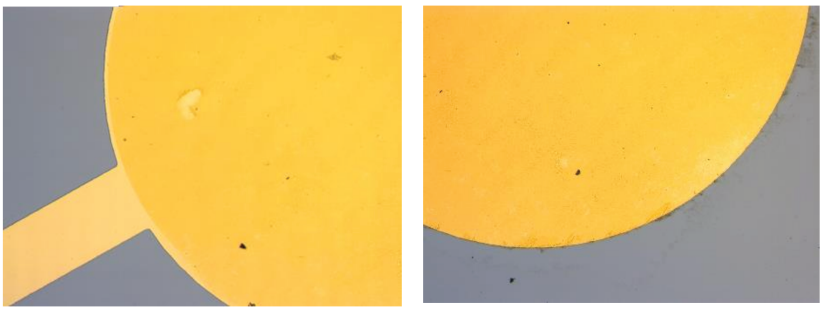

(B)

Figure 3.27 (A) Scanning electron microscope (SEM) images of patterned surface-attached hydrogel. (B) A photograph of patterned 2D hydrogel using UV irradiation for 2.5 hours. The patterns were obtained by using 8 Watt fluorescent lamp with aluminum foil mask.

Figure 3.28 shows the influence of the irradiation time on PAA film thickness. The experiments were performed using a commercial 8 Watt, 16 Watt and 32 Watt fluorescent lamp at a wavelength of 254 nm. The film thickness increases with the exposure time and reach a plateau after 2.5 hours irradiation for the 0.5 % PAA (with molecular weight of 250 kg/mol), using 8 Watt fluorescent lamp. The variation of the film thickness with the exposure time during the first two hours is probably due to partial crosslinking of polymer chains, the uncrosslinked chains being removed by washing. Over radiation seems to cause the degradation of the PAA hydrogel film for both the 16 Watt and 32 Watt experiments and hence, 2.5 hours (8 W) was chosen.

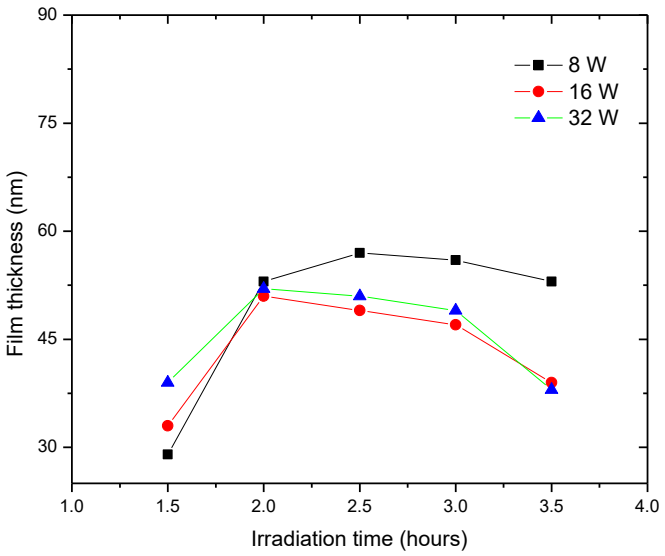

Figure 3.28: The dry thickness of the 0.5 % PAA hydrogel film coating (the average molar mass is 250 kg/mol) as function of UV-irradiation time. The data are given for three different UV power.

3.3.3.3 Film thickness evaluation: Effect of polymer concentration

The dry thickness remains the same after many steps of immersion in solvent, demonstrating that the stability of polymer films is due to covalent bond between chains and with the substrate. In general, the hydrogel thin films fabricated are stable and durable due to covalent bonds between chains and with the surface. If there is no chemical (or covalent) cross-linking, the hydrogel films were demonstrated to not be stable and polymer (free) chains will be removed during samples washing (see section 3.4.1).

The thickness of surface attached hydrogel thin film formed on thiol modified gold substrate, prepared by spin-coating depends on the viscosity of the solution, the speed of rotation and the evaporation rate of the solvents used. In the spin-coating process, the film thinning can be modeled by hydrodynamic equations describing radial out-flow and solvent evaporation. It is given by the expression: $h \alpha \omega^{-1/2} \eta^{1/2} Cp$ where h is the final thickness, ω the rotation speed, η is the viscosity of the solution and Cp is its polymer concentration. The power law dependence of the viscosity with the exponent of ½ is preferred to the value of 1/3 assuming that all the solvent flashes off at a certain time. This assumption is in agreement with our spin-coating conditions with the use of

very volatile solvent such as methanol. As the viscosity of polymer solution can be expressed as function of the concentration and the molecular weight as Cp M α where α is the Mark-Houwink parameter between 0.5 for theta solvents and 0.8 for good solvents. Hence, the thickness of polymer hydrogel thin films is given by the expression: $h \alpha \omega^{-1/2} M^{\alpha/2} Cp^{3/2}$.

For the thickness measurement, the samples are prepared from polymer solutions at different concentrations to obtain different thicknesses. It is important to note that in our spin-coating experiments, the spin speed was fixed at 3000 rpm for 30 seconds, but the variation of this parameter could be as valuable as that of polymer concentration and molecular weight to reach the desired thickness. The film thickness is plotted as $M^{\alpha/2} Cp^{3/2}$ using $\alpha = 0.8$.

The thickness of the hydrogel as a function of polymer concentration is shown in figure 3.29. The dry thickness is measured before and after rinsing with methanol. For the measurement of thickness, we have previously characterized the gold surface by ellipsometry, which allowed us to obtain the optical constants (n and k) of the substrate.

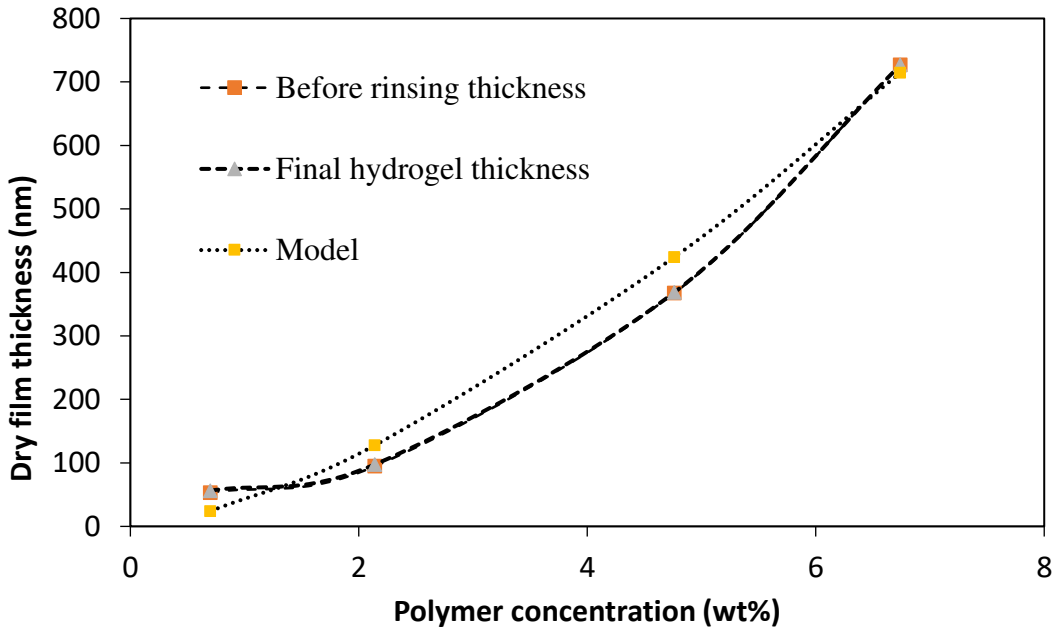

Figure 3.29 : Dry thickness of PAA hydrogel films as function of polymer concentration before rinsing (■), after rinsing (▲), theoretical model (■) for average molar mass of 250 kg/mol using ellipsometry. The ellipsometric measurements corresponds to the mean of three measurements.

The comparison of the experimental and theoretical curves confirms the spin-coating theory linking the final thin film thickness to the $Cp^{3/2}$ polymer concentration. We also note that the thickness varies very little between these different measurements. This means that almost all the polymer deposited by spin-coating has been grafted on the surface and is not fallen off/delaminated by rinsing and ultra-sonication (the curves before and after rinsing are overlapping).

3.3.3.4 Electrochemical characterization of hydrogel surface

Looking in to the separation potential and current density of the cyclic voltammetry experiments carried out for different polymer concentrations, it is shown in figure 3.30 that the current density decreasing from 0.5 % to 6% and the separation potential increasing from 0.5 % to 6 %. The imaging techniques, using optical microscopy, showed a slight degradation of the hydrogel especially for the 6% PAA hydrogel. Hence, for the experiments carried out in this study to construct the aptasensor, we decided to use 0.5% PAA.

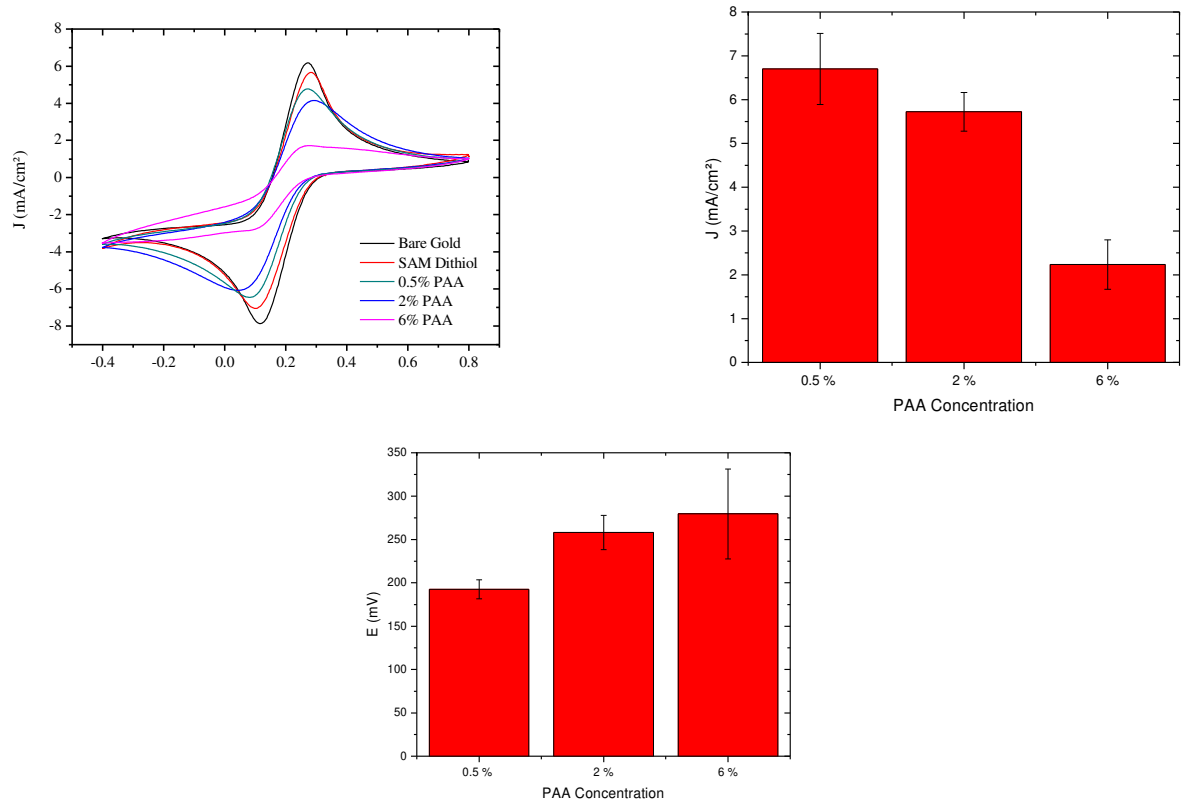

Figure 3.30: CVs and Evolution of the ΔE and ΔJ of hydrogel modified electrode in a solution of $[Fe(CN)6]^{3-/4-}$ 50 mM + KCl 100 mM (50 mV/s)solution

Taking into consideration the pKa of PAA, 4.5, the 0.5% PAA hydrogel modified electrode was electrochemically analyzed to see how the electrode behaves as a function of the pH. The voltammetry for a variety of redox molecules at our hydrogel modified electrodes provides additional qualitative information about the nature of the material and the basic kinetic performance of the electrode. The voltammetric reversibility of highly charged redox ions is markedly influenced by the attractive/repulsive interactions with the polyanionic layer that the ions must penetrate to reach the electrode surface. The voltammetry for three redox markers of ferricyanide($^{3-/4-}$), Ferrocenemethanol (FcMeOH) and ruthenium hexaammine($^{3+/2+}$), at hydrogel modified electrodes at a concentration of 5 mM in 0.1M buffers of different pH is given in Figure 3.31. For the reversible reaction that involves the transfer of one electron, the difference between the potentials of the cathodic and anodic peaks should equal ΔEpeak = 59 mV. Also, the ratio of the peak heights should equal unity and the difference in the I-E profiles (voltammetry measurements) of the hydrogel modified electrode are interpreted accordingly.

As shown in figure 3.31, the voltammetry for the redox markers at hydrogel modified electrodes is clearly affected by electrostatic interactions, and the reduction of ferricyanide is less reversible at pH 9 and 7 than at the pH 3, as evidenced by the increased separation potential (ΔE), 245 mV, 157 mV and 149 mV respectively. The variation observed in separation potential, for the quasi-reversible behavior of what is expected to be a reversible redox couple using the different pH studies, particularly for the increased irreversibility for the redox couple at pH 7 and 9 is due to the repulsive electrostatic interactions between the deprotonated PAA at these pH values and the negatively charged probe, impeding the ability of anions to reach the electrode surface.

Conversely, the reversibility of the reduction of positive probe used, ruthenium hexaammine (RuHex), is enhanced at hydrogel modified electrode suggesting that the RuHex is able to approach the electrode surface more closely, the reduction proceeding at the diffusion limited rate. A surface wave for RuHex is observed as a postwave shoulder when the voltammetry is measured and the reduction of RuHex is enhanced, the return oxidation is still diminished, as evidenced by the broader diffusive wave shape and lower peak current (figure 3.31(B)). The voltammetry for the oxidation of a neutral probe, Ferrocenemethanol, is nearly identical for the hydrogel modified electrodes at the different pH with similar separation potential of 60 mV. In general, the results obtained indicated that the hydrogel modified electrode is responsive to different pH and is stable in different media.

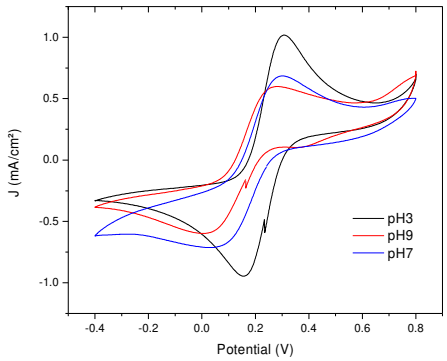

(A)

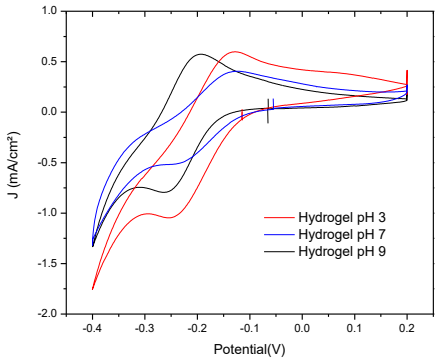

B)

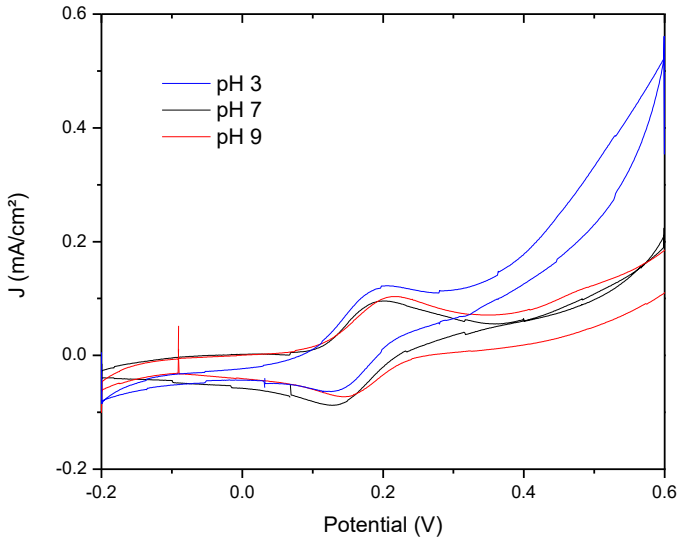

(C)

Figure 3.31: Cyclic voltammograms of hydrogel modified electrode in different buffer containing 5 mM (A) $K_4[Fe(CN)_6]$ (B)$[Ru(NH_3)_6]Cl_3$ (C)FcMeOH

Table 3.3: Parameters obtained from cyclic voltammetry (CV) recorded in different solution containing 5mM $[Fe(CN)_6]^{4-}$, $[Ru(NH_3)_6]^{3+}$ and FcMeOH at 50 mV s^{-1} for hydrogel modified electrode

	pH 3				pH 7				pH 9			
Probe	**Epa(V)**	**Epc(V)**	**ΔE**	**Ipc/Ipa**	**Epa(V)**	**Epc(V)**	**ΔE**	**Ipc/Ipa**	**Epa(V)**	**Epc(V)**	**ΔE**	**Ipc/Ipa**
FcMeoH	0.19	0.13	60	0.78	0.19	0.13	60	0.84	0.21	0.14	60	0.7
$[Fe(CN)_6]^{3-/4-}$	0.286	0.06	149	0.97	0.30	0.15	220	0.93	0.26	0.01	245	1.0
$[Ru(NH3)6]^{3+/2+}$	-0.137	-0.248	111	0.33	-0.2	-0.25	90	0.47	-0.13	-0.23	57	0.43

E_{pa} and **E_{pc}:** Anodic and cathodic peak potential respectively;

ΔE(mV): difference between anodic and cathodic peak potential;

Ipc/Ipa: cathodic/anodic current peak ratio.

Figure 3.32 shows the behavior response of the surface attached hydrogel using the negative probe. The voltammogram obtained shows at relatively high pH, for which the PAA hydrogel is swollen and dissociated, when comes in contact with the negative redox probe, $Fe(CN)_6^{3-/4-}$, it causes electrostatic repulsion which will affect the interfacial electron-transfer rate of the probe and a decrease in peak current and increased separation potential in comparison to the bare gold and thiol-modified electrodes. Moreover, this can be explained with the study that describes polyacid brushes at low pH are fully protonated and adopt a conformation similar to that of neutral brushes[31]. At high pH, the acid groups on the brush become dissociated and the brush behaves as an extended polyelectrolyte brush in the osmotic or Pincus regime[32].

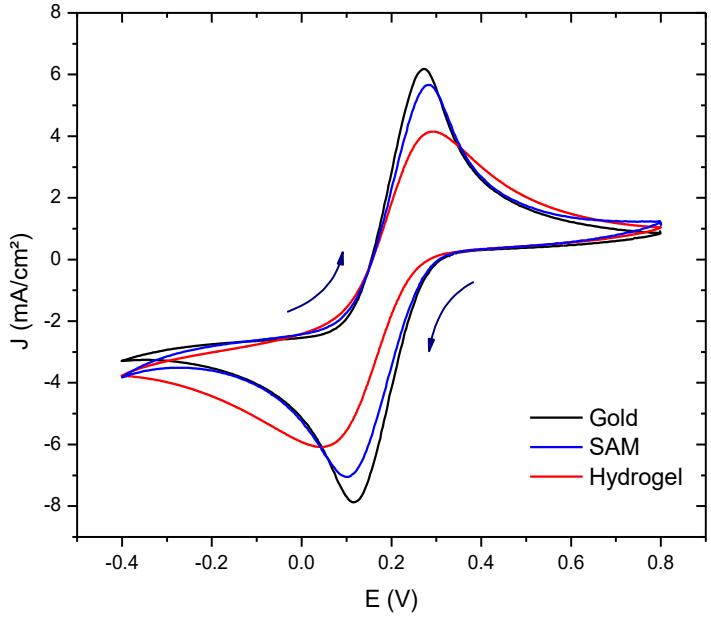

Figure 3.32 : Characterization of the sensing interface by cyclic voltammetry at 50 mV.s^{-1} in a solution of KCl 0.1 M containing 5 10^{-2} M $K_4[Fe(CN)_6]$ and $K_3[Fe(CN)_6]$: bare gold electrode (black), thiol monolayer (blue), PAA hydrogel film (red).

3.3.3.5 Adhesion between the surface attached hydrogel and electrode substrate

Adhesion between the surface attached hydrogel and the gold electrode substrate plays an important role for long-term use and hence we studied if we have an efficient adhesion to ensure chronical electro activity of the modified electrode otherwise, the coating may be delaminated and fall off from the electrode after a period of time in use. Table 3.4 displays the adhesive property between Au substrate and the surface attached hydrogel (0.5 % PAA) thin film and also as a control sample, adhesive property between thiol modified gold electrode and 0.5% PAA hydrogel without cross linker, physically adsorbed on the surface is listed in the table. The physical adsorption could not resist desorption caused by water diffusion and the surface attached thin film detached easily.

Table 3.4: The adhesive property between Au substrate and the surface attached hydrogel (0.5 % PAA) thin film.

Electrodes	Conditions		
	Immersion in DI water	**CV(20 cycles)**	**Ultrasonication**
Control Sample	Fall off after 1 min	NA	Fall of after 10s
Hydrogel modified electrode	Intact after 1 month	Good condition/Intact	Fall off/delaminated after 10 minutes

The adhesion to the substrate for the hydrogel coating fabricated via the CLAG approach and modified thin film synthesis described above, however, was observed to be more stable. The coating was not detached in water even after 1 month. Further microscopy study also showed that no delamination of the hydrogel from substrate was observed and the hydrogel modified electrode remained intact. Moreover, no electro activity attenuation was observed after cyclic sweeping for 20 cycles as shown in Fig. 3.33, indicating that the hydrogel coating was well adhered to the substrate and the hydrogel modified electrode retained good stability. However, CV test could not be applied to the control due to its instability in the testing solution. Adhesion is, presumably, improved by the fact that the hydrogel network is chemically crosslinked and grafted to the electrode by covalently anchoring, which inhibits the diffusion of the formed chains away from the electrode substrate.

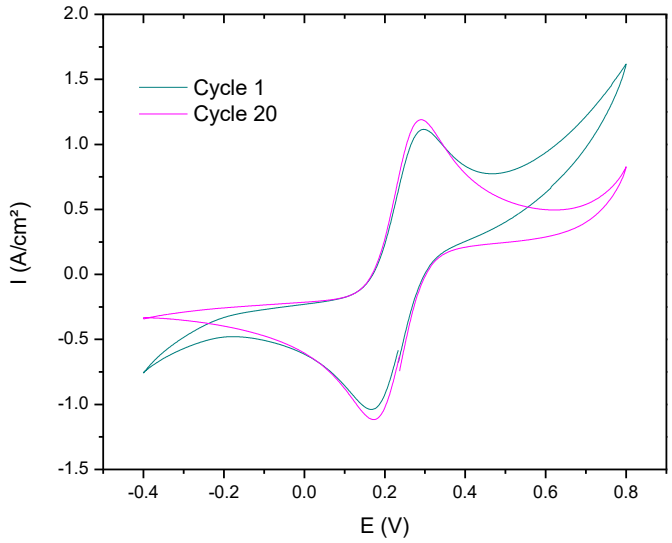

Figure 3.33: CV of hydrogel modified electrode after cyclic sweeping for different cycles.

3.4 WCA and Topography features of electrode-attached hydrogel films

3.4.1. Water contact angle

For the different stages of electrode construction, contact angle measurements were performed to evaluate the presence of the different layers put on and hence, the same is confirmed by analyzing the materials hydrophobicity and/or hydrophilicity. Though the water contact angle (WCA) value shows relatively a hydrophobic surface for the silicon wafer, after the plasma cleaning the wafer exhibited dramatic differences in the contact angle indicating the surface change from a hydrophobic state to hydrophilic. The WCA of the cleaned bare gold is ~62°.

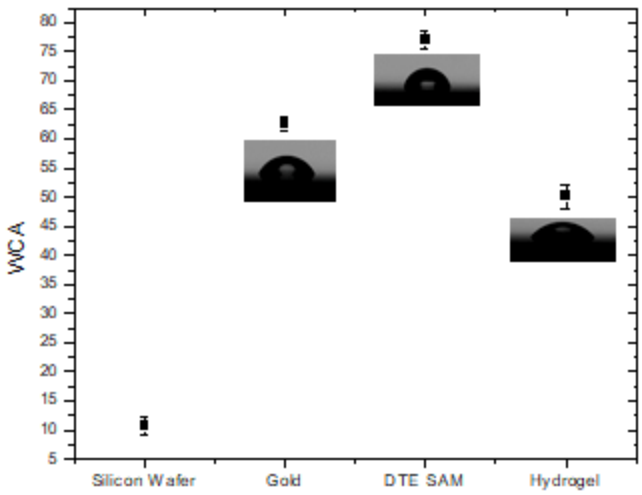

Figure 3.34: Water contact angle of the different stages of electrode fabrication

The WCA on the DTE modified gold exhibited higher contact angles (~75°) compared to that of the clean gold electrode, evidencing the modification of gold surface properties. The WCA measurements of SAMs are reported to have a parity (or odd-even) *vs* chain-length relationship [33,34].

After the formation of PAA hydrogel on thiol-modified gold electrode, the water contact angle is around 50°. Accounting for the homogeneity and smoothness of the thin PAA film, the contact angle expresses the presence of polymeric polyelectrolyte surface and this result is consistent with a previous study described for the water contact angle of hydrophilic and negatively charged hydrogel at constant grafting density [35].

3.4.2. AFM and SEM analysis

The thickness of both the gold and dry hydrogel layer grafted on a DTE SAM-modified gold substrate was determined using AFM measurements. It was found to be around 100 nm for the bare gold electrode and 57 nm for the PAA hydrogel. The dry thickness of the PAA hydrogel film is consistent with the value found for surface-attached hydrogel films using spin-coated polymer solution with concentration of 0.5 wt % and molecular weight of 250 kg mol^{-1} [13].

Since the PAA modified electrodes will be used in aqueous solutions, it is important to evaluate the properties of the film in humid conditions. The swelling ratio is measured as the ratio of the swollen thickness of hydrogel films (measured in water) to the dry thickness (measured in air). This parameter allows to evaluate the swelling of the PAA film in water. The measurements were

conducted with hydrogel films fabricated with 2 % ene-reactive groups and 30 times the ene-reactive groups excess of dithioerythritol cross-linkers. Both thicknesses (dry and swollen) were evaluated thanks to AFM measurements, as illustrated on Figure 3.35. The swelling ratio was found to be 1.8. This means that the thickness of the hydrogel is almost double in humid conditions. This result is consistent with the study that states for thin films of below 150 nm, the swelling ratio increases with the film thickness and it is independent of the thickness in the whole range from 150 nm to a few micrometers [13,36]. This is related to the strong effect that the surface attachment has on the swelling of films and hence, nanometric hydrogel films swell on average less than micrometric layers as a result of the constraint due to the surface attachment.

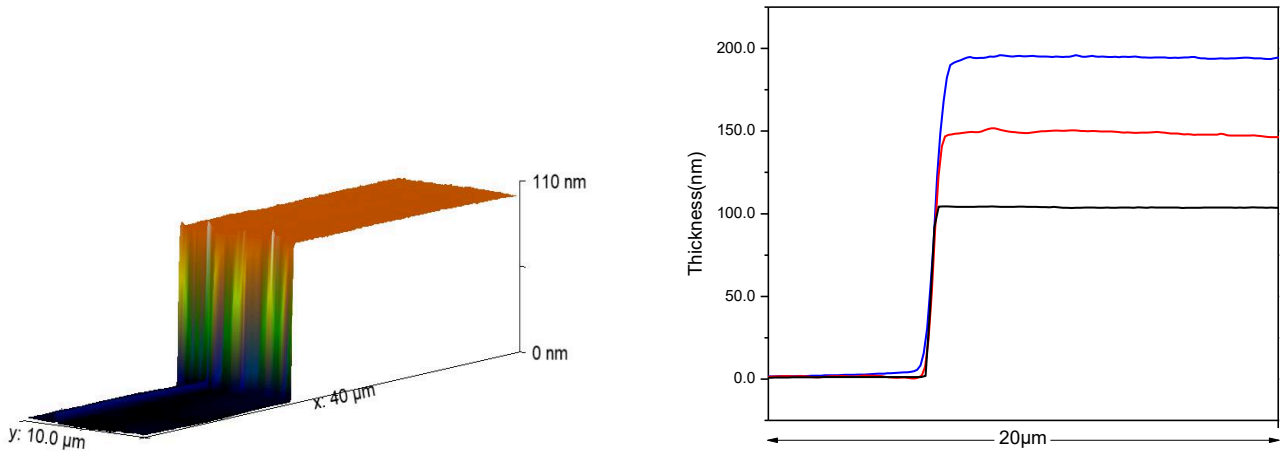

(a) **(b)**

Figure 3.35(a) Schematics of height profiles obtained by AFM for bare gold (blue area : silicon; orange area : gold) (b) Height profiles of gold electrode (in black), PAA hydrogel film in air (red) and PAA hydrogel film in water (blue).

Topographic images and height profiles of the bare gold surface, the surface-attached hydrogel film in air and the surface attached hydrogel immersed in water have been determined by AFM (Figure 3.35 and Figure 3.39) and scanning electron microscopy (SEM) (Figure 3.37 and Figure 3.40). The AFM image obtained for the evaporated gold surface shows a typical grainy structure (Figure 3.36a). To illustrate the roughness difference between the samples on Figure 3.36, a profile line is extracted for each height image and displayed below the image. The roughness of the gold surface can be extracted from the AFM images measuring the half width of the height histogram

of the image. From the Figure 3.36 (a), a roughness of 4 nm is obtained. It is important to underline that the same roughness value (~ 4 nm) is obtained for both images using different scanning area (1 µm- and 10 µm-scales), proving that the roughness is independent of the size of the sample and is homogeneous. In the general case, the roughness strongly depends on the image size, but here, the roughness of the sample is completely determined by the morphology of the coated gold on the (plane) silicon wafer. It means that increasing the image size does not reveal additional lower spatial frequency. All in all, the large homogeneity of the bare gold electrode at 10 µm-scale and the granular structure at 1 µm-scale observed by AFM are also confirmed by SEM (Figure 3.37).

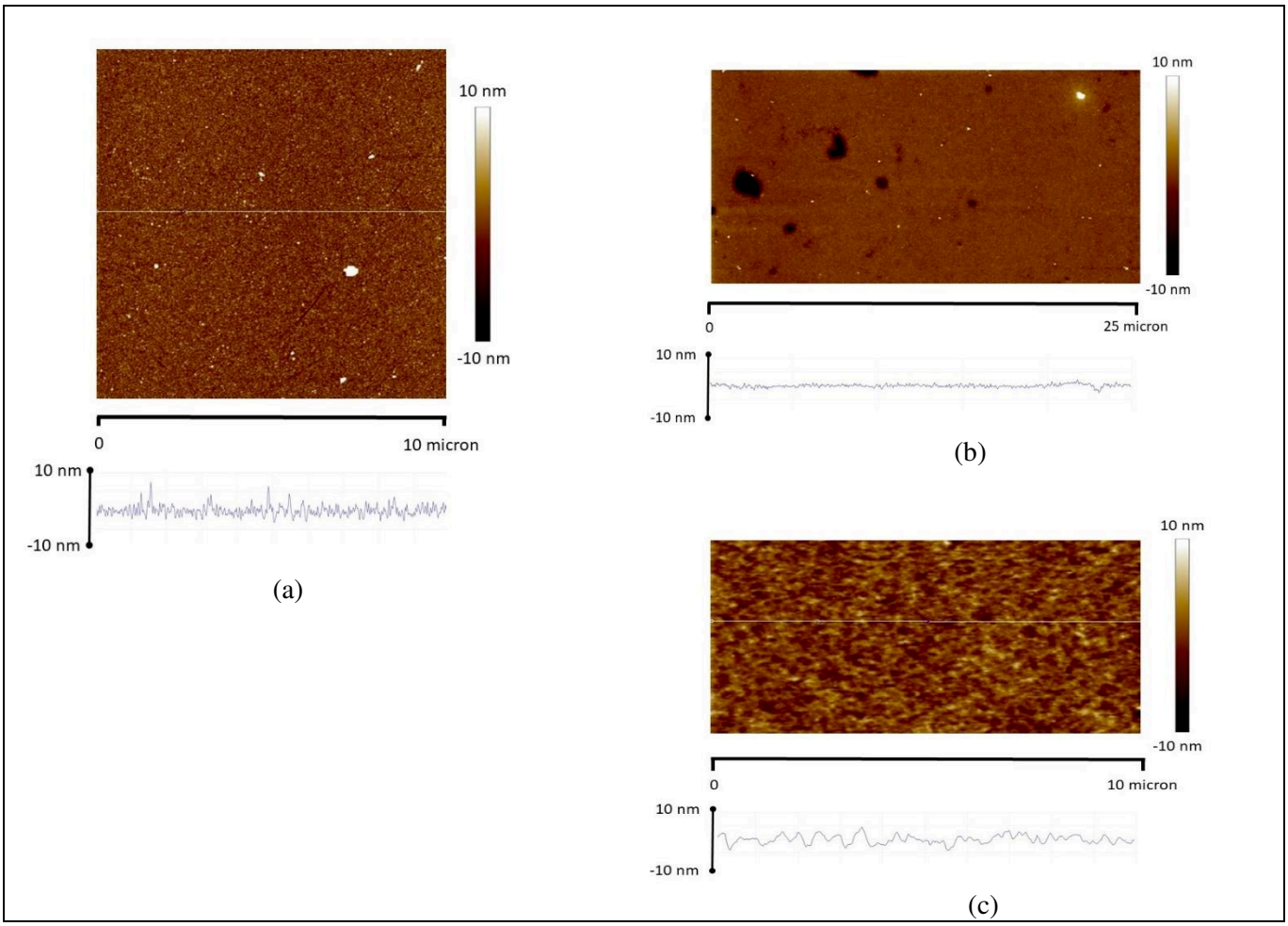

Figure 3.36: AFM tapping height images of the bare gold electrode surface (a), AFM tapping height images of the hydrogel film in air (b) and AFM height contact images of the hydrogel film immersed in water (c).

The AFM images of PAA hydrogel film in air (Figure 3.36b) also show that the roughness, estimated to 1 nm (half width of the height histogram of the image), is homogeneous. Even though the thickness of the hydrogel film (~ 57 nm) is much higher than the roughness, the surface of the hydrogel film replicates that of the gold electrode and follows strictly the same granular structure. The replication of the morphology of the gold surface is confirmed by SEM. In Figure 3.38, the SEM image displays the frontier between the hydrogel film (dark region) and the bare gold surface. The inset enables to highlight the granular structure on both surfaces of the gold electrode and the hydrogel film with a slightly lower topography contrast in the hydrogel region. The observation of the hydrogel region (upper part of Figure 3.38) on the large scale (50 μm-) confirms the high planarity of the hydrogel surface. Finally, the hydrogel film immersed in water (Figure 3.36c) showed higher roughness (~ 4 nm) than that in air, as the gel swells (recalling that the swelling ratio is 1.8). As a result, we show that the roughness of the hydrogel film surface is due to the replication of the granular morphology of the gold electrode. It is anyway much lower than the thickness of the layer, so that the hydrogel film can be considered as fully homogeneous and plane.

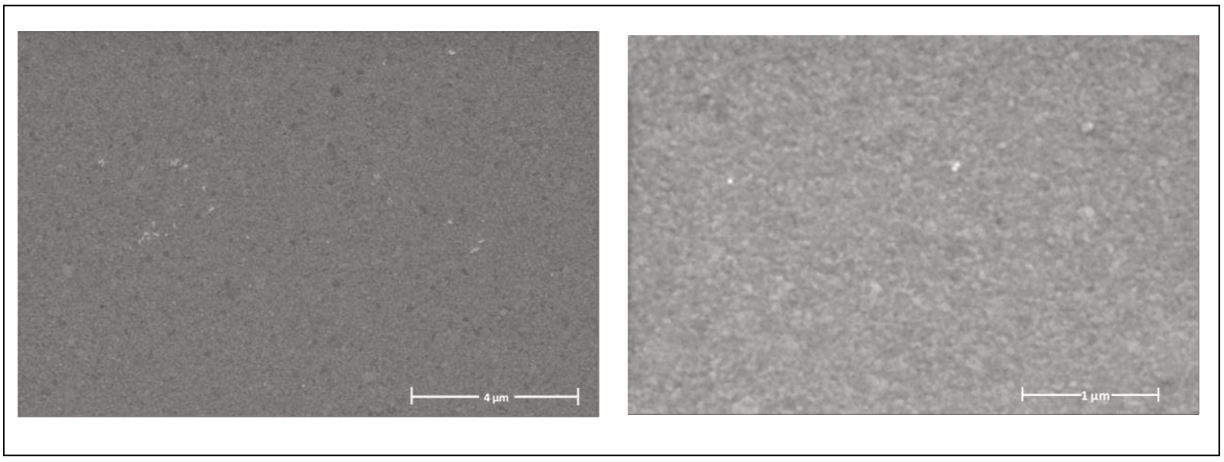

Figure 3.37: SEM images of the bare gold electrode surface at different scales

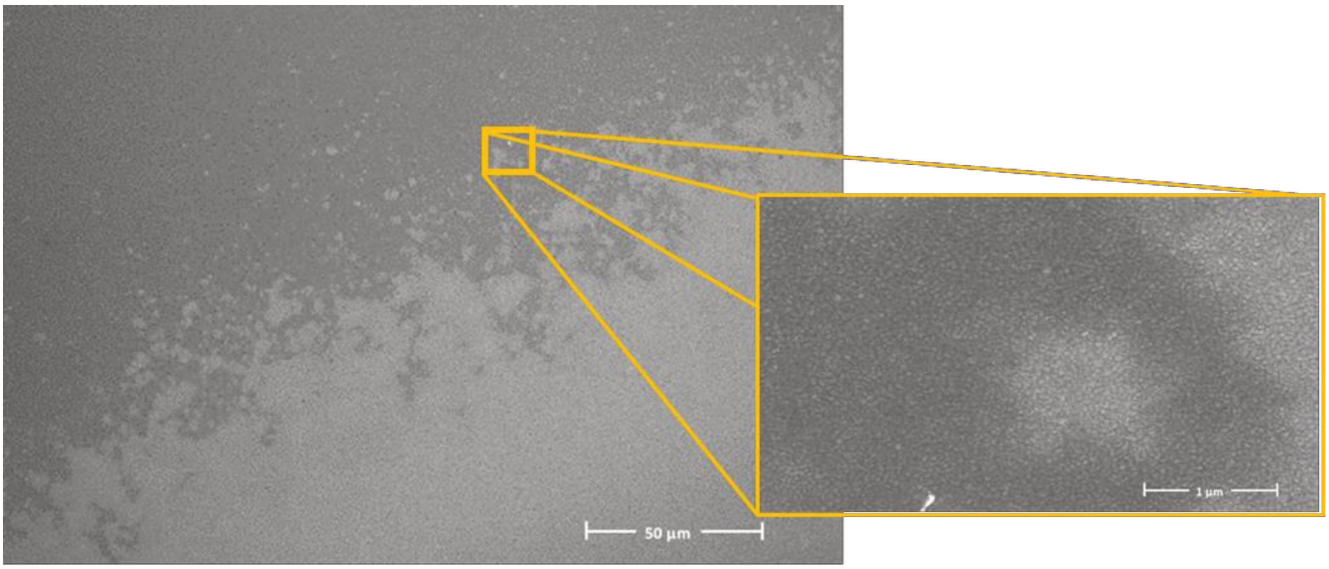

Figure 3.38 :. Surface morphology of hydrogel (dark area) and gold (white area) visualized using scanning electron microscope (SEM)

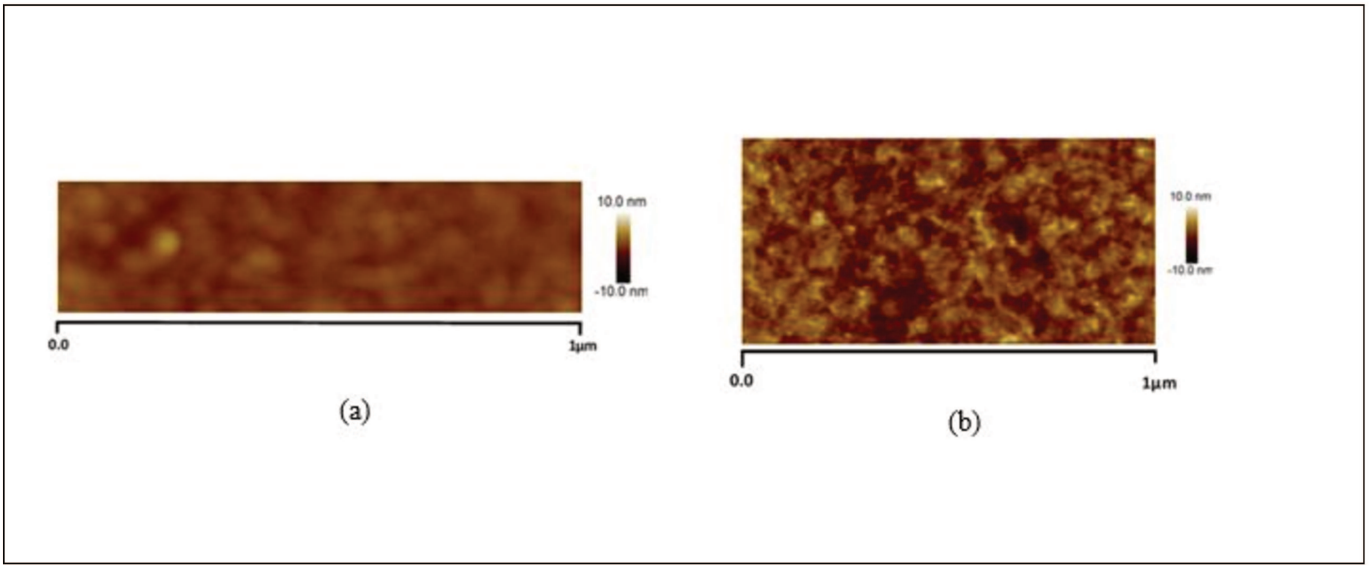

Figure 3.39: AFM height images of the hydrogel film in air (a) and height images of the hydrogel film immersed in water (b)

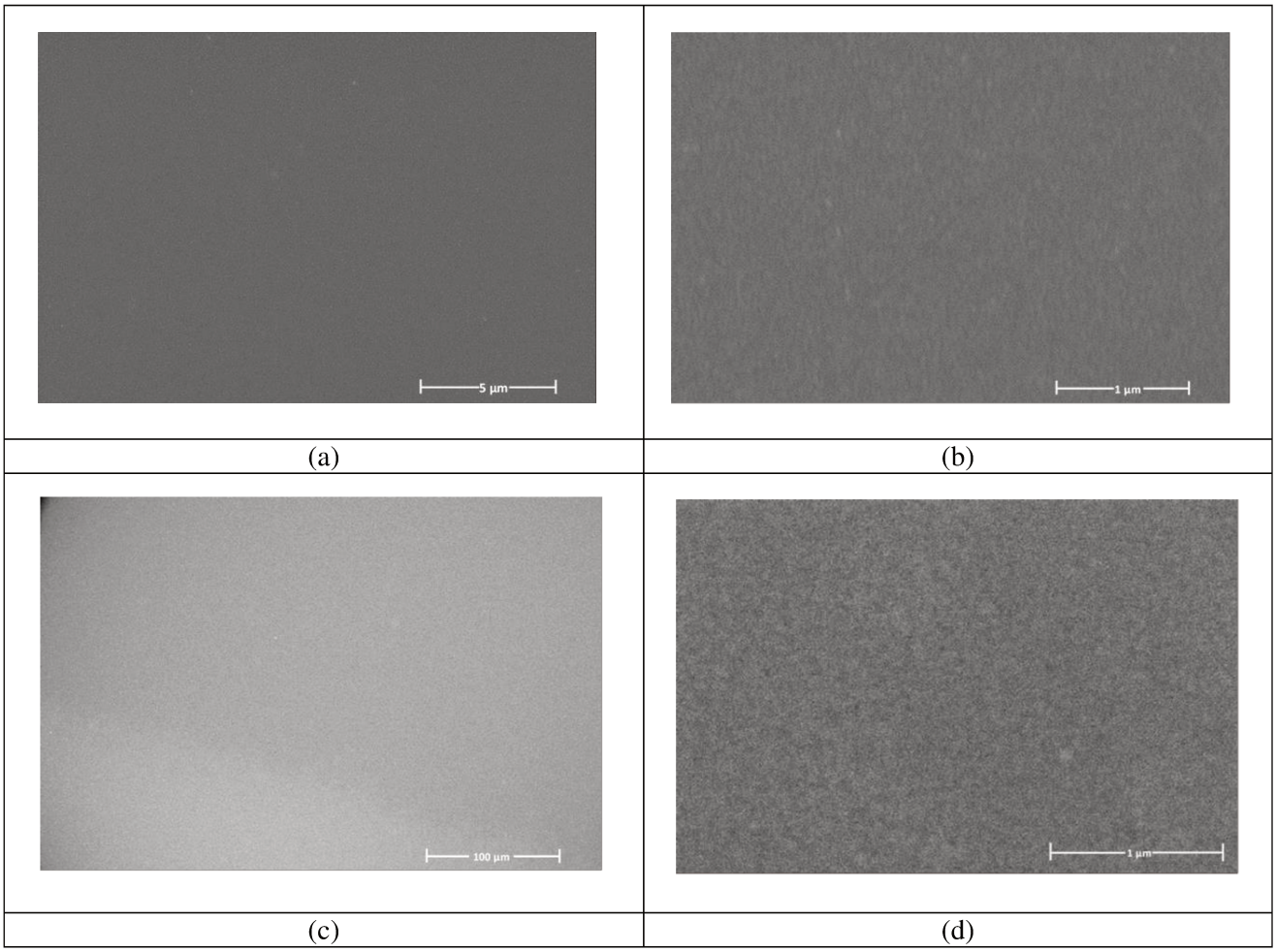

Figure 3.40: Surface morphology using SEM of hydrogel film in air (a and b) hydrogel film after immersing in water (c and d)

3.5 ATR-IR Characterization of the hydrogel-modified electrode

Electrodes were also characterized by ATR-FTIR spectroscopy and electrochemistry, after cross-linking and grafting of PAA to evidence the presence of the hydrogel on the electrode surface. Figure 3.41 shows the ATR-FTIR spectra between 500 and 4000 cm^{-1} of the gold electrode after thiol modification and after the formation of PAA hydrogel. As the contact between the ATR-diamond waveguide and the solid silicon substrate cannot be reproducible for different samples, the absorbance is in arbitrary unit. This representation also enables to highlight the absorption bands. The spectrum on figure 3.41 (a) exhibits the presence of the large band in the range of 500 to 750 cm^{-1}, which can be assigned to the stretch mode of C-S bond showing the presence of covalent gold-sulfur bonds. Secondly, the vibration mode of alkyl thiol is observed at 2917 cm^{-1}. Moreover, the peaks at 1017 cm^{-1} correspond to the O-H deformation mode. The O–H stretching

vibrations in the range of 3100–3500 cm^{-1} can also be clearly seen. The presence of these bands demonstrates that the gold electrode is modified by thiol molecules.

The FTIR-ATR spectrum on Figure 3.41 (b) is obtained with the gold electrode modified by the PAA hydrogel. It evidences the O-H stretching band in 3400 cm^{-1} region and the CH2 (asymmetric) stretching at 2925 cm^{-1}. Also, the bands at 1700 cm^{-1} are assigned to C=O stretching band of PAA. Comparing spectra (a) and (b), it could be noticed that the O–H stretching vibration in the range of 3100 – 3500 cm^{-1} is different. The absorption band of the PAA hydrogel which is characteristics of hygroscopic compound is broader due to the presence of H-bonds (in comparison with the O-H stretching band of thiol monolayer). The decrease of the O-H band at 1017 cm^{-1} is due to the arbitrary unit of the absorbance. Finally, it should be noted that the presence of C-S band in PAA hydrogel spectrum is not surprising as the thickness of the hydrogel film is much less than the penetration depth of the evanescent wave of the ATR-infrared beam (a few microns).

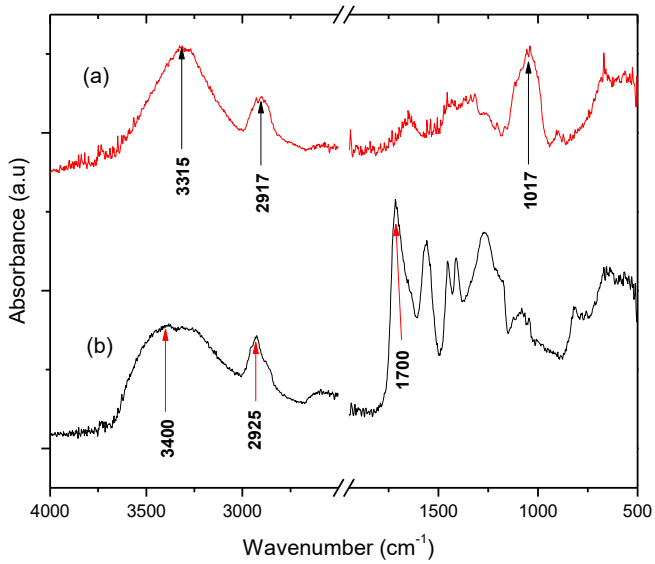

Figure 3.41: FTIR-ATR spectra of thiolated gold electrode (a) and PAA hydrogel grafted gold electrode (b).

3.6 Functionalization of PAA films and Immobilization of the Aptamer

3.6.1 Covalent Immobilization of the Aptamer

The covalent immobilization of the aptamer on the surface of the PAA hydrogel film grafted on the underlying electrode was achieved through two stages EDC/NHS chemistry. A standard method for immobilization of NH_2-containing biomolecules onto carboxyl-containing substrates via covalent amide bond is using N-ethyl-N'-(3-(dimethylamino)propyl)carbodiimide (EDC) and N-hydroxysuccinimide (NHS), which is well-known in peptide synthesis[37]. The EDC/NHS activation approach possesses many merits: high conversion efficiency, mild reaction conditions, excellent biocompatibility with little influence on the bioactivity of target molecules, and much cleaner products than other crosslinking reagents such as glutaraldehyde and formaldehyde. Activation commonly consists of forming a reactive NHS-ester by a two-step reaction between the acid and a carbodiimide to form O-acylurea followed by a reaction between O-acylurea and NHS to yield the activated NHS-ester[38] (figure 3.42).

The activation of carboxylic acids is a complex reaction (figure 3.43), competitive paths are formation of anhydride by dehydration of O-acylurea with a neighboring carboxylic acid (reaction 2 in figure 3.43), which may further evolve to NHS-ester depending on its structural stability, and formation of stable N-acylurea via an intramolecular acyl rearrangement (reaction 1 in figure 3.43), which is negligible at the well accepted reaction conditions and only becomes serious at extreme conditions such as high temperatures and high concentrations.[39] Anhydride is also a linking moiety and can react directly with primary amine, resulting in equal quantities of two products, amide and carboxylic acid. NHS-ester, however, reacts with primary amine to produce only a single product of amide. From the product viewpoints, obviously the cross-linking efficiency of anhydride is only half that of NHS-ester. In addition, different structural anhydrides have much different hydrolysis rates, not like NHS-esters which have similar hydrolytic behavior during the amidation reaction. Therefore, NHS-ester is preferred in amidation even though anhydride can be easily obtained by using only EDC for dehydration of carboxylic acids.

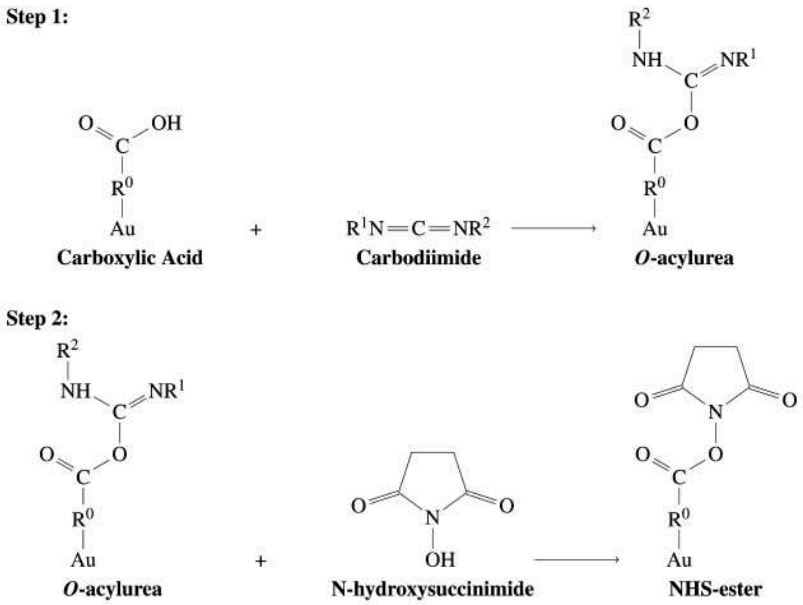

Figure 3.42 : Activation of carboxylic Acids by Carbodiimide and NHS without Byproducts[38]

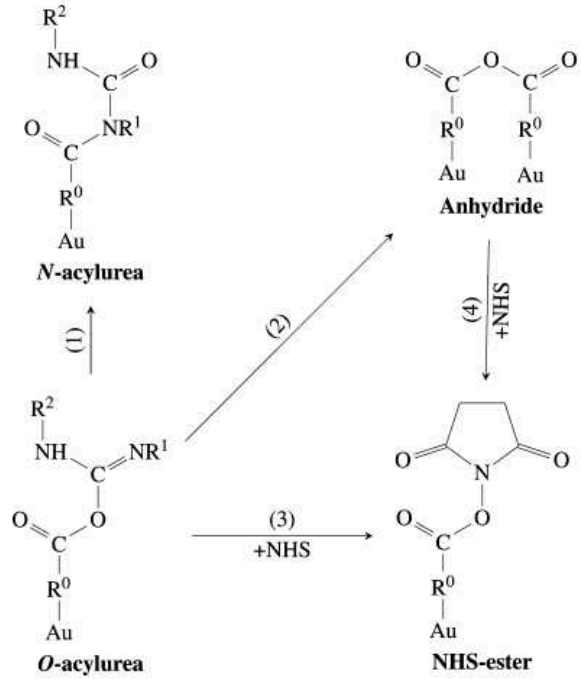

Figure 3.43 : Possible Derivatizations of O-Acylurea in the presence of NHS, including the expected NHS-Ester and Main Byproducts and Anhydride [38]

Although prepared NHS or Sulfo-NHS esters are sufficiently stable to process in a two-step reaction scheme, both groups will hydrolyze within hours or minutes, depending on water-content and pH of the reaction solution. (NHS esters have a half-life of 4-5 hours at pH 7, 1 hour at pH 8 and only 10 minutes at pH 8.6 [40].

The activation reaction with EDC and Sulfo-NHS is most efficient at pH 4.5-7.2, and EDC reactions are often performed in MES buffer at pH 4.7-6.0. Reaction of Sulfo-NHS-activated molecules with primary amines is most efficient at pH 7-8, and Sulfo-NHS-ester reactions are usually performed in phosphate-buffered saline (PBS) at pH 7.2-7.5[37]. Based on this, a semi-optimization for the covalent coupling of the aptamer was done first for a model molecule used, P-nitroaniline, and later applied to the aptamer immobilization.

Figure 3.44 shows the ATR-FTIR spectra at different stages of the sensor construction: the PAA hydrogel, the activated PAA hydrogel and the grafting of the aptamer. The spectrum of the activated hydrogel shows three characteristic bands at 1815, 1790, and 1750 cm^{-1} which are representative of the carbonyl stretch modes in the COO-NHS ester moiety. After aptamer immobilization, the anhydride and NHS ester peaks disappear and new amide bands appear around 1580 cm^{-1} and 1660 cm^{-1} (characteristics of amide I and amide II), thus confirming the efficient covalent immobilization of aptamer on the PAA hydrogel surface.

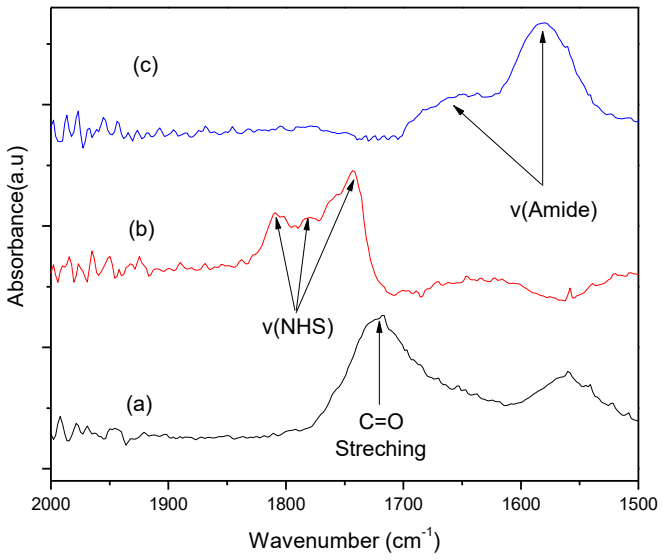

Figure 3.44: ATR-FTIR spectra of Au/PAA hydrogel (a), Au/activated PAA hydrogel (b) and Au/PAA hydrogel/grafted DCL aptamer (c).

The modified electrodes were also analyzed by impedance spectroscopy. Figure 3.45 displays the Nyquist diagrams of the sensor involving different construction steps. The Nyquist plots of the electrodes include a semi-circle at the highest frequency range explored, and linear portion at the lowest frequencies. The semicircle is related to charge transfer resistance (Rct). The linear part is ascribed to diffusion processes. Its slope is not affected by PAA presence nor by the aptamer immobilization. A change in the value of Rct is related to the blocking effect of the stepwise modification procedure of the electrode. The double-layer capacitance (Cdl) and Rct are associated to the dielectric and insulating properties at the electrode/electrolyte interface, therefore they are affected by the variations occurring on the electrode surface [41].

.

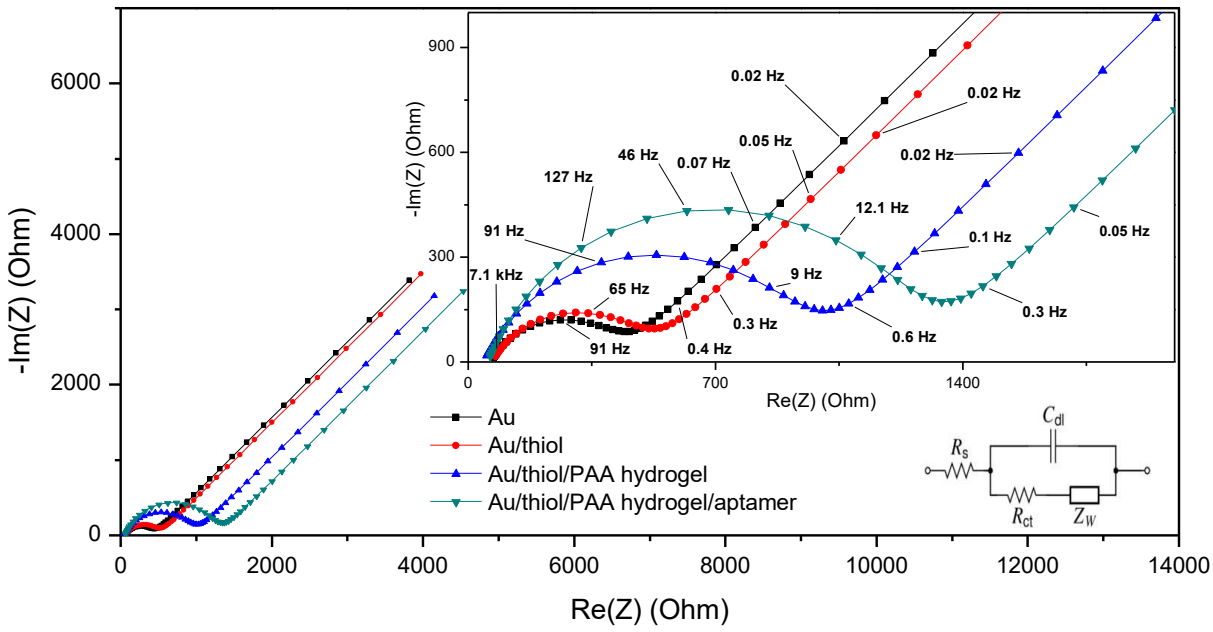

Figure 3.45 : Nyquist plots of Au (■), Au/thiol (●), Au/thiol/PAA hydrogel (▲), Au/thiol/PAA hydrogel/aptamer (▼) electrodes in 0.1 M PBS containing 5 mM $K_4[Fe(CN)_6]$ and $K_3[Fe(CN)_6]$ in the frequency range of 10 kHz to 0.1 Hz.

When the gold electrode surface is modified using DTE layer, the Rct value slightly increased (451 ohm). There is no very significant difference, in contrary to the insulator property of thiol self-assembled monolayer (380 ohm). This is due to the dithiol short chain used in this study as it has been discussed during cyclic voltammetry study. In contrast, when the electrode is grafted by PAA hydrogel film, because of repulsive interaction occurring between the negatively charged PAA

hydrogel and anionic redox probe, the Rct value increased reaching 932 ohm. After immobilization of the aptamer on the electrode, a semi-circle with fairly large diameter was monitored, leading to Rct of 1237 ohm . The observed increase in the value of Rct was attributed to the electron transfer hindrance by the negatively charged aptamer. The different analysis of the gold electrode surface at each stage of its modification have evidenced the formation of PAA hydrogel and its modification with aptamer thanks to a covalent coupling.

3.6.2 Quantitation of Aptamer Coverage Density

The surface area and aptamer coverage density dictate the magnitude of the Rct response that could be observed, and hence first, the effective area of the sensing platform was estimated by using the Randles–Sevcik equation (3.1) [42] using cyclic voltammetry, where the peak current is related to the surface area and the scan rate via the Eq. (1).

$$i_p = 2.68 \text{ X } 10^5 \text{ n}^{2/3}\text{AD}^{1/2}\text{v}^{1/2}\text{ c} \qquad (3.1)$$

Where *n* is the number of transferred electrons for the redox reaction (in this case 1), D is the diffusion coefficient for ferrocyanide (cm^2s^{-1}), c is its molar concentration (mol/cm^3), A is the effective surface area (cm^2), and v is the scan rate ($V\ s^{-1}$). By rearranging Equation 3.1, the electroactive surface area of the modified working electrodes were calculated.

From equation (3.1), a linear relationship exists between i_p and $v^{1/2}$, see Figure 3.46, and by performing linear regression of i_p versus $v^{1/2}$, the slope was obtained. Cyclic voltammetry experiments at different scan rates were performed for bare Au electrode and hydrogel modified electrode for 1 mM $[Fe(CN)_6]^{3-/4-}$ in 0.1 M KCl aqueous solution. The ferricyanide couple was chosen for this study as it has highly reproducible electrochemistry and has been studied extensively in the literature.

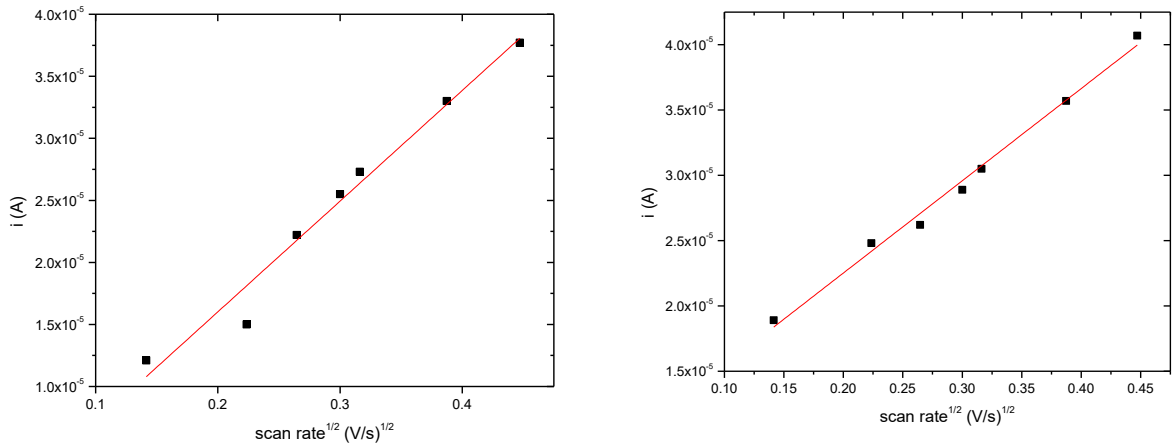

(A) (B)

Figure 3.46: Linear regression between the peak current and the square root of different scan rates for (A) gold electrode and (B) Hydrogel modified electrode with 1 mM $Fe(CN)_6^{3-/4-}$ in 0.1 M KCl solution.

From a plot of Ip versus $v^{1/2}$, a slope of 7.06×10^{-5} A $s^{1/2}$/ $V^{1/2}$ was found for the bare electrode and 9.1×10^{-5} A $s^{1/2}$/ $V^{1/2}$ for the hydrogel modified electrode. The system is considered to be electrochemically reversible, assuming semi-infinite linear diffusion normal to the electrode. From the D value for 7.6×10^{-6} cm^2 s^{-1} [43], and n = 1, the surface areas from gold electrode and hydrogel modified electrodes were estimated to be 0.123 cm^2 and 0.095 cm^2 respectively, while the geometric area were 0.076 cm^2. The hydrogel decreased the effective area and thus decreasing the effective surface area available for signal transduction. This observation is also in agreement with impedance characterization of bare electrode, and modified with hydrogel, whereas the latter present increased impedance, in the form of larger Rct.

The coverage density of DCL aptamer on the electrode surface was estimated using the number of cationic redox molecules that electrostatically associated to the anionic phosphate backbone of the DNA aptamer using Chronocoulometry as reported by [44]. The measured charge acquired from the reduction of the RuHex that is electrostatically associated with the negatively charged backbone of the surface-bound aptamers is used to calculate the number of moles of phosphate (and thus number of probe DNAs) immobilized on the surface. In this method, the DNA aptamer modified electrode is exposed to a solution containing a cationic redox marker $Ru(NH_3)_6^{3+}$

(RuHex) , which electrostatically binds to DNA to balance its negative charge. The molar amount of RuHex is measured via chronocoulometry. Charge is collected after stepping the voltage to activate the redox reaction. The diffusive component can be measured and separated by time resolving charge collection according to the integrated Cottrell expression;

$$Q = \frac{2nFAD_0^{1/2}c_0^*}{\pi^{1/2}} t^{1/2} + Q_{dl} + nFA\Gamma_{Ru} \quad (3.2)$$

Where Q is charge; n is the number of electrons per molecule in the redox reaction; F is the Faraday constant (C/mol); A is the electrode area (cm^2) of the working electrode, D_o is the diffusion coefficient (cm^2/s);C^*_o is the bulk concentration (mol/cm^2), Q_{dl} is the capacitive charge, $nFA\Gamma_{Ru}$is the charge from the reduction of adsorbed redox marker [C_{Ru} (mol/cm^2)], and Γ_{Ru} the excess surface density of RuHex.

The intercept at t = 0 is then calculated as the sum of the double layer charging and the surface excess terms. The surface excess is determined from the difference in intercepts for the identical potential step experiment in the presence and absence of redox marker. Assuming the double layer capacitance with and without RuHex to be approximately equal, the double layer capacitative charge Qdl for the fixed voltage step can be considered constant. According to the integrated Cottrell expression, the excess charge from adsorbed RuHex, $nFA\Gamma_{Ru}$, can therefore be determined from the y-intercept in a plot of integrated charge versus $t^{1/2}$. The assumption of negibible Q_{dl} is verified via the negligible difference in y-intercepts in plots of Q vs. $t^{1/2}$ with and without RuHex when the aptamer was omitted. The DNA surface density is determined from the excess surface density of RuHex as;

$$\Gamma_{aptamer} = \Gamma_{Ru}\left(\frac{z}{m}\right)N_A \quad (3.3)$$

Where $\Gamma_{aptamer}$ is the probe surface density ($molecules/cm^2$); m is the number of phosphate groups on the probe DNA (75 for the main DCL aptamer used in this study); z is the charge on the redox molecule (3 for RuHex), and N_A is Avogadro's number.

Values reported for aptamer packing density range from $\sim 10^{11}$ to 10^{13} aptamers/cm^2 [45,46]. These values represent ≤ 10% of the maximum packing density of $\sim 9 \times 10^{13}$ molecules/cm^2 assuming a 0.7 nm cross-sectional radius for fully extended, single-stranded DNA [47]. The optimal packing density for a given aptamer sequence, as determined by sensor performance, is dependent on the

aptamer geometry (tertiary structure) as well as the size and structure of the target analyte [46]. In general, steric interactions between neighboring aptamers can inhibit target accessibility and aptamer folding at high aptamer packing densities. The latter can significantly alter the observed binding affinity (Kd) of the sensor [45,46]. When aptamer packing densities become too low, the number of aptamers on the surface may not produce an appreciable faradaic signal above the background.

In order to determine the packing densities of the 75-mer DCL aptamer-attached electrode, chronocoulometric experiments were acquired at ambient temperature using 10 mM tris buffer (pH 7.4) or 150 µM $Ru(NH_3)_6^{3+}$ (RuHex) in 10 mM tris buffer (pH 7.4). For this experiment, we used Princeton Applied Research VersaSTAT 3 potentiostat/galvanostat. Two step coulometry was performed stepping from 0.2 V to -0.5 V with a pulse width of 0.25 s. Typical chronocoulometric response curves for 75-mer functionalized electrode in the absence and presence of 150 µM $Ru(NH_3)_6^{3+}$ is shown Fig.3.47.

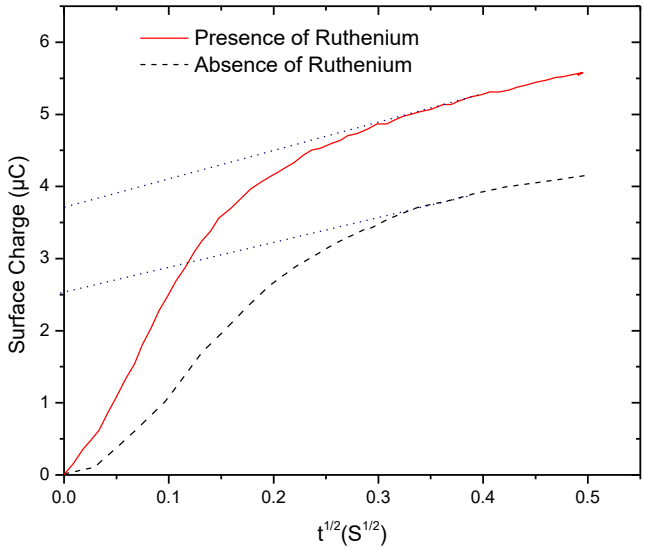

Figure 3.47: Determination of coupled 75-mer aptamer density via chronocoulometry. The extrapolated y-intercepts shown by dotted lines indicate the surface excess charge for measurements with (solid curve) and without (dashed curved) the RuHex

From the difference of y-intercepts; $nFA\Gamma_{Ru}$=1.1 μC. Substituting Faraday's constant, n=1, and the electrode area A measured via cyclic voltammetry, we find; $\Gamma_{Ru} = 1.25 \times 10^{-9}$ mole/cm^2 which leads to the surface density of DNA aptamer after substituting z=3, m=75, and $N_A = 6.02 \times 10^{23}$ mol^{-1}. Hence, the measured aptamer density was found to be 3.0 x 10^{13} aptamer/cm^2 (surface coverage density of 1 aptamer per 3 nm^2), taking the surface area measured by cyclic votammetry.

From the measurement of the dry thickness of the hydrogel film (h = 57 nm) and the swelling ratio (S = 1.8), we can calculate the concentrations of acrylic acid unit. The volume concentration C_V can be calculated by: $C_V = \rho/(S\text{x}M)$ where ρ is the density of poly(acrylic acid) and M is the molecular weight of acrylic acid unit. The surface concentration C_S is calculated by: $C_S = (h\text{x}\rho)/M$. We obtained C_V = 8 10^3 mol/L and C_s = 0.82 10^{-3} mol/m^2.

Assuming 50% of the acid groups of the hydrogel dissociating at pH 7, we have a 0.41 10^{-3} mol/m^2 acrylic acid unit readily available for the covalent immobilization of aptamer. From the aptamer density calculated above(3.0 x 10^{13} aptamer/cm^2), we have 5.0 x 10^{-7} mol/m^2 and in comparison to the surface concentration of acrylic acid unit available, we can deduce the resulting surface coverage is high enough to expect a responsive interface but not excessively high that the aptamers should interfere with their neighbors when undergoing conformational changes assuming a 0.7 nm cross-sectional radius for fully extended single-stranded DNA. The relatively higher packing density achieved with this aptamer is consistent and found to be optimal with previous studies for nanoparticle-based diclofenac aptasensor [48].

3.7 Performances of the aptasensor for diclofenac

Among the different electrochemical transduction methods available for assessing the performance of an aptasensor, we have selected to use in this work impedimetric method as it is one of the most powerful tool for directly probing the interfacial reaction mechanisms and monitoring the dynamics of biomolecular interactions, and also based on its comparative advantages of sensitivity, simplicity use, capacity for label-free detection, being nondestructive technique and cost-efficient technique [259].

Basically, electrochemical impedance spectroscopy (EIS) is based on applying an AC potential to an electrochemical cell and measuring the current through the cell. When a process occurs in a electrochemical cell, it can be modelled using combination of resistors, capacitors,... using the principle of the equivalent circuits. This principle consists on obtaining values of electrical parameters such as resistance, capacitance, etc. when an experimental spectra is fitted with a theoretical curve corresponding to the selected circuit model. If it is applied a sinusoidal potential excitation, E_t *:*

$$E_t = E_0 \cdot \sin(\omega \cdot t) \tag{3.4}$$

Where E_t is the potential at time t, E_0 is the amplitude of the signal and $\omega = 2\pi f$ is the radial frequency (f is the frequency expressed in Hertz (Hz)).

$$I_t = I_0 \cdot \sin(\omega \cdot t + \varphi) \tag{3.5}$$

An AC current signal with a current intensity I_t is obtained in response to this potential applied. I_t also depending on t with the same frequency but with an amplitude I_0 and a phase angle φ depending on the impedance of the system, as shown in Figure 3.48.

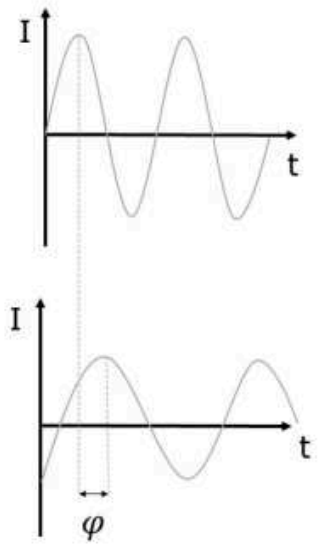

Figure 3.48: AC excitation signal and sinusoidal current response in the system under study

To calculate the impedance of the system, an expression analogous to ohm's law is used:

$$z = \frac{E_t}{I_t} = \frac{E_o \cdot \sin(\omega \cdot t)}{I_o \cdot \sin(\omega \cdot t \quad +\varphi)} = Z_o \cdot \frac{\sin(\omega \cdot t)}{\sin(\omega \cdot t + \varphi)} \tag{3.6}$$

According to Euler's expression:

$$\exp(j\varphi) = \cos\varphi + j \cdot \sin\varphi \tag{3.7}$$

A common way to represent the impedance vector model is to use complex notation:

$$E_{(t)} = E_o \cdot \exp(j\omega \cdot t) \tag{3.8}$$

$$I(t) = I_0 \cdot \exp(j\omega \cdot t - j\varphi) \tag{3.9}$$

Therefore impedance is represented as:

$$z = \frac{E}{i} = z_0 \exp(j\varphi) = Z_0(\cos\varphi + j\sin\varphi) = z_r + j \cdot Z_i \tag{3.10}$$

where z_r is the real part of the impedance and Z_i the imaginary part. In order to acquire an impedimetric spectrum, an AC excitation signal is applied to the system within a certain frequency range, obtaining an AC current response for each analyzed frequency value.

The most common graphical representation of impedimetric data is the "Nyquist Diagram", in which the imaginary part of the impedance Z_i is plotted versus the real part z_r . In this plot, each point corresponds to a different frequency. In Figure 3.49 is represented a Nyquist diagram, where the impedance vector with magnitude |Z| (|Z| correspond to Z0) forms with the X-axis an angle corresponding to the phase angle *cp.* The high frequency data are represented on the left part of the diagram whilst the low frequency are on the right one.

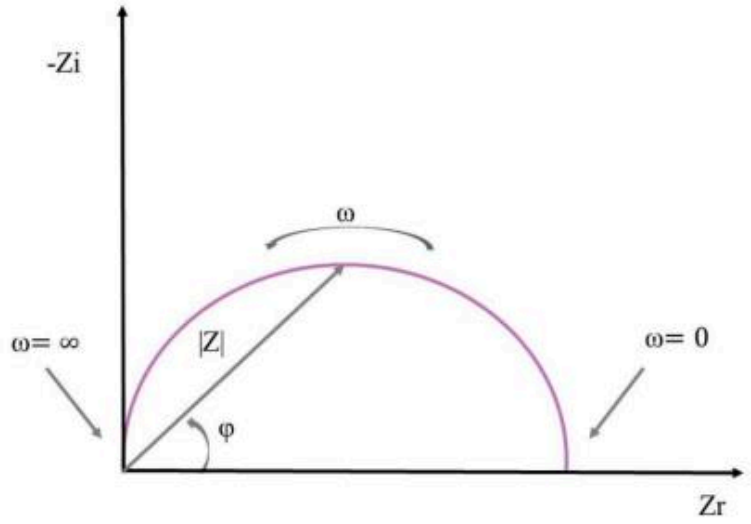

Figure 3.49: Nyquist diagram representing the impedance vector in the complex plane

Another way of representation data is "Bode Diagram" where the modulus of the impedance (Log|Z|) and the phase angle *(cp)* between the AC potential and the AC current as a function of the frequency (log co) are plotted. As shown in Figure 3.50, the impedance data which are frequency independent represent the behavior of the resistive processes (phase angles close to 0) whereas the ones that are dependent on the frequency are more related to capacitive or diffusive processes (phase angles between -90° or -45°). Each type of representation can be chosen according to different experiment and needs for parameter visualization.

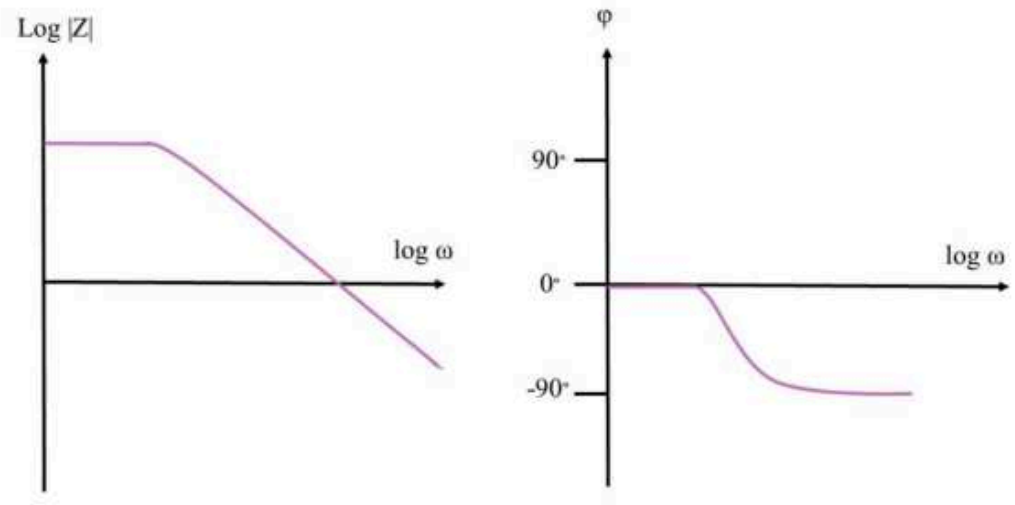

Figure 3.50: Bode diagrams

The interpretation of impedimetric spectra consists on the correlation among the obtained data with equivalent circuits formed by basic electrical elements (resistance, capacitor, inductance,...).

Figure 3.51 shows an example of Nyquist diagram to a simple equivalent circuit formed by resistance Ri in series with the parallel combination of a capacitance C and another R2 (Ri(R2C)). This important circuit is observed for very well behaved electrochemical reaction occurring onto a metallic electrode. The impedance spectra is represented by a semicircle beginning in the point corresponding to R_1 value (a) and ending in the point (b) corresponding to the equal $R_1 + R_2$. The value of capacitance of the capacitor C is obtained by the maximum value of imaginary impedance in the spectrum. Most of impedance spectra corresponding to electrochemical systems can be fitted to this type of equivalent circuit. In that cases, the parameter R_1 represents the resistance of the solution (Rs), R_2 corresponds to the resistance (Rct) to the charge transfer between the solution and the electrode surface and C is the capacitance of the double layer due to the interface between the electrode and the electrolytic solution.

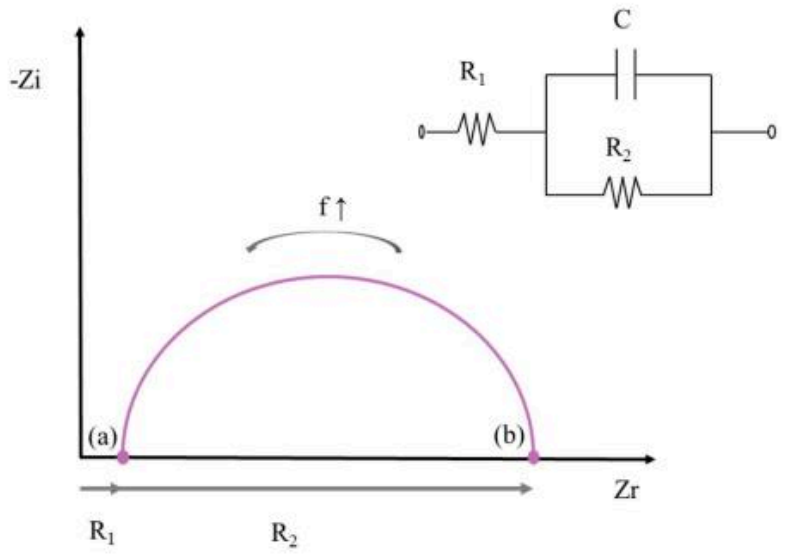

Figure 3.51: Nyquist diagram and the corresponding equivalent circuit.

A Warburg impedance parameter should be considered when it is recorded at low frequencies. This parameter is related to the mass transfer between the solution and the electrode surface and can be modeled as a frequency dependent reactance with equal real and imaginary components.

$$z_w = \sigma \cdot (\omega)^{-\frac{1}{2}} \cdot (1 - j) \qquad (3.11)$$

Where ω is the radial frequency and σ is the Warburg coefficient (constant for a defined system). The Warburg impedance appears on a Nyquist diagram as a diagonal line with a slope of 45°. In an electrochemical system or process, it represents the diffusion of electrochemical species in the solution. Figure 3.52 shows the impedimetric spectra and the most favorite model of equivalent circuit for a simple electrochemical reaction called Randles equivalent circuit [5].

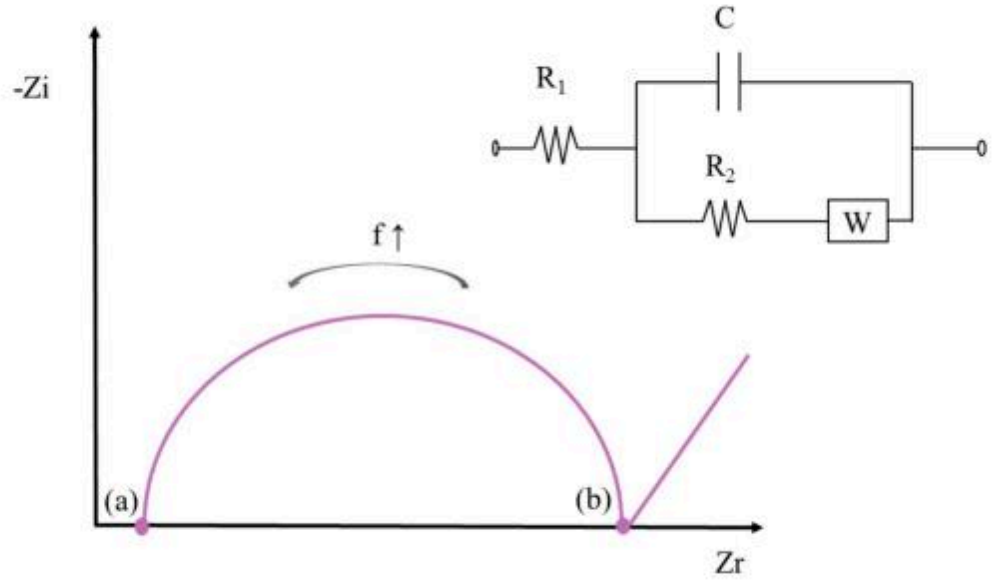

Figure 3.52: Nyquist diagram and the corresponding equivalent Randles circuit.

In some cases, the semicircles of Nyquist diagrams present a depressed and not completely symmetric shape, this is due to the non-ideal behavior of most capacitors in electrochemical systems. In order to fit better the experimental data to the theoretical curves, a Constant Phase Element (CPE) is used instead of a capacitor. The impedance of a CPE is represented by:

$$z_{CPE} = (j \cdot \omega)^{-\alpha/C} \qquad (3.12)$$

Where ω is radial frequency, C *is* capacitance and α is a exponent, $\alpha(0-1)$.In a constant phase element, the exponent α is lower than 1,even though $\alpha = 1$ corresponds to the ideal capacitor.

3.7.1. Sensitivity

The sensitivity of the aptamer-modified electrode for the detection of DCL was carried out by impedance spectroscopy. To this end, the aptamer-modified electrode was incubated for 50 minutes with DCL solutions at different concentrations, from 1 fmol L^{-1} to 1 µmol L^{-1}. Then, the aptasensor was rinsed and its performances of the aptasensor was investigated by recording its EIS responses in 0.1 M PBS containing 5 mM $[Fe(CN)_6]^{3-/4-}$ solution.

As illustrated in Figure 3.53, when the DCL concentration increases Rct decreases. This can be attributed to the fact that higher concentrations of DCL cause changes in the spatial conformation of the aptamer. The results demonstrate that these conformational changes lower the negative charge density on the surface and therefore, they decrease the interfacial charge transfer resistance to the negatively charged redox probe[49].

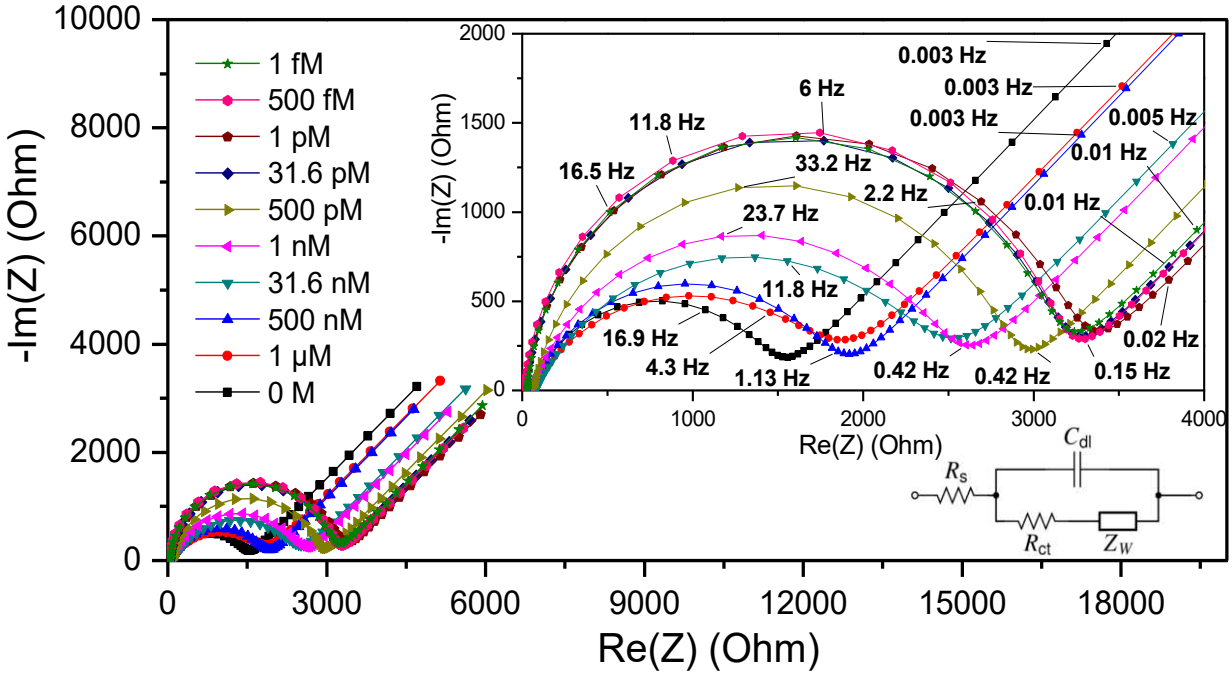

Figure 3.53: Nyquist plot obtained in 0.1 M PBS containing 5 mM $K_4[Fe(CN)_6]$ and $K_3[Fe(CN)_6]$ after treatment of the aptasensor with different concentrations of DCL in the frequency range of 100 kHz to 1 mHz.

3.7.2. Determination of the limit of detection

The change in charge-transfer resistance (Fig. 3.54) was reported as a function of the logarithm of DCL concentration. As shown on Figure 3.54, Rct was found to be linear with target concentration in the range of 30 pM to 1 µM, according to the following equation:

$$Rct = -310.23\ [DCL] - 99.637.\ (R^2 = 0.9787).$$

The detection limit was calculated to be 0.02 nmol L^{-1} from the intersection between the linear part and the non-sensitive linear region of the Rct vs log(DCL) curve (Figure 3.54).

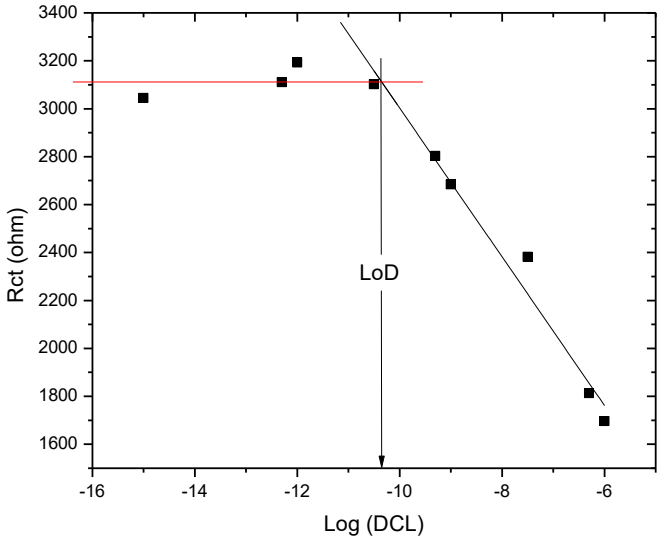

Figure 3.54: Calibration curve using Rct vs. Log DCL concentration

3.8 Stability, Reproducibility, and Selectivity of the Aptasensor

3.8.1 Stability and Reproducibility Study

Once the response of the sensor to DCL is demonstrated, the stability and reproducibility merits of the protocol developed were evaluated. The operational stability and performances of the developed aptasensor was assessed for a long-term storage at 4°C using five different aptasensors. The impedance response of the aptasensor was evaluated and it was observed that the aptasensor retained 96 % of its initial response after 7 days storage and 92.3 % after 14 days storage (detection of 500 pM of DCL), indicating a good stability.

Furthermore, in order to evaluate the reproducibility of the aptasensor, five aptasensors were treated with 500 pM DCL, and Rct was recorded in 0.1 M PBS containing 5mM $[Fe(CN)_6]^{3-/4-}$. The reproducibility of the different stages of electrode construction was also evaluated (Figure 3.55) by measuring the relative standard deviation (RSD) of their response. The relative standard deviation was found to be 5 %. This shows that the reproducibility of the aptasensor is quite reliable.

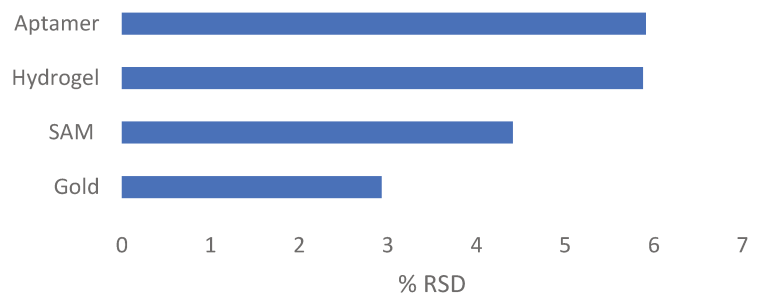

Figure 3.55 : Relative standard deviation of the recorded electron transfer resistance (Rct) of different stages of electrode construction in 0.1M PBS containing 5mM $[Fe(CN)_6]^{3-/4-}$.

3.8.2 Selectivity and Cross-reactivity of the Aptasensor

Real sample matrices provide an important challenge for the development of sensitive and specific detection systems. Matrix interference may either involve signal suppression or enhancement. False negative results due to reduced sensitivity of the test or false positives due to lack or specificity may result from co-extraction of compounds having similar physicochemical properties [50,51]. The selectivity of the aptasensor played an important role in analyzing real samples *in situ* without separation, and for the successful determination of target molecules, some common potentially interfering substances were investigated to test the selectivity of the DCL aptasensor and also the cross reactivity, due to structural similarity. We choose to assess the selectivity of the developed aptasensor against three reported control compounds: paracetamol, 4-Amino phenyl acetic acid and tryptophan (Figure 3.56).

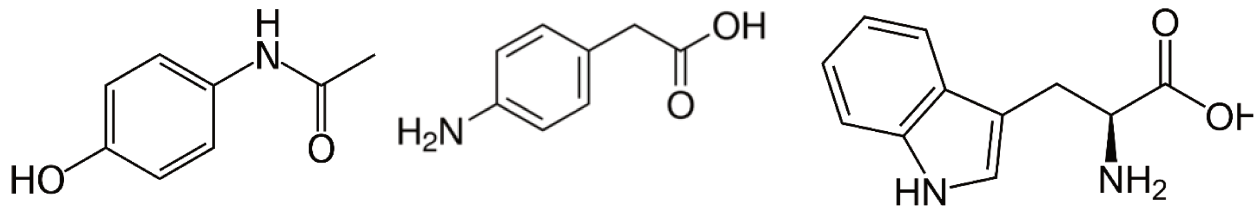

(A) **(B)** **(C)**

Figure 3.56: Chemical structure of the interfering substances: (A) Paracetamol, (B) 4-Amino phenyl acetic acid (C) Tryptophan.

The selectivity study was carried out by incubating the aptamer-modified electrode (aptasensor) with the interference species solutions at concentrations 1000-fold higher than that of DCL (15 nM) and the performances of the aptasensor was investigated by recording its EIS responses in 0.1 M PBS containing 5 mM $[Fe(CN)_6]^{3-/4-}$ solution (Figure 3.57).

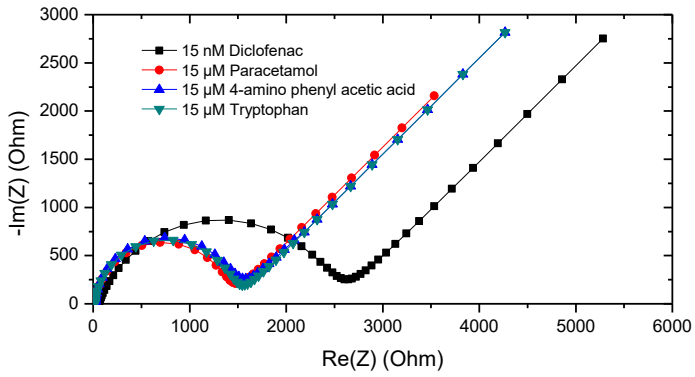

Figure 3.57: Impedimetric response of the selectivity of the aptasensor recorded in 0.1 M PBS containing 5 mM $[Fe(CN)_6]^{3-/4-}$ solution after being incubated in the following samples under the same experimental conditions: (■) 15 nM DCL (●) 15 µM Paracetamol (▲) 15 µM 4-amino phenyl acetic acid(▼) 15 µM Tryptophan.

The results summarized as histogram on Figure 3.58 show that the presence of interfering compounds, at concentration level of 15 µM (Column B to D), exhibits Rct values close to that obtained in absence of target analyte and different in comparison to the Rct obtained in the presence of 15 nM DCL (Column A), showing that these interferences could not interact with the DCL-aptamer.

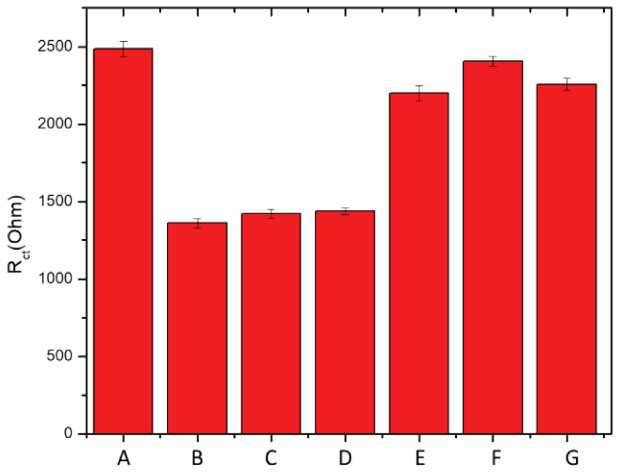

Figure 3.58 : Charge transfer resistance deduced from EIS measurements at the aptasensor, recorded in 0.1 M PBS containing 5 mM $[Fe(CN)_6]^{3-/4-}$ solution after incubation of the aptasensor in the following samples under the same experimental conditions: (A) 15 nmol L^{-1} DCL (B) 15 µmol L^{-1} Paracetamol (C) 15 µmol L^{-1} 4-amino phenyl acetic acid (D) 15 µ mol L^{-1} Tryptophan (E) 15 nmol L^{-1} DCL + 15 µM Paracetamol (F) 15 nmol L^{-1} DCL + 15 µmol L^{-1} 4-amino phenyl acetic acid (G) 15 nmol L^{-1} DCL + 15 µmol L^{-1} Tryptophan. Error bars indicate the range of two independent experiments.

To confirm the selectivity of the aptasensor, the cross-sensitivity of the aptasensor was also investigated in a mixed sample, containing 15 nM DCL coexisting with a high concentration of interfering components (15 µM), as shown on figure 3.59. In spite of 1000-fold higher concentration of interferences compared with DCL concentration, the Rct obtained from the response of three complex samples (Figure 3.58, Columns E to G) were almost the same as the Rct obtained from only DCL, which obviously revealed that the interferences had almost negligible influence for DCL detection. These results confirm the high selectivity of the developed aptasensor associated with the highly specific bindings between the target DCL, and the corresponding aptamer and its possible applicability for the selective quantification of DCL without interference.

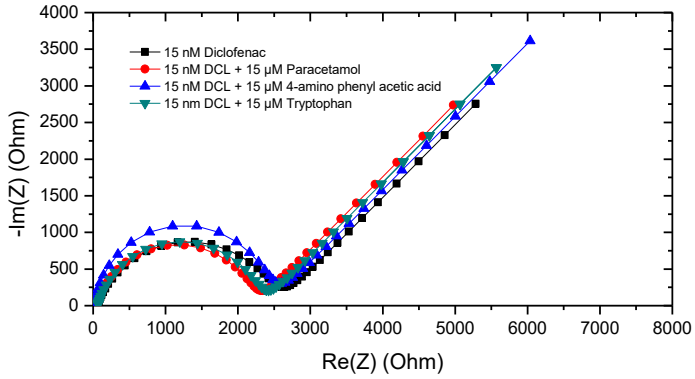

Figure 3.59: Impedimetric response of the selectivity of the aptasensor recorded in 0.1 M PBS containing 5 mM $[Fe(CN)_6]^{3-/4-}$ solution after being incubated in the following samples under the same experimental conditions: (■) 15 nM DCL (●)15 nM DCL + 15 µM Paracetamol (▲)15 nM DCL + 15 µM 4-amino phenyl acetic acid (▼)15 nm DCL + 15 µM Tryptophan.

Furthermore, in order to prove the specific interaction between the aptamer and the DCL, control experiments were conducted by performing the EIS measurements at PAA hydrogel modified electrode in 0.1 M PBS containing 5 mM $[Fe(CN)_6]^{3-/4-}$ solution, after incubating with 15 nM diclofenac and interfering compounds (15 µM), was recorded (Figure 3.60 (A)). As summarized and shown on the histogramms of Figure 3.60 (B), no recognizable change of EIS response was obtained for the hydrogel modified electrode incubated with 15 µM interfering compounds (column C and D) and 15 nM diclofenac (column E) while the response of the aptamer modified electrode showed a remarkable change in EIS response when DCL binding aptamer modified electrode is incubated with 15 nM diclofenac (column A). This result indicates that almost no interaction is detectable between the electrode modified with the PAA hydrogel only and the target and also with the interfering compounds used in this study, confirming the specific interaction between the aptamer and the DCL.

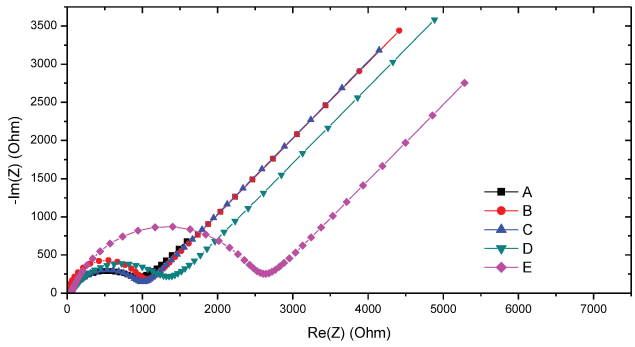

(A)

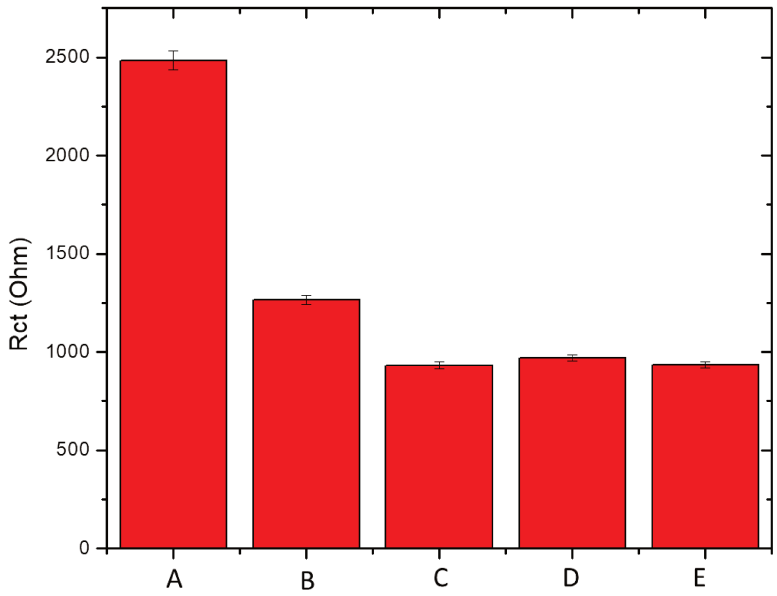

(B)

Figure 3.60: ***(A)*** *Impedimetric response of :(A) Hydrogel modified electrode incubated in 15 nmol L^{-1} diclofenac (B) Hydrogel modified electrode incubated in 15 µmol L^{-1} 4-amino phenyl acetic acid (C) Hydrogel modified electrode incubated in 15 µmol L^{-1} Paracetamol (D) Aptamer modified electrode (E) aptasensor incubated in 15 nmol L^{-1} Diclofenac.* ***(B)*** *Histograms of: (A) aptasensor incubated in 15 nmol L^{-1} Diclofenac (B) Aptamer modified electrode (C) Hydrogel modified electrode incubated in 15 µmol L^{-1} Paracetamol (D) Hydrogel modified electrode incubated in 15 µmol L^{-1} 4-amino phenyl acetic acid (E) Hydrogel modified electrode incubated in 15 nmol L^{-1} diclofenac. Error bars indicate the range of two independent experiments.*

3.10 Comparative Data

As mentioned in Chapter 1, several electroanalytical methods have been reported for the determination of DCL based on potentiometry, differential pulse voltammetry, square wave voltammetry, linear sweep voltammetry, photo electrochemical and electrochemical impedance spectroscopy. The figure of merits of different electrochemical methods for detection of DCL are summarized in Table 3.5. The LOD reached with most of these techniques are not lower than a few tens of nanomole L^{-1}. Improvement of target detection at the transducing surface using biomolecules specific for DCL have been tried before and published using nucleic acid aptamers. In this regard, the latest improved LOD (in the nmol L^{-1} range) achieved for detection of DCL using aptamers is the one demonstrated by okoth *et al.* [54], using gold nanoparticles and graphene-doped Cadmium sulfide structured electrode. To the best of our knowledge, there are no reports on the utilization of surface-attached hydrogel thin films used for immobilization of aptamer, used for detection of DCL, which is the focus of the present study. Thanks to the polymeric environment used for immobilizing the aptamer, the proposed method of ours has demonstrated the lowest limit of detection and sensitivity for DCL analysis.

Table 3.5. Comparison between analytical performances of reported techniques for DCL detection.

Detection method	**Modifier**	**Linear range**	**LOD**	**Refs.**
Potentiometry	Membrane containing β- cyclodextrin coupled with magnetite ferric oxide (CV-Fe(beta-CD))	10 µM to 10 mM	$11x10^3$ nM	[53]
Photoelectrochemical (PEC)	DCL Aptamer/Gold nanoparticles (Au NPs) and graphene-doped CdS (GR-CdS)(Au/GR-CdS/Aptamer)	1 to 150 nM	0.78 nM	[54]
Differential Pulse Voltammetry (DPV)	Functionalized multi-walled carbon nanotubes (f-MWCNTs) and gold–platinum bimetallic nanoparticles (Au–PtNPs) (Au–PtNPs/fMWCNTs/Au)	0.5 to 1000 µM	300 nM	[55]
Electrochemical Impedance Spectroscopy (EIS)	DCL Aptamer immobilized on the surface of the glassy carbon electrode (GCE)(GCE/AHA/Aptamer)	0 – 5 µM ;10 µM to 1 mM	270 nM	[49]
Differential Pulse Voltammetry (DPV)	A diclofenac (DCL) imprinted polymer	16.8 to 270 µM	$3.72x10^3$ nM	[56]
Electrochemical Impedance Spectroscopy (EIS)	Platinum nanoparticles (PtNPs) on carbon nanotubes (CNTs) functionalized with polyethyleneimine (PEI) (PtNPs/PEI/CNTs/Aptamer)	10 to 200 nM	2.7 nM	[52]
Linear Sweep Voltammetry (LSV)	A multi-walled carbon nanotubes (MWNTs)–dihexadecyl hydrogen phosphate (DHP) film-coated glassy carbon electrode (MWNTs–DHP/GCE)	0.17 to 2.5 µM	80 nM	[57]
Potentiometry	Modified graphite pencil electrode (MGPE) with doped polypyrrole films (MGPE/ PPy–DCL)	310 µM to11 mM	$190x10^3$ nM	[58]
Differential Pulse Voltammetry (DPV)	Multiwalled carbon nanotube and ionic liquid modified carbon ceramic electrode (MWCNT–IL/CCE)	0.05 to 50 µM	18 nM	[59]
Electrochemical Impedance Spectroscopy (EIS)	Aptamer immobilized on the Surface of hydrogel matrix modified gold electrode (Au/SAM/hydrogel/Aptamer)	30 pM to 1 µM	0.02 nM	This work

REFERENCES

[1] J.M. Pingarrón, P. Yáñez-Sedeño, A. González-Cortés, Gold nanoparticle-based electrochemical biosensors, Electrochimica Acta. 53 (2008) 5848–5866. https://doi.org/10.1016/j.electacta.2008.03.005.

[2] J. Yao, Y. Sun, M. Yang, Y. Duan, Chemistry, physics and biology of graphene-based nanomaterials: new horizons for sensing, imaging and medicine, J. Mater. Chem. 22 (2012) 14313. https://doi.org/10.1039/c2jm31632c.

[3] L. Angnes, E.M. Richter, M.A. Augelli, G.H. Kume, Gold Electrodes from Recordable CDs, Anal. Chem. 72 (2000) 5503–5506. https://doi.org/10.1021/ac000437p.

[4] A. Ulman, Formation and Structure of Self-Assembled Monolayers, Chem. Rev. 96 (1996) 1533–1554. https://doi.org/10.1021/cr9502357.

[5] Kern W & Puotinen D A. Cleaning solutions based on hydrogen peroxide for use in silicon semiconductor technology. RCA Rev. 31:187-206, 1970., (n.d.) 1.

[6] W. Kern, The Evolutionof Silicon Wafer Cleaning Technology, J Electrochem Soc. 137 (1990) 6.

[7] C. Spégel, A. Heiskanen, J. Acklid, A. Wolff, R. Taboryski, J. Emnéus, T. Ruzgas, On-Chip Determination of Dopamine Exocytosis Using Mercaptopropionic Acid Modified Microelectrodes, Electroanalysis. 19 (2007) 263–271. https://doi.org/10.1002/elan.200603720.

[8] M.F.M. Noh, I.E. Tothill, Development and characterisation of disposable gold electrodes, and their use for lead(II) analysis, Anal. Bioanal. Chem. 386 (2006) 2095–2106. https://doi.org/10.1007/s00216-006-0904-5.

[9] A.R. Heiskanen, C.F. Spégel, N. Kostesha, T. Ruzgas, J. Emnéus, Monitoring of *Saccharomyces cerevisiae* Cell Proliferation on Thiol-Modified Planar Gold Microelectrodes Using Impedance Spectroscopy, Langmuir. 24 (2008) 9066–9073. https://doi.org/10.1021/la800580f.

[10] L.M. Fischer, M. Tenje, A.R. Heiskanen, N. Masuda, J. Castillo, A. Bentien, J. Émneus, M.H. Jakobsen, A. Boisen, Gold cleaning methods for electrochemical detection applications, Microelectron. Eng. 86 (2009) 1282–1285. https://doi.org/10.1016/j.mee.2008.11.045.

[11] R.K. Mendes, R.S. Freire, C.P. Fonseca, S. Neves, L.T. Kubota, Characterization of self-assembled thiols monolayers on gold surface by electrochemical impedance spectroscopy, J. Braz. Chem. Soc. 15 (2004) 849–855. https://doi.org/10.1590/S0103-50532004000600011.

[12] O. Azzaroni, M.E. Vela, H. Martin, A. Hernández Creus, G. Andreasen, R.C. Salvarezza, Electrodesorption Kinetics and Molecular Interactions at Negatively Charged Self-Assembled Thiol Monolayers in Electrolyte Solutions, Langmuir. 17 (2001) 6647–6654. https://doi.org/10.1021/la010019v.

[13] B. Chollet, M. Li, E. Martwong, B. Bresson, C. Fretigny, P. Tabeling, Y. Tran, Multiscale Surface-Attached Hydrogel Thin Films with Tailored Architecture, ACS Appl. Mater. Interfaces. 8 (2016) 11729–11738. https://doi.org/10.1021/acsami.6b00446.

[14] C.E. Hoyle, C.N. Bowman, Thiol-Ene Click Chemistry, Angew. Chem. Int. Ed. 49 (2010) 1540–1573. https://doi.org/10.1002/anie.200903924.

[15] B. Chollet, L. D'Eramo, E. Martwong, M. Li, J. Macron, T.Q. Mai, P. Tabeling, Y. Tran, Tailoring Patterns of Surface-Attached Multiresponsive Polymer Networks, ACS Appl. Mater. Interfaces. 8 (2016) 24870–24879. https://doi.org/10.1021/acsami.6b07189.

[16] C. Zhao, S. Nie, M. Tang, S. Sun, Polymeric pH-sensitive membranes—A review, Prog. Polym. Sci. 36 (2011) 1499–1520. https://doi.org/10.1016/j.progpolymsci.2011.05.004.

[17] Q. Zhao, J.W.C. Dunlop, X. Qiu, F. Huang, Z. Zhang, J. Heyda, J. Dzubiella, M. Antonietti, J. Yuan, An instant multi-responsive porous polymer actuator driven by solvent molecule sorption, Nat. Commun. 5 (2014) 4293. https://doi.org/10.1038/ncomms5293.

[18] Q. Zhao, M. Yin, A.P. Zhang, S. Prescher, M. Antonietti, J. Yuan, Hierarchically Structured Nanoporous Poly(Ionic Liquid) Membranes: Facile Preparation and Application in Fiber-Optic pH Sensing, J. Am. Chem. Soc. 135 (2013) 5549–5552. https://doi.org/10.1021/ja402100r.

[19] M.-J. Yin, M. Yao, S. Gao, A.P. Zhang, H.-Y. Tam, P.-K.A. Wai, Rapid 3D Patterning of Poly(acrylic acid) Ionic Hydrogel for Miniature pH Sensors, Adv. Mater. 28 (2016) 1394–1399. https://doi.org/10.1002/adma.201504021.

[20] R.M. Rasal, D.E. Hirt, Micropatterning of Covalently Attached Biotin on Poly(lactic acid) Film Surfaces, Macromol. Biosci. 9 (2009) 989–996. https://doi.org/10.1002/mabi.200800374.

[21] E.N. Chiang, R. Dong, C.K. Ober, B.A. Baird, Cellular Responses to Patterned Poly(acrylic acid) Brushes, Langmuir. 27 (2011) 7016–7023. https://doi.org/10.1021/la200093e.

[22] I.-T. Hwang, M.-S. Oh, C.-H. Jung, J.-H. Choi, Direct patterning of poly(acrylic acid) on polymer surfaces by ion beam lithography for the controlled adhesion of mammalian cells, Biotechnol. Lett. 36 (2014) 2135–2142. https://doi.org/10.1007/s10529-014-1569-3.

[23] M. Yin, C. Wu, L. Shao, W.K.E. Chan, A.P. Zhang, C. Lu, H. Tam, Label-free, disposable fiber-optic biosensors for DNA hybridization detection, The Analyst. 138 (2013) 1988. https://doi.org/10.1039/c3an36791f.

[24] D. Buenger, F. Topuz, J. Groll, Hydrogels in sensing applications, Prog. Polym. Sci. 37 (2012) 1678–1719. https://doi.org/10.1016/j.progpolymsci.2012.09.001.

[25] G. Miquelard-Garnier, S. Demeures, C. Creton, D. Hourdet, Synthesis and rheological behavior of new hydrophobically modified hydrogels with tunable properties, Macromolecules. 39 (2006) 8128–8139. https://doi.org/10.1021/ma061361n.

[26] A. George, J.E. ten Elshof, Sub-50 nm patterning of functional oxides by soft lithographic edge printing, J. Mater. Chem. 22 (2012) 9501. https://doi.org/10.1039/c2jm31121f.

[27] R. Dong, S. Krishnan, B.A. Baird, M. Lindau, C.K. Ober, Patterned Biofunctional Poly(acrylic acid) Brushes on Silicon Surfaces, Biomacromolecules. 8 (2007) 3082–3092. https://doi.org/10.1021/bm700493v.

[28] G. Wu, Y. Xia, S. Yang, Buckling, symmetry breaking, and cavitation in periodically micro-structured hydrogel membranes, Soft Matter. 10 (2014) 1392–1399. https://doi.org/10.1039/C3SM51640G.

[29] Y. Mi, Y. Chan, D. Trau, P. Huang, E. Chen, Micromolding of PDMS scaffolds and microwells for tissue culture and cell patterning: A new method of microfabrication by the self-assembled micropatterns of diblock copolymer micelles, Polymer. 47 (2006) 5124–5130. https://doi.org/10.1016/j.polymer.2006.04.063.

[30] X. Chen, J. Sun, J. Shen, Patterning of Layer-by-Layer Assembled Organic−Inorganic Hybrid Films: Imprinting versus Lift-Off, Langmuir. 25 (2009) 3316–3320. https://doi.org/10.1021/la804133w.

[31] G. Sudre, D. Hourdet, C. Creton, F. Cousin, Y. Tran, pH-Responsive Swelling of Poly(acrylic acid) Brushes Synthesized by the Grafting Onto Route, Macromol. Chem. Phys. 214 (2013) 2882–2890. https://doi.org/10.1002/macp.201300477.

[32] B. Lego, W.G. Skene, S. Giasson, Swelling Study of Responsive Polyelectrolyte Brushes Grafted from Mica Substrates: Effect of pH, Salt, and Grafting Density, Macromolecules. 43 (2010) 4384–4393. https://doi.org/10.1021/ma902588j.

[33] Y.-T. Tao', Structures of Self-Assembled Monolayers of Aromatic-Derivatized Thiols on Evaporated Gold and Silver Surfaces: Implication on Packing Mechanism, (n.d.) 14.

[34] P.E. Laibinis, A.N. Parikh, R.G. Nuzzo, Comparison of the Structures and Wetting Properties of Self-Assembled Monolayers of n-Alkanethiols on the Coinage Metal Surfaces, Cu, Ag, Au', (n.d.) 16.

[35] V. Yadav, A.V. Harkin, M.L. Robertson, J.C. Conrad, Hysteretic memory in pH-response of water contact angle on poly(acrylic acid) brushes, Soft Matter. 12 (2016) 3589–3599. https://doi.org/10.1039/C5SM03134F.

[36] M. Li, B. Bresson, F. Cousin, C. Fretigny, Y. Tran, Submicrometric Films of Surface-Attached Polymer Network with Temperature-Responsive Properties, Langmuir. 31 (2015) 11516–11524. https://doi.org/10.1021/acs.langmuir.5b02948.

[37] J.V. Staros, R.W. Wright, D.M. Swingle, Enhancement by N-hydroxysulfosuccinimide of water-soluble carbodiimide-mediated coupling reactions, Anal. Biochem. 156 (1986) 220–222. https://doi.org/10.1016/0003-2697(86)90176-4.

[38] S. Sam, L. Touahir, J. Salvador Andresa, P. Allongue, J.-N. Chazalviel, A.C. Gouget-Laemmel, C. Henry de Villeneuve, A. Moraillon, F. Ozanam, N. Gabouze, S. Djebbar, Semiquantitative Study of the EDC/NHS Activation of Acid Terminal Groups at Modified Porous Silicon Surfaces, Langmuir. 26 (2010) 809–814. https://doi.org/10.1021/la902220a.

[39] D. Lin-Vien, ed., The Handbook of infrared and raman characteristic frequencies of organic molecules, Academic Press, Boston, 1991.

[40] A.J. Lomant, G. Fairbanks, Chemical probes of extended biological structures: Synthesis and properties of the cleavable protein cross-linking reagent [35S]dithiobis(succinimidyl propionate), J. Mol. Biol. 104 (1976) 243–261. https://doi.org/10.1016/0022-2836(76)90011-5.

[41] L. Alfonta, A. Bardea, O. Khersonsky, E. Katz, I. Willner, Chronopotentiometry and Faradaic impedance spectroscopy as signal transduction methods for the biocatalytic precipitation of an insoluble product on electrode supports: routes for enzyme sensors,

immunosensors and DNA sensors, Biosens. Bioelectron. 16 (2001) 675–687. https://doi.org/10.1016/S0956-5663(01)00231-7.

[42] A.J. Bard, L.R. Faulkner, Electrochemical methods: fundamentals and applications, 2nd ed, Wiley, New York, 2001.

[43] A.C. Dillon, T. Gennett, K.M. Jones, J.L. Alleman, P.A. Parilla, M.J. Heben, A Simple and Complete Purification of Single-Walled Carbon Nanotube Materials, (n.d.) 5.

[44] A.B. Steel, T.M. Herne, M.J. Tarlov, Electrochemical Quantitation of DNA Immobilized on Gold, Anal. Chem. 70 (1998) 4670–4677. https://doi.org/10.1021/ac980037q.

[45] F. Ricci, R.Y. Lai, A.J. Heeger, K.W. Plaxco, J.J. Sumner, Effect of Molecular Crowding on the Response of an Electrochemical DNA Sensor, Langmuir. 23 (2007) 6827–6834. https://doi.org/10.1021/la700328r.

[46] R.J. White, N. Phares, A.A. Lubin, Y. Xiao, K.W. Plaxco, Optimization of Electrochemical Aptamer-Based Sensors via Optimization of Probe Packing Density and Surface Chemistry, Langmuir. 24 (2008) 10513–10518. https://doi.org/10.1021/la800801v.

[47] A.B. Steel, R.L. Levicky, T.M. Herne, M.J. Tarlov, Immobilization of Nucleic Acids at Solid Surfaces: Effect of Oligonucleotide Length on Layer Assembly, Biophys. J. 79 (2000) 975–981. https://doi.org/10.1016/S0006-3495(00)76351-X.

[48] L. Kashefi-Kheyrabadi, M.A. Mehrgardi, Design and construction of a label free aptasensor for electrochemical detection of sodium diclofenac, Biosens. Bioelectron. 33 (2012) 184–189. https://doi.org/10.1016/j.bios.2011.12.050.

[49] L. Kashefi-Kheyrabadi, M.A. Mehrgardi, Design and construction of a label free aptasensor for electrochemical detection of sodium diclofenac, Biosens. Bioelectron. 33 (2012) 184–189. https://doi.org/10.1016/j.bios.2011.12.050.

[50] T. G., I. Smukste, K. R., Y. Wang, D. McKearn, R. E., Identifying and Overcoming Matrix Effects in Drug Discovery and Development, in: J. Prasain (Ed.), Tandem Mass Spectrom. - Appl. Princ., InTech, 2012. https://doi.org/10.5772/32108.

[51] S.F. Kingsmore, Multiplexed protein measurement: technologies and applications of protein and antibody arrays, Nat. Rev. Drug Discov. 5 (2006) 310–321. https://doi.org/10.1038/nrd2006.

[52] H. Derikvand, M. Roushani, A.R. Abbasi, Z. Derikvand, A. Azadbakht, Design of folding-based impedimetric aptasensor for determination of the nonsteroidal anti-inflammatory drug, Anal. Biochem. 513 (2016) 77–86. https://doi.org/10.1016/j.ab.2016.06.013.

[53] H.T. Elbalkiny, A.M. Yehia, S.M. Riad, Y.S. Elsaharty, Potentiometric diclofenac detection in wastewater using functionalized nanoparticles, Microchem. J. 145 (2019) 90–95. https://doi.org/10.1016/j.microc.2018.10.017.

[54] O.K. Okoth, K. Yan, J. Feng, J. Zhang, Label-free photoelectrochemical aptasensing of diclofenac based on gold nanoparticles and graphene-doped CdS, Sens. Actuators B Chem. 256 (2018) 334–341. https://doi.org/10.1016/j.snb.2017.10.089.

[55] M.M. Eteya, G.H. Rounaghi, B. Deiminiat, Fabrication of a new electrochemical sensor based on Au Pt bimetallic nanoparticles decorated multi-walled carbon nanotubes for determination of diclofenac, Microchem. J. 144 (2019) 254–260. https://doi.org/10.1016/j.microc.2018.09.009.

[56] M. Mostafavi, M.R. Yaftian, F. Piri, H. Shayani-Jam, A new diclofenac molecularly imprinted electrochemical sensor based upon a polyaniline/reduced graphene oxide nano-composite, Biosens. Bioelectron. 122 (2018) 160–167. https://doi.org/10.1016/j.bios.2018.09.047.

[57] X. Yang, F. Wang, S. Hu, Enhanced oxidation of diclofenac sodium at a nano-structured electrochemical sensing film constructed by multi-wall carbon nanotubes–surfactant composite, Mater. Sci. Eng. C. 28 (2008) 188–194. https://doi.org/10.1016/j.msec.2006.11.006.

[58] M.C. Oliveira, E.H. Bindewald, L.H. Marcolino, M.F. Bergamini, Potentiometric determination of Diclofenac using an ion-selective electrode prepared from polypyrrole films, J. Electroanal. Chem. 732 (2014) 11–16. https://doi.org/10.1016/j.jelechem.2014.08.006.

[59] K. Sarhangzadeh, A.A. Khatami, M. Jabbari, S. Bahari, Simultaneous determination of diclofenac and indomethacin using a sensitive electrochemical sensor based on multiwalled carbon nanotube and ionic liquid nanocomposite, J. Appl. Electrochem. 43 (2013) 1217–1224. https://doi.org/10.1007/s10800-013-0609-3.

GENERAL CONCLUSION AND PERSPECTIVES

GENERAL CONCLUSION AND PERSPECTIVES

A bibliographic study showed the harmful effects of an emergent pollutant: the diclofenac, when exposed to a few ng L^{-1} to tens of mg L^{-1} of DCL in tap waters and thereby described the strong need for rapid detection of DCL in environmental samples, not only to improve the current state of knowledge regarding its pathways, fate and effects in the environment, but also to determine the efficiency of water treatment procedures.

Until now, the DCL detection mostly relied on conventional techniques, such as HPLC and GC/MS. Though highly sensitive, these analytical techniques are time-consuming, expensive, require a lot of expertise to be operated and are not easy to be deployed in the field. Overcoming these limitations, electrochemical methods have attracted attention in recent years for environmental, pharmaceutical and biological compounds analysis and they offer numerous advantages over optical, piezoelectric or thermal detection. In comparison with optical methods, electrochemical transduction offers several benefits including simple-to-operate, rapid, cost effective, highly sensitive and selective, compatible with novel micro-fabrication techniques, disposable, easy to miniaturize and robust. Electrochemical reactions usually provide an electronic signal directly, avoiding the requirement of expensive signal transduction equipment.

Among the electrochemical methods, various amperometric and potentiometric techniques have been reported for the determination of DCL. Modified electrodes including Cu-doped zeolite-expanded graphite-epoxy electrode and catalytic DCL electro oxidation on graphene or carbon nanotubes have been also used. In order to improve the limit of detection (LOD), biomolecules that are specific for the DCL have been utilized by using antibodies also.

When it comes to electrochemical sensing, aptasensors are promising biosensors, as they take advantage of using aptamers as a recognition element. Aptamers are short single-stranded nucleic acid oligomers (DNA or RNA) capable of folding into highly organized, complex structures enabling ligation to molecular targets with high affinity. Their multiple advantages include their high specificity and affinity, their easy and highly reliable production by enzymatic or chemical synthesis, their regenerability by simple means and their storability. They are also stable, with no loss of activity under a wide range of buffer conditions, and resistant to harsh treatments such as

physical or chemical denaturation. Aptamers can be functionalized, offering diverse immobilization ways.

Thus, combination of the excellent characteristics of aptamers and the leading detection platform techniques, such as optical, electrochemical, or mass sensitive techniques with high sensitivity and specificity draws a promising view for the application of the aptasensors for the detection of harmful small toxic chemicals and their real-time monitoring in the environments. Among the different electrochemical detection techniques, electrochemical impedance spectroscopy (EIS) has appeared as a promising strategy.

Studies on detection of DCL using aptasensors are rarely reported to the best of our knowledge, and recently a very few EIS aptasensors have been designed and constructed based on monitoring the interfacial property changes. The main challenge to develop highly sensitive and selective aptasensors is related to the issue of stable immobilization of the aptamer; the issue to preserve the aptamer active and functional structure, the inability to immobilize a large amount of the aptamers and the selective affinity of the aptamer to the target.

Hence, so as to achieve a stable, large amounts of immobilization of DCL aptamer while retaining its bioactivity, among different materials, a surface-attached hydrogel thin films, have been chosen as an immobilization matrix for aptamers and have demonstrated advantages in the context of developing relatively simple but effective strategies to exploit the advantages of aptamers in detection of DCL

In this thesis we have developed a novel aptasensor for DCL. To this end, a new class of surface-attached hydrogel thin films was grafted on conductive transducer and used as biocompatible matrix for aptamer immobilization, tuned for the conception of biosensor. The polymeric network environment favors the stable immobilization of the aptamer and the selective affinity to the target and sensitive electrochemical detection, by providing the aptamer excellent environments to preserve its active and functional structure. Surface-attached hydrogel thin films present then many advantages as immobilization matrix: they are stable, robust, multiscale and multifunctional materials, with thickness widely ranging from low nanometers to high micrometers. The deformability, permeability and porosity of the hydrogel films can also be easily and finely adjusted with the film thickness and the network crosslinks density.

A simple and versatile approach for the synthesis of reliable and reproducible hydrogel films, the so-called CLAG process (Cross-Linking And Grafting), was followed in this study. The process consists of preforming functionalized polymers using thiol-ene click chemistry. The advantage of the approach is that the synthesis of preformed reactive chains avoids the difficulty of working under a controlled atmosphere as oxygen inhibits radical polymerization. This versatile approach provides then the facile adjustment of chemical properties (platform for covalent immobilization) and physical properties (size and architecture) of hydrogel films.

The surface-attached hydrogel thin films were grafted on conductive transducer with well-controlled geometry. The different stages of development of the aptasensor including the photolithography and lift-off process, to create a process for manufacturing electrodes adapted to the needs of the study, were optimized to achieve a reproducible gold transducer. The challenge for UV-patterning of hydrogel was also tackled up by using low cost, easily available material instead of the classical quartz-based photomask

The surface-attached hydrogel thin films obtained with controlled geometry were characterized by spectroscopy and electrochemical techniques including atomic force microscopy (AFM), cyclic voltammetry (CV) and electrochemical impedance spectroscopy (EIS). These measurements confirmed the covalent immobilization of hydrogel on the gold surface electrodes and found to be stable for many weeks at 4°C. The proof of concept of the biomolecule immobilization on the hydrogel through the peptide synthesis method was performed using the P-nitro aniline as a model molecule. The conditions of the model molecule covalent immobilization were optimized and the grafting was characterized using the IR-ATR technique. The performed methodology was then adapted for covalent immobilization of DCL aptamer onto the PAA hydrogel. The covalent attachments between the hydrogel and the DCL aptamer were confirmed by ATR-FTIR and EIS studies. We obtained electrochemical impedance spectroscopy biosensor for DCL detection with high sensitivity. The Surface-attached hydrogel film with controlled architecture, fabricated as immobilization matrix, was finely characterized.

The electrochemical properties of the biosensor in different media and its stability were then studied. The recognition of DCL by the aptamer-based electrode results in an electron transfer resistance change for the $[Fe(CN)6]^{3-/4-}$ as probed by the EIS technique. The difference of the signal before and after the addition of targets shows a linear increase with the concentration of

DCL. EIS aptasensor for DCL with nanomolar detection limit was evidenced. This improvement of the limit of detection compared to the values of the literature be attributed to the three-dimensional environment of the hydrogel which improves the grafting density of aptamer compared to other matrices.

The stability and reproducibility of the biosensor were also proved. The selectivity of the developed aptasensor towards its target analyte (DCL) was also studied against three reported control compounds: paracetamol, 4-Amino phenylacetic acid, and tryptophan. The results confirmed the high selectivity of the developed aptasensor to DCL.

The aptasensor designed provides a platform for simple, selective and more importantly rapid detection of DCL. The sensing platforms can serve as a molecular recognition of different targets in the field of health, or in the field of environment. Furthermore, increased sensitivity and specificity can be achieved by incorporating nanostructured metallic materials like gold nanoparticles inside the hydrogel network.

Another way of covalent aptamer grafting could be tested for the immobilization of DCL aptamers that involves the covalent entrapment of the aptamer into the three-dimensional matrices before the hydrogel grafting and the reticulation step. This way is to be tested with the aim of achieving even an increased coupling density. Another track of characterization and optimization of the EIS-aptasensor, which is currently ongoing work, is the coupling with the quartz microbalance. We can optimize the EIS aptamer-based sensor by using the QCM-D, as the combination of QCM-D with EIS techniques will provide further insight into the effects of mass loading and charge effects that govern the response of an EIS aptasensor.

RÉSUMÉ DE LA THÈSE EN FRANCAIS

1. Introduction

Les médicaments sont utilisés pour le traitement de nombreuses maladies et pathologies. Malgré leurs bénéfices pour la santé humaine, une partie des médicaments se retrouve dans l'environnement. Ainsi, la détection des résidus de médicaments en tant que contaminants dans les aliments et l'eau revêt une grande importance dans les domaines de l'environnement et de la santé humaine. L'un des anti-inflammatoire couramment utilisé depuis plusieurs décennies est le diclofénac (noté DCL) ou acide 2-(2-((2,6-dichlorophényl)amino)phényl)- acétique. Cet anti-inflammatoire non stéroïdien (AINS) possède des propriétés analgésiques, anti-inflammatoires et antipyrétiques[1]. Cependant, ses effets sur l'environnement peuvent être délétères [2]. Vendu sous la marque Voltaren® entre autres, DCL est fréquemment prescrit pour les plaintes rhumatismales, les inflammations articulaires aiguës et les douleurs légères à modérées [3, 4]. En raison de son utilisation massive, les résidus de DCL ont souvent été détectés dans les milieux d'eau douce [5-7]. Ainsi, le diclofénac est considérée comme un des contaminants émergents (CE) dans l'environnement par l'Union européenne en raison de sa présence dans les eaux de surface et de sa toxicité potentielle pour les organismes aquatiques [8,9]. Les CE comprennent un large panel de substances comme les perturbateurs endocriniens, les produits pharmaceutiques et les produits de soins personnels. Ils se caractérisent par une distribution extensive dans l'environnement en raison de leur utilisation quotidienne massive et de leur persistance [10,11]. Les CE, généralement présents à l'état de traces, ont été associés à des effets négatifs sur la santé humaine et animale (par exemple : dommages au système nerveux, toxicité ou perturbation du système immunitaire) [12]. Plusieurs études ont décrit les effets nocifs sur différents organismes lorsqu'ils sont exposés au DCL [13,14] présent dans l'environnement. Sa teneur peut varier de quelques ng L^{-1} à quelques dizaines de mg L^{-1} [15] dans les eaux usées et les eaux environnementales. Dans ce contexte, la quantification du DCL dans les eaux environnementales revêt une grande importance, non seulement pour améliorer l'état actuel des connaissances concernant leurs voies de pénétration, leur devenir et leurs effets dans l'environnement, mais aussi pour déterminer l'efficacité des stations de traitement des eaux usées [16]. Jusqu'à présent, la détection du DCL repose principalement sur des techniques conventionnelles, telles que la HPLC [17,18] et la GC/SM [19]. Bien que robustes, ces techniques analytiques sont difficilement mises en œuvre sur le terrain, prennent beaucoup de temps, sont coûteuses, et exigent beaucoup d'expertise.Une alternative potentielle consiste en l'utilisation de méthodes électrochimiques, qui peuvent être utilisées pour l'analyse des composes environnementaux, pharmaceutiques et biologiques. Elles offrent plusieurs

avantages, dont la simplicité d'utilisation, la rapidité, la rentabilité, la sensibilité et la sélectivité, la compatibilité avec les nouvelles techniques de microfabrication, le jetable, la miniaturisation facile et la robustesse [20-29]. Les réactions électrochimiques fournissent généralement un signal électronique directement, évitant ainsi l'utilisation d'équipements coûteux de transduction de signaux.

Parmi les méthodes électrochimiques, diverses techniques ampérométriques [30-33] et potentiométriques [24, 34-36] ont été rapportées pour la détermination de la DCL. On a également utilisé des électrodes modifiées, y compris l'électrode [37] en graphite-époxy expansé de zéolithe dopée au cuivre et l'électrooxydation catalytique DCL sur nanotubes de graphène ou de carbone [38,39]. Afin d'améliorer la limite de détection (LOD), des biomolécules spécifiques de la DCL ont été utilisées en utilisant également des anticorps [40,41].

Lorsqu'il s'agit de détection électrochimique, les aptasenseurs sont des biocapteurs prometteurs, car ils tirent avantage de l'utilisation des aptamères comme élément de reconnaissance [42]. Les aptamères sont de courts oligomères d'acides nucléiques monocaténaires (ADN ou ARN) capables de se plier en structures complexes hautement organisées permettant la ligature à des cibles moléculaires à haute affinité [43]. Leurs multiples avantages comprennent leur haute spécificité et affinité [44-47], leur production facile et très fiable par synthèse enzymatique ou chimique [44,45], leur régénérabilité par des moyens simples [46,48] et leur capacité de stockage [46,49]. Ils sont également stables, sans perte d'activité dans une large gamme de conditions tampons, et résistants aux traitements agressifs tels que la dénaturation physique ou chimique. Les aptamères peuvent être fonctionnalisés, offrant ainsi diverses possibilités d'immobilisation [50].

Ainsi, la combinaison des excellentes caractéristiques des aptamères et des principales techniques de plates-formes de détection, telles que les techniques optiques, électrochimiques ou sensibles à la masse avec une sensibilité et une spécificité élevées, offre une perspective prometteuse pour l'application des aptasensors à la détection des petits produits chimiques toxiques nocifs et leur surveillance en temps réel dans les environnements. Parmi les différentes techniques de détection électrochimique, la spectroscopie d'impédance électrochimique (SIE) apparaît comme une stratégie prometteuse [52,53].

Les études sur la détection de la DCL à l'aide d'aptasenseurs sont rarement rapportées au meilleur de nos connaissances, et récemment, très peu d'aptasenseurs EIS ont été conçus et construits sur la base du suivi des changements des propriétés interfaciales [29,54].

Ce travail de thèse est orienté vers le développement d'une nouvelle classe d'aptacapteur. La cible choisie a été le diclofénac du fait de son importante en tant que poilluant émergent dans l'environnement, tel qu'explicité en introduction. Un des objectifs a été d'évaluer l'utilisation une nouvelle classe de couches minces d'hydrogel greffées en surface sur un transducteur conducteur et utilisée comme matrice biocompatible pour l'immobilisation des aptamères, qui serviront de biorécepteurs sélectifs au diclofénac. Nous avons ainsi évalué si l'environnement réseau polymère permet de favoriser l'immobilisation stable de l'aptamère tout en permettant de conserver l'affinité sélective de l'aptamère pour sa cible. Un autre paramètre évalué concerne l'étude des performances pour la détection électrochimique de la cible. Les couches minces d'hydrogel fixées en surface présentent de nombreux avantages en tant que matrice d'immobilisation : elles sont stables, robustes, multi-échelles et multifonctionnelles, avec des épaisseurs allant du faible nanomètre au micromètre. La déformabilité, la perméabilité et la porosité des films d'hydrogel peuvent également être finement ajustées tout comme l'épaisseur du film et la densité des réticulations du réseau.

Une approche polyvalente pour la synthèse de films d'hydrogel fiables et reproductibles, appelée procédé CLAG (Cross-Linking And Grafting), a été utilisée dans cette étude. Ce procédéconsiste à préformer des polymères fonctionnalisés à l'aide de la chimie du clic thiol-ène. L'avantage de cette approche, telle que décrite par Chollet et al. [56], est que la synthèse de chaînes réactives préformées évite de travailler sous atmosphère contrôlée, le dioxygène inhibant la polymérisation radicalaire. Cette approche polyvalente permet ensuite d'ajuster facilement les propriétés chimiques (plate-forme d'immobilisation covalente) et physiques (taille et architecture) des films hydrogel.

La première partie du résumé présente la conception des transucteurs électrochimiques, consituées d'électrodes d'or préparées sur des wafer en silicium, nécessaires pour la synthèse contrôlée des hydrogels. La seconde partie est centrée sur l'optimisation du greffage des hydrogels et l'étude de leurs propriétés physico-chimiques. La dernière partie est consacrée à la conception de l'aptacapteur et à l'étude de ses performances analytiques pour la détection du diclofénac en milieu aqueux.

2. Partie experimentale

2.1 Produits chimiques

Poly(acide acrylique) (PAA) (MW ~ 250 kg/mol, solution à 35 % en poids dans l'eau), allylamine, N-hydroxysuccinimide (NHS), 1-éthyl-3-(3-diméthylaminopropyl)carbodiimide (EDC), 1,4-dithioérythritol (DTE), diclofénac (DCL), ferricyanure de potassium[$K_3Fe(CN)_6$], ferricyanure de potassium[$K_4Fe(CN)_6$] et potassium/phosphate de sodium monobasique/dibasique ont été achetés à Sigma-Aldrich et utilisés tels quels. Du chloroforme, du méthanol et des solvants à base d'acide formique ont également été achetés à Sigma-Aldrich.

L'aptamer utilisé pour la détection (aptamer DCL à terminaison amine marqué par fluorescence (75 bases)) avait la séquence 5'-/5AmMC6/ATA CCA GCT TCA TCA ATT GCA GCA ACG TGG CGG TCA TCA GTC AGC GGG TGG TGG TGG T CGG TCC AGA TAG TAA GTG CAA TCT/36-FAM/-3' et fut acheté des technologies ADN intégrées.

Une solution tampon de phosphate (0,1 M, pH 7,4) a été utilisée pour la préparation de la solution aptamère. 100 µM de solution mère d'aptamère a été préparée et conservée à -20 °C et les solutions d'aptamère de travail ont été préparées par dilution à la concentration finale souhaitée.

Sauf indication contraire, les autres produits chimiques utilisés dans cette étude étaient de qualité analytique et utilisés tels quels. De l'eau désionisée (18,2 MΩ/cm) purifiée par un système Pure Labflex (Elga Water, Veolia, France) a été utilisée tout au long de l'expérience pour la préparation de la solution aqueuse.

Pour la détermination de la DCL dans l'échantillon d'eau, une solution mère de 100 mM de DCL a été préparée quotidiennement, puis diluée à différentes concentrations avec 200 µL de tampon de lavage liant (BWB) (2 mM Tris-HCl à pH 7,5 contenant 10 mM NaCl, 0,5 mM KCl, 0,2 mM $MgCl_2$, 0,1 mM $CaCl_2$ et 5% éthanol).

Détection de cibles

La détection des DCL a été réalisée par incubation de l'électrode modifiée par l'aptamère dans une solution BWB de 200 µL contenant la concentration souhaitée de DCL pendant 50 minutes à température ambiante. Après incubation, l'électrode a été lavée trois fois à l'aide du tampon BWB pour éliminer toute cible seulement adsorbée en surface .

2.2 Méthodes de caractérisation de l'aptacapteur

Mesures de l'EIS

Une cellule conventionnelle à trois électrodes a été utilisée avec une electrode au calomel saturée (SCE, saturated calomel electrode) comme électrode de référence, un fil de platine comme contre-électrode et une électrode en or modifié comme électrode de travail. L'ensemble des voltammogrammes cycliques et des mesures de spectroscopie d'impédance électrochimique (EIS, electrochemical impedance spectroscopy) a été effectué à l'aide d'un potentiostat Bio-Logic (Bio-Logic SP-300) équipé du logiciel EC-Lab. Les mesures d'EIS ont été enregistrées en appliquant un potentiel égal à 0 V (par rapport à l'OCP), le potentiel d'oscillation de 10 mV sur la gamme de fréquences de 10 kHz à 1 mHz. Les mesures d'impédance ont été effectuées en présence d'un mélange $K_3[Fe(CN)_6]/K_4[Fe(CN)_6]$ (1:1, 5mM), dans une solution tampon phosphate, noté PBS (0,1 M à pH 7,4).

Microscopie à force atomique (AFM)

L'électrode en or et les électrodes fonctionnalisées à l'hydrogel de PAA ont été caractérisées par microsocpie à force atomique (AFM). Toutes les images ont été acquises avec un microscope Bruker ICON contrôlé par un Nanoscope V. L'épaisseur de l'électrode en or et de l'hydrogel PAA est déterminée sur le bord du motif. Les images en hauteur de la surface de l'or et des films d'hydrogel dans l'air ont été obtenues en mode tapping à 300 kHz avec une pointe standard de rigidité de 40 N/m. La rugosité est définie comme la demi-largeur de l'histogramme de distribution de hauteur extraite des images. Les conditions d'imagerie d'hydrogel dans l'eau ont été examinées en détail par Li et al. [57]. Comme la matière très molle est sondée, une pointe avec une rigidité inférieure est préférée si l'adhérence n'est pas prépondérante. Dans notre cas, un compromis a été choisi avec une pointe de contact typique avec une rigidité de 0,2 N/m. Pour sonder les films d'hydrogel dans l'eau, le mode tapping est préférable. Dans ce mode, la sonde et l'échantillon sont mis en contact de façon intermittente pendant une courte période et peuvent être considérés comme une succession de courbes d'approche-rétraction réalisées à haute fréquence (1 kHz) et limitées par une force de réglage maximale qui peut être réglée avec précision. Ce mode permet de réduire les forces latérales et de cisaillement pendant le balayage. Les images des forces maximales dans l'eau ont été obtenues à l'aide d'un cantilever de rigidité de 0,7 N/m, avec un point de consigne de force typique de 1 nN. L'amplitude du tapping était d'environ 200 nm. La taille des images est de 1 µm.

Autres techniques de caractérisation

L'ATR-FTIR a été réalisée sur un appareil Agilent Cary 660. Les mesures de l'angle de contact avec l'eau des différentes étapes de fabrication des électrodes ont été obtenues avec l'analyseur de forme de goutte KRUSS selon la méthode Sessile Drop en utilisant une goutte d'eau posée sur la surface étudiée.

L'imagerie électronique secondaire des différentes étapes de la construction a été réalisée à l'aide d'un microscope électronique à balayage FEI Thermo Fischer Magellan équipé d'une source FEG.

2.3 Construction de l'aptacapteur

Le schéma 1 illustre les étapes succesives de fabrication de l'aptacapteur électrochimique. L'étape préalable consiste en la préparation des electrodes d'or par lithographie positive (A). Ensuite, la première étape consiste à modifier l'électrode d'or par une monocouche auto-assemblée avec des molécules de dithiol (B). Une fois la SAM formée, et simultanément à faire fonctionner le PAA par réaction de clic thiol-ène pour la formation de matrice hydrogel (C) à surface fixée.

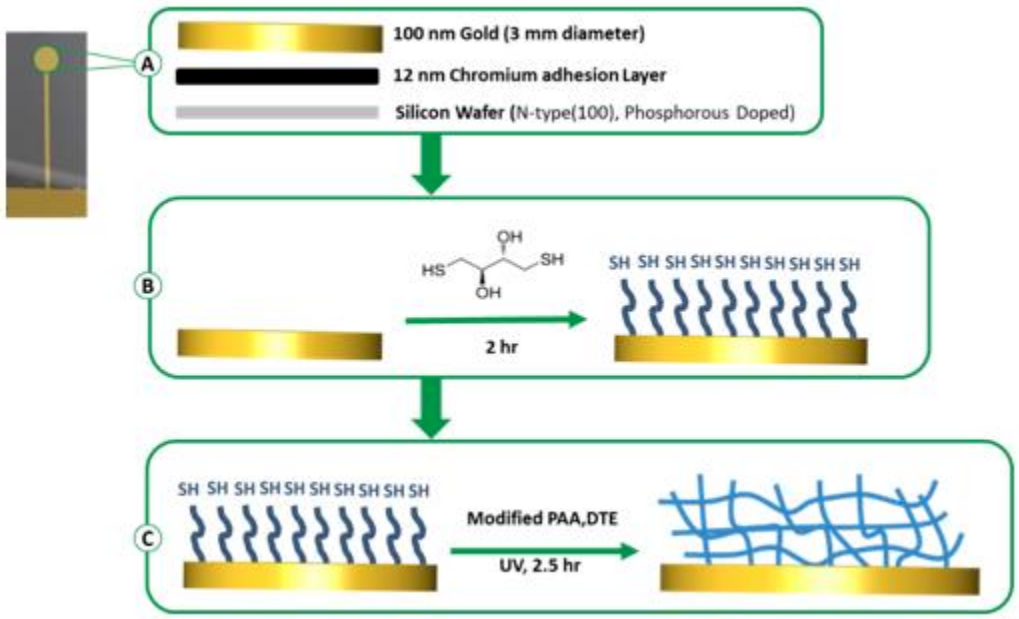

Schéma 1 : Représentation schématique des différentes étapes de la construction des aptasenseurs ;(A) électrode en or réalisée par photolithographie positive ; (B) modification thiol de l'électrode en or par une monocouche aauto-assemblée de thiol ; (C) greffage de l'hydrogel en utilisant la chimie du clic thiol-ène.

Préparation et fonctionnalisation thiol d'un transducteur d'électrode en or

Tout d'abord, le transducteur a été préparé sous la forme d'une électrode en or à couche mince déposée sur une tranche de silicium. A cette fin, des plaquettes de silicium dopées au phosphore de type N avec 100 orientations (résistivité : 1-20 ohm.cm) ont été utilisées comme substrats dans la préparation des films d'or évaporés. Les plaquettes de silicium ont été nettoyées au plasma d'oxygène avant le revêtement pour favoriser l'adhérence et la propreté. Les couches minces d'or ont été préparées par évaporation thermique de ∼100 nm d'Au sur une couche d'adhésion de chrome de ∼12 nm en utilisant un procédé photolithographique positif.

L'électrode de travail à couche mince en or, d'un diamètre de 3 mm, a ensuite été nettoyée dans 50 mM KOH et 25 % H_2O_2 pendant 30 minutes. Les électrodes ont ensuite été caractérisées par voltampérométrie cyclique à 50 mV/s dans une solution aqueuse de $K_3[Fe(CN)_6]$ pour vérifier la réversibilité du couple redox et comparer les courants de pointe expérimentaux et théoriques .

Les surfaces aurifères activées ont ensuite été fonctionnalisées avec des monocouches auto-assemblées de thiol en utilisant une solution de 1 mM de dithioérythritol (DTE) dans du chloroforme pendant 2 heures. Les surfaces modifiées au thiol ont ensuite été rincées et soniquées au chloroforme et séchées à l'azote.

Greffe d'hydrogels sur électrodes en or

Les chaînes polymères d'acide poly(acrylique) ont été fonctionnalisées de façon aléatoire avec des groupes ènes à leurs sites acides carboxyliques. Une réaction peptidique a été utilisée pour greffer de l'allylamine sur des chaînes polymères en présence d'EDC comme agent de déshydratation et de NHS comme agent d'addition pour augmenter les rendements et diminuer les réactions secondaires [58]. Brièvement, une solution à 20 % en poids de PAA dans de l'eau Milli-Q a été mélangée avec EDC et NHS à un pH de 4,5 pendant 2 heures à 60 °C. L'allylamine a ensuite été ajoutée (le rapport molaire AA/allylamine/EDC/NHS étant fixé à 10/1/1,5/1,5/1,5) et le pH a été ajusté à 10 avant que la réaction puisse se poursuivre pendant 16 heures à 60°C. Enfin, le polymère a été récupéré par lyophilisation après 3 jours de dialyse dans une solution de NaCl 0,1 M et 3 jours de dialyse dans de l'eau Milli-Q.

Des films minces d'hydrogel de PAA ont été synthétisés à la surface de l'électrode par réticulation et greffage simultanés de chaînes de polymères préformées par la voie chimique du clic thiol-ène,

comme décrit par Chollet et al. [56] et Li et al. [57]. Plus précisément, le polymère PAA fonctionnalisé à l'énène (0,5 % en poids) a été dissous dans le mélange de méthanol et d'acide formique 7:3 (V/V) et la solution a été agitée pendant une nuit. Les revêtements ont été réalisés par centrifugation de la solution polymère fonctionnalisée par l'éne-fonctionnalisation sur des électrodes en or fonctionnalisées par des thiols, avec ajout de réticulants à base de dithiol à 3000 tr/min pendant 30 secondes.

Une feuille d'aluminium a été utilisée comme masque pour les motifs. Les CLAG ont été obtenus simultanément en exposant l'ensemble à un rayonnement UV à 254 nm pendant 2,5 heures. L'électrode a ensuite été rincée dans du méthanol à l'aide d'un bain ultrasonique pendant 1 minute pour éliminer tous les polymères n'ayant pas réagi, puis séchée avec un flux de N_2. On a obtenu des films homogènes avec une épaisseur bien contrôlée, l'épaisseur à sec étant d'environ 57 nm.

Immobilisation de l'aptamère sur un transducteur modifié par un hydrogel

La fixation covalente de l'aptamère marqué sur l'électrode modifiée par l'hydrogel PAA a été réalisée par une une méthode de couplage en deux étapes. L'électrode modifiée par le PAA a d'abord été incubée pendant 30 minutes à 20ºC dans un tampon phosphate de pH 6,2 contenant 50 mM EDC et 100 mM NHS. L'électrode a ensuite été rincée avec un tampon phosphate (pH 7,4), puis incubée avec 10 µM d'aptamère dans une solution tampon phosphate de pH 7,4 pendant 1 h à 20ºC. Avant la fixation, la solution d'aptamère a été chauffée à 75ºC pendant 5 minutes. Après la fixation, l'électrode a été lavée avec une solution tampon de phosphate pour éliminer tout aptamère n'ayant pas réagi.

3. Optimisation et caracterisation des hydrogels

Dans un premier temps, des etudes ont été menées afin d'optimiser la fabrication des electrodes d'or et de determiner les conditions permettant l'obtention d'un comportement électrochimique. La partie présentée ci-après concerne l'étude et l'optimisation de la formation des films d'hydrogel sur les electrodes d'or conçues.

3.1 Caractérisation de la mouillabilité des films d'hydrogel fixés à l'électrode

Le greffage des films d'hydrogel sur les électrodes en or est mené en deux étapes, telles que décrite sur le schéma 1. L'angle de contact a ainsi été mesuré aux différentes étapes de préparation des électrodes et de leurs modifications de surface. Les mesures ont d'abord permis d'évaluer la mouillabilité du wafer en silicium qui sert de support pour la préparation des électrodes d'or en couche mince. Le mesures réalisées sur ce wafer avant et après son nettoyage par un plasma montre que la surface devient mouillante (angle de contacte de 12°) après le nettoyage au plasma. Après dépôt de l'électrode d'or, la mesure est également faite sur l'électrode d'or, montrant un angle de contact supérieur à celui du silicium initial, et égal à 62° Les mesures de l'angle de contact ont ensuite été effectuées sur l'or après les deux étapes de modification pour évaluer la présence des différentes couches, .

Le WCA obtenue pour l'or modifié par une monocouche auto-assemblée de DTE SAM présente un angle de contact plus élevé (~75°) que celui de l'électrode en or initiale, ce qui témoigne de la modification des propriétés de surface de l'or. Les mesures WCA des MAS ont une relation de parité (ou pair-impair) par rapport à la longueur de la chaîne [59,60].

Après la formation de l'hydrogel PAA sur l'électrode en or modifié par le SAM thiol, l'angle de contact diminue par rapport à l'élecrode modifiée par le SAM et est évalué à 50°, montrant que la surface est plus mouillante. Cette modification est indicative de la présence d'un film plus hydrophile en surface. Ce résultat est conforme à une étude antérieure décrivant pour l'angle de contact de pour des films d'hydrogel PAA, qui est hydrophile et chargé négativement [61].

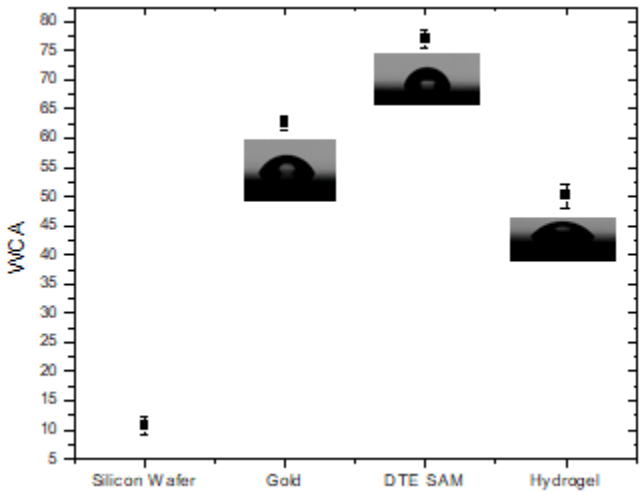

Figure 1. Mesures d'angles de contact (WCA : water contact angle) avec l'eau aux différentes étapes de la modification de surface des électrodes. Chaque mesure représente la moyenne de 3 mesures.

3.2 Epaisseur et topographie des électrodes modifiées par les films d'hydrogel

La microscopie à force atomique a été utilisée afin d'évaluer l'épaisseur et la topographie des électrodes après le greffage de l'hydrogel. Il est à noter que la caractérisation AFM des films d'hydrogel a été faite dans des conditions sèches et humides afin de mesurer la capacité de gonglement des films en présence d'eau.

La figure 2 présente les profils de hauteur obtenus par AFM. La caractérisation de l'électrode d'or a permis de montrer que la couche mince d'or déposée sur le silicium est de 100 nm. L'épaisseur du film d'hydrogel sec est de 57 nm. Cette épaisseur à sec du film d'hydrogel PAA correspond à la valeur trouvée dans la littérature pour des films d'hydrogel fixés sur or à l'aide d'une solution polymère déposée par centrifugation à une concentration de 0,5 % en poids et un poids moléculaire de 250 kg mol 1 [56].

Le taux de gonflement est mesuré en calculant le rapport entre l'épaisseur des films d'hydrogel mesurée dans l'eau et l'épaisseur des films secs (mesurée dans l'air). Ce taux a été évalué à 1,8 pour des films d'hydrogel fabriqués avec 2 % de groupes réactifs à l'énérythritol et 30 fois l'excès de groupes réactifs à l'énérythritol des réticulants dithioérythritol. Ce résultat est cohérent avec une

étude antérieure selon laquelle, pour les films minces de moins de 150 nm, le taux de gonflement augmente avec l'épaisseur du film et est indépendant de l'épaisseur dans toute la gamme allant de 150 nm à quelques micromètres [56,57]. Ceci est lié au fort effet de l'attachement de surface sur le gonflement des film. Par conséquent, les films d'hydrogel nanométriques gonflent en moyenne moins que les couches micrométriques en raison de la contrainte due à leur greffage avec la surface.

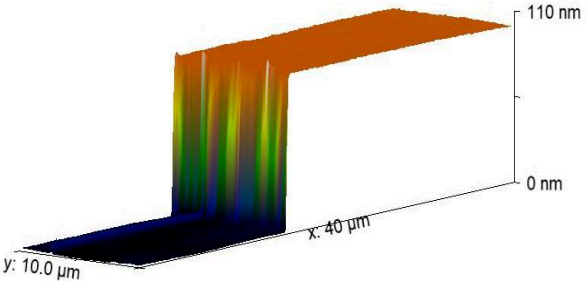

(c)

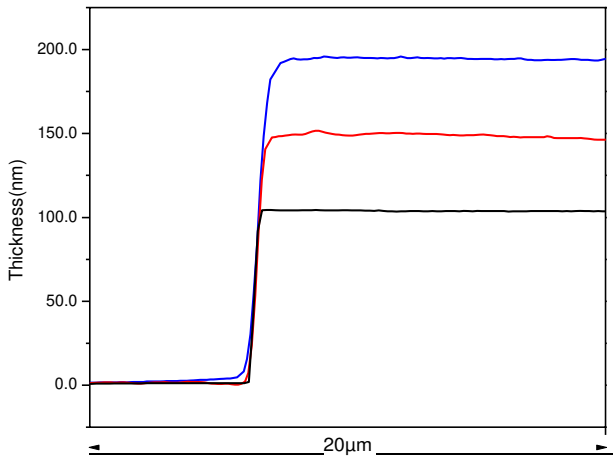

(d)

Figure 2. (a) Schémas des profils de hauteur obtenus par AFM pour l'or non modifié (bleu : surface de silicium, rouge : surface d'or non modifiée). b) Profils de hauteur de l'électrode en or non modifié (en noir), du film hydrogel PAA dans l'air (rouge) et du film hydrogel PAA dans l'eau (bleu). L'épaisseur nulle correspond à la surface de silicium.

Les images topographiques AFM de la surface d'or modifiée ou non par le film d'hydrogel fixé (à sec ou immergé dans l'eau) sont présentés sur la figure 3 . L'image en hauteur obtenue à partir de la surface de l'or évaporé montre une structure granuleuse typique (figure 3a). Pour illustrer la différence de rugosité entre les échantillons de la figure 3, une ligne de profil est extraite pour chaque image en hauteur et affichée sous l'image. La rugosité de la surface d'or peut être extraite des images AFM mesurant la demi-largeur de l'histogramme de hauteur de l'image. La figure 3 (a) donne une rugosité de 4 nm. De plus, la même valeur (~ 4 nm) est obtenue pour les deux images

(échelles de 1 µm et 10 µm), prouvant que la rugosité est indépendante de la taille de l'échantillon et est homogène. L'homogénéité de l'électrode en or nu à l'échelle de 10 µm et la structure granulaire à l'échelle de 1 µm observée par AFM sont également confirmées par SEM (figure 4). et microscopie électronique à balayage (SEM) (figure 4 et figure S4 (renseignements à l'appui)

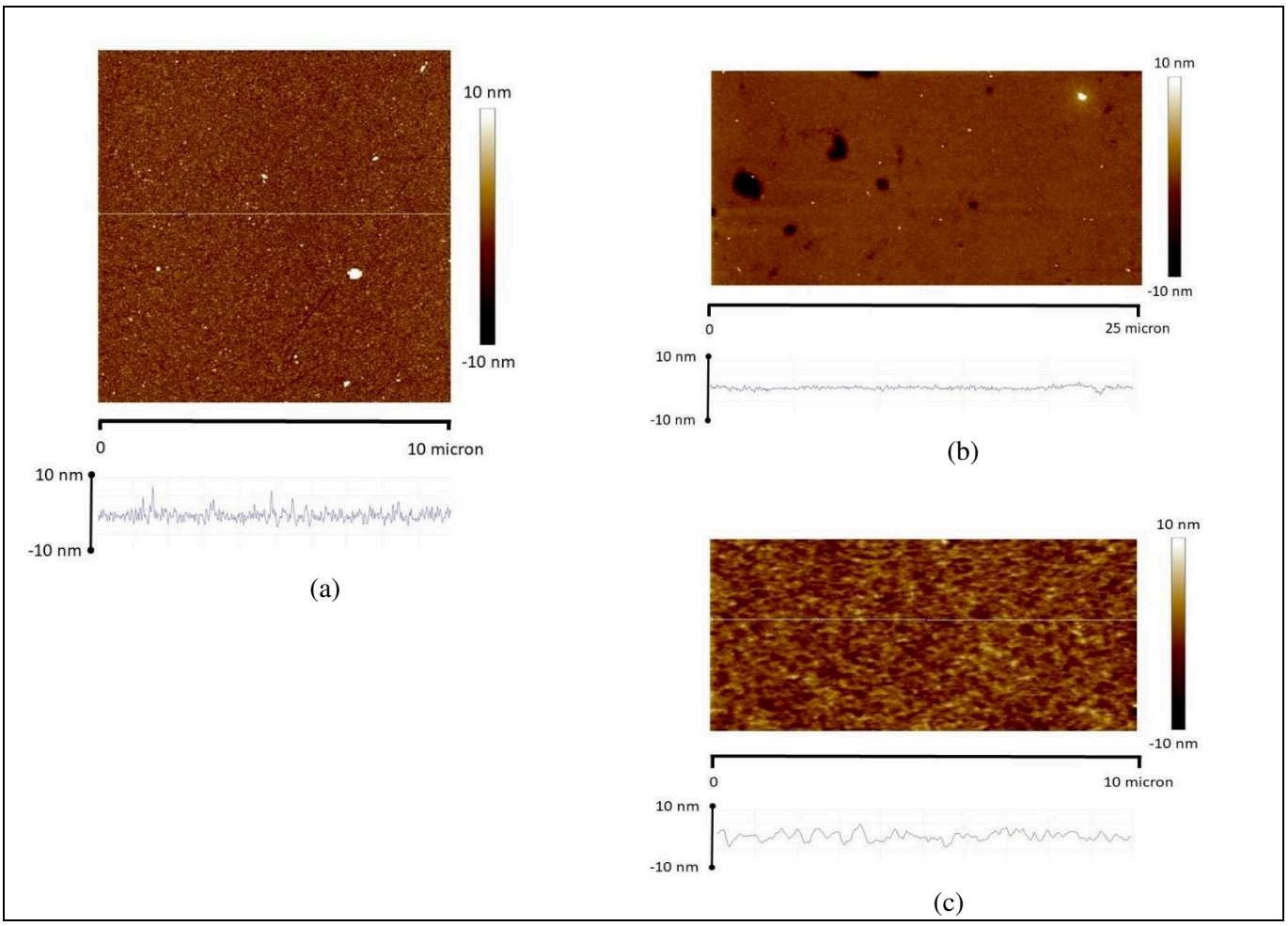

Figure 3. Images topographiques (10 x 10 µm) obtenues par AFM en mode tapping pour l'électrode d'or non mpodifée (a), le film d'hydrogel sec (b) et le film d'hydrogel immergé dans l'eau (c).

Les images AFM du film d'hydrogel PAA dans l'air (Figure 3b) montrent que sa rugosité, estimée à 1 nm, est homogène. Bien que l'épaisseur du film d'hydrogel (~ 57 nm) soit beaucoup plus élevée que sa rugosité, la surface du film d'hydrogel reproduit celle de l'électrode en or sous-jacente et suit strictement la même structure granulaire que l'électrode d'or initiale. La réplication de la morphologie de la surface de l'or est confirmée par microscopie électronique à balayage, sur les

figures 4 et 5. L'image MEB de la figure 5 permet d'observer la frontière entre le film d'hydrogel (région sombre) et la surface de l'or non modifiée. L'insert montre la structure granulaire sur les deux surfaces de l'électrode en or et du film d'hydrogel, avec un contraste topographique légèrement inférieur dans la région de l'hydrogel. L'observation de la région de l'hydrogel (partie supérieure de la figure 5) à grande échelle (50 µm) confirme la planéité de la surface de l'hydrogel.

Le film d'hydrogel immergé dans l'eau (figure 3c) présente une rugosité supérieure (~ 4 nm) à celle obtenue à sec, lorsque le gel gonfle (le taux de gonflement est de 1,8). Ainsi, la rugosité de la surface du film d'hydrogel est due à la réplication de la morphologie granulaire de l'électrode en or. Elle est beaucoup plus faible que l'épaisseur de la couche, de sorte que le film d'hydrogel peut être considéré comme totalement homogène et plan.

A partir de la mesure de l'épaisseur sèche (épaisseur = 57 nm) et du taux de gonflement (S = 1,8), il est possible de calculer la concentration en acide acrylique en surface. En effet, la concentration volumique C_V peut être calculée par : $C_V = \rho/(SxM)$ où ρ est la densité de l'acide poly(acrylique) et M est le poids moléculaire du motif acide acrylique. La concentration de surface C_S est calculée par : $C_S = (hx\rho)/M$. On obtient finalement $C_V = 8\ 10^{+3}$ mol L^{-1} et Cs = 0,82 10^{-3} mol/m^2.

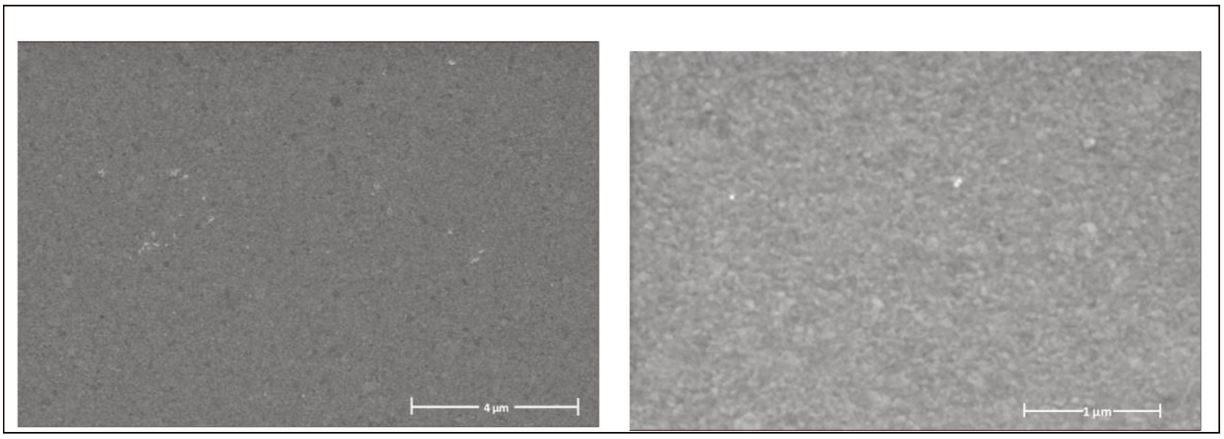

Figure 4. Images MEB de la surface de l'électrode en or nu à différentes échelles

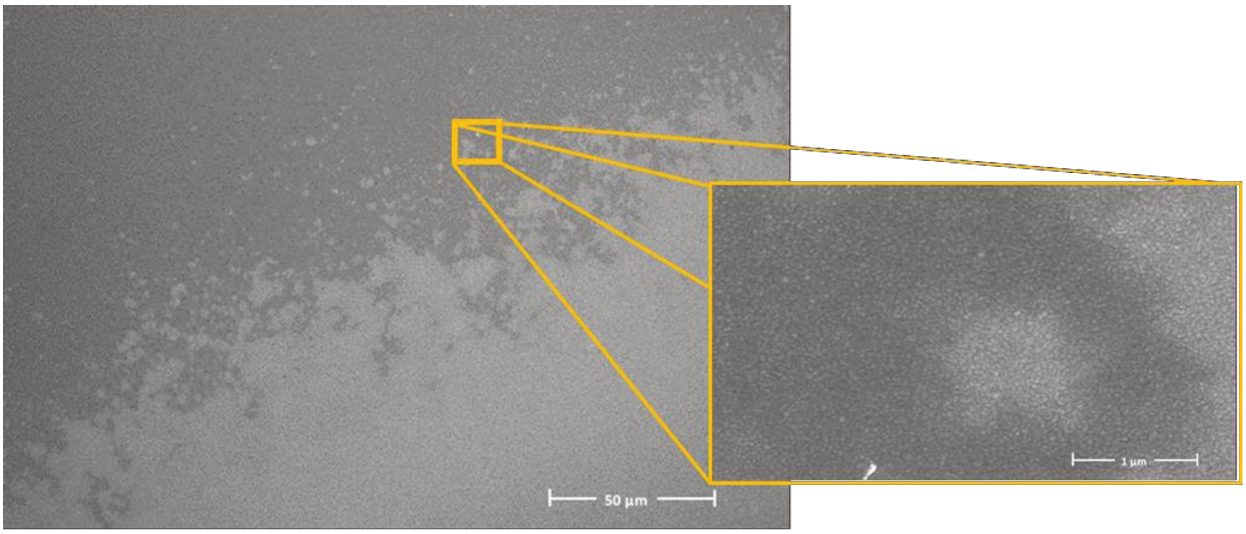

Figure 5. Morphologie de surface de l'hydrogel (zone sombre) et de l'or (zone blanche) visualisée au microscope électronique à balayage (MEB)

3.3 Caractérisation infra-rouge des électrodes modifiées par hydrogel

Les électrodes ont également été caractérisées par spectroscopie ATR-FTIR et électrochimie, après réticulation et greffe de PAA pour mettre en évidence la présence de l'hydrogel à la surface de l'électrode. La figure 6 montre les spectres ATR-FTIR entre 500 et 4000 cm^{-1} de l'électrode en or après modification du thiol et formation de l'hydrogel PAA. Comme le contact entre le guide d'onde ATR-diamant et le substrat de silicium solide ne peut être reproductible pour différents échantillons, l'absorbance est en unité arbitraire. Cette représentation permet également de mettre en évidence les bandes d'absorption. Le spectre (a) démontre clairement que l'électrode en or est modifiée par des molécules de thiol. Tout d'abord, la liaison covalente or-soufre est prouvée par la présence d'une large bande de l'ordre de 500 à 750 cm^{-1}, qui peut être affectée au mode d'étirement de la liaison C-S. Deuxièmement, le mode vibratoire de l'alkylthiol est observé à 2917 cm^{-1}. De plus, les pics à 1017 cm^{-1} correspondent au mode de déformation O-H. Les vibrations d'étirement O-H de l'ordre de 3100-3500 cm^{-1} sont également clairement visibles.

Le spectre FTIR-ATR (b) est obtenu avec l'électrode en or modifiée par l'hydrogel PAA. Il met en évidence la bande d'étirement O-H dans la région 3400 cm^{-1} et l'étirement CH_2 (asymétrique) à 2925 cm^{-1}. De plus, les bandes à 1700 cm^{-1} sont assignées à la bande d'étirement C=O du PAA. En comparant les spectres (a) et (b), on peut remarquer que les vibrations d'étirement O-H dans la gamme de 3100 à 3500 cm^{-1} sont différentes. La bande d'absorption de l'hydrogel de PAA qui est

caractéristique du composé hygroscopique est plus large en raison de la présence de liaisons H (en comparaison avec la bande d'étirement O-H de la monocouche de thiol). La diminution de la bande O-H à 1017 cm^{-1} est due à l'unité arbitraire de l'absorbance. Enfin, il faut noter que la présence de la bande C-S dans le spectre de l'hydrogel PAA n'est pas surprenante car l'épaisseur du film d'hydrogel est bien inférieure à la profondeur de pénétration de l'onde évanescente du faisceau infrarouge ATR (quelques microns).

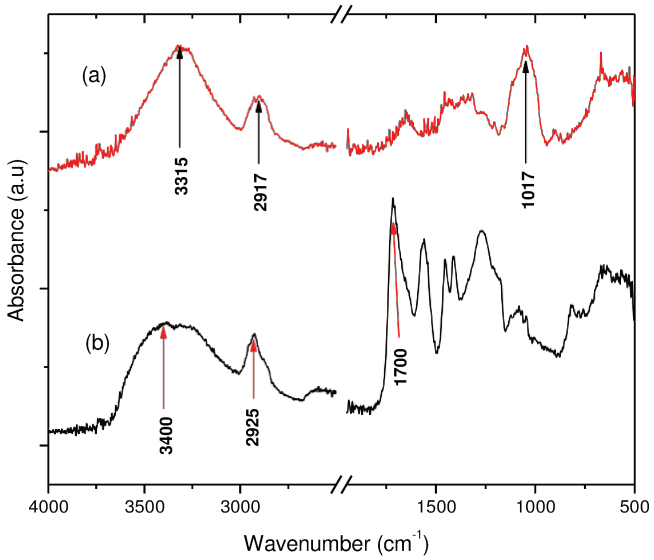

Figure 6. Spectre FTIR-ATR de l'électrode en or thiolé (a) et de l'électrode en or greffé par hydrogel PAA (b).

3.4. Caractérisation électrochimique de l'électrode modifiée par hydrogel

L'électrode modifiée par hydrogel PAA a également été analysée électrochimiquement par voltampérométrie cyclique. La figure 7 montre les voltammogrammes de $Fe(CN)_6^{3-/4-}$ de l'électrode en or à différentes étapes de la préparation du film d'hydrogel : électrode en or nu, monocouche de thiol et film d'hydrogel PAA.

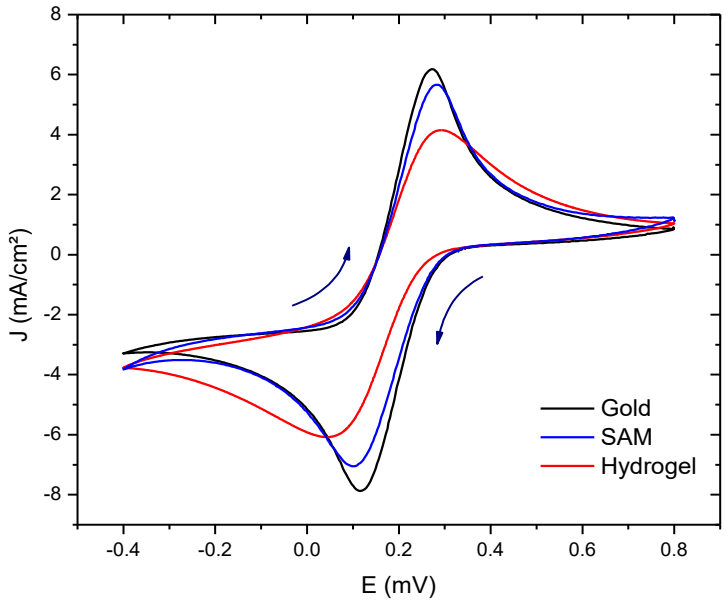

Figure 7. Caractérisation de l'interface de détection par voltampérométrie cyclique à 50 $mV.s^{-1}$ dans une solution de KCl 0,1 M contenant 5 10^{-2} M $K_4[Fe(CN)_6]$ et $K_3[Fe(CN)_6]$: électrode or nu (noire), monocouche thiol (bleue), film hydrogel PAA (rouge).

Le voltammogramme de $Fe(CN)_6^{3-/4-}$ obtenu avec une électrode modifiée avec les groupements thiols est presque similaire au voltammogramme observé avec une électrode en or nu. Ceci est attribué au fait que les molécules de thiol forment une monocouche non dense [62]. L'introduction de groupements -SH, -COOH, -OH, $-NH_2$ au lieu du groupement $-CH_3$ entraîne généralement une diminution des couches auto-assemblées [63]. Ainsi, la monocouche de petites molécules de DTE thiol sur or est plus mince pour pouvoir bloquer efficacement le transfert d'électrons sur une surface en or.

A un pH relativement élevé pour lequel l'hydrogel de PAA est gonflé et dissocié et au contact de la sonde d'oxydoréduction négative $Fe(CN)_6^{3-/4}$, la répulsion électrostatique affectera le taux de transfert d'électrons interfacial de la sonde et on observe une diminution du courant maximal et une augmentation du potentiel de séparation par rapport aux électrodes en or nues et modifiées. De plus, ceci peut s'expliquer par l'étude qui décrit que les brosses en polyacide à faible pH sont entièrement protonées et adoptent une conformation similaire à celle des brosses neutres [64]. A pH élevé, les groupes acides de la brosse se dissocient et la brosse se comporte comme une brosse polyélectrolyte étendue en régime osmotique ou Pincus [65].

4. Etude de l'immobilisation covalente de l'aptamere sur les films d'hydrogel

L'immobilisation covalente de l'aptamère sur la surface du film d'hydrogel de PAA greffé sur l'électrode sous-jacente a été réalisée par deux étapes chimiques EDC/NHS.

La figure 8 montre les spectres ATR-FTIR à différents stades de la construction du capteur : l'hydrogel PAA, l'hydrogel PAA activé et la greffe de l'aptamère. Le spectre de l'hydrogel activé présente trois bandes caractéristiques à 1815, 1790 et 1750 cm^{-1}. Ces bandes sont représentatives des modes d'étirement carbonyle dans la le groupement COO-NHS. Après immobilisation de l'aptamère, les pics de l'anhydride et de l'ester NHS disparaissent et de nouvelles bandes dues aux groupements amide apparaissent autour de 1580 cm^{-1} et 1660 cm^{-1} (caractéristiques des amides I et II), ce qui confirme le couplage de l'aptamère sur le film d'hydrogel.

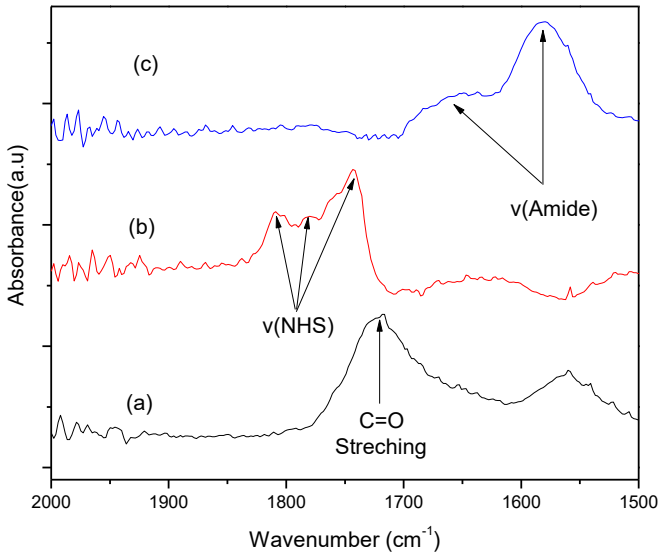

Figure 8. Spectre ATR-FTIR de l'hydrogel Au/PAA (a), de l'hydrogel Au/PAA activé (b) et de l'aptamère Au/PAA hydrogel/DCL greffé (c).

La figure 9 présente les diagrammes de Nyquist de l'électrode modifiée par l'aptamère, aux différentes étapes de modification. Le diagramme de Nyquist représente l'opposé de l'impédance imaginaire en fonction de l'impédance réelle pour chacune des fréquences d'excitation

L'impédance est modélisée à l'aide d'un circuit équivalent (schéma en bas de la Figure 9) dont les éléments sont expliqués :

- Résistance de la solution (Rs) : la résistance de la solution, modélise le phénomène de passage du courant entre l'électrode de travail et la contre électrode. Elle dépend, principalement, de la résistivité de la solution, de l'aire et de la géométrie de l'électrode de travail.
- Résistance de transfert de charge (Rct) : la résistance de transfert de charge est la résistance liée au mécanisme de transfert de charge pour des réactions redox à l'électrode.
- Elément de phase constante (CPE) : l'élément de constante de phase CPE représente une grandeur empirique, qui prend en considération les irrégularités interfaciales (porosité, géométrie, rugosité, diffusion, etc.). Ce paramètre CPE est défini par une capacité C_d et un nombre n qui peut prendre les valeurs -1, 0, 0.5 ou 1 et qui correspondent respectivement à une inductance, impédance pure, terme de Warburg ou capacitance.
- Impédance de Warburg (Z_W) : l'impédance de Warburg est l'impédance résultant de la diffusion d'une espèce à l'électrode. C'est le premier élément électrochimique qui a été présenté dans la description de l'impédance de la diffusion semi-infinie. Cette impédance dépend de la fréquence de la perturbation, du potentiel appliqué et de la concentration des espèces qui diffusent [66].

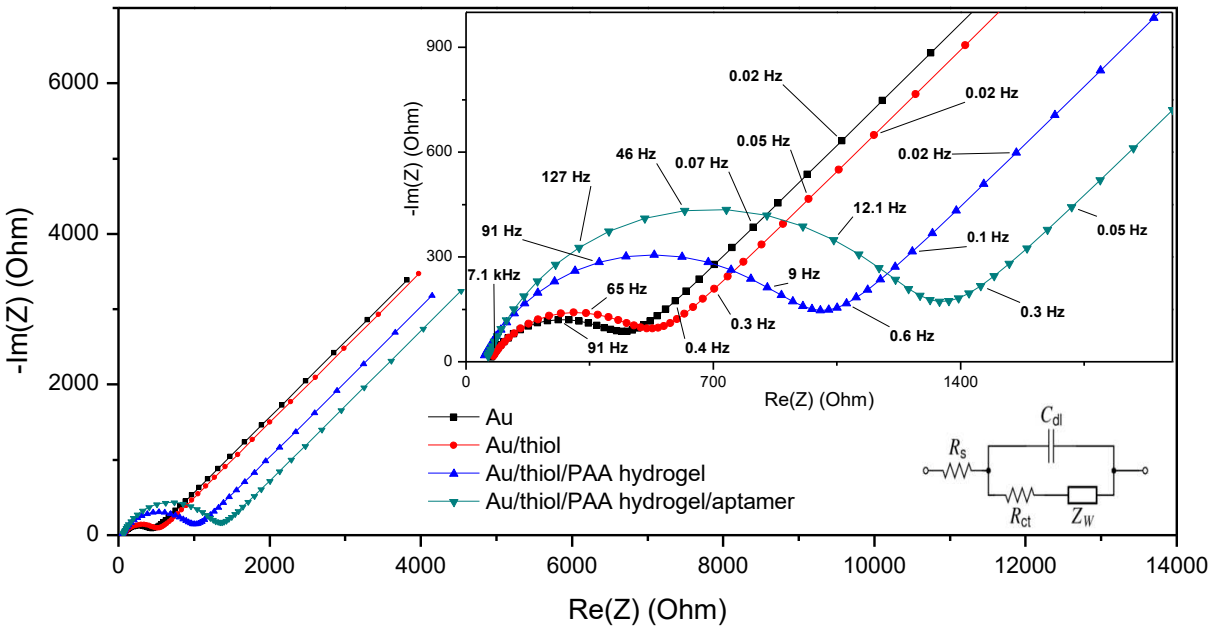

Figure 9. Diagrammes Nyquist de Au (■), Au/thiol (●), Au/thiol/PAA hydrogel (▲), Au/thiol/PAA hydrogel/aptamer (▼) dans des électrodes 0,1 M PBS contenant 5 mM $K_4[Fe(CN)_6]$ et $K_3[Fe(CN)_6]$ dans la gamme de fréquences allant de 10 kHz à 0,1 Hz.

Lorsque la surface de l'électrode en or est modifiée en utilisant la couche DTE, la valeur Rct augmente légèrement (451 ohm). Il n'y a pas de différence très significative, contrairement à la propriété isolante de la monocouche auto-assemblée thiol. Ceci est dû à la courte chaîne de dithiol utilisée dans cette étude, telle qu'elle a été discutée lors de l'étude de voltampérométrie cyclique. En revanche, lorsque l'électrode est greffée par un film d'hydrogel de PAA, en raison de l'interaction répulsive entre l'hydrogel de PAA chargé négativement et la sonde redox anionique, la valeur Rct augmente pour atteindre 932 ohms. Après immobilisation de l'aptamère sur l'électrode, un demi-cercle de diamètre assez grand a été surveillé. L'augmentation observée de la valeur de Rct a été attribuée à l'empêchement du transfert d'électrons par l'aptamère chargé négativement.

5. Performances de l'aptacapteur pour la detection du dcl

5.1 Détection du diclofénac

La détection de DCL a été effectuée par incubation de l'électrode modifiée par l'aptamer avec des solutions de DCL à différentes concentrations. Les performances de l'aptasenseur ont été étudiées en enregistrant les réponses EIS dans une solution de PBS 0,1 M contenant 5 mM $[Fe(CN)_6]^{3-/4-}$.

Comme l'illustre la figure 10, lorsque la concentration de DCL augmente, Rct diminue. Cela peut être attribué au fait que des concentrations plus élevées de DCL provoquent des changements dans la conformation spatiale de l'aptamère. Les résultats démontrent que ces changements de conformation réduisent la densité de charge négative en surface et, par conséquent, la résistance au transfert de charge interfaciale à la sonde d'oxydoréduction à charge négative [29].

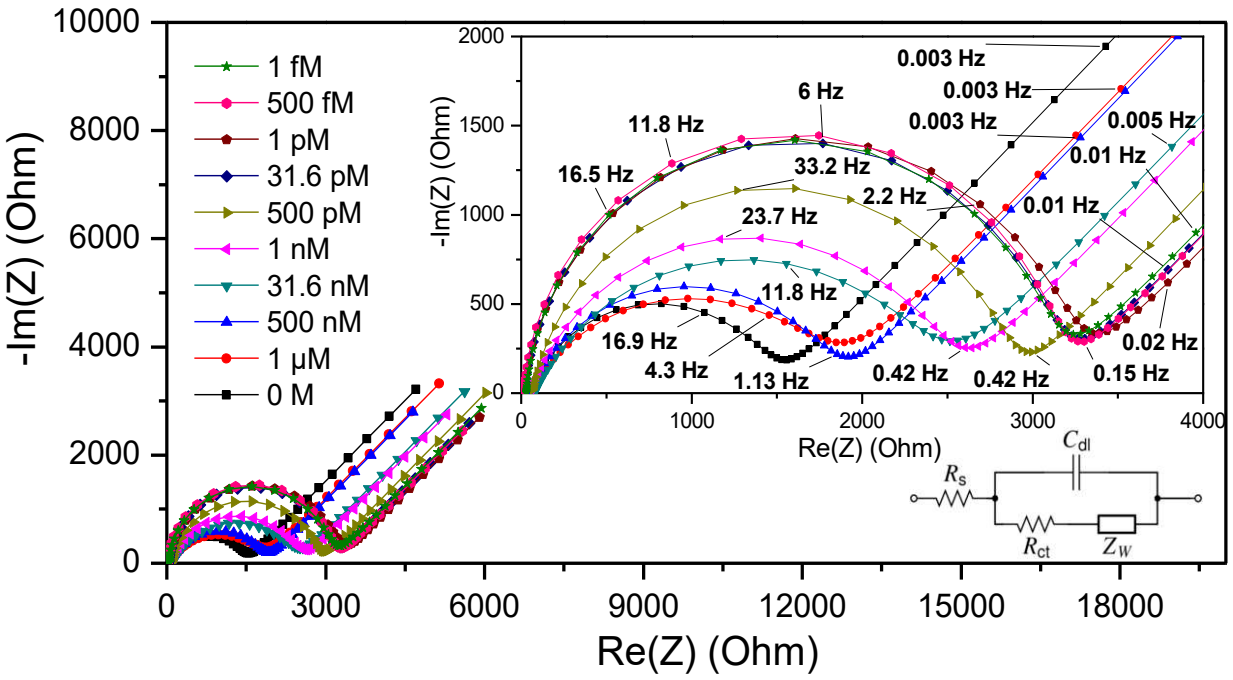

Figure 10. Diagramme de Nyquist obtenu dans du PBS 0,1 M contenant 5 mM de $K_4[Fe(CN)_6]$ et $K_3[Fe(CN)_6]$ après traitement de l'aptasenseur avec différentes concentrations de DCL dans la gamme de fréquences de 100 kHz à 1 mHz.

La variation de la résistance de transfert de charge (Fig. 10) est linéaire avec une concentration de la molécule cible comprise entre 30 pM et 1 µM. Une bonne relation linéaire entre Rct et la concentration de DCL a été obtenue (R^2 = 0,9787), selon l'équation suivante :

Rct= - 310.23[DCL] - 99.637.

La limite de détection est de 0,02 nM (Fig. 11).

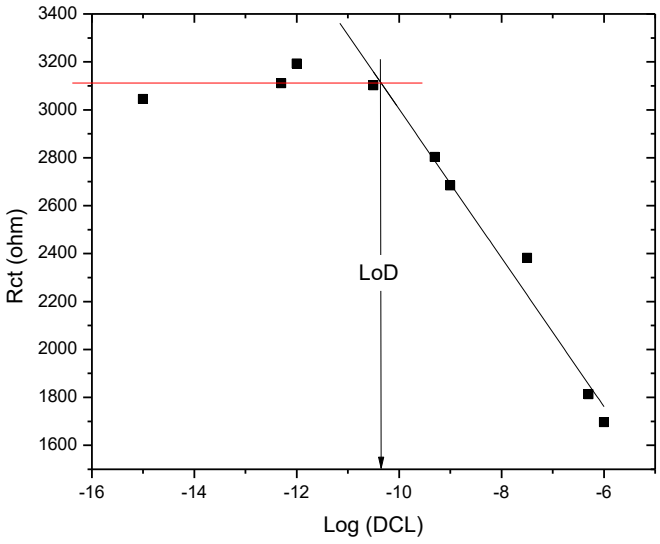

Figure 11. Courbe d'étalonnage représentant la concentration de Rct en fonction du logarithme de la concentration de DCL l

5.2 Stabilité et reproductibilité des aptacapteurs

Une fois que la réponse du capteur au diclofénac démontrée, la stabilité et la reproductibilité du protocole développé ont été évaluées. La stabilité opérationnelle et les performances de l'aptasenseur développé ont été évaluées pour un stockage à long terme à 4°C en utilisant cinq électrodes différentes modifiées par des aptamères. La réponse d'impédance de l'aptasenseur a été évaluée et il a été observé que l'aptasenseur conservait 95,6 % de sa réponse initiale après 7 jours de stockage et 92,3 % après 14 jours de stockage (détection de 500 pM de DCL), indiquant une bonne stabilité.

De plus, afin d'évaluer la reproductibilité de l'aptasenseur, cinq aptasenseurs ont été traités avec 500 pM de DCL, et la Rct a été enregistrée dans 0,1M PBS contenant 5mM de $[Fe(CN)_6]^{3-/4-}$. L'écart-type relatif (RSD) de leur réponse était de 4,8 %. Cela montre que la reproductibilité de l'aptasensor est fiable. La reproductibilité des différentes étapes de la construction des électrodes a également été évaluée (figure 12). Les variations observées peuvent s'expliquer par plusieurs facteurs difficilement controlables qui peuvent affecter les résultats impédimétriques puisque les électrodes sont fabriquées à la main.

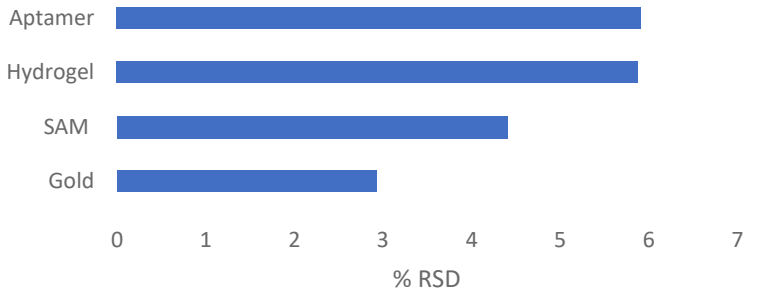

Figure 12. Écart-type relatif de la résistance de transfert d'électrons (Rct) enregistrée à différents stades de la construction des électrodes dans 0,1M PBS contenant 5mM $[Fe(CN)_6]^{3-/4-}$.

5.3 Sélectivité de l'aptacapteur

La sélectivité de la detection a également été évaluée en utilisant deux interférents potentiels dans la detection du DCL. En effet, les matrices d'échantillons réels constituent un défi important pour le développement de systèmes de détection sensibles et spécifiques. Les interférences de la matrice peuvent entraîner une suppression ou une augmentation du signal obtenu. Des faux négatifs dus à une sensibilité réduite du test ou des faux positifs dus à un manque de spécificité peuvent résulter notamment de la co-extraction de composés ayant des propriétés physico-chimiques similaires à la cible [33,34]. La sélectivité de l'aptacapteur joue un rôle important dans l'analyse d'échantillons réels in situ sans pré-traitement, et nous avons choisi d'étudier certaines substances potentiellement interférentes pour évaluer la sélectivité de l'aptacapteur DCL ainsi que la réactivité croisée, en utilisant des échantillons contenant un mélange de la cible et des interférents. Les espèces interférentes choisies ont été : le paracétamol, l'acide 4-amino-phényl-acétique et le tryptophane, leur structure étant présentée sur la figure 13.

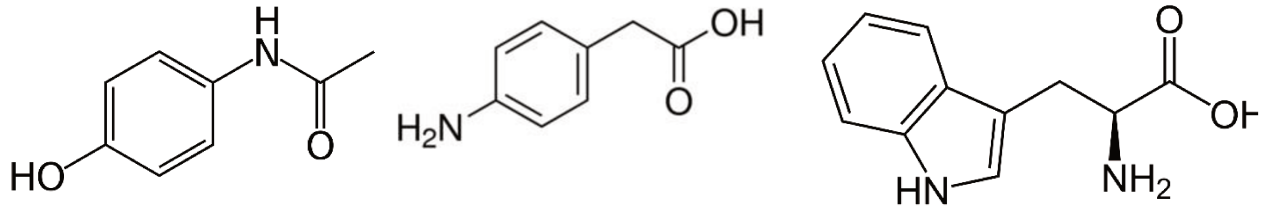

(A) **(B)** **(C)**

Figure 13: Strcutures des molecules pontentiellement interférentes: (A) Paracétamol, (B) Acide 4-Amino phenyl acétique (C) Tryptophane.

L'étude de sélectivité a été réalisée par incubation de l'électrode modifiée par l'aptamère au DCL (aptacapteur) avec les solutions des interférents à une concentration 1000 fois supérieure à celle du DCL (15 nM). Les performances ont été étudiées en enregistrant ses réponses SIE dans un milieu PBS 0,1 M contenant 5 mM $[Fe(CN)_6]^{3-/4-}$ (Figure 14), dans les memes conditions que pour la detection du DCL seul.

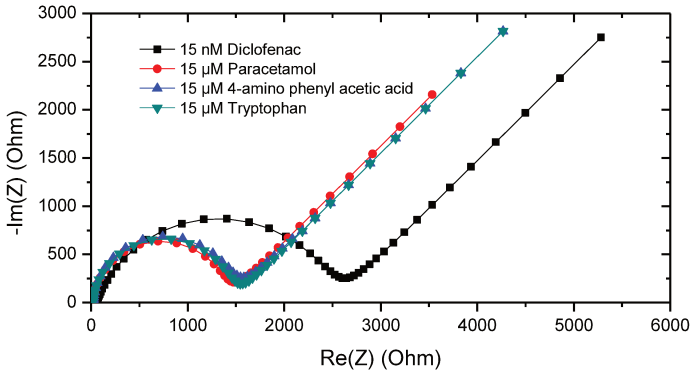

Figure 14 : Allure typique de la réponse SIE de l'aptacapteur en milieu PBS 0,1 M contenant 5 mM $[Fe(CN)_6]^{3-/4-}$ après incubation dans les échantillons suivants: (■) 15 nM DCL (●) 15 µM Paracetamol (▲) 15 µM acide 4-amino phenyl acetique (▼) 15 µM Tryptophane.

Les résultats résumés sous forme d'histogramme sur la figure 15 montrent que la réponse obtenue en présence de composés interférents, à un niveau de concentration de 15 µM (colonnes B à D), est proche de celle obtenue en l'absence d'analyte cible et est différente de celle obtenue en présence de 15 nM DCL (colonne A), montrant que ces composes interférents ne peuvent interagir avec l'aptamère DCL.

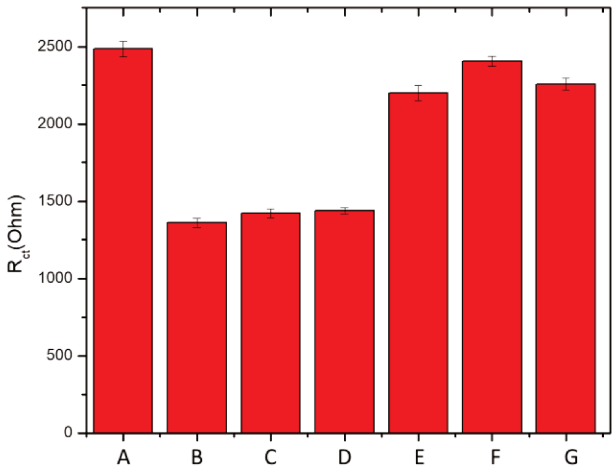

Figure 15: Résistance au transfert de charge déduite des mesures SIE avec l'aptacapteur, réalisées en milieu PBS 0,1 M contenant 5 mM $[Fe(CN)_6]^{3-/4-}$ après incubation de l'aptacapteur dans les échantillons suivants: (A) 15 nmol L^{-1} DCL (B) 15 µmol L^{-1} Paracétamol (C) 15 µmol L^{-1} acide 4-amino phenyl acétique (D) 15 µmol L^{-1} Tryptophane (E) 15 nmol L^{-1} DCL + 15 µM Paracétamol (F) 15 nmol L^{-1} DCL + 15 µmol L^{-1} acide 4-amino phenyl acétique (G) 15 nmol L^{-1} DCL + 15 µmol L^{-1} Tryptophane. Chaque point est la moyenne faite sur deux experiences indépendantes.

Pour confirmer la sélectivité de l'aptacapteur, la sensibilité croisée de l'aptacapteur a également été étudiée dans un échantillon mixte, contenant 15 nM de DCL en presence d'une concentration élevée d'interférents (15 µM), comme le montre la figure 16. Malgré une concentration en interférent 1000 fois plus élevée que la concentration de DCL, le Rct obtenu à partir de la réponse de trois échantillons complexes (Figure 15, colonnes E à G) est similaire au Rct obtenu en presence de DCL uniquement. Ces résultats montrent que les espèces interférentes étudiées ont une influence négligeable sur la détection du DCL. Ces résultats confirment la sélectivité de l'aptacapteur développé associée aux liaisons spécifiques entre le DCL et son aptamère et son application possible pour la quantification sélective de la DCL sans interférence.

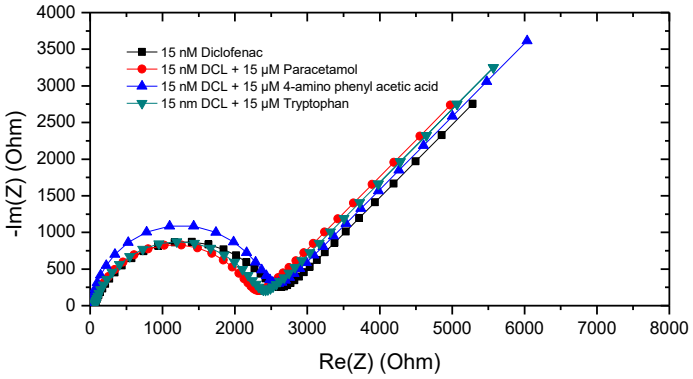

Figure 16: Mesures SIE avec l'aptacapteur, réalisées en milieu PBS 0,1 M contenant 5 mM $[Fe(CN)_6]^{3-/4-}$ après incubation de l'aptacapteur dans les échantillons suivants: : (■) 15 nM DCL (●)15 nM DCL + 15 µM Paracétamol (▲)15 nM DCL + 15 µM 4-amino phenyl acetic acid (▼)15 nm DCL + 15 µM Tryptophane.

De plus, afin de montrer l'interaction spécifique entre l'aptamère et le DCL, des contrôles ont été effectués en rélaisant des mesures SIE sur une électrode modifiée par hydrogel PAA uniquement (sans aptamère), après incubation avec 15 nM de DCL et des composés interférents (15 µM) (Figure 17(i)). Les diagrammes de la figure 17(ii) montrent qu'il n'y a pas changement de la réponse EIS pour l'hydrogel qu'il soit incubé ou non, soit avec les composés interférents (colonnes C et D) ou avec le diclofénac (colonne E) tandis que la réponse de l'électrode modifiée avec l'aptamère présente une modification de la réponse SIE après incubation avec du diclofénac 15 nm (colonne A). Ce résultat indique qu'il n'y a pas d'interaction détectable par SIE entre l'électrode modifiée avec l'hydrogel PAA et la cible ainsi ou avec les composés interférents utilisés dans cette étude, ce qui confirme l'interaction spécifique entre l'aptamère et le DCL.

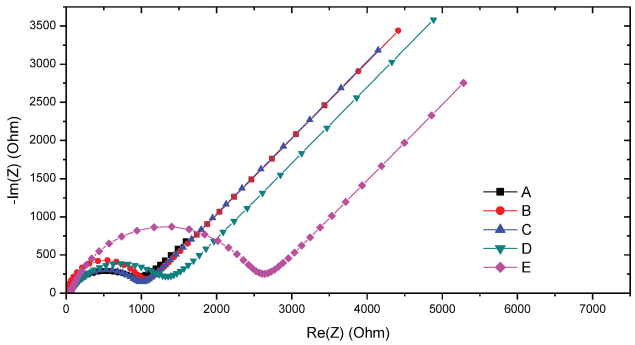

(i)

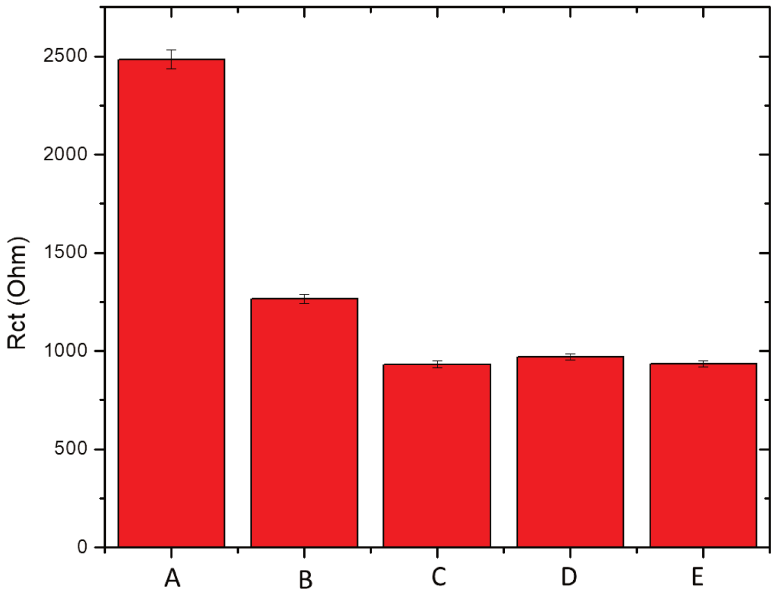

(ii)

Figure 17: **(i)** Résistance au transfert de charge obtenue par mesures d'impédance avec electrode modifiée par l'hydrogel et incubée dans une solution de diclofenac 15 nmol L^{-1} (A) ou dans 15 µmol L^{-1} acide 4-amino phenyl acétique (B) ou dans 15 µmol L^{-1} Paracétamol. Résistance au transfert de charge obtenue par mesures d'impédance avec electrode modifiée par l'aptamère (D) incubé dans 15 nmol L^{-1} Diclofenac (E). **(ii)** Histogramme correspondant à la figure (i) (A) electrode modifiée par l'aptamère incubé dans 15 nmol L^{-1} Diclofenac (B) electrode modifiée par l'aptamère (C) electrode modifiée par l'hydrogel incubée dans 15 µmol L^{-1} Paracétamol (D) electrode modifiée par l'hydrogel incubée dans 15 µmol L^{-1} d'acide 4-amino phenylacetique (E) electrode modifiée par l'hydrogel incubée dans 15 nmol L^{-1} diclofenac. Chaque point est la moyenne faite sur deux experiences indépendantes.

.

5.4 Comparaison des performances aux capteurs de la littérature

Comme mentionné en introduction, plusieurs méthodologies électroanalytiques ont été rapportées dans la littérature pour la détermination de la DCL basées sur différentes méthodes de détection et sur des modifications d'électrodes plus ou moins complexes. L'amélioration de la détection des cibles à la surface transductrice à l'aide de biomolécules spécifiques au DCL a été publiée à l'aide d'aptamères. A cet égard, la dernière LOD améliorée (dans la plage nM) obtenue pour la détection des DCL à l'aide d'aptamères est celle démontrée par Derikvand et al. [54], qui utilise des électrodes nanostructurées. A notre connaissance cependant, notre étude est la première à proposer l'utilisation de films d'hydrogel fixés en surface pour une meilleure immobilisation de l'aptamère et donc une détection accrue de la DCL par des méthodes électrochimiques. Le tableau 1 résume ainsi les caractéristiques des principales méthodes électrochimiques de détection des DCL La méthode que nous proposons présente une limite de détection plus faible que celles reportées dans la littérature pour l'analyse DCL.

Tableau 1. Comparaison entre les performances analytiques des techniques rapportées pour la détection des DCL.

Méthode de détection	**Modification de surface**	**Gamme dynamique**	**LOD**	**Refs.**
Potentiométrie	Membrane contenant la β- cyclodextrine et de la magnetite (CV-Fe(beta-CD))	10 µM to 10 mM	$11x10^3$ nM	36
Photoélectrochemie (PEC)	Apatmère DCL / nanoparticles d'or (Au NPs) et graphène-dopé CdS (GR-CdS) (Au/GR-CdS/Aptamère)	1 to 150 nM	0,78 nM	67
Volampérométrie différentielle à impulsion (DPV)	Nanotubes de carbone multifeuillets (f-MWCNTs) et nanoparticules bimétalliques Or-platine (Au–PtNPs) (Au–PtNPs/fMWCNTs/Au)	0.5 to 1000 µM	300 nM	68
Spectroscopie d'impédance électrochimique (EIS)	Aptamère DCL immobilisé sue carbone vitreux (GCE)(GCE/AHA/Aptamer)	0 – 5 µM ;10 µM to 1 mM	270 nM	29
Volampérométrie différentielle à impulsion (DPV)	Polymère à empreinte moléculaire DCL	16.8 to 270 µM	$3,72x10^3$ nM	23
Spectroscopie d'impédance électrochimique (EIS)	Nanoparticles de Pt (PtNPs) sur nanotubes de carbone (CNTs) fonctionnalisés avec la polyethyleneimine (PEI) et l'aptamère DCL (PtNPs/PEI/CNTs/Aptamère)	10 to 200 nM	2,7 nM	54
Voltampérométrie linéaire (LSV)	Nanotubes de carbone multi-feuillets (MWNTs) – film dihexadecyl hydrogen phosphate (DHP) déposé sur électrode de carone vitreux (MWNTs–DHP/GCE)	0.17 to 2.5 µM	80 nM	31
Potentiométrie	Electrode crayon (MGPE) modifiée par un film de polypyrrole dopé DCL (MGPE/PPy–DCL)	310 µM to11 mM	$190x10^3$ nM	34
Volampérométrie différentielle à impulsion	Nanotubes de carbone multi-feuillets et liquide ionique sur électrode de carbone céramique (MWCNT–IL/CCE)	0.05 to 50 µM	18 nM	38
Spectroscopie d'impédance électrochimique (EIS)	Aptamère immobilisé sur un hydrogel sur électrode d'or (Au/SAM/hydrogel/Aptamer)	30 pM to 1 µM	0,02 nM	Ce travail

6. Conclusion

Une étude bibliographique a montré les effets nocifs d'un polluant émergent : le diclofénac, lorsqu'il est exposé à quelques ng L^{-1} à quelques dizaines de mg L^{-1} de DCL dans l'eau du robinet et a ainsi décrit le besoin urgent de détecter rapidement les DCL dans les échantillons environnementaux, non seulement pour améliorer l'état actuel des connaissances concernant ses voies de pénétration, son devenir et ses effets dans l'environnement, mais également pour déterminer l'efficacité des procédures de traitement des eaux.

La détection DCL repose principalement sur des techniques analytiques conventionnelles, telles que la HPLC et la GC/MS. Malgré leurs performances analytiques intéressantes, ces methods d'analyse prennent beaucoup de temps, sont coûteuses, exigent beaucoup d'expertise et ne sont pas faciles à mettre en œuvre sur le terrain. Aussi, les méthodes électrochimiques sont promstteuses pour l'analyse des composés environnementaux, pharmaceutiques et biologiques. La transduction électrochimique offre plusieurs avantages : elle est simple à utiliser, rapide, économique, très sensible et sélective, compatible avec les nouvelles techniques de microfabrication, jetable, facile à miniaturiser, utilizable sur le terrain et robuste. Les réactions électrochimiques fournissent généralement un signal électronique directement, évitant ainsi l'utilisation d'équipements coûteux de transduction de signaux.

Des méthodes électrochimiques ampérométriques et potentiométriques ont été rapportées pour la détermination de la DCL, via l'utilisation d'électrodes modifies par des nanomatériaux tells que des nanotubes de graphène ou de carbone notamment. Afin d'améliorer la limite de détection (LOD), des biomolécules spécifiques de la DCL ont également été utilisées.

Les aptacapteurs électrochimiques sont des biocapteurs prometteurs, car ils tirent avantage de l'utilisation des aptamères comme élément de reconnaissance spécifique d'une cible. Les aptamères sont de courts oligomères d'acides nucléiques monocaténaires synthétiques (ADN ou ARN), capables de se former des structures complexes hautement organisées permettant de se lier spécifiquement à des cibles moléculaires à haute affinité. Leurs avantages sont nombreux: leur grande spécificité et affinité, leur production facile et très fiable par synthèse enzymatique ou chimique, leur regeneration par des moyens simples et leur aptitude au stockage. Ils sont également stables, sans perte d'activité dans une large gamme de conditions tampons, et résistants aux

traitements agressifs tels que la dénaturation physique ou chimique. Les aptamères peuvent être fonctionnalisés, offrant diverses façons de pouvoir les immobilizer sur des surfaces.
Ainsi, la combinaison des excellentes caractéristiques des aptamères et d'un transudcteur électrochimique offre une perspective prometteuse pour la conception d'aptacapteurs dédiés à la détection des petits produits chimiques toxiques nocifs et leur surveillance en temps réel dans l'environnement. Parmi les différentes techniques de détection électrochimique, la spectroscopie d'impédance électrochimique (SIE) est apparue comme une stratégie prometteuse. Peu d'études ont été menées sur la détection du DCL à l'aide d'aptacapteurs et encore moins basés sur une detection par impedance électrochimique.
Le principal challenge du développement d'aptacapterus hautement sensibles et sélectifs est lié à l'immobilisation stable de l'aptamère sur la surface de l'électrode pour permettre la préservation de leur structure active et fonctionnelle, leur affinité sélective avec la cible, et d'immobiliser une grande quantité d'aptamères. Ainsi, afin d'obtenir une immobilisation stable de l'aptamère DCL tout en conservant son affinité, nous avons choisi d'utiliser des films minces d'hydrogel fixés en surface comme matrice d'immobilisation pour les aptamères.

Dans cette thèse, nous avons développé une nouvelle classe d'aptacapteur pour le diclofénac. A cette fin, une nouvelle classe de couches minces d'hydrogel fixées en surface a été greffée sur un transducteur conducteur en or et utilisée comme matrice biocompatible pour l'immobilisation des aptamères, adaptée à la conception du biocapteur. L'environnement réseau polymère favorise l'immobilisation stable de l'aptamère et l'affinité sélective avec la cible et la détection électrochimique sensible, en fournissant à l'aptamère des environnements excellents pour préserver sa structure active et fonctionnelle. Les couches minces d'hydrogel fixées en surface présentent alors de nombreux avantages en tant que matrice d'immobilisation : elles sont stables, robustes, multi-échelles et multifonctionnelles, avec des épaisseurs allant du faible nanomètre au micromètre élevé. La déformabilité, la perméabilité et la porosité des films d'hydrogel peuvent également être ajustées avec l'épaisseur du film et la densité des réticulations du réseau.

Une approche simple et polyvalente a été utilisée pour la synthèse de films d'hydrogel fiables et reproductibles, base sur le procédé CLAG (Cross-Linking And Grafting). Ce procédé consiste à préformer des polymères fonctionnalisés à l'aide de la chimie clic thiol-ène. L'avantage de cette approche est que la synthèse de chaînes réactives préformées évite la difficulté de travailler sous

atmosphère contrôlée car l'oxygène inhibe la polymérisation radicalaire. Cette approche polyvalente permet ensuite d'ajuster facilement les propriétés chimiques (plate-forme d'immobilisation covalente) et physiques (taille et architecture) des films hydrogel.

Les couches minces d'hydrogel fixées en surface ont été greffées sur un transducteur conducteur à géométrie bien contrôlée. Les différentes étapes de développement de l'aptacapteur, y compris la photolithographie et le procédé de décollage, pour créer un procédé de fabrication d'électrodes adapté aux besoins de l'étude, ont été optimisées pour obtenir un transducteur en or reproductible. Le défi du motif UV de l'hydrogel a également été relevé par l'utilisation d'un matériau peu coûteux et facilement disponible à la place du photomasque classique à base de quartz.

Les couches minces d'hydrogel fixées en surface obtenues avec une géométrie contrôlée ont été caractérisées par spectroscopie et par des techniques électrochimiques, notamment la microscopie à force atomique (AFM), la voltampérométrie cyclique (CV) et la spectroscopie à impédance électrochimique (EIS). Ces mesures ont confirmé l'immobilisation covalente de l'hydrogel sur les électrodes de surface en or et se sont révélées stables pendant plusieurs semaines à 4°C. La preuve de concept de l'immobilisation des biomolécules sur l'hydrogel par la méthode de synthèse peptidique a été réalisée en utilisant la P-nitro aniline comme molécule modèle. Les conditions d'immobilisation covalente de la molécule modèle ont été optimisées et la greffe a été caractérisée par la technique IR-ATR. La méthodologie réalisée a ensuite été adaptée pour l'immobilisation covalente de l'aptamère DCL sur l'hydrogel PAA. Les attaches covalentes entre l'hydrogel et l'aptamère DCL ont été confirmées par des études ATR-FTIR et spectroscopie d'impédance.

La detection du diclofénac a ensuite été réalisée par spectroscopie d'impédance électrochimique (SIE). La reconnaissance du DCL par l'électrode à base d'aptamère entraîne une variation de la résistance de transfert d'électrons pour le couple $[Fe(CN)_6]^{3-/4-}$ mesuré par SIE. La différence de signal avant et après l'addition de DCL à différentes concentrations a permis de montrer une augmentation linéaire de la résistance de transfert de charge avec la concentration en DCL. Les résultats ont mis en evidence une limite de détection nanomolaire pour le DCL avec l'aptacpateur conçu. Nous avons ainsi obtenu un biocapteur à spectroscopie d'impédance électrochimique pour la détection de DCL à haute sensibilité. L'amélioration de la limite de détection par rapport aux valeurs de la littérature est à attribuer à l'environnement tridimensionnel de l'hydrogel, qui améliore la densité de greffage de l'aptamère par rapport aux autres matrices de la littérature. La stabilité et la reproductibilité du biocapteur ont également été prouvées. La sélectivité de l'aptacapteur

développé par rapport à son analyte cible (DCL) a également été étudiée vis-à-vis trois composés interférents : le paracétamol, l'acide 4-amino-phénylacétique et le tryptophane. Les résultats ont confirmé la grande sélectivité de l'aptacapteur conçu par rapport au DCL.

L'aptacapteur conçu a donc permis de fournir une plate-forme pour une détection simple, sensible et sélective du DCL. Il est envisageable d'améliorer la sensibilité de l'aptacapteur en incorporant par exemple des matériaux métalliques nanostructurés tels que des nanoparticules d'or dans le réseau hydrogel.

Une autre méthode de greffage covalent des aptamères covalente pourra être testée pour qui implique le piégeage covalent de l'aptamère dans les matrices tridimensionnelles avant de greffer d'hydrogel et de le réticuler sur la surface. Cette méthode doit être testée dans le but d'obtenir une densité de greffage encore plus élevée. Une autre piste de caractérisation et d'optimisation de l'aptacapteur SIE qui est actuellement en cours de développement, est le couplage avec la microbalance à quartz. Ce couplage permettra de mieux comprendre les effets de masse et de charges qui régissent la réponse de l'aaptacapteur SIE conçu.

La stratégie développée a permis de concevoir des plates-formes de détection qui sont transposables à la reconnaissance moléculaire d'autres cibles, en utilisant les aptamères adequats, dans le domaine de la santé ou de l'environnement.

REFERENCES

(1) Solomon, D. H.; Avorn, J.; Stürmer, T.; Glynn, R. J.; Mogun, H.; Schneeweiss, S. Cardiovascular Outcomes in New Users of Coxibs and Nonsteroidal Antiinflammatory Drugs: High-Risk Subgroups and Time Course of Risk. *Arthritis Rheum.* **2006**, *54* (5), 1378–1389. https://doi.org/10.1002/art.21887.

(2) Tiedeken, E. J.; Tahar, A.; McHugh, B.; Rowan, N. J. Monitoring, Sources, Receptors, and Control Measures for Three European Union Watch List Substances of Emerging Concern in Receiving Waters – A 20 Year Systematic Review. *Sci. Total Environ.* **2017**, *574*, 1140–1163. https://doi.org/10.1016/j.scitotenv.2016.09.084.

(3) Altman, R.; Bosch, B.; Brune, K.; Patrignani, P.; Young, C. Advances in NSAID development: evolution of diclofenac products using pharmaceutical technology, Drugs **2015**, 75, 859–877. https://doi.org/10.1007/s40265-015-0392-z.

(4) Gan, T. J. Diclofenac: an update on its mechanism of action and safety profile, Curr. Med. Res. Opin. **2010**, 26, 1715–1731. https://doi.org/10.1185/03007995.2010.486301.

(5) Paíga, P.; Santos, L. H. M. L. M.; Ramos, S.; Jorge, S.; Silva, J. G.; Delerue-Matos, C. Presence of pharmaceuticals in the Lis river (Portugal): sources, fate and seasonal variation, Sci. Total Environ. **2016**, 573, 164–177. https://doi.org/10.1016/j.scitotenv.2016.08.089.

(6) Lonappan, L.; Brar, S. K.; Das, R. K.; Verma, M.; Surampalli, R. Y. Diclofenac and its transformation products: environmental occurrence and toxicity - a review, Environ. Int. **2016**, 96, 127–138. https://doi.org/10.1016/j.envint.2016.09.014.

(7) Zhang, Y.; Geißen, S.U.; Gal, C. Carbamazepine and diclofenac: removal in waste water treatment plants and occurrence in water bodies, Chemosphere **2008**, 73, 1151–1161. https://doi.org/10.1016/j.chemosphere.2008.07.086.

(8) Petrie, B.; Barden, R.; Kasprzyk-Hordern, B. A review on emerging contaminants in wastewaters and the environment: current knowledge, understudied areas and recommendations for future monitoring, Water Res. **2014**, 72, 3–27. https://doi.org/10.1016/j.watres.2014.08.053.

(9) Richardson, S. D.; Ternes, T. A. Water analysis: emerging contaminants and current issues, Anal. Chem. **2014**, 86, 2813 – 2848. https://doi.org/10.1021/ac500508t.

(10) Albero, B.; Sanchez-Brunete, C.; García-Valcarcel, A. I.; Perez, R. A.; Tadeo, J. L. Ultrasound-assisted extraction of emerging contaminants from environmental samples, TrAC Trends Anal. Chem. **2015**, 71, 110 – 118. https://doi.org/10.1016/j.trac.2015.03.015.

(11) Sui, Q.; Cao, X.; Lu, S.; Zhao, W.; Qiu, Z.; Yu, G. Occurrence, sources and fate of pharmaceuticals and personal care products in the ground water: a review, Emerg. Contam. **2015**, 1, 14 – 24. https://doi.org/10.1016/j.emcon.2015.07.001.

(12) Luo, Y.; Guo, W.; Ngo, H. H.; Nghiem, L. D.; Hai, F. I.; Zhang, J.; Liang, S.; Wang, X. C. A review on the occurrence of micropollutants in the aquatic environment and their fate and removal during wastewater treatment, Sci. Total Environ. **2014**, 473–474, 619–641. https://doi.org/10.1016/j.scitotenv.2013.12.065.

(13) Hoeger, B.; Köllner, B.; Dietrich, D. R.; Hitzfeld, B. Water-borne diclofenac affects kidney and gill integrity and selected immune parameters in brown trout (Salmo trutta f. fario), Aquat. Toxicol. **2005**, 75, 53 – 64. https://doi.org/10.1016/j.aquatox.2005.07.006.

(14) Triebskorn, R.; Casper, H.; Scheil, V. J. Schwaiger, Ultrastructural effects of pharmaceuticals (carbamazepine, clofibric acid, metoprolol, diclofenac) in rainbow trout (Oncorhynchus mykiss) and common carp (Cyprinus carpio), Anal. Bioanal. Chem. **2007**, 387, 1405–1416. https://doi.org/10.1007/s00216-006-1033-x.

(15) Ebele, A. J.; Abou-Elwafa Abdallah, M.; Harrad, S.; Pharmaceuticals and personal care products (PPCPs) in the freshwater aquatic environment, Emerg. Contam. **2017**, 3, 1–16. https://doi.org/10.1016/j.emcon.2016.12.004.

(16) Cleuvers, M. Mixture Toxicity of the Anti-Inflammatory Drugs Diclofenac, Ibuprofen, Naproxen, and Acetylsalicylic Acid. *Ecotoxicol. Environ. Saf.* **2004**, *59* (3), 309–315. https://doi.org/10.1016/S0147-6513(03)00141-6.

(17) Arcelloni, C.; Lanzi, R.; Pedercini, S.; Molteni, G.; Fermo, I.; Pontiroli, A.; Paroni, R. High-Performance Liquid Chromatographic Determination of Diclofenac in Human Plasma after Solid-Phase Extraction. *J. Chromatogr. B. Biomed. Sci. App.* **2001**, *763* (1–2), 195–200. https://doi.org/10.1016/S0378-4347(01)00383-8.

(18) Yilmaz, B.; Asci, A.; Palabiyik, S. S. HPLC Method for Determination of Diclofenac in Human Plasma and Its Application to a Pharmacokinetic Study in Turkey. *J. Chromatogr. Sci.* **2011**, *49* (6), 422–427. https://doi.org/10.1093/chrsci/49.6.422.

(19) Auroux, P.-A.; Iossifidis, D.; Reyes, D. R.; Manz, A. Micro Total Analysis Systems. 2. Analytical Standard Operations and Applications. *Anal. Chem.* **2002**, *74* (12), 2637–2652. https://doi.org/10.1021/ac020239t.

(20) Karimi-Maleh, H.; Biparva, P.; Hatami, M. A Novel Modified Carbon Paste Electrode Based on NiO/CNTs Nanocomposite and (9, 10-Dihydro-9, 10-Ethanoanthracene-11, 12-Dicarboximido)-4-Ethylbenzene-1, 2-Diol as a Mediator for Simultaneous Determination of Cysteamine, Nicotinamide Adenine Dinucleotide and Folic Acid. *Biosens. Bioelectron.* **2013**, *48*, 270–275. https://doi.org/10.1016/j.bios.2013.04.029.

(21) Ensafi, A. A.; Karimi-Maleh, H.; Mallakpour, S.; Hatami, M. Simultaneous Determination of N-Acetylcysteine and Acetaminophen by Voltammetric Method Using N-(3,4-Dihydroxyphenethyl)-3,5-Dinitrobenzamide Modified Multiwall Carbon Nanotubes Paste Electrode. *Sens. Actuators B Chem.* **2011**, *155* (2), 464–472. https://doi.org/10.1016/j.snb.2010.12.048.

(22) Sanghavi, B. J.; Mobin, S. M.; Mathur, P.; Lahiri, G. K.; Srivastava, A. K. Biomimetic Sensor for Certain Catecholamines Employing Copper(II) Complex and Silver Nanoparticle Modified Glassy Carbon Paste Electrode. *Biosens. Bioelectron.* **2013**, *39* (1), 124–132. https://doi.org/10.1016/j.bios.2012.07.008.

(23) Mostafavi, M.; Yaftian, M. R.; Piri, F.; Shayani-Jam, H. A New Diclofenac Molecularly Imprinted Electrochemical Sensor Based upon a Polyaniline/Reduced Graphene Oxide Nano-Composite. *Biosens. Bioelectron.* **2018**, *122*, 160–167. https://doi.org/10.1016/j.bios.2018.09.047.

(24) Lenik, J. A New Potentiometric Electrode Incorporating Functionalized β-Cyclodextrins for Diclofenac Determination. *Mater. Sci. Eng. C* **2014**, *45*, 109–116. https://doi.org/10.1016/j.msec.2014.08.072.

(25) Wang, C.; Jiang, T.; Zhao, K.; Deng, A.; Li, J. A Novel Electrochemiluminescent Immunoassay for Diclofenac Using Conductive Polymer Functionalized Graphene Oxide as Labels and Gold Nanorods as Signal Enhancers. *Talanta* **2019**, *193*, 184–191. https://doi.org/10.1016/j.talanta.2018.09.103.
(26) Wang, S.; Liu, Q.; Li, H.; Li, Y.; Hao, N.; Qian, J.; Zhu, W.; Wang, K. Fabrication of Label-Free Electrochemical Impedimetric DNA Biosensor for Detection of Genetically Modified Soybean by Recognizing CaMV 35S Promoter. *J. Electroanal. Chem.* **2016**, *782*, 19–25. https://doi.org/10.1016/j.jelechem.2016.09.052.
(27) Asif, M.; Aziz, A.; Azeem, M.; Wang, Z.; Ashraf, G.; Xiao, F.; Chen, X.; Liu, H. A Review on Electrochemical Biosensing Platform Based on Layered Double Hydroxides for Small Molecule Biomarkers Determination. *Adv. Colloid Interface Sci.* **2018**, *262*, 21–38. https://doi.org/10.1016/j.cis.2018.11.001.
(28) Sanati, A. L.; Karimi-Maleh, H.; Badiei, A.; Biparva, P.; Ensafi, A. A. A Voltammetric Sensor Based on NiO/CNTs Ionic Liquid Carbon Paste Electrode for Determination of Morphine in the Presence of Diclofenac. *Mater. Sci. Eng. C* **2014**, *35*, 379–385. https://doi.org/10.1016/j.msec.2013.11.031.
(29) Kashefi-Kheyrabadi, L.; Mehrgardi, M. A. Design and Construction of a Label Free Aptasensor for Electrochemical Detection of Sodium Diclofenac. *Biosens. Bioelectron.* **2012**, *33* (1), 184–189. https://doi.org/10.1016/j.bios.2011.12.050.
(30) Rodríguez, J. A.; Barrado, E.; Castrillejo, Y.; Santos, J. R.; Lima, J. L. F. C. Validation of a Tubular Bismuth Film Amperometric Detector. *J. Pharm. Biomed. Anal.* **2007**, *45* (1), 47–53. https://doi.org/10.1016/j.jpba.2007.05.025.
(31) Yang, X.; Wang, F.; Hu, S. Enhanced Oxidation of Diclofenac Sodium at a Nano-Structured Electrochemical Sensing Film Constructed by Multi-Wall Carbon Nanotubes–Surfactant Composite. *Mater. Sci. Eng. C* **2008**, *28* (1), 188–194. https://doi.org/10.1016/j.msec.2006.11.006.
(32) Hajjizadeh, M.; Jabbari, A.; Heli, H.; Moosavi-Movahedi, A. A.; Haghgoo, S. Electrocatalytic Oxidation of Some Anti-Inflammatory Drugs on a Nickel Hydroxide-Modified Nickel Electrode. *Electrochimica Acta* **2007**, *53* (4), 1766–1774. https://doi.org/10.1016/j.electacta.2007.08.026.
(33) Daneshgar, P.; Norouzi, P.; Ganjali, M.; Dinarvand, R.; Moosavi-Movahedi, A. Determination of Diclofenac on a Dysprosium Nanowire- Modified Carbon Paste Electrode Accomplished in a Flow Injection System by Advanced Filtering. *Sensors* **2009**, *9* (10), 7903–7918. https://doi.org/10.3390/s91007903.
(34) Oliveira, M. C.; Bindewald, E. H.; Marcolino, L. H.; Bergamini, M. F. Potentiometric Determination of Diclofenac Using an Ion-Selective Electrode Prepared from Polypyrrole Films. *J. Electroanal. Chem.* **2014**, *732*, 11–16. https://doi.org/10.1016/j.jelechem.2014.08.006.
(35) Kormosh, Zh. A.; Hunka, I. P.; Bazel, Ya. R. A Potentiometric Sensor for the Determination of Diclofenac. *J. Anal. Chem.* **2009**, *64* (8), 853–858. https://doi.org/10.1134/S1061934809080140.
(36) Elbalkiny, H. T.; Yehia, A. M.; Riad, S. M.; Elsaharty, Y. S. Potentiometric Diclofenac Detection in Wastewater Using Functionalized Nanoparticles. *Microchem. J.* **2019**, *145*, 90–95. https://doi.org/10.1016/j.microc.2018.10.017.
(37) Manea, F.; Ihos, M.; Remes, A.; Burtica, G.; Schoonman, J. Electrochemical Determination of Diclofenac Sodium in Aqueous Solution on Cu-Doped Zeolite-Expanded Graphite-

Epoxy Electrode. *Electroanalysis* **2010**, *22* (17–18), 2058–2063. https://doi.org/10.1002/elan.201000074.

(38) Sarhangzadeh, K.; Khatami, A. A.; Jabbari, M.; Bahari, S. Simultaneous Determination of Diclofenac and Indomethacin Using a Sensitive Electrochemical Sensor Based on Multiwalled Carbon Nanotube and Ionic Liquid Nanocomposite. *J. Appl. Electrochem.* **2013**, *43* (12), 1217–1224. https://doi.org/10.1007/s10800-013-0609-3.

(39) Karuppiah, C.; Cheemalapati, S.; Chen, S.-M.; Palanisamy, S. Carboxyl-Functionalized Graphene Oxide-Modified Electrode for the Electrochemical Determination of Nonsteroidal Anti-Inflammatory Drug Diclofenac. *Ionics* **2015**, *21* (1), 231–238. https://doi.org/10.1007/s11581-014-1161-9.

(40) Huebner, M.; Weber, E.; Niessner, R.; Boujday, S.; Knopp, D. Rapid Analysis of Diclofenac in Freshwater and Wastewater by a Monoclonal Antibody-Based Highly Sensitive ELISA. *Anal. Bioanal. Chem.* **2015**, *407* (29), 8873–8882. https://doi.org/10.1007/s00216-015-9048-9.

(41) Hlaváček, A.; Farka, Z.; Hübner, M.; Horňáková, V.; Němeček, D.; Niessner, R.; Skládal, P.; Knopp, D.; Gorris, H. H. Competitive Upconversion-Linked Immunosorbent Assay for the Sensitive Detection of Diclofenac. *Anal. Chem.* **2016**, *88* (11), 6011–6017. https://doi.org/10.1021/acs.analchem.6b01083.

(42) Hayat, A.; Marty, J. L. Aptamer Based Electrochemical Sensors for Emerging Environmental Pollutants. *Front. Chem.* **2014**, *2*. https://doi.org/10.3389/fchem.2014.00041.

(43) Joeng, C. B.; Niazi, J. H.; Lee, S. J.; Gu, M. B. SsDNA Aptamers That Recognize Diclofenac and 2-Anilinophenylacetic Acid. *Bioorg. Med. Chem.* **2009**, *17* (15), 5380–5387. https://doi.org/10.1016/j.bmc.2009.06.044.

(44) Strehlitz, B.; Reinemann, C.; Linkorn, S.; Stoltenburg, R. Aptamers for Pharmaceuticals and Their Application in Environmental Analytics. *Bioanal. Rev.* **2012**, *4* (1), 1–30. https://doi.org/10.1007/s12566-011-0026-1.

(45) Radom, F.; Jurek, P. M.; Mazurek, M. P.; Otlewski, J.; Jele?, F. Aptamers: Molecules of Great Potential. *Biotechnol. Adv.* **2013**, *31* (8), 1260–1274. https://doi.org/10.1016/j.biotechadv.2013.04.007.

(46) Balamurugan, S.; Obubuafo, A.; Soper, S. A.; McCarley, R. L.; Spivak, D. A. Designing Highly Specific Biosensing Surfaces Using Aptamer Monolayers on Gold. *Langmuir* **2006**, *22* (14), 6446–6453. https://doi.org/10.1021/la060222w.

(47) Tombelli, S.; Minunni, M.; Mascini, M. Analytical Applications of Aptamers. *Biosens. Bioelectron.* **2005**, *20* (12), 2424–2434. https://doi.org/10.1016/j.bios.2004.11.006.

(48) Hamula, C.; Guthrie, J.; Zhang, H.; Li, X.; Le, X. Selection and Analytical Applications of Aptamers. *TrAC Trends Anal. Chem.* **2006**, *25* (7), 681–691. https://doi.org/10.1016/j.trac.2006.05.007.

(49) Tom, S.; Jin, H.-E.; Lee, S.-W. Aptamers as Functional Bionanomaterials for Sensor Applications. In *Engineering of Nanobiomaterials*; Elsevier, 2016; pp 181–226. https://doi.org/10.1016/B978-0-323-41532-3.00006-3.

(50) Menger, M.; Glökler, J.; Rimmele, M. Application of Aptamers in Therapeutics and for Small-Molecule Detection. In *RNA Towards Medicine*; Erdmann, V., Barciszewski, J., Brosius, J., Eds.; Springer-Verlag: Berlin/Heidelberg, 2006; Vol. 173, pp 359–373. https://doi.org/10.1007/3-540-27262-3_18.

(51) Nguyen, V.-T.; Kwon, Y. S.; Gu, M. B. Aptamer-Based Environmental Biosensors for Small Molecule Contaminants. *Curr. Opin. Biotechnol.* **2017**, *45*, 15–23. https://doi.org/10.1016/j.copbio.2016.11.020.

(52) Hayat, A.; Haider, W.; Rolland, M.; Marty, J.-L. Electrochemical Grafting of Long Spacer Arms of Hexamethyldiamine on a Screen Printed Carbon Electrode Surface: Application in Target Induced Ochratoxin A Electrochemical Aptasensor. *The Analyst* **2013**, *138* (10), 2951. https://doi.org/10.1039/c3an00158j.

(53) Hayat, A.; Andreescu, S.; Marty, J.-L. Design of PEG-Aptamer Two Piece Macromolecules as Convenient and Integrated Sensing Platform: Application to the Label Free Detection of Small Size Molecules. *Biosens. Bioelectron.* **2013**, *45*, 168–173. https://doi.org/10.1016/j.bios.2013.01.059.

(54) Derikvand, H.; Roushani, M.; Abbasi, A. R.; Derikvand, Z.; Azadbakht, A. Design of Folding-Based Impedimetric Aptasensor for Determination of the Nonsteroidal Anti-Inflammatory Drug. *Anal. Biochem.* **2016**, *513*, 77–86. https://doi.org/10.1016/j.ab.2016.06.013.

(55) Feng, L.; Wang, L.; Hu, Z.; Tian, Y.; Xian, Y.; Jin, L. Encapsulation of Horseradish Peroxidase into Hydrogel, and Its Bioelectrochemistry. *Microchim. Acta* **2009**, *164* (1–2), 49–54. https://doi.org/10.1007/s00604-008-0030-5.

(56) Chollet, B.; Li, M.; Martwong, E.; Bresson, B.; Fretigny, C.; Tabeling, P.; Tran, Y. Multiscale Surface-Attached Hydrogel Thin Films with Tailored Architecture. *ACS Appl. Mater. Interfaces* **2016**, *8* (18), 11729–11738. https://doi.org/10.1021/acsami.6b00446.

(57) Li, M.; Bresson, B.; Cousin, F.; Fretigny, C.; Tran, Y. Submicrometric Films of Surface-Attached Polymer Network with Temperature-Responsive Properties. *Langmuir* **2015**, *31* (42), 11516–11524. https://doi.org/10.1021/acs.langmuir.5b02948.

(58) Miquelard-Garnier, G.; Demeures, S.; Creton, C.; Hourdet, D. Synthesis and Rheological Behavior of New Hydrophobically Modified Hydrogels with Tunable Properties. *Macromolecules* **2006**, *39* (23), 8128–8139. https://doi.org/10.1021/ma061361n.

(59) Chang, S. C.; Chao, I.; Tao, Y.-T. Structures of Self-Assembled Monolayers of Aromatic-Derivatized Thiols on Evaporated Gold and Silver Surfaces: Implication on Packing Mechanism. J. Am.Chem.Soc.**1994**, 116, 6792-6805.

(60) Laibinis, P. E.; Parikh, A. N.; Nuzzo, R. G. Comparison of the Structures and Wetting Properties of Self-Assembled Monolayers of n-Alkanethiols on the Coinage Metal Surfaces, Cu, Ag, Au. J.Am.Chem.Soc.**1991**,113,7152-7167.

(61) Yadav, V.; Harkin, A. V.; Robertson, M. L.; Conrad, J. C. Hysteretic Memory in PH-Response of Water Contact Angle on Poly(Acrylic Acid) Brushes. *Soft Matter* **2016**, *12* (15), 3589–3599. https://doi.org/10.1039/C5SM03134F.

(62) Mendes, R. K.; Freire, R. S.; Fonseca, C. P.; Neves, S.; Kubota, L. T. Characterization of Self-Assembled Thiols Monolayers on Gold Surface by Electrochemical Impedance Spectroscopy. *J. Braz. Chem. Soc.* **2004**, *15* (6), 849–855. https://doi.org/10.1590/S0103-50532004000600011.

(63) Azzaroni, O.; Vela, M. E.; Martin, H.; Hernández Creus, A.; Andreasen, G.; Salvarezza, R. C. Electrodesorption Kinetics and Molecular Interactions at Negatively Charged Self-Assembled Thiol Monolayers in Electrolyte Solutions. *Langmuir* **2001**, *17* (21), 6647–6654. https://doi.org/10.1021/la010019v.

(64) Sudre, G.; Hourdet, D.; Creton, C.; Cousin, F.; Tran, Y. PH-Responsive Swelling of Poly(Acrylic Acid) Brushes Synthesized by the Grafting Onto Route. *Macromol. Chem. Phys.* **2013**, *214* (24), 2882–2890. https://doi.org/10.1002/macp.201300477.

(65) Lego, B.; Skene, W. G.; Giasson, S. Swelling Study of Responsive Polyelectrolyte Brushes Grafted from Mica Substrates: Effect of PH, Salt, and Grafting Density. *Macromolecules* **2010**, *43* (9), 4384–4393. https://doi.org/10.1021/ma902588j.

(66) Alfonta, L.; Bardea, A.; Khersonsky, O.; Katz, E.; Willner, I. Chronopotentiometry and Faradaic Impedance Spectroscopy as Signal Transduction Methods for the Biocatalytic Precipitation of an Insoluble Product on Electrode Supports: Routes for Enzyme Sensors, Immunosensors and DNA Sensors. *Biosens. Bioelectron.* **2001**, *16* (9–12), 675–687. https://doi.org/10.1016/S0956-5663(01)00231-7.

(67) Okoth, O. K.; Yan, K.; Feng, J.; Zhang, J. Label-Free Photoelectrochemical Aptasensing of Diclofenac Based on Gold Nanoparticles and Graphene-Doped CdS. *Sens. Actuators B Chem.* **2018**, *256*, 334–341. https://doi.org/10.1016/j.snb.2017.10.089.

(68) Eteya, M. M.; Rounaghi, G. H.; Deiminiat, B. Fabrication of a New Electrochemical Sensor Based on Au Pt Bimetallic Nanoparticles Decorated Multi-Walled Carbon Nanotubes for Determination of Diclofenac. *Microchem. J.* **2019**, *144*, 254–260. https://doi.org/10.1016/j.microc.2018.09.009.

RÉSUMÉ

Une grande variété de polluants émergents se trouvent dans les sources d'eau naturelles et traitées. Les méthodes traditionnelles de détection et de quantification de ces polluants font appel à la spectrométrie de masse, souvent associées à la chromatographie en phase gazeuse ou liquide. Ils sont coûteux, lents, nécessitent de gros appareillages et mobilisent des experts. Pour surmonter ces limitations, la mise au point de capteurs rapides, économiques et faciles d'utilisation, destinés à l'analyse des polluants dans l'eau, revêt une importance capitale. Ces dernières années les biocapteurs électrochimiques font l'objet d'une attention considérable pour la détection et la quantification des polluants dans l'eau. Ils offrent l'avantage de détecter les contaminants à l'état de traces dans différentes matrices, telles que les échantillons d'eaux naturelles et traitées. Nous avons développé un nouveau biocapteur basé sur l'utilisation d'un aptamère pour la reconnaissance moléculaire d'un polluant émergent pharmaceutique : le diclofénac (DCL). Une nouvelle classe de polymères a été utilisée comme matrice biocompatible pour l'immobilisation de l'aptamère. Il s'agit d'un film mince d'hydrogel greffé à la surface du transducteur conducteur. L'immobilisation de l'aptamère sur l'hydrogel offre un environnement biodégradable qui permet de préserver la structure active et fonctionnelle de l'aptamère tout en permettant la détection du DCL. Le greffage de l'aptamère s'obtient par la formation de liaisons amides *via* l'activation des groupes acide carboxylique de l'hydrogel Poly(Acide Acrylique) (PAA). La sensibilité du biocapteur est améliorée grâce à la densité de greffage élevée de l'apatmère et à la structure 3D de l'hydrogel. La spectroscopie d'impédance électrochimique (EIS) a été utilisée pour détecter le DCL dans l'eau. La variation de la résistance au transfert de charge est linéaire avec une concentration cible comprise entre 30 pM et 1 µM. La limite de détection est de 0,02 nM.

MOTS CLÉS

Aptacapteurs impédimétriques; Hydrogel; Aptamère; Diclofenac; Polluants émergents

ABSTRACT

A wide variety of emerging pollutants are found in natural and treated water sources. Traditional methods to detect and quantify these pollutants involve mass spectrometry, often in combination with gas or liquid chromatography. They are expensive, time-consuming and require laboratory facilities for sample analysis by an expert. To overcome these limitations, the development of rapid, low cost, easy, point of use sensors for pollutant determination in water is of vital importance. Electrochemical biosensors for the detection of environmental pollutants have received considerable attention in recent years. They provide a great advantage to detect trace levels of contaminants in different matrices, such as in natural and treated water samples. We have developed a novel biosensor dedicated to a molecular recognition level of a pharmaceutical emerging pollutant: the diclofenac based on the use of aptamer. We have designed the biosensor using a novel class of grafted polymers, a surface-attached hydrogel thin films on conductive transducer as a biocompatible matrix for the aptamer immobilization. The immobilization of the aptamer onto the hydrogel by covalent attachment provided a biodegradable shelter, giving the aptamer an excellent environment to preserve its active and functional structure while allowing the detection of DCL. The grafting of the aptamer is obtained using the formation of amide bonds *via* the activation of carboxylic acid groups of the poly (acrylic acid) (PAA) hydrogel thin film, and for improved sensitivity and higher stability of the aptasensor, a high density of immobilized aptamer was enabled. The surface potential was probed *via* Electrochemical Impedance Spectroscopy (EIS) and the impedance spectra were analyzed by using a modified Randles equivalent circuit model. The change in charge-transfer resistance was found to be linear with the target concentration in the range of 30 pM to 1 µM, with a detection limit of 0.02 nM.

KEYWORDS

Impedimetric aptasensors; Hydrogel; Aptamer; Diclofenac; Emerging pollutants